Mixed Matrix Membranes For Mixture Gas Separation Of Butane Isomers

A Thesis
Presented to
The Academic Faculty

by

Omoyemen Edoamen Esekhile

In Partial Fulfillment
of the Requirements for the Degree
Doctor of Philosophy in the
School of Chemical and Biomolecular Engineering

Georgia Institute of Technology
December 2011

Mixed Matrix Membranes For Mixture Gas Separation Of Butane Isomers

Approved by:

Dr. William Koros, Advisor
School of Chemical &
Biomolecular Engineering
Georgia Institute of Technology

Dr. Amyn Teja
School of Chemical &
Biomolecular Engineering
Georgia Institute of Technology

Dr. Victor Breedveld
School of Chemical &
Biomolecular Engineering
Georgia Institute of Technology

Dr. Karl Jacob
School of Material Science &
Engineering
Georgia Institute of Technology

Dr. Carson Meredith
School of Chemical &
Biomolecular Engineering
Georgia Institute of Technology

Date Approved: October 26th 2011

This thesis is dedicated to my parents,
Mr. Joseph and Mrs. Helen Esekhile

The best siblings in the world,
Dr. Ehizokhale, Miss. Osedebamen, and Mr. Osezua Esekhile

And my loving fiancé,
Mr. James Ofoegbu

ACKNOWLEDGEMENTS

It has been a long and very rewarding journey in so many ways. I would like to express my appreciation to God for the grace he gave me through this period of my career. Without his help I do not know where I would be. My heartfelt gratitude to my parents and siblings. They have been the greatest support I could ever ask for. With their constant prayers, words of encouragement, and their belief in me especially when I stop believing. I can't thank them enough.

I would like to thank my advisor, Dr. Bill Koros for the support he has given me through the years. He is a very dedicated professor, extremely hardworking and focused. Seating in Mass Transfer class with Dr. Koros as the professor was both nerve wrecking and challenging. I knew I had to be prepared for questions being thrown at me. My desire to work under Dr. Koros' supervision was based on his skill as a teacher, and his commitment to his work. I recall when he presented me with the project; he mentioned it would involve some modeling. I made it clear that I didn't know anything about modeling, and he assured me we would get through it together. We did, with long periods of brainstorming and going back and forth. That is just an example of how wonderful he is.

Many thanks to the diverse group of intelligent people I had the opportunity to work with. Thanks to Dr. Liu for showing me the ropes, technical discussions, and the interesting collaboration experience. I would like to acknowledge ExxonMobil and KAUST for funding this project. Thanks to the GT-EM group which consisted of Dr. Jones, Dr. Nair, Dr. Meredith, Dr. Breedveld, Dr. Koros, Dr. Liu, Dr. Olanrewaju, Dr.

Bae, and Dr. Hyun. The monthly meetings were truly helpful. Thank to my research committee, your inputs were greatly appreciated

I would also like to appreciate other group members that made my stay amazing, with friendly discussions about things ranging from research to other aspects of life. Liren Xu, Nitesh Bhuwania, Dr. Jong Suk Lee, Dr. Chien-Chiang Chen, Dr. Kuang Zhang, and Dr. Ryan Lively, much thanks. To Dr. JR. Johnson and Dr. Oguz Karvan, my utmost gratitude for your help. I know it seemed I always needed something moved, installed, fixed or built, but you came through for me. Thanks a lot. To Carine Saha Kuete, I know you are still fairly new to the group, but you have made the last year so much more exciting. Thanks to my roommate Kendra Maxwell, I appreciate your support, and wiliness to listen when I needed to vent, as well as the laughs we shared.

To my fiancé James Ofoegbu, how can I thank you enough. You supported me right from the beginning which includes applying to Georgia Tech. You encouraged me through the different stages, the qualifiers, proposal, conferences, paper writing, job applications and interviews not to mention keeping me on track. You are truly God sent.

TABLE OF CONTENTS

LIST OF TABLES

LIST OF FIGURES

SUMMARY

The goal of this project was to understand and model the performance of hybrid inorganic-organic membranes under realistic operating conditions for hydrocarbon gas/vapor separation, using butane isomers as the model vapors and a hybrid membrane of 6FDA-DAM-5A as an advanced separation system.

To achieve the set goal, three objectives were laid out. The first objective was to determine the factors affecting separation performance in dense neat polymer. One main concern was plasticization. High temperature annealing has been reported as an effect means of suppressing plasticization. A study on the effect of annealing temperature was performed by analyzing data acquired via sorption and permeation measurements. Based on the findings from this study, a suitable annealing temperature was determined. Another factor studied was the effect of operating temperature. In deciding a suitable operating temperature, factors such as its possible effect on plasticization as well as reducing heating/cooling cost in industrial application were considered.

Based on the knowledge that industrial applications of this membrane would involve mixture separation, the second objective was to understand and model the complexity of a mixed gas system. This was investigated via permeation measurements using three feed compositions. An interesting transport behavior was observed in the mixed gas system, which to the best of our knowledge, has not been observed in other mixed gas systems involving smaller penetrants. This mixed gas transport behavior presented a challenge in predictability using well-established transport models. Two hypotheses were made to explain the observed transport behavior, which led to the

development of a new model termed the HHF model and the introduction of a fitting parameter termed the CAUFFV fit. Both the HHF model and CAUFFV fit showed better agreement with experimental data than the well-established mixed gas transport model.

The final objective was to explore the use of mixed matrix membranes as a means of improving the separation performance of this system. A major challenge with the fabrication of good mixed matrix membranes was the adhesion of the zeolite particle with the polymer. This was addressed via sieve surface modification through a Grignard treatment process. Although a Grignard treatment procedure existed, there was a challenge of reproducibility of the treatment. This challenge was addressed by exploring the relationship between the sieves and the solvent used in the treatment, and taking advantage of this relationship in the Grignard treatment process. This study helped identify a suitable solvent, which allowed for successful and reproducible treatment of commercial LTA sieves; however, treatment of lab-made sieves continues to prove challenging. Based on improved understanding of the Grignard treatment reaction mechanism, modifications were made to the existing Grignard treatment procedure, resulting in the introduction of a "simplified" Grignard treatment procedure. The new procedure requires less control over the reaction process, thus making it more attractive for industrial application.

Permeation measurements were made using mixed matrix membranes in both single and mixed gas systems. Selectivity enhancements were observed under both single and mixed gas systems using sieve loadings of 25 and 30wt%. The Maxwell model was used to make predictions of mixed matrix membrane performance. Although the experimental results were not in exact agreement with Maxwell predictions, the observed

selectivity enhancement was very encouraging and shows potential for future application. Recommendations were made for future study of this system.

CHAPTER 1
MOTIVATION AND INTRODUCTION

1.1. MEMBRANES FOR GAS SEPARATION

The separation of gases by thin barriers termed membranes is a dynamic and rapidly growing field. Membranes are being used to separate gases from their mixtures by differential permeation of the components through them. Membrane separation processes offer potential advantages in terms of low energy use and capital investments [1]. Membranes were known to have the potential to separate important gas mixtures long before 1980, but the technology to fabricate high-performance membranes and modules was lacking [2]. Ample opportunities to extend the membrane market for gas and vapor separation exists; however, exploitation of these opportunities is limited by the inadequacy of existing economical membrane materials, membrane structures and formation processes [3]. There are currently only eight or nine polymer materials used to make 90% of the total installed gas separation membranes base. New polymer membranes with substantially higher permeabilities and selectivities have been reported, but they do not meet other necessary criteria for useful membranes [2]. The key criteria for membrane material selection for a given application are durability, mechanical integrity at the operating conditions, productivity and separation efficiency, which must all be balanced against cost. The operating cost of membranes is dependent on the driving force required to achieve a certain separation, while the capital cost is dependent on the flux through the membrane. For low operational and capital cost, it is desired for the

membrane to provide high selectivity and high flux thus requiring smaller membrane areas and minimal need for recycle.

Asymmetric and composite membranes consist of thin dense selective skins and a thicker porous matrix layer that provides physical support to the thin skin. Practically speaking, the selective skin must be either dense or molecular sieving in nature. Although convective flow or bulk flow can occur in nonselective porous membranes when the pore diameter is larger than the mean free path of permeates, such membranes offer no molecular separation and are not useful. Knudsen diffusion, which occurs in porous membranes when the pore diameter is smaller than the mean free path of penetrants results when the molecules collide more frequently with the pore walls than with other co-permeating gas species. In totally dense membranes or dense layers of asymmetric and composite membranes, the so-called sorption-diffusion mechanism applies. In this mechanism the gas molecules first sorb into the polymer matrix to an extent dependent on their individual condensability and diffuse across the membrane under a concentration gradient at rates dependent on their molecular sizes, and finally desorb on the downstream end of the membrane. Schematic of these mechanisms are shown in figure 1.1. Molecular sieving media are simply a limiting case of standard sorption-diffusion media in which microscopic pores enable only one of the two penetrants to diffuse through the porous structure at a significant rate while the other is effectively excluded.

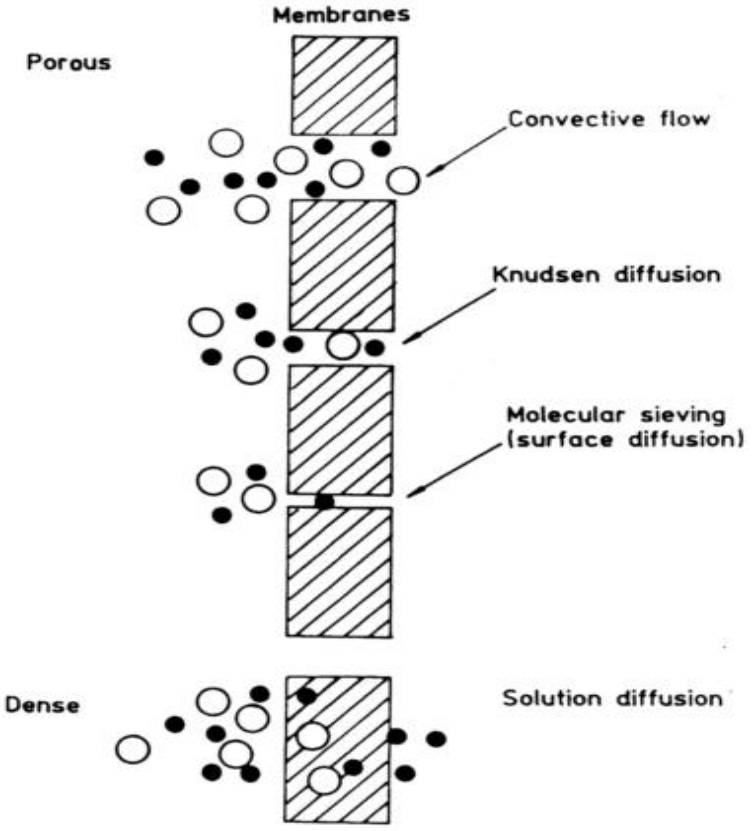

Figure 1.1: Schematic of diffusion mechanism of gas through membranes [1]

1.2. MIXED MATRIX MEMBRANES FOR GAS SEPARATION

There are two main technical challenges facing the current membrane technology that hinders commercialization. These are: 1) achieving higher efficiency and maintaining productivity comparable with the current separation plants while offering a cost benefit, and 2) maintaining these properties in the presence of complex and aggressive feeds [3]. Robeson has shown the existence of an upper bound limit in the separation performance of pure polymeric membranes that can be processed using economical solution formation techniques. Polymeric membranes exhibit a trade-off in

selectivity with increasing productivity and vice-versa. Commercially attractive membranes will need to exhibit separation performance that exceeds this upper bound line as indicated in the cross-hatched region in figure 1.2. Polymeric membranes are easy to produce but undergo plasticization in the presence of highly condensable penetrants.

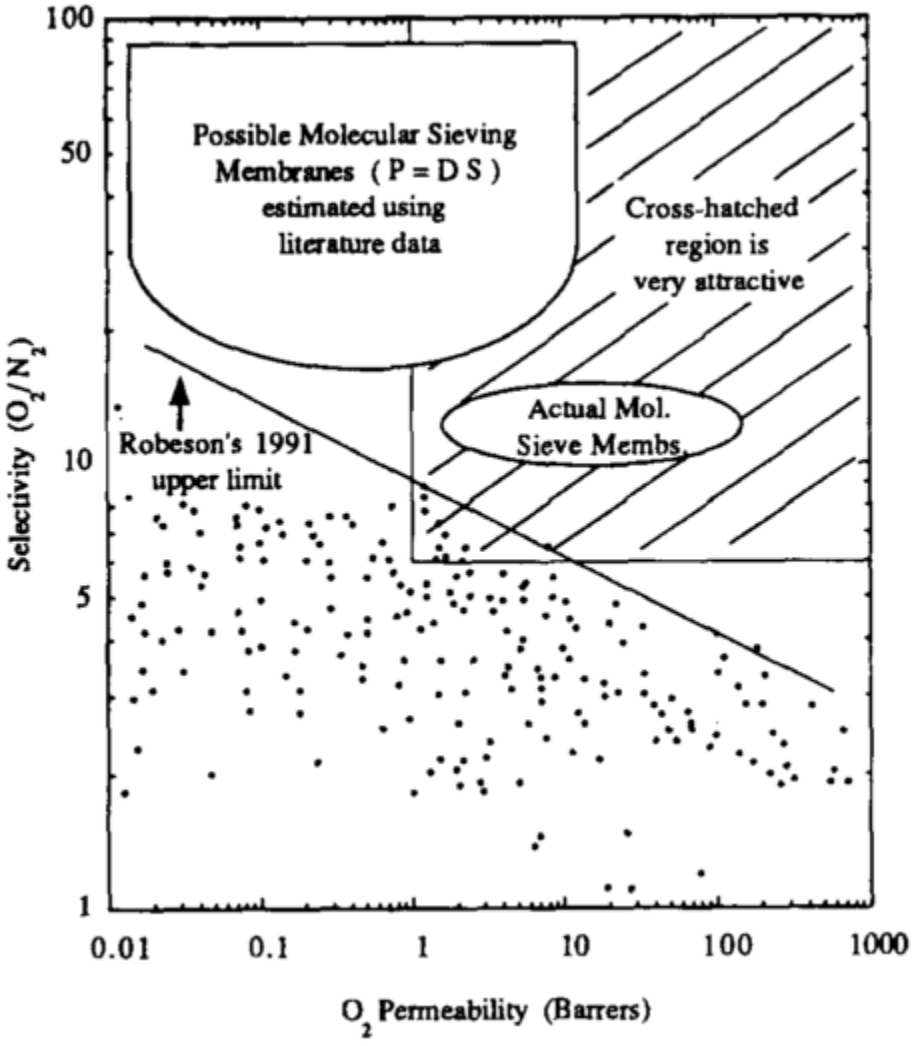

Figure 1.2: Robeson Trade-off curve for O_2/N_2 [4]

Molecular sieving membranes such as zeolite membranes have shown separation performances that are commercially attractive. These membranes are rigid and stable in

adverse conditions of high temperature, pressure, and highly sorbing components; however, they are difficult and costly to produce [3]. Mixed matrix membranes comprise highly selective molecular sieves as the dispersed phase with the continuous phase being polymer. These membranes take advantage of the high selectivity of the sieves and the ease of production of the polymers, and have been shown to exhibit separation performances that exceed the upper bound line as seen in figure 1.3.

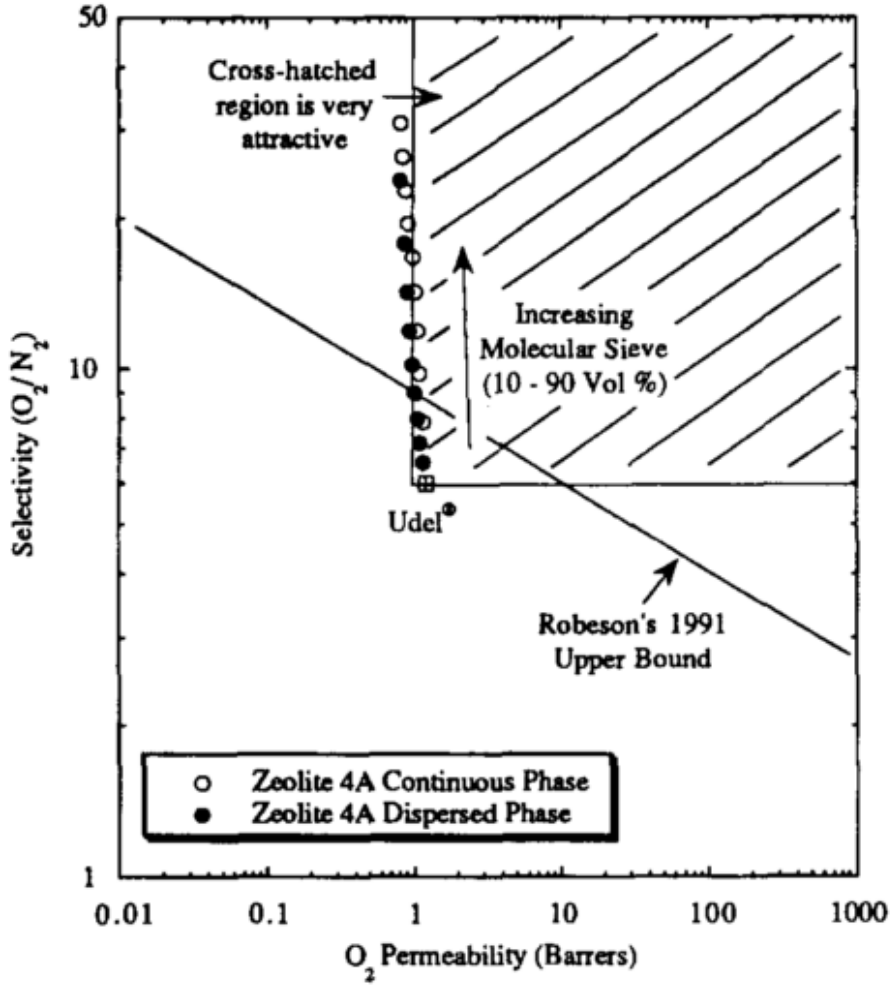

Figure 1.3: Mixed matrix membranes of zeolite 4A and Udel for O2/N2 separation [4]

Though mixed matrix membranes have shown potential in improved gas separation performance, there are significant challenges faced in the fabrication of defect-free membranes. These challenges mainly result from the poor adhesion of the molecular sieves to the polymer, which leads to poor selectivity. Researchers have investigated means of improving the adhesion problem, which will be discussed in subsequent chapters. Another challenge is in spinning these mixed matrix membranes into asymmetric hollow fibers, which provide high membrane area per volume and are the industrially favored configuration.

1.3. SEPARATION OF BUTANE ISOMERS

Normal butane is a highly flammable natural gas obtained from the refining of crude oil. It is a straight chain alkane with four carbon atoms and ten hydrogen atoms. Normal butane can be isomerized via the so-called butamer™ process to produce isobutane. The UOP butamer process is a fixed-bed catalytic process. The reaction is equilibrium limited and favored by lower temperature [5].

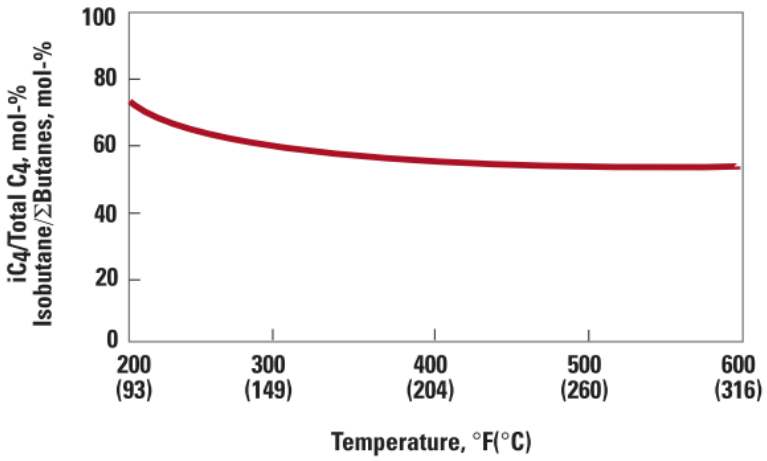

Figure 1.4: Isobutane Equilibrium [5]

As shown in figure 1.4, the butamer™ process yields a composition of ~60 mol% isobutane with a balance of normal butane. The mixture is then separated, and isobutane is further processed to isobutylene, which is a feed for motor fuel alkylates for reformulated gasoline. Also, isobutane has replaced carbon fluorocarbon as a refrigerant due to its zero ozone depletion potential. The unconverted normal butane is recycled to the butamer™ unit.

The current separation process is based on fractional distillation, which depends on the boiling point difference of the isomers (nC4 (bp. -0.5°C), iC4 (bp. -11.7°C)). The close boiling points of these isomers make the separation difficult, requiring many stages, and large amounts of energy [6]. The introduction of membrane units in the separation process would serve to debottleneck the distillation towers and make the separation process more energy efficient, requiring less operational and capital cost. Figure 1.5 shows a schematic of the proposed membrane-distillation separation set-up.

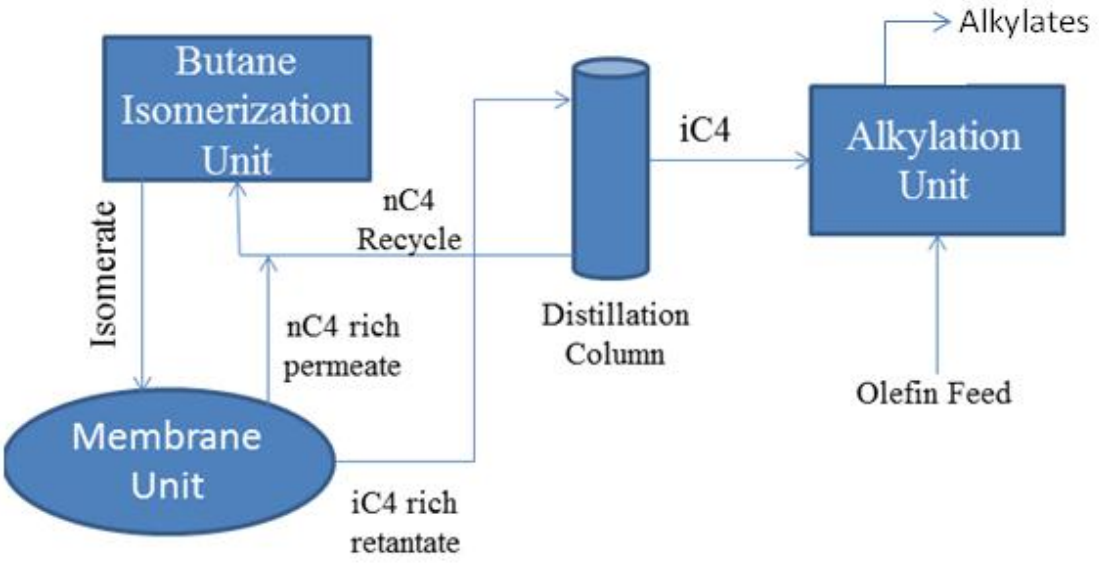

Figure 1.5: Schematic of membrane-distillation separation set-up for butane isomers

1.4. RESEARCH GOAL

The aim of this research study was to both understand and model the performance of hybrid inorganic-organic membranes under realistic operating conditions for hydrocarbon gas/vapor separation. The approach utilized butane isomers as the model vapors, and a hybrid membrane of 6FDA-DAM-5A zeolites as an advanced separation system. In order to achieve this goal, specific objectives were established.

Objective 1: Characterize and analyze the factors that impact the separation performance of dense 6FDA-DAM membranes for the model isobutane/n-butane system.

Annealing of glassy polymers at high temperatures below their glass transition temperature, T_g, physically ages the film by facilitating free volume diffusion out of the

glass. This allows the packing defect in glassy polymers to diffuse out, leading to lower free volumes, and permeability. Another common effect of annealing in polyimides is the formation of charge-transfer-complexes (CTC's), which are evidenced by a change in color of the film. CTC's are a result of change in molecular orientation in the polymer that leads to change in electron density. Polyimides like 6FDA-DAM are very susceptible to CTC formation due to the abundance of ring structures which act as sites for the formation of weak bonds via π-electron transfer. Annealing has been shown to reduce the susceptibility of glassy polymeric membranes to plasticization. Plasticization is the swelling induced increase in diffusion coefficient due to high feed pressures of strongly sorbing gases. The swelling causes an increase in fractional free volume (FFV), and loss of selectivity.

Objective 2: Identify and model factors affecting separation performance of dense 6FDA-DAM membranes for gas/vapor mixtures of the model n-butane/isobutane system.

There are three common factors reported in the literature to influence mixed gas transport though glassy polymers. These are: 1) Competitive sorption in the limited Langmuir environment present in glassy polymers, 2) Bulk flow effect or convective flow effect, which may be important when there is a significant difference in the fluxes of the gases in the mixture and 3) Plasticization of the polymer in the presence of highly condensable gases. Tanaka et al. [7] studied mixture gas/vapor separation of propylene, C_3H_6 and propane, C_3H_8 (50/50 mol%) using 6FDA-DAM. Their study showed a decrease in the permeability of the faster C_3H_6, an increase in the permeability of the

slower C_3H_8 and thus an overall decrease in selectivity compared to single gas studies. They also observed a drop in selectivity with increase in total pressure. This increase in permeability of C_3H_8 in the presence of C_3H_6 could be due to competitive sorption and bulk flow effect [8]. Plasticization, which is a known effect of C_3H_6 and C_3H_8 in 6FDA-based polymers [9], could also be responsible for the transport behavior observed by Tanaka et al.

Objective 3: Extend analysis to include hybrid inorganic-organic membranes under realistic operating conditions.

The most desirable membrane polymers for gas separation should provide both high permeability and selectivity. Unfortunately, an inverse permeability/selectivity behavior exists for pure polymeric membranes. As noted earlier, this behavior has been studied by Robeson [10], who suggested the existence of a hypothetical upper bound between permeability and selectivity. It has been the focus of recent research to push the bound into a more economically attractive region. Recent work in mixed matrix has shown enhanced separation properties above the trade-off line. The main challenge faced while making mixed matrix membranes is the lack of adhesion of the sieves to the polymer, which results in no separation enhancement.

Shu [11] and Husain [12] developed a method of Grignard treatment of the sieves, which changes their surface structure, improving their adhesion to the polymer. Grignard treatment produces whisker structures of magnesium hydroxide on the surface of zeolite sieves, making them more hydrophobic. As depicted in figure 1.6, the magnesium

hydroxide whiskers are hypothesized to decrease the change in entropy of the polymer during contact with the sieves, thus improving adhesion.

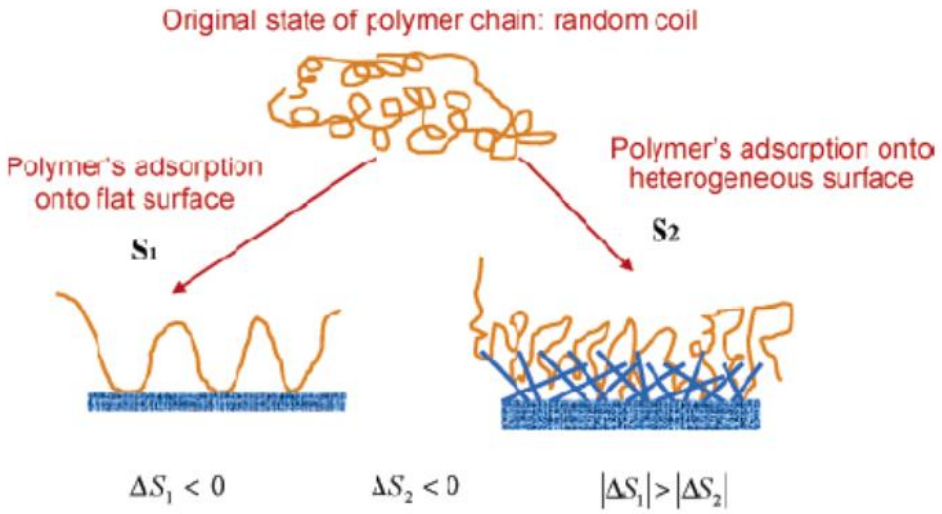

Figure 1.6: Schematic illustrating the benefit of sieve roughing or "whiskering" for adhesion by the polymer matrix [13]

Mixed matrix membranes, like neat polymer membranes can experience bulk flow effects and plasticization in mixed gas tests. To increase n-butane/isobutane selectivity, one needs to reduce the permeability of isobutane relative to n-butane. This can be achieved by using mixed matrix membranes of 6FDA-DAM and molecular sieves with pore size smaller than the kinetic diameter of isobutane.

1.5. DISSERTATION OUTLINE

This dissertation is divided into seven chapters including this introduction. Chapter 2 will provide details on the background and theory of gas transport through membranes. It will introduce the well-established models used in this work.

Chapter 3 will describe the materials used in this study. This includes the polymer, molecular sieves and solvents. This chapter will also describe the experimental methods and characterization techniques used.

Chapter 4 will address the surface modification of LTA 5A via Grignard treatment. It will discuss the recently developed "*simplified*" Grignard treatment method, which was used for most of the mixed matrix work in this project.

Chapter 5 will address the transport behavior of butane isomers in 6FDA-DAM-based dense films, in pure gas systems. The effect of annealing temperatures of 180°C, and 230°C over 24 hrs, will be covered as well as the effect of operating temperature with regards to permeation and sorption, thus addressing objective 1. The chapter will also address transport in 6FDA-DAM-5A mixed matrix membranes.

Chapter 6 will address the transport behavior of butane isomers in 6FDA-DAM-based dense films, in mixed gas systems. It will introduce new models used to describe the observed transport behavior in this system.

Chapter 7 will review the successes and challenges of this research and will make recommendations for future work for the advancement of this project.

1.6. REFERENCES

1. Pandey, P. and R.S. Chauhan, *Membranes for gas separation.* Progress in Polymer Science, 2001. **26**(6): p. 853-893.

2. Baker, R.W., *Future Directions of Membrane Gas Separation Technology.* Industrial & Engineering Chemistry Research, 2002. **41**(6): p. 1393-1411.

3. Koros, W.J. and R. Mahajan, *Pushing the limits on possibilities for large scale gas separation: which strategies?* Journal of Membrane Science, 2000. **175**(2): p. 181-196.

4. Zimmerman, C.M., A. Singh, and W.J. Koros, *Tailoring mixed matrix composite membranes for gas separations.* Journal of Membrane Science, 1997. **137**(1-2): p. 145-154.

5. http://xa.yimg.com/kq/groups/3862917/709231331/name/Butamer.pdf.

6. Seader, J.D. and E.J. Henley, *Separation Process Principles*: John Wiley & Sons, Inc.

7. Tanaka, K., et al., *Permeation and separation properties of polyimide membranes to olefins and paraffins.* Journal of Membrane Science, 1996. **121**(2): p. 197-207.

8. Kamaruddin, D.H. and W.J. Koros, *Some observations about the application of Fick's first law for membrane separation of multicomponent mixtures.* J. Mem. Sci., 1997. **135**(2): p. 147-159.

9. Das, M., *Membranes for Olefin/Paraffin Separation*, in *Chemical and Biomolecular Engineering*. 2009, Georgia Institute of Technology: Atlanta, GA.

10. Robeson, L.M., *Correlation of separation factor versus permeability for polymeric membranes.* Journal of Membrane Science, 1991. **62**(2): p. 165-185.

11. Shu, S. Husain, and W.J. Koros, *Formation of Nanostructured Zeolite Particle Surfaces via a Halide/Grignard Route.* Chemistry of Materials, 2007. **19**(16): p. 4000-4006.

12. Husain, S. and W.J. Koros, *Mixed matrix hollow fiber membranes made with modified HSSZ-13 zeolite in polyetherimide polymer matrix for gas separation.* Journal of Membrane Science, 2007. **288**(1-2): p. 195-207.

13. Shu, S., *Engineering the performance of mixed matrix membranes for gas separation*, in *Chemical and Biomolecular Engineering* 2007, Georgia Institute of Technology: Atlanta

CHAPTER 2
BACKGROUND AND THEORY

2.1. ABSTRACT

This chapter provides insight into the background material relevant to the research covered in the subsequent chapters. The transport mechanisms of gases through polymers, zeolites and mixed matrix membranes will be discussed in more detail to provide a basis for understanding the subsequently presented results. Factors affecting mixed gas transport through membranes will be addressed and models used to account for these factors will be presented.

2.2. GAS TRANSPORT IN GLASSY POLYMERS

The sorption-diffusion theory describes transport of penetrants through polymeric membranes and molecular sieving media [1, 2]. This transport occurs in three stages: First the penetrants sorb at the surface of the membrane on the high-pressure feed side, then diffuse through the polymer matrix via a concentration gradient, and finally desorb at the low pressure permeate side. The intrinsic ability of the membrane to transport a particular penetrant via a given transmembrane driving force reflects its productivity or permeability. The permeability of a gas through a polymer is defined as the flux of the gas A, normalized by the thickness of the film and the partial pressure difference across the membrane, viz, [3, 4]

$$P_A = Flux_A * \frac{l}{\Delta p_A} \tag{2.1}$$

where P_A is the permeability, l is the thickness of the film, Δp_A is the partial pressure difference of the gas/vapor penetrant A across the film.

Permeability can also be described as the product of the diffusion and solubility coefficient of a penetrant in the polymer, viz, [5-7]

$$P_A = D_A \times S_A \tag{2.2}$$

where D_A is the diffusion coefficient, and S_A is the solubility coefficient.

The efficiency of a membrane to achieve gas separation is reflected by the permselectivity or selectivity of the membrane for a particular gas pair. The permselectivity is defined as the ratio of the permeability of the penetrants, and could also be viewed as the product of the diffusivity selectivity and solubility selectivity under ideal conditions with a vacuum downstream, viz,

$$\alpha^*_{A/B}(ideal) = \frac{P_A}{P_B} = \frac{flux_A}{flux_B} * \frac{\Delta p_B}{\Delta p_A} = \frac{D_A}{D_B} * \frac{S_A}{S_B} \tag{2.3}$$

In a mixed gas system, the separation factor is defined as the ratio of the permeate mole fractions divided by the ratio of the feed mole fractions [4, 8]. The mole fractions are determined via gas chromatogram (GC) analysis, which will be discussed in detail in chapter 3.

$$\alpha_{A/B} = \frac{y_A/y_B}{x_A/x_B} \tag{2.4}$$

where, A and B are the individual penetrants that constitute the gas mixture, y and x are the permeate and feed mole fractions respectively. Under conditions where the ratio of downstream to upstream pressure approaches zero, $\alpha_{A/B} \rightarrow \alpha^*_{A/B}$.

2.2.1. Gas sorption in glassy polymers

The sorption coefficient of penetrants into polymeric membranes is determined by measuring the sorption capacity of the penetrant in the membrane as a function of external penetrant partial pressure or fugacity. Sorption is a thermodynamic process, which is dependent on the condensability of the gas and the polymer-penetrant interaction [9]. The condensability effect is dominant in the absence of specific interaction, so the solubility increases with increase in the condensability of the gas, which can be qualified using its critical temperature, or energy parameters [10]. Figure 2.1 shows an increase in solubility with increase in energy parameter of various gases.

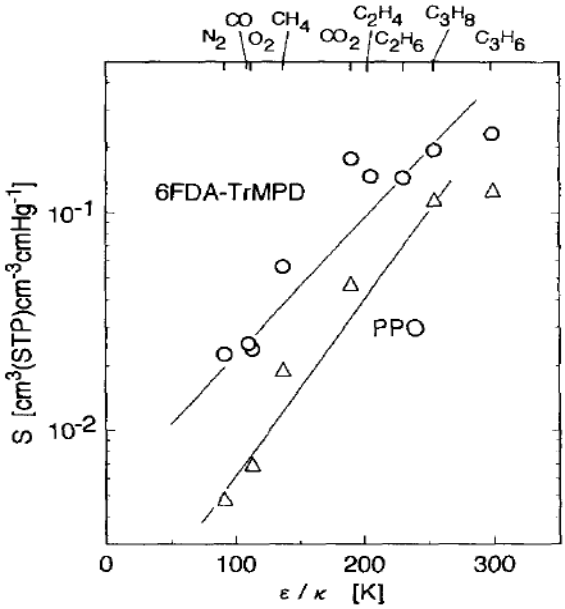

Figure 2.1: Correlation of gas solubility with their energy parameter [10]

Sorption isotherms of gases in glassy polymers typically exhibit non-linearity. Several models have been proposed to describe the non-linearity, these include the dual-mode model, the gas-polymer matrix model, and predictive equation of state models such as the nonequilibrium lattice fluid model [9]. The most suitable and commonly used model is the dual-mode [5, 11]. Glassy polymers such as 6FDA-DAM exist in a non-equilibrium state below their glass transition temperatures, T_g [12]. The non-equilibrium state means that the chains are frozen in place without reaching their most thermodynamically stable state. As a result, there are "holes" or molecular scale microvoids within the matrix whose total amount can be referred to as unrelaxed free volume. The microvoids are non-equilibrium elements, which arise during quenching to the glassy state from the rubbery state [13]. These microvoids though limited in volume, allow for penetrant sorption into the polymer. Figure 2.2 shows a schematic of the unrelaxed free volume present in glassy polymers.

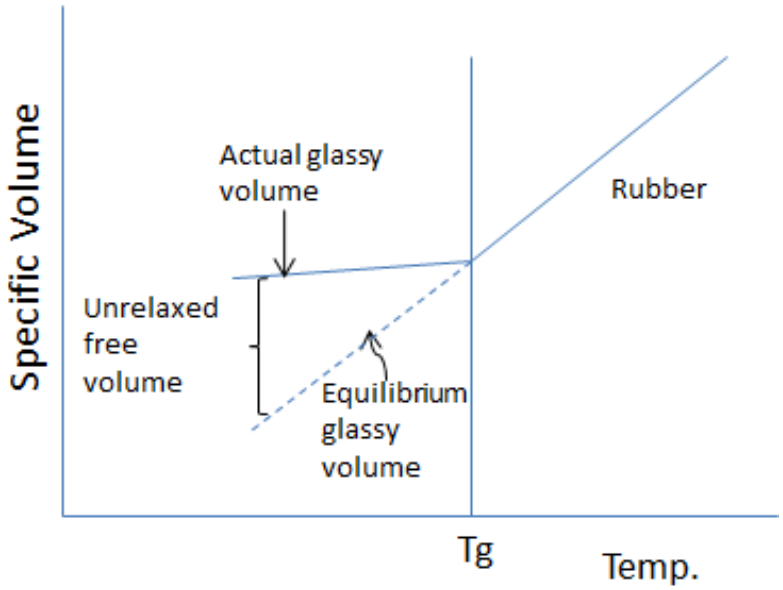

Figure 2.2: Schematic of the unrelaxed free volume

Glassy polymers are ideally viewed as exhibiting two types of sorption environments. The so-called equilibrium densified environment is also known as the Henry's environment and it is representative of an equilibrium segmental packing. Sorption in this mode is generally expressed as a concentration (C_D), which is directly proportional to the partial pressure of the penetrant, with a proportionality constant k_D also referred to as the Henry's constant. To characterize the deviation of the glassy state from equilibrium, so-called unrelaxed free volume or "holes" or microvoids provide an environment to accommodate an additional population, C_H, is generally accepted to exist. Associated with this additional microvoid or "hole" environment is a so-called "Langmuir Capacity Parameter", C'_H. The affinity of a particular penetrant for the Langmuir environment, b, and the partial pressure or fugacity (for non-ideal gases at high pressures) of the penetrant provide a measure of the tendency of a given penetrant to saturate this limited additional microvoid capacity. The overall sorption concentration, C,

is the sum of the concentrations in both environments and is described using the dual mode sorption model in equation 2.5.

$$C_A = C_{D_A} + C_{H_A} = k_{D_A} p_A + \frac{C'_{H_A} b_A p_A}{1 + b_A p_A} \tag{2.5}$$

Sorption into the Langmuir environment is based on the well-established assumptions that:

- Sorption does not proceed beyond saturation of the fixed Langmuir capacity
- All sorption sites are equally available, and the sorption site energies are uniform
- The ability of a gas molecule to sorb at a particular site is independent of the occupation of neighboring sites
- A dynamic equilibrium exists between the sorbed molecules and the free gas molecules

The amount and size distribution of the excess unrelaxed free volume factors into the sorption capacity of the gas. The unrelaxed free volume in a glassy polymer is described as the difference between the specific volume of a glass, V_g and the hypothetical liquid volume, V_l.

$$Unrelaxed\ free\ volume\ (FV) = V_g - V_l \tag{2.6}$$

The size distribution and amount of unrelaxed free volume can change as a result of aging [12, 14, 15], or high temperature (sub-T_g) annealing [16]. Sub-T_g annealing will be addressed in more detail in chapter 5.

The saturated Langmuir sorption constant of a gas in a glassy polymer can be described by the unrelaxed free volume fraction, as in equation 2.7 [17-20]:

$$C'_{H_A} = \left(\frac{V_g - V_l}{V_g}\right)\rho_A^* \tag{2.7}$$

where, ρ_A^* is the liquid-like molar density of the specific penetrant in the Langmuir region.

Koros [21] extended the dual mode sorption model to account for binary gas sorption. This extended model accounts for the presence of competitive sorption in the Langmuir environment, and assumes that the model parameters remain unaffected by the presence of a second penetrant. Due to the limited Langmuir sorption sites, in a mixed gas system, individual penetrants have to compete for these sites, thus resulting in a decrease in the sorption capacity of a particular penetrant with increase in the partial pressure of the other penetrant.

$$C_A = k_{D_A}p_A + \frac{C'_{H_A}b_A p_A}{1 + b_A p_A + b_B p_B} \tag{2.8}$$

The sorption coefficient of gas for a polymeric membrane is defined as the ratio of its sorption capacity and partial pressure.

$$S_A = \frac{C_A}{p_A} = k_{D_A} + \frac{C'_{H_A}b_A}{1 + b_A p_A + b_B p_B} \tag{2.9}$$

2.2.2. Diffusion of gases through glassy polymers

Diffusion of a gas through a polymer is dependent on the polymer chain mobility, which results from temperature fluctuations and intrinsic flexibility of the backbone. The diffusion coefficient is dependent on the jump frequency, f and the jump length, λ [22].

$$D = \frac{\lambda^2 f}{6} \tag{2.10}$$

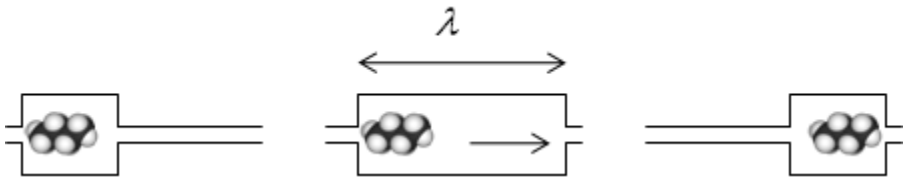

Figure 2.3: Schematic of diffusion mechanism of a gas molecule through polymeric membrane

In order for a gas molecule to make a diffusive jump, the polymer segments must separate locally sufficiently to create a microscopic passage for the gas molecule to pass through. The frequency of jumps decreases with increase in kinetic diameter of the gas, thus leading to a similar trend in the diffusion coefficient, as shown in figure 2.4.

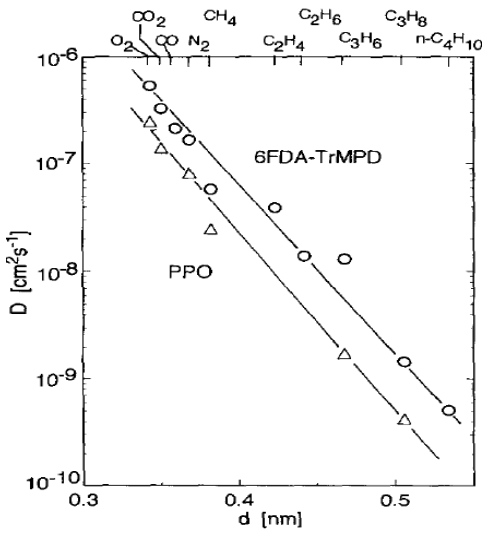

Figure 2.4: Correlation of diffusion coefficient with the kinetic diameter of penetrants [10]

Barrer [23] identified 4 types of diffusion jumps in glassy matrices:

1. D→D. Jump of a penetrant from a dissolved region to another dissolved environment via a chemical potential gradient. The diffusion coefficient associated with this jump is defined as D_{DD}.
2. H→D. Jump of a penetrant from a Langmuir site to a dissolved region via a chemical potential gradient. The diffusion coefficient associated with this jump is defined as D_{HD}.
3. D→H. Jump of a penetrant from a dissolved region to a Langmuir site via a chemical potential gradient. This jump is dependent on the availability of the Langmuir site and the probability of finding a Langmuir site adjacent to the dissolved molecule. The diffusion coefficient associated with this jump is defined as D_{DH}.
4. H→H. Jump of a penetrant from a Langmuir site to another Langmuir site via a chemical potential gradient. This jump is dependent on the availability of the

Langmuir site, and the probability of finding two Langmuir sites adjacent to each other. The diffusion coefficient associated with this jump is defined as D_{HH}.

The Barrer model which defines permeability by accounting for the four types of diffusion jumps in glassy polymer is provided in equation 2.11 [23].

$$P = k_D \left[D_{DD} + \frac{(D_{HD} + D_{HH})\, bC'_H / k_D - D_{DH}}{1 + bp} + \frac{2D_{DH}}{bp} ln(1 + bp) \right] \tag{2.11}$$

Due to the relative scarcity of Langmuir sites, D_{DH} and D_{HH} are considered negligible. So the two main types of diffusion jumps are D_{DD} and D_{HD}, which are commonly referred to as D_D and D_H respectively. This reduces equation 2.11 to the simpler and more commonly used form in equation 2.14 where, $p_B = 0$.

The diffusion-based flux of a penetrant through a polymer as defined in Fick's law is the product of the diffusion coefficient and the local concentration gradient, which serves as a "surrogate" for the local chemical potential gradient, viz., [2]

$$N_A = -D(C)_A \frac{\partial C_A}{\partial z} \tag{2.12}$$

where N is the flux, and z is the membrane thickness.

Paul and Koros [24] explained the existence of partial immobilization in the Langmuir sites. It is assumed that only a fraction F, of the Langmuir sorption capacity, C_H, is mobile, so the flux can be described via the dual mode mobility model.

$$N_A = -D_{D_A}\frac{\partial\left(C_{D_A} + FC_{H_A}\right)}{\partial z} = -D_{D_A}\frac{\partial C_{D_A}}{\partial z} - D_{H_A}\frac{\partial C_{H_A}}{\partial z} \tag{2.13}$$

Following from the definition of permeability, the dual mode mobility and sorption models are combined to derive the dual mode transport model that defines the diffusion-based permeability, P^*, of a gas through a glassy polymer in a system with downstream vacuum, viz.

$$P_A^* = k_{D_A}D_{D_A} + \frac{C'_{H_A}D_{H_A}b_A}{1 + b_Ap_A + b_Bp_B} = k_{D_A}D_{D_A}\left(1 + \frac{K_AF_A}{1 + b_Ap_A + b_Bp_B}\right) \tag{2.14}$$

where,

$$F = \frac{D_H}{D_D} \tag{2.15}$$

and

$$K = \frac{C'_Hb}{k_D} \tag{2.16}$$

According to Fick's law of diffusion, the permeation flux through polymeric membranes with respect to a fixed frame of reference is equal to the sum of the bulk and diffusional flux.

$$n_A = n_A^{bulk} + n_A^{diff} \tag{2.17}$$

$$n_A^{bulk} = \left(n_A + n_B + n_p\right)\omega_A \tag{2.18}$$

$$n_A^{diff} = -\rho D_A\frac{d\omega_A}{dz} \tag{2.19}$$

where, n_p is the flux of the polymer, which is stationary. So, $n_p = 0$, and ω is the mobile weight fraction of the penetrant in the polymer.

Kamarrudin and Koros [25] discuss in detail the bulk flow contribution to the overall flux. In a mixture system, the bulk fraction, which is dependent on the sorption level of the penetrants and the overall flux of the mobile components, may be significant and so should be accounted for in analyzing permeation data. The bulk flow effect suggests that the slower moving gas is being carried along by the faster gas, leading to an increase in permeability of the slower gas with negligible effect on the faster gas. This accounts for some of the drop in selectivity generally observed when comparing permselectivity from single gas system to that attained from mixed gas system.

The total mass flux of each penetrant is obtained by integrating equation 2.19 with the boundary conditions:

$$\begin{aligned} z = 0; \quad & \omega_A = \omega_{A1}, \quad \omega_B = \omega_{B1} \\ z = l; \quad & \omega_A = \omega_{A2}, \quad \omega_B = \omega_{B2} \end{aligned}$$

In a system with vacuum downstream, ω_{A2} and $\omega_{B2} \approx 0$.

$$n_A l = \frac{\rho D_A \ln\left[\frac{1-\omega_{A2}(1+1/r)}{1-\omega_{A1}(1+1/r)}\right]}{(1+1/r)} \approx \frac{\rho D_A \ln\left[\frac{1}{1-\omega_{A1}(1+1/r)}\right]}{(1+1/r)} \qquad (2.20)$$

$$n_B l = \frac{\rho D_B \ln\left[\frac{1-\omega_{B2}(1+r)}{1-\omega_{B1}(1+r)}\right]}{(1+r)} \approx \frac{\rho D_B \ln\left[\frac{1}{1-\omega_{B1}(1+r)}\right]}{(1+r)} \qquad (2.21)$$

where,

$$r = \frac{n_A}{n_B}; \quad (n_A > n_B)$$

ρ is the density of the polymer, l is the thickness of the film, and ω is the mobile weight fraction of the gas in the polymer, and is calculated using equation 2.22.

$$\omega_A = \left(1 + \frac{F_A K_A}{1 + b_A p_A + b_B p_B}\right) \frac{k_{D_A} p_A M_A}{22400\rho} \tag{2.22}$$

where, M_A is the molecular weight of the penetrant.

Using equations 2.23 and 2.24, the observed permeability of gases A and B ($n_A > n_B$) through a glassy polymer in a mixed gas system can be determined.

$$P_A = \frac{P_A^*}{(1 - \pi_A^{bulk})} = \frac{\ln\left[\frac{1}{1 - \omega_{A1}(1 + 1/r)}\right] P_A^*}{\omega_{A1}(1 + 1/r)} \tag{2.23}$$

$$P_B = \frac{P_B^*}{(1 - \pi_B^{bulk})} = \frac{\ln\left[\frac{1}{1 - \omega_{B1}(1 + r)}\right] P_B^*}{\omega_{B1}(1 + r)} \tag{2.24}$$

Equations 2.23 and 2.24 are permeability models that account for both competition in the Langmuir environment, and bulk flow effect. These are used to make transport predictions for mixed gas systems, using model parameters derived from single gas transport systems. As shown in figure 2.5, Das [26] obtained good agreement to experimental data using equations 2.23 and 2.24 for a mixed gas system of propane/propylene in 6FDA-6FpDA. Similarly, Koros and Kammarudin [25] obtained good agreement to experimental data for a mixed gas system of CO_2/CH_4 in 6FDA-TADPO.

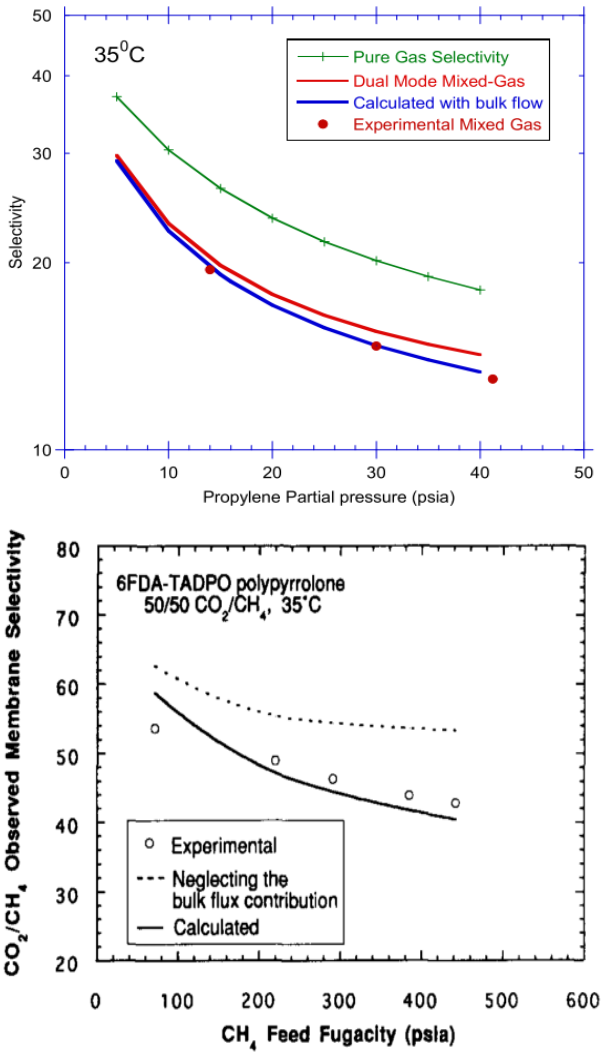

Figure 2.5: Shows good agreement of mixed gas model using equations 2.23 and 2.24 for, (a) 50%/50% propane/propylene in 6FDA-6FpDA [26], and (b) 50%/50% CO2/CH4 in 6FDA-TADPO polypyrrolone [25]

2.2.3. Plasticization

Plasticization is a swelling induced increase in segmental mobility in the presence of highly sorbing penetrants [27, 28]. The swelling introduces an added free volume, which results in an increase in permeability of the polymer but drastically reduces its selectivity.

The feed pressure at which plasticization first occurs is termed the "plasticization pressure". It is observed at an upswing in the isothermal plot of permeability with feed pressure in glassy polymers. Permeability in glassy polymers typically decrease with increase in feed pressure, then reaches an asymptotic value indicating saturation of Langmuir sorption sites. In the presence of a plasticizing penetrant, an increase in permeability is observed upon further increase in feed pressure. The feed pressure at which the upswing begins is termed the plasticization pressure.

To avoid the complications of plasticization, all measurements were made within the plasticization-free pressure range as shown in figure 5.4.

2.2.4. Temperature effect on gas transport through polymers

Gas diffusion through polymers is dependent on temperature, and can be represented by an Arrhenius relationship via equation 2.25.

$$D = D_0 \exp\left(\frac{-\Delta E_D}{RT}\right) \tag{2.25}$$

where, D_0 is the pre-exponential factor, ΔE_D is the apparent activation energy for diffusion, R is the universal gas constant, and T is the operating temperature in Kelvin. Solubility coefficient dependence on temperature is described by the van't Hoff equation (equation 2.26).

$$S = S_0 \exp\left(\frac{-\Delta H_S}{RT}\right) \tag{2.26}$$

where, S_0 is the pre-exponential factor, and ΔH_S is the apparent heat of sorption. Equations 2.25 & 2.26 can be combined into the Arrhenius expression for permeability.

$$P_0 = D_0 S_0 \tag{2.27}$$

$$\Delta E_P = \Delta E_D + \Delta H_S \tag{2.28}$$

$$P = P_0 \exp\left(\frac{-\Delta E_P}{RT}\right) \tag{2.29}$$

where, P_0 is a pre-exponential factor and ΔE_P is the apparent activation energy for permeation.

2.3. GAS TRANSPORT THROUGH ZEOLITES

The transport of gas through zeolite is via molecular sieving. Inorganic zeolite particles have specific pore sizes, thus permitting passage of gas molecules with small enough kinetic sizes, and hindering passage of larger gas molecules. As a result of their rigid structure, they are highly selective materials [29].

The permeability of a penetrant through molecular sieves is also defined as the flux through the sieve, normalized by the pressure difference, and the particle length, as in equation 2.1.

$$P_A = Flux_A * \frac{l}{\Delta p_A} \tag{2.1}$$

$$Flux_A = -D_A \frac{dC_A}{dz} \tag{2.12}$$

Zeolites unlike glassy polymers typically only have one type of sorption site, which is the Langmuir sorption site. The sorption capacity is described viz,

$$C_A = \frac{C'_{H_A} b_A p_A}{1 + b_A p_A + b_B p_B} = C'_{H_A} \theta_A \tag{2.30}$$

The Stefan-Maxwell equation is used to determine the diffusion coefficient through molecular sieves.

$$D_A = D_{0_A} \frac{d \ln(p_A)}{d \ln(C_A)} \tag{2.31}$$

where D_0 is the mobility diffusion coefficient of the penetrant in the sieves. This can be estimated to be the diffusion coefficient at low concentrations, which can be deduced from transient sorption measurements. The diffusion coefficient can be deduced graphically or mathematically using Cranks solution for the time-dependent uptake in a sphere of radius, R.

$$\left(\frac{M_t}{M_\infty}\right)_A = 1 - \sum_{n=0}^{\infty} \frac{8}{\pi^2 (2n+1)^2} exp\left(\frac{-D_A (2n+1)^2 \pi^2 t}{R^2}\right) \tag{2.32}$$

where, M_t and M_∞ are the masses of the penetrants sorbed at times t and ∞.

Combining equations 2.1, 2.12, 2.30 and 2.31, the flux and permeability of a penetrant through sieves can be described as:

$$Flux_A = -\frac{D_{0_A}}{1 - \theta_A} C'_{H_A} \frac{d\theta_A}{dz} \tag{2.33}$$

$$P_A = -\frac{D_{0_A} C'_{H_A}}{1-\theta_A}\left[\frac{d\theta_A}{dp_A}\right] = -\frac{D_{0_A} C'_{H_A}}{p_A}\ln[1-\theta_A] \tag{2.34}$$

assuming downstream is under vacuum.

2.4. GAS TRANSPORT THROUGH MIXED MATRIX MEMBRANES

As noted earlier in section 1.2, it is well known that there is an upper bound (trade-off) line in the separation performance of pure polymeric membranes, and mixed matrix membranes have shown potential in achieving gas separation performance that exceeds the upper bound line.

The performance of mixed matrix membranes is largely dependent on some matching criteria, and the nature of the interface between the zeolite and the polymer. Several models have been proposed for describing the permeability through mixed matrix membranes [30]. The most commonly used model is the Maxwell Model developed in 1873 to predict the permittivity of a dielectric [31]. Based on the similarity of the equations governing electrical potential and the flux through membranes, Maxwell's model is applicable to transport in mixed matrix membranes. This model as presented in equation 2.35, is acceptable at dilute dispersion of spherical particles as it is based on the assumption that the streamlines around particles are not affected by the presence of nearby particles [31]. It also assumes proper dispersion of sieves in the membrane, and proper adhesion of the sieve surface to the polymer.

$$P_{MMM_A} = P_{M_A}\left(\frac{P_{D_A} + 2P_{M_A} - 2\varphi_D\left(P_{M_A} - P_{D_A}\right)}{P_{D_A} + 2P_{M_A} + \varphi_D\left(P_{M_A} - P_{D_A}\right)}\right) \tag{2.35}$$

The Maxwell model takes into account the permeability through the polymer matrix, P_{M_A}, the permeability through the dispersed phase (sieves), P_{D_A}, and the volume fraction of the sieves, φ_D. In order to achieve maximum separation performance the separation properties of the sieves have to complement those of the polymer. The matching criteria vary for each system and polymer/sieve pair. Figure 2.6 can be used to explain the matching requirement.

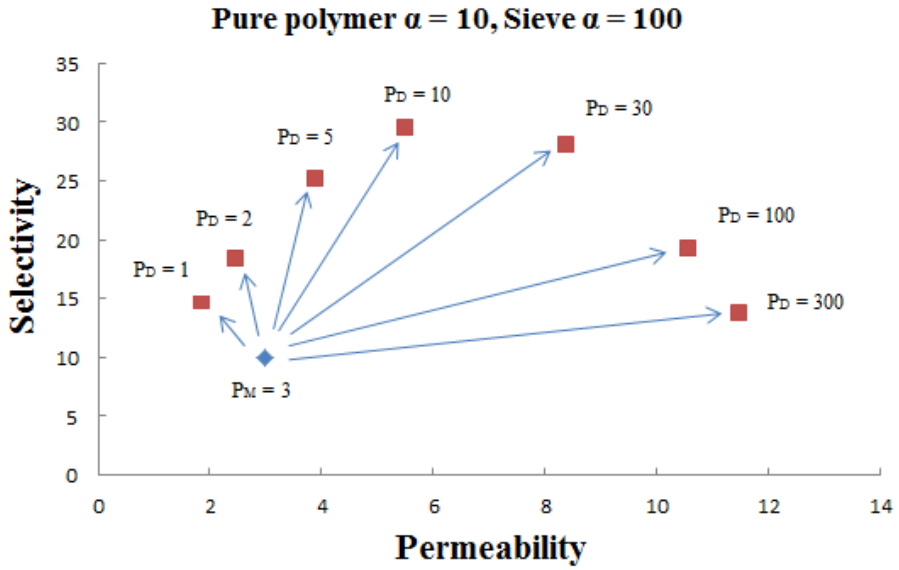

Figure 2.6: Maxwell model prediction of separation performance of hypothetic mixed matrix membrane

Figure 2.6 shows a system with the permeability of the fast gas being 3 Barrer, and selectivity in pure polymer of 10, while selectivity in the sieve is 100. For a particular sieve volume fraction, the mixed matrix membrane separation performance is greatly affected by the gas permeability in the sieve. If the gas is more permeable in the polymer matrix, the presence of the sieves reduces the permeability with only a slight increase in

selectivity, since the sieve will be mostly by-passed for the less diffusion resistant polymer. On the other end, if the sieves are much more permeable than the polymer, there will be an increase in the permeability with no selectivity enhancement. This results from the permeability of both gases being equally enhanced by the sieves.

The second main factor that affects the separation performance of mixed matrix membrane is the nature of the interface between the zeolite and the polymer. Non-ideal mixed matrix membrane morphologies have been identified [32]. These are: plugged sieves, matrix rigidification, leaky interface and sieve-in-cage morphology. Plugged sieves occur as a result of strongly held molecules completely preventing passage of the penetrant. Matrix rigidification, leaky interface and sieve-in-cage can be related to the stress generated from removal of solvent during film formation [32-34]. Plugged sieves result in decrease in permeability with no effect on the selectivity, because the polymer provide a path of less diffusion resistance, thus the mixed matrix membrane retains the intrinsic selectivity of the polymer. Matrix rigidification results in decrease in permeability with some increase in selectivity. This is because, though diffusion is hindered within the rigidified region, the penetrants still have access to the sieves, thus resulting in selectivity enhancement. Leaky interface which is the case with voids around the interface of the zeolite and polymer results in increase in permeability and decrease in selectivity. Unlike sieve-in-cage, these voids are not visible through SEM as they are on the order of the penetrant size (~5Å), so both penetrants have access to the less diffusion resistant voids. Sieve-in-cage results in increased permeability with no change in selectivity. In this case, the sieves are caged in by the polymer, so the intrinsic selectivity of the polymer is retained. Although sieve-in-cage results in increased permeability,

which may seem favorable; however, it will be difficult to prepare asymmetric hollow fibers with such morphology without loss in selectivity.

Due to the importance of the polymer-zeolite interface in the separation performance of mixed matrix membranes, researchers have identified various means of improving adhesion [34-36]. Based on the understanding that stress encountered from solvent evaporation during film formation contributes to poor interfacial adhesion, researchers have investigated increasing polymer flexibility and decreasing stress by decreasing T_g. This was done by incorporation of plasticizers to decrease T_g, using low volatile solvents and casting films at elevated temperatures [33]. The result of this strategy showed good sieves dispersion, adhesion and selectivity but decreased permeability. Another attempt at improving interfacial adhesion was to use silane coupling. This was aimed at achieving a chemical bond between the sieve and polymer [35]. The result of this strategy showed better adhesion confirmed by SEM, but a decrease in selectivity. The decrease in selectivity despite improvement in adhesion was attributed to the presence of "nonselective leakage" (i.e. leaky interface). Also attempted was the use of polymers with carboxylic acid group to promote formation of strong hydrogen bonds with the hydroxylated surface of sieves [36]. This resulted in improved adhesion and selectivity; however, the polymers have poor intrinsic separation performance. Since the desire is to make successful mixed matrix membranes with minimal alteration to the well-established and industrially viable spinning process, further research has been done to modify the sieve surface. Zeolite surface modification via Grignard treatment has shown improved mixed matrix performance. This treatment process as developed by Husain and Shu [37] results in the growth of magnesium

hydroxide ($Mg(OH)_2$) nanowhiskers on the zeolite surface that promote interlocking of the polymer chains. Liu [38] has shown good adhesion of Grignard treated MFI with 6FDA-DAM. Grignard treatment will be used in this work for sieve surface modification.

2.5. REFERENCES

1. Wijmans, J.G. and R.W. Baker, *The solution-diffusion model: a review.* Journal of Membrane Science, 1995. **107**(1-2): p. 1-21.

2. Wang, R., C. Cao, and T.-S. Chung, *A critical review on diffusivity and the characterization of diffusivity of 6FDA-6FpDA polyimide membranes for gas separation.* Journal of Membrane Science, 2002. **198**(2): p. 259-271.

3. Lin, H., et al., *Plasticization-Enhanced Hydrogen Purification Using Polymeric Membranes.* Science, 2006. **311**(5761): p. 639-642.

4. Ghosal, K. and B.D. Freeman, *Gas separation using polymer membranes: an overview.* Polymers for Advanced Technologies, 1994. **5**(11): p. 673-697.

5. Koros, W.J., A.H. Chan, and D.R. Paul, *Sorption and transport of various gases in polycarbonate.* Journal of Membrane Science, 1977. **2**: p. 165-190.

6. Barrer, R.M., J.A. Barrie, and J. Slater, *Sorption and diffusion in ethyl cellulose. Part III. Comparison between ethyl cellulose and rubber.* Journal of Polymer Science, 1958. **27**(115): p. 177-197.

7. Koros, W.J., *Simplified analysis of gas/polymer selective solubility behavior.* Journal of Polymer Science: Polymer Physics Edition, 1985. **23**(8): p. 1611-1628.

8. O'Brien, K.C., et al., *A new technique for the measurement of multicomponent gas transport through polymeric films.* Journal of Membrane Science, 1986. **29**(3): p. 229-238.

9. Merkel, T.C., et al., *Sorption and transport of hydrocarbon and perfluorocarbon gases in poly(1-trimethylsilyl-1-propyne).* Journal of Polymer Science Part B: Polymer Physics, 2000. **38**(2): p. 273-296.

10. Tanaka, K., et al., *Permeation and separation properties of polyimide membranes to olefins and paraffins.* Journal of Membrane Science, 1996. **121**(2): p. 197-207.

11. Vieth, W.R., J.M. Howell, and J.H. Hsieh, *Dual sorption theory.* Journal of Membrane Science, 1976. **1**: p. 177-220.

12. Strum, L.C.E., *Physical aging in plastics and other glassy materials.* Polymer Engineering & Science, 1977. **17**(3): p. 165-173.

13. Koros, W.J., D.R. Paul, and G.S. Huvard, *Energetics of gas sorption in glassy polymers.* Polymer, 1979. **20**(8): p. 956-960.

14. Huang, Y., X. Wang, and D.R. Paul, *Physical aging of thin glassy polymer films: Free volume interpretation.* Journal of Membrane Science, 2006. **277**(1-2): p. 219-229.

15. Victor, J.G. and J.M. Torkelson, *On measuring the distribution of local free volume in glassy polymers by photochromic and fluorescence techniques.* Macromolecules, 1987. **20**(9): p. 2241-2250.

16. Chan, A.H. and D.R. Paul, *Effect of sub-Tg annealing on CO2 sorption in polycarbonate.* Polymer Engineering & Science, 1980. **20**(1): p. 87-94.

17. Wonders, A.G. and D.R. Paul *Effect of CO2 exposure history on sorption and transport in polycarbonate.* J. Mem. Sci., 1979. **5**: p. 63-75.

18. Kanehashi, S. and K. Nagai, *Analysis of dual-mode model parameters for gas sorption in glassy polymers.* J. Mem. Sci., 2005. **253**(1-2): p. 117-138.

19. Koros, W.J. and D.R. Paul, *CO2 sorption in poly(ethylene terephthalate) above and below the glass transition.* J. Poly. Sci.: Poly. Phys. Ed., 1978. **16**(11): p. 1947-1963.

20. Koros, W.J. and D.R. Paul, *Transient and steady-state permeation in poly(ethylene terephthlate) above and below the glass transition.* J. Poly. Sci.: Poly. Phys. Ed., 1978. **16**(12): p. 2171-2187.

21. Koros, W.J., *Model for sorption of mixed gases in glassy polymers.* Journal of Polymer Science: Polymer Physics Edition, 1980. **18**(5): p. 981-992.

22. Koros, W.J. and G.K. Fleming, *Membrane-based gas separation.* Journal of Membrane Science, 1993. **83**(1): p. 1-80.

23. Barrer, R.M., *Diffusivities in glassy polymers for the dual mode sorption model.* J. Mem. Sci., 1984. **18**: p. 25-35.

24. Paul, D.R. and W.J. Koros, *Effect of partially immobilizing sorption on permeability and the diffusion time lag.* Journal of Polymer Science: Polymer Physics Edition, 1976. **14**(4): p. 675-685.

25. Kamaruddin, D.H. and W.J. Koros, *Some observations about the application of Fick's first law for membrane separation of multicomponent mixtures.* J. Mem. Sci., 1997. **135**(2): p. 147-159.

26. Das, M., *Membranes for Olefin/Paraffin Separation*, in *Chemical and Biomolecular Engineering*. 2009, Georgia Institute of Technology: Atlanta, GA.

27. Ismail, A.F. and W. Lorna, *Penetrant-induced plasticization phenomenon in glassy polymers for gas separation membrane.* Separation and Purification Technology, 2002. **27**(3): p. 173-194.
28. E.S, S., *Penetrant-induced plasticization and gas permeation in glassy polymers.* Journal of Membrane Science, 1988. **37**(1): p. 63-80.

29. Hillock, A.M.W., S.J. Miller, and W.J. Koros, *Crosslinked mixed matrix membranes for the purification of natural gas: Effects of sieve surface modification.* Journal of Membrane Science, 2008. **314**(1-2): p. 193-199.

30. Gonzo, E.E., M.L. Parentis, and J.C. Gottifredi, *Estimating models for predicting effective permeability of mixed matrix membranes.* Journal of Membrane Science, 2006. **277**(1-2): p. 46-54.

31. Vu, D.Q., W.J. Koros, and S.J. Miller, *Mixed matrix membranes using carbon molecular sieves: II. Modeling permeation behavior.* Journal of Membrane Science, 2003. **211**(2): p. 335-348.

32. Moore, T.T. and W.J. Koros, *Non-ideal effects in organic-inorganic materials for gas separation membranes.* Journal of Molecular Structure, 2005. **739**(1-3): p. 87-98.

33. Mahajan, R., et al., *Challenges in forming successful mixed matrix membranes with rigid polymeric materials.* Journal of Applied Polymer Science, 2002. **86**(4): p. 881-890.

34. Husain, S. and W.J. Koros, *Mixed matrix hollow fiber membranes made with modified HSSZ-13 zeolite in polyetherimide polymer matrix for gas separation.* Journal of Membrane Science, 2007. **288**(1-2): p. 195-207.

35. Mahajan, R. and W.J. Koros, *Mixed matrix membrane materials with glassy polymers. Part 1.* Polymer Engineering & Science, 2002. **42**(7): p. 1420-1431.

36. Mahajan, R. and W.J. Koros, *Mixed matrix membrane materials with glassy polymers. Part 2.* Polymer Engineering & Science, 2002. **42**(7): p. 1432-1441.

37. Shu, S. Husain, and W.J. Koros, *Formation of Nanostructured Zeolite Particle Surfaces via a Halide/Grignard Route.* Chemistry of Materials, 2007. **19**(16): p. 4000-4006.

38. Liu, J., et al., *Butane isomer transport properties of 6FDA-DAM and MFI-6FDA-DAM mixed matrix membranes.* J. Mem. Sci., 2009. **343**(1-2): p. 157-163.

CHAPTER 3
MATERIALS AND EXPERIMENTAL METHODS

3.1. ABSTRACT

This chapter will introduce the materials used in this work, and their properties. Characterization techniques for both polymer and molecular sieves will be introduced, along with the experimental procedure used for making permeation and sorption measurements both for single and mixed gas systems. This chapter will also cover the original procedure for surface modification of zeolite sieves along with the modified process used in this work.

3.2. MATERIALS

This section will give basic information about the materials used in this work and their sources. The reasons for polymer and molecular sieve selection will be addressed.

3.2.1. Polymer

The polyimide, 6FDA-DAM (repeat structure shown in figure 3.1) (T_g = 395°C, ρ = 1.35g/cm^3) was used as the polymer base for the membranes studied in this work. 6FDA-DAM is a fluorinated glassy polymer, with relatively high fractional free volume. The high fractional free volume allows for high productivity and its rigid backbone supports high selectivity. Unlike rubbery polymers that are known to favor permeation of the most condensable gas, and thus gas separation is solubility driven [1, 2], gas

separation in glassy polymers is diffusivity-based due to their rigid chains. This supports the selection of a glassy polymer for this work because butane isomers have similar condensability (T_c values are: n-C4 = 152°C, i-C4 = 134.9°C). Past studies compared the separation performance of fluorinated glassy polymers [3] and as shown in table 3.1, 6FDA-DAM has the best balance of permeability and selectivity.

Table 3.1: Separation performance of various polymers for butane isomers [3]

Polymer	n-C4 Permeability (Barrers)	Selectivity $\alpha_{n/i}$
6FDA-6FpDA	0.12	-
6FDA-DAM-DABA (3:2)	0.35	24 ± 2
6FDA-DAM	3.70	21 ± 1

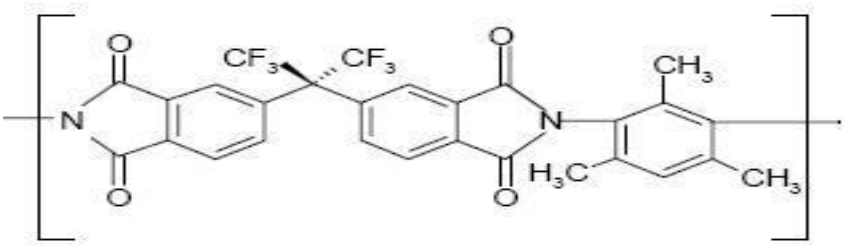

Figure 3.1: Repeat structure of 6FDA-DAM

The polymer is synthesized in-lab using a step growth polymerization method with details reported elsewhere [4]. The monomers 6FDA (2,2-bis(3,4-carboxyphenyl) hexafluoropropane dianhydride) and DAM (diaminomesitylene) were purchased from Sigma Aldrich and purified by sublimation before polymerization.

3.2.2. Molecular sieves

The inorganic molecular sieve used in this work is LTA 5A. With a pore size of ~4.3Å, it allows passage of n-C4 (3.95-4.0Å) and completely prevents entrance of i-C4 (6.0Å). Two sources of 5A were used in this work. The commercial source was purchased from Sigma Aldrich, and the Lab-made source was synthesized by Dr. Tae Hyun Bae from Jones/Nair research group at Georgia Tech. The commercial sieves have an average size of 1-2µm, various sizes of sieves were received from Dr. Bae ranging from 300nm to 1µm.

Zeolite LTA, $[Na_{12}(Al_{12}Si_{12}O_{48})27H_2O]$ has a three dimensional pore structure with pores running perpendicular to each other in the x, y, and z plane. The pore diameter is defined by an eight member oxygen ring, and has a Si/Al ratio of 1. LTA zeolite has 2 types of cages, β (sodalite cage), and α (supercage) which can host different cations [5]. Figure 3.2 shows the structural framework of LTA zeolite.

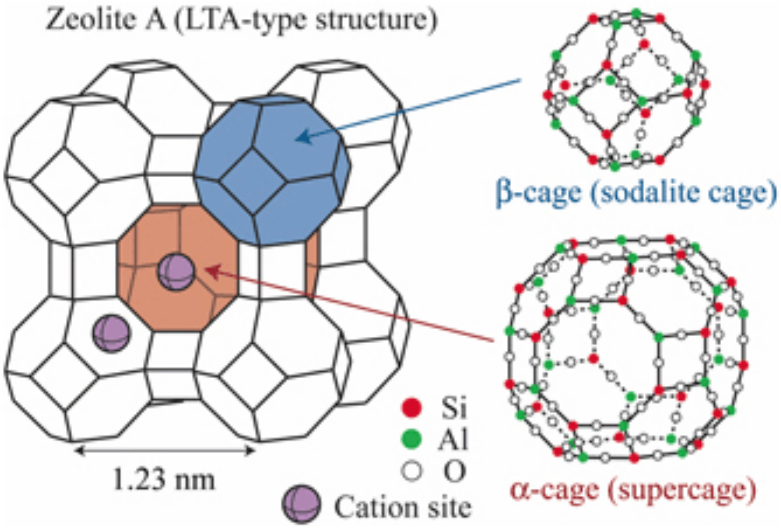

Figure 3.2: Structural framework of aluminosilica LTA zeolite [6]

The lab-made sieves received from Dr. Bae were LTA 4A (Na cations). These were ion-exchanged to 5A by stirring it in 1M $Ca(NO_3)_2.4H_2O$ solution for ~ 1hr. The solution is centrifuged out and replaced with a fresh solution. On the third time, temperature of the mixture is raised to 60°C. DI water rinse is used to wash off the loose Ca^{2+} deposits on the surface. Energy Dispersive X-Ray Spectroscopy (EDS) analysis is used to confirm the presence of Ca^{2+} ions and deficiency of Na^{+} ions.

3.2.3. Solvents and reagents

All solvents and reagents used in this project were purchased from Sigma Aldrich. Solvents and reagents used were anhydrous tetrahydrofuran, THF (purity: 99.9%, inhibitor-free), anhydrous 2-methyltetrahydrofuran, MeTHF (purity: 99%, inhibitor-free), anhydrous toluene (purity: 99.8%), anhydrous 2-propanol, IPA (purity: 99.5%), methyl magnesium bromide, CH_3MgBr (3.0M solution in diethyl ether).

3.2.4. Gases

The gases used in this project are nitrogen, N_2, oxygen, O_2, n-butane, n-C4, isobutane, i-C4, mixtures of n-butane and isobutane, propane, C_3H_8, propylene, C_3H_6, mixtures of propane and propylene, air, and helium, He. All the gases were research grade, and purchased from AirGas and Matheson Tri-gas.

3.3. CHARACTERIZATION METHODS

The various characterization methods used throughout this work will be highlighted in this section.

3.3.1. Scanning electron microscopy (SEM)

Scanning Electron Microscopy (SEM) was used to observe the surface morphology of molecular sieves prior to, and after surface treatment, and to observe the adhesion of sieves to polymer in mixed matrix membranes. The SEM instruments used were LEO 1530, and 1550, which are equipped with a thermally assisted field emission gun. The samples of molecular sieves for SEM were prepared in either of two ways. A small amount of sieves are dispersed in acetone, and deposited on a flat SEM mount. Upon evaporation of acetone, the sieves are left on the mount. The second approach was to stick a piece of double-sided carbon tape on a flat mount, and smear some sieves on the tape. The tape holds the sieves in place. Samples of films for SEM, are prepared by soaking a piece of film in hexane for ~2mins, freezing and breaking it in liquid nitrogen. On a 90°-stage SEM mount, the film is stuck to a piece of double-sided carbon tape, with the edge of the film that was broken in liquid nitrogen facing upwards. The soak in hexane and freezing in liquid nitrogen is essential to maintain the mechanical structure of the film during breaking to preserve the morphology after fracture. The film is gold sputter coated prior to insertion in the SEM chamber. Figure 3.3 are examples of SEM pictures of zeolite and mixed matrix membranes.

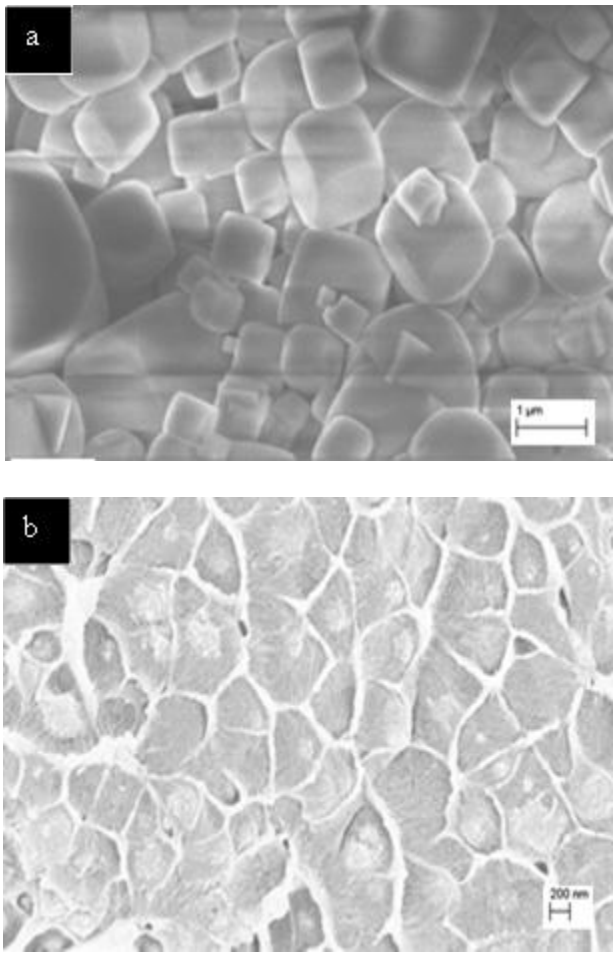

Figure 3.3: SEM pictures of: a. LTA zeolite, b. Mixed matrix membrane

3.3.2. Energy dispersive x-ray

Energy dispersive x-ray analysis, EDS, was used to identify the surface elemental composition of the molecular sieves. This analysis is done in conjunction with SEM. The electron beam in the SEM collides with the electrons in the sample, knocking some out of their orbit. They are replaced by x-ray emitting electron which are analyzed, and used to determine the elemental composition [7]. Figure 3.4 is an example of an EDS spectrum of LTA 5A zeolite.

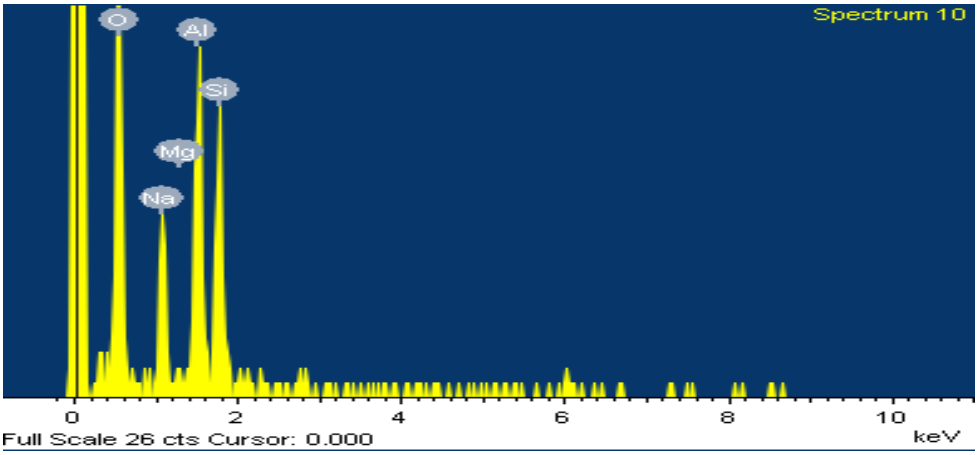

Figure 3.4: EDS spectrum of surface modified LTA 5A

3.3.3. Gas chromatograph (GC)

The Agilent 6890N GC, and GasPro GSC capillary column were used throughout this project. It operated with a thermal conductivity detector (TCD) and helium as the carrier gas. The GasPro column is an open column made of stainless steel, 30 m x 0.32mm, ID. The elution sequence of the butane isomers were identified by injecting the gases individual to the GC. The next step was to develop a method that would separate the elusion peaks for proper identification. The method used for butane isomers is: oven temperature of 75°C for 2mins with a temperature ramp of 20°C/min to 175°C, inlet temperature of 51°C, split ratio of 5:1, Helium flowrate of 1.3ml/min. Figure 3.5 is a GC spectrum of n-C4/i-C4 mixture. The peaks at elation times of 2.383, 6.154 and 6.403 are nitrogen from air due to leaks, i-C4, and n-C4 respectively.

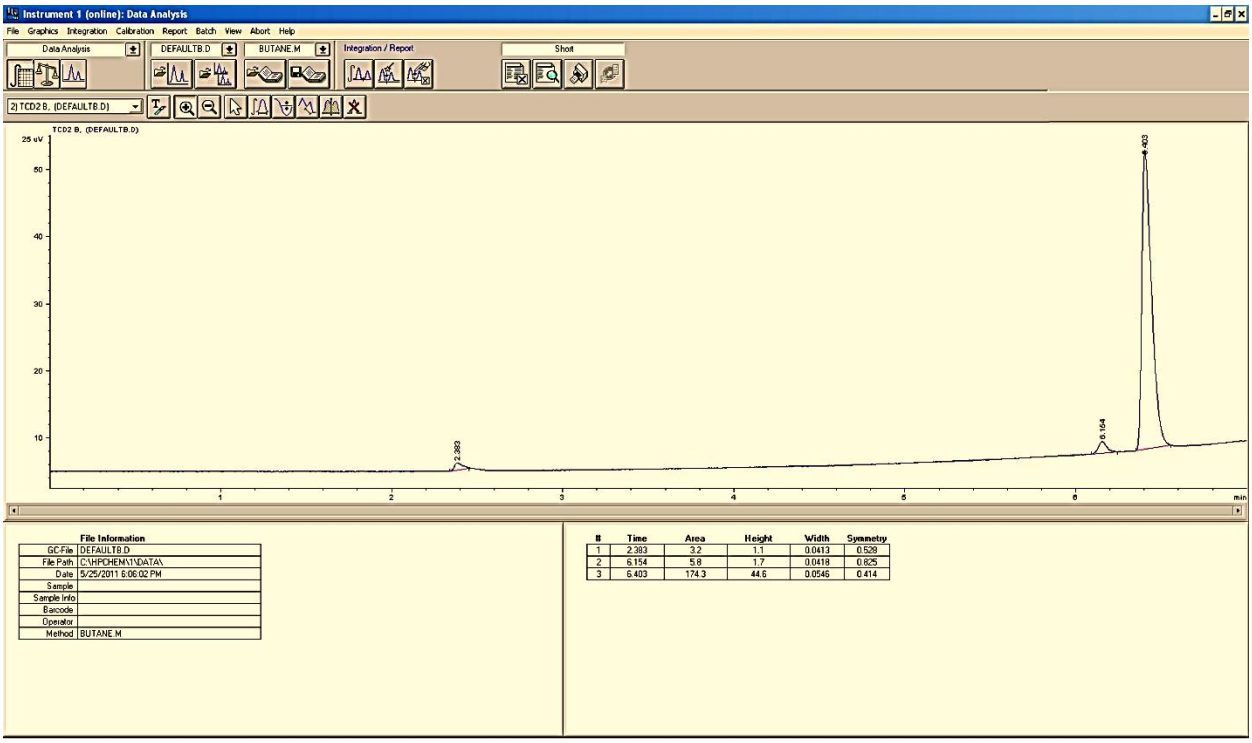

Figure 3.5: GC spectrum

With the method set, the GC was calibrated using three known mixture compositions: %nC4/%iC4 – 5.01/94.99, 29, 98/70.02, and 94.99/5.01. The calibration plots are provided in figures 3.6 and 3.7.

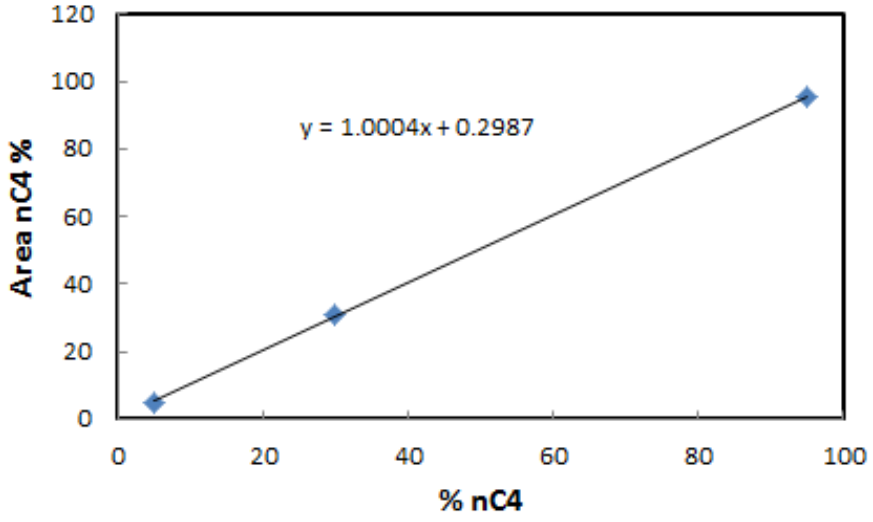

Figure 3.6: Correlation of GC Area% with %nC4

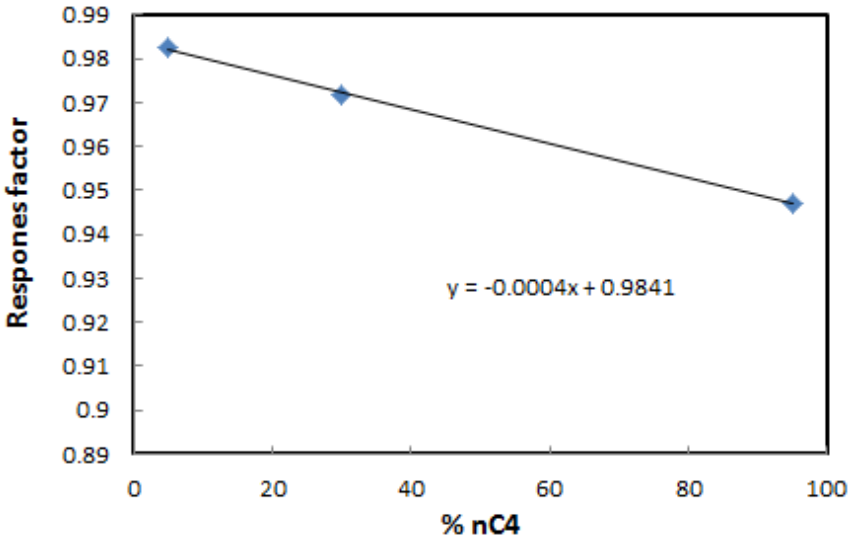

Figure 3.7: Correlation of response factor with %nC4

Response factor, β, is defined as:

$$\beta = \frac{x_{nC4}}{x_{iC4}} \frac{A_{iC4}}{A_{nC4}} \tag{3.1}$$

The mole fractions are determined viz.,

$$y_{iC4} = \frac{1}{\left(1 + \beta \left(\frac{A_{nC4}}{A_{iC4}}\right)\right)} \tag{3.2}$$

$$y_{nC4} = 1 - y_{iC4} \tag{3.3}$$

3.4. PERMEATION MEASUREMENT

This section will address the process of making both single and mixed gas measurements in dense polymeric films. The preparation of dense films both neat polymer and mixed matrix membranes will be covered. This section will also outline masking of the film and then permeation procedure.

3.4.1. Dense film preparation

Polymer is placed in a 10ml glass vial, covered with aluminum foil with holes punched in to allow escape of moisture when dried in vacuum oven at 180°C overnight. The polymer is weighed, and THF is added to make the desired weight percent of polymer. The dope is placed on a roller overnight to make a homogenous dope.

For mixed matrix membranes, sieves are dried in a glass vial at 100°C overnight. THF is added to the sieves and the vial is placed in a sonication bath to disperse the sieves. The sieves are primed by adding 10% of the required polymer from the prior prepared polymer dope. The remaining polymer is added from prior prepared polymer dope, and left on the roller overnight.

In a glove bag saturated with THF for 4hrs, the dope was poured onto a silane coated glass plate and draw cast using a draw knife of appropriate clearance to produce the desired film thickness. The film was left in the glove bag overnight for solvent evaporation. Dense film casting set-up is shown in figure 3.8. Initial saturation of the glove bag with the solvent THF helps to reduce the rate of evaporation, which minimizes the stress on the film. Prior to making measurements the film is annealed in a vacuum oven at the desired annealing temperature for a set period. The importance of annealing will be discussed in detail in chapter 5.

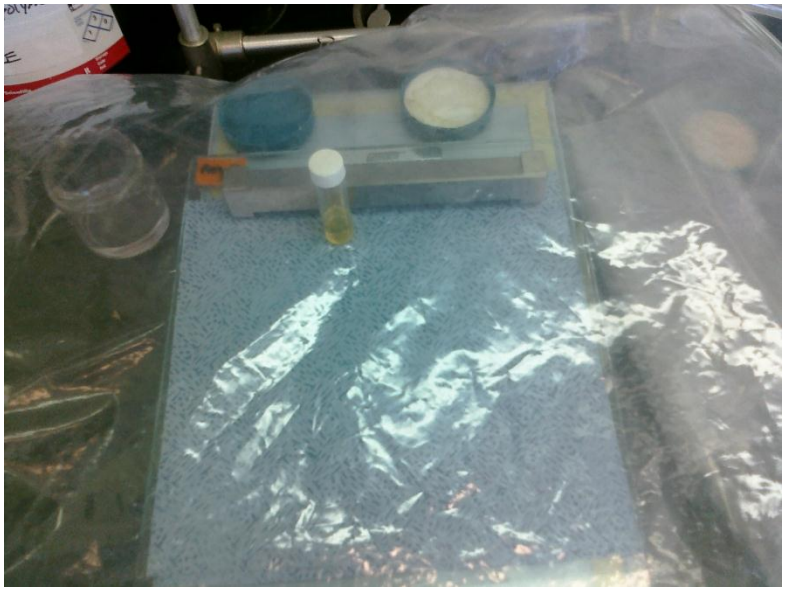

Figure 3.8: Dense film casting set-up

3.4.2. Single gas permeation measurement

Permeation measurements are performed in a temperature controlled permeation box. The film is masked onto a dense film permeation cell, which is mounted in a permeation box. Masking of dense film is done by placing a piece of film between two circular aluminum tapes with concentric circle cut in the tape (see figure 3.9). Using a larger circular aluminum tape, the sandwiched film is taped to the permeation cell.

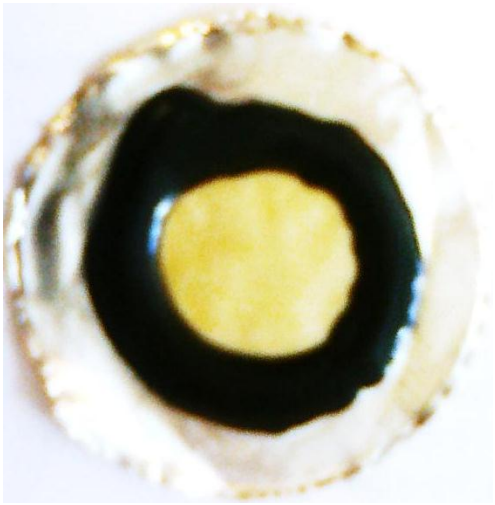

Figure 3.9: Sample of masked dense film

The bottom half of the permeation cell has a fritted disk to support the film. Two paper filters are placed on the stage before the sandwiched film is taped on. This is to provide more support and also protect the film. High temperature epoxy was used to seal the interface between the film and aluminum tape to prevent leak. The permeation cell is mounted into the permeation box (see Figure 3.10), via VCR fittings.

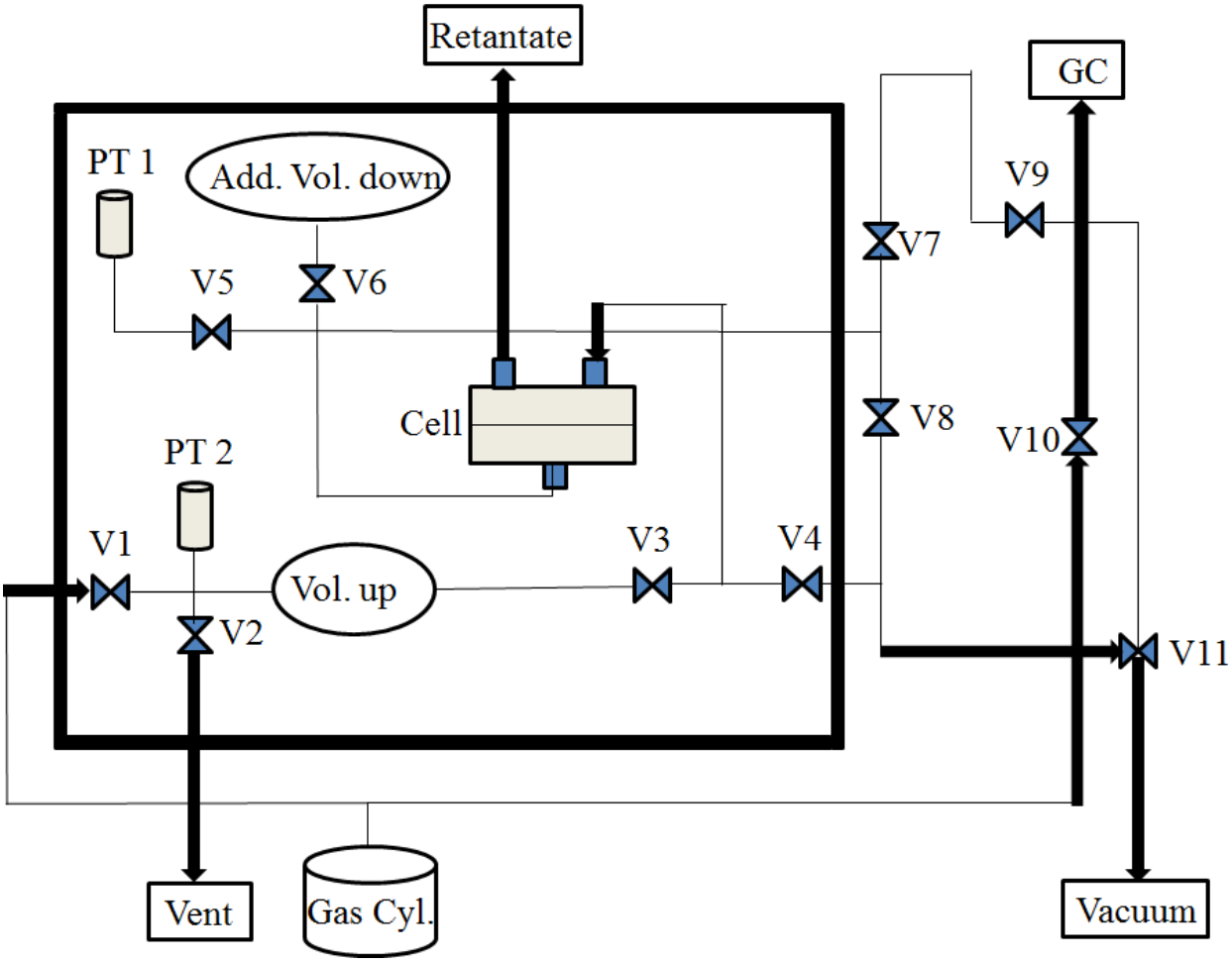

Figure 3.10: Schematic of Dense Film Permeation System

For single gas measurements, the gas is introduced via valve V1 into the upstream cylinder. Valves V4, V8 and V11 are open to keep the film under vacuum. When the system temperature is stable, valve V4 and valve V8 are closed, and valve V3 is open to introduce the gas to the upstream of the film. The upstream pressure transducer, PT2 displays the upstream pressure and the downstream pressure transducer PT1, is linked to a data acquisition system, LabView, and the permeate pressure buildup is recorded over time. This permeation measurement method is referred to as the time-lag method. Time-

lag is related to the time it takes for the gas to achieve a constant permeate rate through the film. Permeation is allowed to continue until ~6 times time-lag has been reached to ensure steady state has been attained. Valve V8 is opened to pump down the permeate pressure and closed to allow it to build up again, and repeated once more, to get a good average of the permeation rate. The permeation rate is related to the steady state slope in a plot of permeate pressure versus time. Equation 3.4 is used to determine the permeability.

$$P = \frac{22400 \frac{\Delta p_{downstream}}{\Delta t} Vl}{p_{upstream} RT * A} * 10^{10} [=] Barrer \quad (3.4)$$

Where V is the downstream volume, A is the membrane area, R is the gas constant, and T is the system temperature. Using the time-lag θ, the apparent diffusion coefficient can be deduced via equation 3.5.

$$\theta = \frac{l^2}{6D} \quad (3.5)$$

where l is the thickness of the film and D is the apparent diffusion coefficient.

3.4.3. Mixed gas permeation measurement

Mixed gas permeation measurements are made in a similar manner as single gas permeation measurements. Research grade gas mixtures of known composition are purchased from AirGas and Matheson Tri-gas. The major difference in the experimental setup is the addition of a retentate flow on the upstream, and a GC connection to the

downstream. The retentate flow is set to <1% stage cut to prevent concentration polarization [8]. The flowrate of the retentate is checked using a 1ml bubble flowmeter.

$$stage\ cut = \frac{permeate\ molar\ flow\ rate\ of\ faster\ gas}{feed\ molar\ flow\ rate} \tag{3.6}$$

The GC is calibrated to allow composition analysis within 2% error. Details of GC calibration have been previously addressed. After steady state is reached, valves V7 and V9 are opened to send the permeate gas to the GC. The vacuum pump is used to adjust the injection pressure. After GC analysis, the downstream is vacuumed and allowed to build up again. Consistency within ± 2% indicates that the system is at steady state and the permeate composition is accurate.

3.5. SORPTION MEASUREMENTS

This section will address the procedure involved for single and mixed gas sorption. The data analysis process is also presented.

3.5.1. Single gas sorption measurement

Sorption measurements of both polymeric films and molecular sieves were performed via pressure decay method using the sorption equipment in figure 3.11. The pressure decay method has been described by Koros and Paul [9].

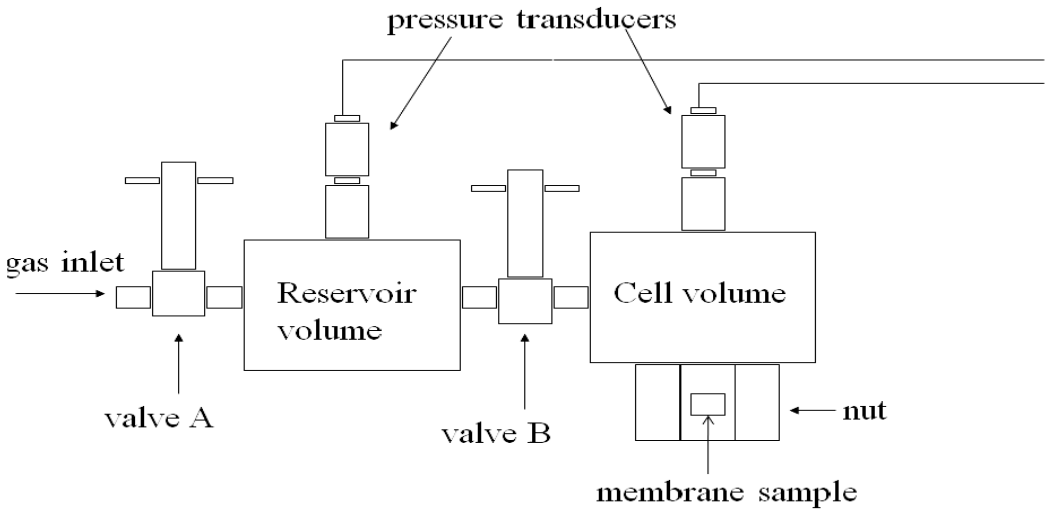

Figure 3.11: Schematic of Pressure-Decay Sorption Equipment

For sorption measurements of polymeric films, the film is first annealed at the desired annealing condition, and weighed.

For sorption measurements of molecular sieves, the sieves are loaded into a stainless steel filter, wrapped with aluminum foil, and held in place with a piece of copper wire. The ensemble is dried overnight at 180°C under vacuum to remove all the moisture in the sieves. The weight of the filter, foil, wire and the total ensemble is recorded to determine the weight of the sieve sample. It is assumed that the filter, foil and wire do not sorb any gas, so all the measured sorption is by the sieves.

The procedure for making sorption measurements via pressure decay method is as follows:

1. The cell volume is cleaned with acetone, to ensure there is nothing present that could sorb gas or occupy volume. Accurate volume measurement is essential for data analysis.

2. The sample is placed in the cell volume, and the volume is capped with a Swagelok nut and nickel gasket to ensure an air tight seal. The system is placed in an oil bath, which is set at the desired temperature.
3. The entire system is kept overnight under vacuum by keeping valves A and B open and connected to a vacuum pump.
4. To begin the measurements, valve B is closed to isolate the cell volume, and gas is introduced into the reservoir volume via valve A.
5. Using the attached pressure transducers, and the data acquisition system LabView, pressure readings of the cell and reservoir are being recorded.
6. After a period of about 45mins, to allow for the pressure in the reservoir to be stable, gas is introduced into the cell volume by opening valve B for 3 seconds. The system is then allowed to attain an equilibrium state. Plot of the pressure in the cell over time, is used to determine if equilibrium has been reached.
7. Additional gas is introduced to the reservoir volume and step 6 is repeated.
8. Steps 6 and 7 are repeated until the desired maximum pressure is attained and enough points have been collected for an accurate curve fit.

Mole balance over the system, after step 6, is used to determine the moles of penetrant sorbed into the sample. The mole balance calculation is described in equations 3.7 to 3.11.

$$n_{R,i} + n_{c,i} = n_{R,f} + n_{c,f} \tag{3.7}$$

$$n = \frac{PV}{ZRT} \tag{3.8}$$

$$moles\ sorbed = moles\ lost\ in\ reservoir - moles\ gained\ in\ cell \tag{3.9}$$

$$n_{sorbed} = \left(\frac{P_{R,i}V_R}{Z_{R,i}RT} - \frac{P_{R,f}V_R}{Z_{R,f}RT}\right) - \left(\frac{P_{C,f}V_C}{Z_{C,f}RT} - \frac{P_{C,i}V_C}{Z_{C,i}RT}\right) \tag{3.10}$$

$$C_{sorbed} = \frac{n_{sorbed}}{V_{sample}} \tag{3.11}$$

where, c is cell, r is reservoir, *i* is initial, *f* is final, P is pressure, V is volume, T is temperature, R is the ideal gas constant and Z is the non-ideality factor.

These calculations are used to determine the sorption capacity isotherm.

3.5.2. Mixed gas sorption

Mixed gas sorption measurements were made on polymeric films. The procedure for mixed gas sorption is similar to that for single gas. A schematic of the system is in figure 3.12. Prior to commencing measurements the composition of the gas is analyzed to ensure an accurate account of the initial reservoir composition. After equilibrium is reached in the cell, valve C, is slightly opened and closed quickly. Valve D, is opened to send the gas to the GC, and then closed. The pressure on the line to the GC is adjusted to the desired injection pressure using a vacuum pump. Valve D, is opened and closed again to send gas to the GC for a repeat analysis. The GC analysis is used to determine the final composition of the cell. A mole balance is performed across the system, and similar calculations as in single gas sorption are performed, while accounting of the gas composition in the reservoir cell. The system is allowed to reach equilibrium again, and GC analysis of the gas composition in the cell is repeated to ensure accuracy. Although the composition of gas in the reservoir is expected to remain unchanged, it is confirmed

via GC analysis. Unlike in single gas test, following each measurement, the sample is removed, and a fresh sample is used for the next measurement. This is to prevent errors that may result from back flow of gas from the cell to the reservoir and it also ensures that the sample is completely evacuated when planning to test a different composition.

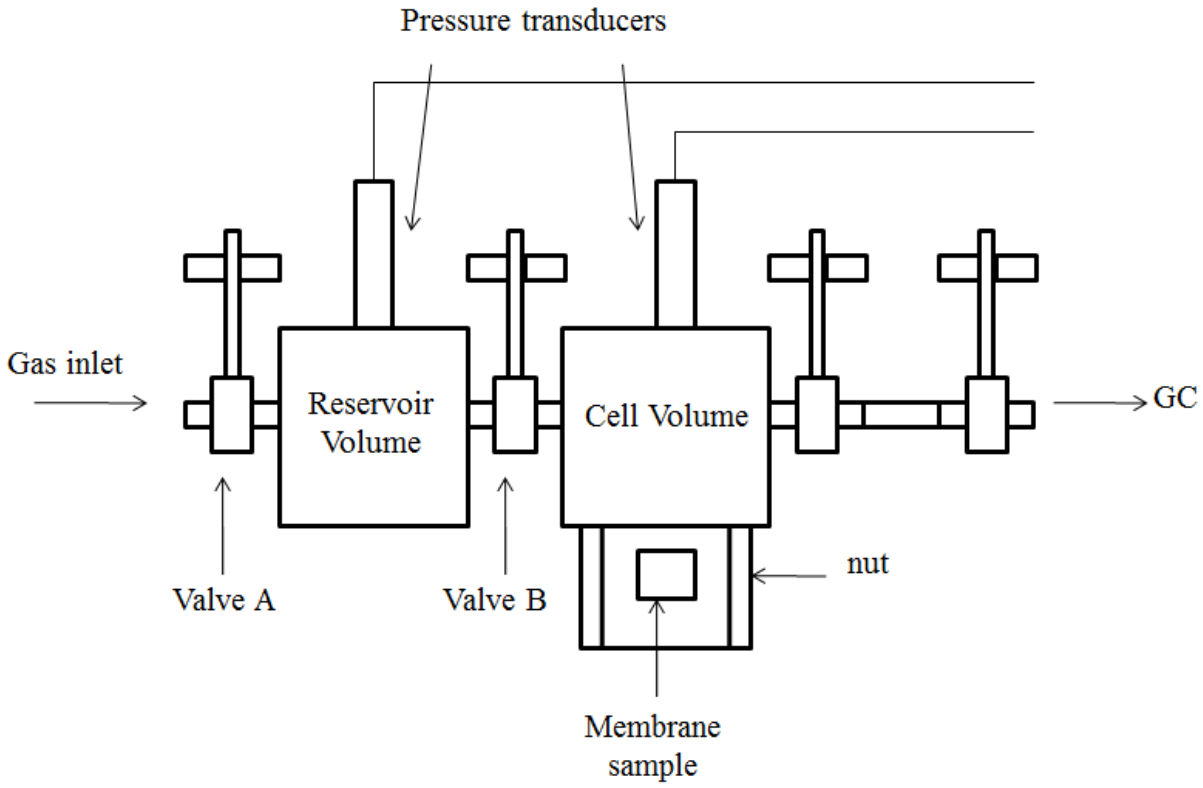

Figure 3.12: Schematic of Mixed Gas Pressure-Decay Sorption Equipment

3.6. SIEVE SURFACE MODIFICATION

Surface modification of LTA zeolite is done via Grignard treatment process. This treatment process was originated by Husain and Shu [10]. The treatment process is aimed

at growing magnesium hydroxide, $Mg(OH)_2$ nanowhiskers on the surface of the sieves to aid adhesion with polymers in mixed matrix membranes. Grignard treatment will be discussed in more detail in chapter 4. In this section, the original procedure and the simplified Grignard treatment process will be addressed.

The original Grignard treatment process as developed by Husain and Shu [10] comprised the following steps:

- Placed 4g of zeolite particles in a three-neck round bottom flask and dried at 150°C overnight along with a magnetic stir bar, an addition funnel, a fitted glass adapter and a vacuum adapter.
- Using a rubber septum, sealed the glassware to prevent moisture. Maintained a low nitrogen sweep through the flask and flame-dried the glassware with a propane torch.
- 80ml of anhydrous toluene and 20ml of thionyl chloride were added to the flask via a dry transfer line.
- The dispersion was sonicated using a sonication bath overnight (~12 hrs) and then, the toluene and remaining thionyl chloride was evaporated using an oil bath at about 90 - 110°C while maintaining a constant nitrogen sweep. The glassware containing the sieves was dried further under vacuum at 80°C.
- 80ml of anhydrous toluene and 15ml of methyl magnesium bromide (3.0M solution in diethyl ether) was added to the flask. The dispersion was sonicated in the sonication bath overnight (~12hrs).
- The flask was transferred to the stirrer, and reacted with 2-propanol (80ml) for about 3hrs.

- The particles were collected in 4 centrifuge vials, and rinsed with 2-propanol three times followed by de-ionized water several times until the conductivity was below 40µs.

Several modifications have been made to the Grignard treatment process to better control the reaction. This includes Grignard treatment via Sol-Gel chemistry. The Sol-Gel Grignard treatment process involves a study of the effect of pH using HCl soln, controlling the amount of water added to the reaction, and $AlCl_X$ deposition on the zeolite surface. Some additional details of Grignard treatment via Sol-Gel will be provided in chapter 4. The modified procedure used in this work is termed the "*Simplified* Grignard Treatment".

The *simplified* Grignard treatment procedure comprises of the following step:

- In a round bottom flask, 4g of zeolite along with a stir bar was dried under vacuum at 150°C overnight (~12hrs)
- 40ml of the solvent was added to the flask, which was stirred for ~10mins, then transferred to a sonication bath for about 1hr to ensure complete dispersion of the sieves in the solvent
- The flask was transferred to the stirrer, and 10ml of methyl magnesium bromide was added, and the dispersion was stirred for ~10mins. The flask was transferred back to the sonication bath and sonicated overnight
- The dispersion was collected in 3 centrifuge vials, and centrifuged to get rid of the unreacted methyl magnesium bromide. The sieves were rinsed with the solvent 3 times.

- The sieves were transferred to the flask, and anhydrous 2-propanol was added. The dispersion was stirred for 3hrs.
- The sieves were collected in centrifuge bottles and centrifuged. The sieves were rinsed 3 times with 2-propanol, followed by de-ionized water until the conductivity was <40µs.

3.7. REFERENCES

1. Merkel, T.C., et al., *Gas sorption, diffusion, and permeation in poly(dimethylsiloxane).* Journal of Polymer Science Part B: Polymer Physics, 2000. **38**(3): p. 415-434.

2. Ghosal, K. and B.D. Freeman, *Gas separation using polymer membranes: an overview.* Polymers for Advanced Technologies, 1994. **5**(11): p. 673-697.

3. Liu, J., et al., *Butane isomer transport properties of 6FDA-DAM and MFI-6FDA-DAM mixed matrix membranes.* J. Mem. Sci., 2009. **343**(1-2): p. 157-163.

4. Vora, R.H. 1989: U.S. Patent.

5. Ríos, C.A., C.D. Williams, and M.A. Fullen, *Nucleation and growth history of zeolite LTA synthesized from kaolinite by two different methods.* Applied Clay Science, 2009. **42**(3-4): p. 446-454.

6. http://cnsi.ctrl.ucla.edu/nanoscience/pages/waterFilt.

7. http://www.mee-inc.com/eds.html.

8. Madden, W.C., *The performance of hollow fiber gas separation membranes in the presence of an aggressive feed stream*, in *Chemical and Biomolecular Engineering*. 2005, Georgia Institute of Technology: Atlanta.

9. Koros, W.J. and D.R. Paul, *Design considerations for measurement of gas sorption in polymers by pressure decay.* J. Poly. Sci.: Poly. Phys. Ed., 1976. **14**(10): p. 1903-1907.

10. Shu, S. Husain, and W.J. Koros, *Formation of Nanostructured Zeolite Particle Surfaces via a Halide/Grignard Route.* Chemistry of Materials, 2007. **19**(16): p. 4000-4006.

CHAPTER 4

SURFACE MODIFICATION OF LTA 5A ZEOLITE PARTICLE VIA GRIGNARD TREATMENT

4.1. ABSTRACT

This chapter will address the challenges and successes of Grignard treatment used to modify the surface of zeolites. Surface modification has been shown to promote adhesion of zeolite to polymer for good mixed matrix membrane fabrication. The original Grignard treatment process as developed by Shu and Husain, led to the formation of $Mg(OH)_2$ nanowhiskers on the surface of zeolite particles; however, the important factors involved in the reaction were not fully known, and the process led to inconsistent results. Several modifications have been made to the Grignard treatment process to achieve better control of the reaction. These modifications include Grignard treatment via sol-gel chemistry, which involved studying the effect of the amount of water added, and the pH of the solution. This chapter will summarize some of the work done with sol-gel chemistry, which was joint work with Dr. Junqiang Liu. Though the sol-gel chemistry based Grignard treatment showed promise, the ideal treatment conditions for lab-made sieves were hard to achieve, which led to further exploration of the reaction chemistry. The choice of solvent was proven to be a significant factor and hypothesized to promote bond formation of the Si-OH on zeolite surface with the Grignard reagent CH_3MgBr. This led to successful treatment of commercial 5A but without success for nominally identical lab-made sieves. Grignard treatment via sol-gel also has the challenge of being time-consuming and requiring excessive control; so a "*simplified*" Grignard treatment

process was developed. This process resulted in well treated commercial 5A, but still did not solve the problem with treating lab-made sieves. Several characterization techniques were used to probe the difference between commercial and lab-made sieves; which may help explain their different response to surface treatment reactions.

4.2. ORIGINAL GRIGNARD TREATMENT

As discussed earlier, a common nonideal morphology of good mixed matrix membranes is so called “sieve-in-cage”, which results from lack of adhesion of the sieves to polymer. To improve adhesion, researchers have identified several methods including, increasing polymer flexibility to reduce stress on the film during solvent evaporation, and silane coupling [1-3]. Though these methods showed some improvement in adhesion, they are not suitable for most sieve-polymer pairs. The original sieve surface modification process via Grignard treatment was developed by Shu and Husian [4]. It is a two-stage process that results in the growth of magnesium hydroxide nanowhiskers on the surface of the sieves. The first stage involves dealumination of the Linde Type A (LTA) zeolite via a thionyl chloride, $SOCl_2$ reaction. The reaction results in the deposition of chlorine-containing species (NaCl and $AlCl_3$ for 4A) on the surface the sieves; which are hypothesized to act as nucleating sites for magnesium hydroxide growth. The second stage involves reacting the Grignard reagent, methyl magnesium bromide (CH_3MgBr) with 2-propanol (IPA) in the presence of the dealuminated LTA.

The hypothesized mechanism for the second stage is [5]:

$$CH_3MgBr + (CH_3)_2CHOH \rightarrow CH_4 + (CH_3)_2CHOMgBr \quad (4.1)$$

This reaction results in white precipitates. Shu [5] identified the precipitate via XPS and XRD to comprise of $MgBr_2$, and $Mg(OH)_2$. After the reaction with 2-propanol, the sieves are collected via centrifuge and washed with DI water. $MgBr_2$ which is highly soluble in water is removed and $Mg(OH)_2$ is left on the sieve surface and grows into a whisker morphology due to the presence of the nucleating sites. Shu [5] investigated the importance of nucleating site on the morphology of $Mg(OH)_2$ and concluded that in the absence of nucleating sites (NaCl and $AlCl_3$), platelet crystals of $Mg(OH)_2$ are deposited on the surface rather than grown into whiskers.

Though some success has been achieved using this process, the results were not always reproducible. Some important factors which were unknown and overlooked have been explored, resulting in a modified Grignard treatment process via sol-gel chemistry.

4.3. GRIGNARD TREATMENT VIA SOL-GEL

This treatment method was developed by Dr. Liu [6]. This method involves converting the Grignard reagent to a magnesium alkoxide, while controlling the hydrolysis and condensation of the magnesium sol as in equations 4.2 – 4.5 [6].

$$Mg(OCH(CH_3)_2)_2 + H_2O \rightleftarrows HOMgOCH(CH_3)_2 + (CH_3)_2CHOH \quad (4.2)$$

$$HOMgOCH(CH_3)_2 + H_2O \rightleftarrows HOMgOH + (CH_3)_2CHOH \quad (4.3)$$

$$-MgOCH(CH_3)_2 + -MgOH \rightleftarrows -MgOMg - + (CH_3)_2CHOH \quad (4.4)$$

$$-MgOH + -MgOH \rightleftarrows -MgOMg - + H_2O \quad (4.5)$$

Two important factors identified to affect the sol-gel product are the amount of water added, and the pH. It was shown that optimum surface modification of commercial sieves (Figure 4.1) was attained after dropwise addition of 1M HCl soln up to 6 times the stoichiometric amount of water required (6S). This amount is determined as shown below:

$$2CH_3MgBr + 2H_2O \rightarrow 2CH_4 + MgBr_2 + Mg(OH)_2 \quad (4.6)$$

$$CH_3MgBr : H_2O$$
$$1mol : 1mol$$

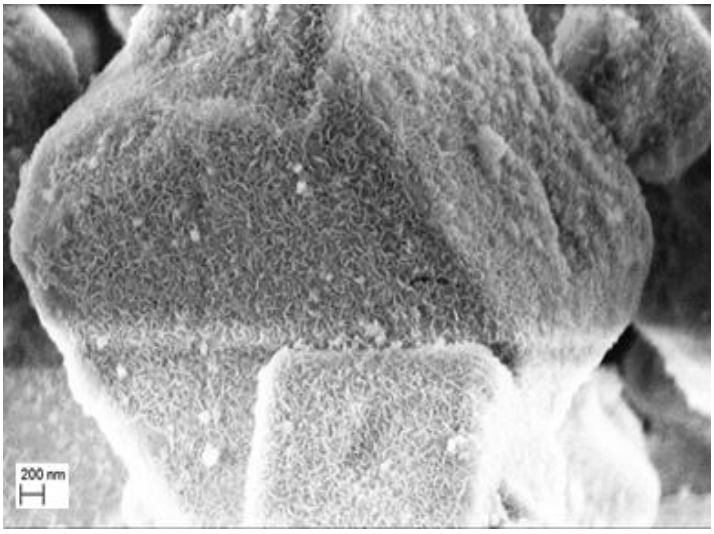

Figure 4.1: Grignard treated commercial 5A via sol-gel method using 6S, 1M HCl soln

The addition of HCl was hypothesized to introduce nucleating sites similar to those formed via dealumination in the original procedure. Dealumination was found to partially clog the pores of the zeolite rendering them ineffective in mixed matrix

membranes. The use of HCl eliminated the need for dealumination via thionyl chloride reaction.

The treatment of lab-made sieves via this method was not successful as it proved difficult to determine the optimum pH and water amount required. Liu [6], investigated the effect of anchoring $AlCl_3$ to the surface of lab-made sieves, to provide the nucleating sites similar to the $AlCl_3$ formed after dealumination. Successful surface modification was achieved using $AlCl_3$ anchored sieves via dropwise addition of DI water up to 6S (shown in figure 4.2a); however, it was observed that a layer of $Al(OH)_3$ gel was formed between the sieves surface and the whiskers; which led to detachment of the whiskers as shown in figure 4.2b. $Al(OH)_3$ is very porous, and acts as a path of less diffusion resistance when these sieves are incorporated in a mixed matrix membrane, thus resulting in poor separation performance. Further investigation of the reaction chemistry was required to successfully treat lab-made sieves.

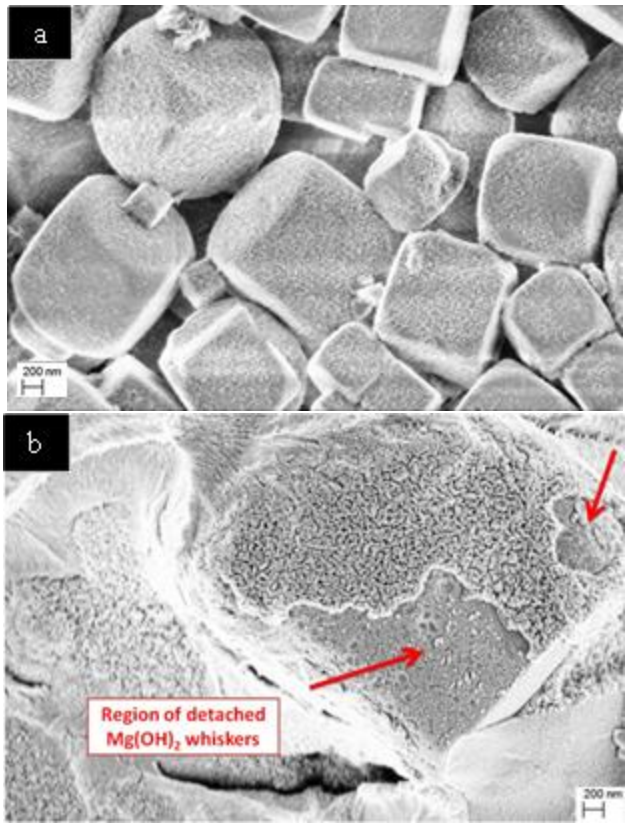

Figure 4.2: a) Grignard treated Lab-made sieves via $AlCl_3$ anchoring, b) Detachment of the whiskers due to presence of $Al(OH)_3$ between sieves surface and whiskers [6]

4.4. SOLVENT EFFECT ON CHARGE FORMATION

The formation of surface charges on particles suspended in aqueous media can be attributed to adsorption or desorption of ions and/or to dissociation of surface groups [7]. Four mechanisms are known to result in the formation of charges in colloidal systems: 1) Dissociation of surface groups, 2) Dissolution of an ion from the crystal surface, 3) Adsorption of a charged ion, and 4) Complex surface equilibria, in which case the net surface charge is determined by the equilibrium constants involved. The surface charging mechanism of particles in non-aqueous liquids is not clearly understood [8, 9]. Generally

in organic liquids two main mechanisms for surface charge formation have been proposed: the relative acid-base character of the solid surface and of the liquid determine the sign of the charge in protic liquids, while the charging in aprotic liquids is explained according to an electron transfer mechanism [9]. In protic liquids with a finite dissociation constant, the charging mechanism is similar to that of water as it involves proton transfer [8]. In aprotic liquids, the direction of electron transfer is determined by the energy levels of both the solids and liquid and can be shown as below [8]:

Strong donor liquid

$$\underset{donor\ molecule}{D:} + \underset{surface\ bond}{X-Y} \rightarrow \underset{donor-acceptor\ complex}{D\cdots X^{\delta+}\cdots Y^{\delta-}}$$

If D: is a strong enough donor, heterolysis of the donor-acceptor complex takes place

$$D\cdots X^{\delta+}\cdots Y^{\delta-} \rightarrow \underset{counterion}{D-X^{+}} + \underset{surface\ charge}{Y^{-}}$$

Proton bearing surfaces

$$D: + HP \rightarrow D\cdots H^{+}\cdots P^{-} \rightarrow \underset{counterion}{DH^{+}} + \underset{surface\ charge}{P^{-}}$$

Strong acceptor liquid

$$\underset{acceptor\ liquid}{A} + \underset{surface\ bond}{X-Y} \rightarrow X^{\delta+}\cdots Y^{\delta-}\cdots A \rightarrow \underset{surface\ charge}{X^{+}} + \underset{counterion}{\underset{complex}{Y-A^{-}}}$$

4.5. SOLVENT EFFECT ON GRIGNARD TREATMENT

Based on the information available on the proposed mechanism of surface charge formation on particles in organic solvents, it was important to study how the choice of solvent for sieve surface modification via Sol-Gel Grignard treatment would affect the outcome. It is hypothesized here that by using a solvent that promotes negative charge formation on the sieve surface, we can promote bond formation with +MgBr. This would lead to the formation of Si-O-MgOH via the reactions below (equations 4.7 – 4.9), which will serve as nucleating sites for the growth of $Mg(OH)_2$ whiskers.

$$Si-OH \;+\; CH_3MgBr \;\rightarrow\; Si-O-MgBr \;+\; CH_4 \tag{4.7}$$

$$2Si-O-MgBr \;+ (CH_3)_2CHO \rightarrow Si-O-MgOCH(CH_3)_2 \;+\; MgBr_2 + Si-OH \tag{4.8}$$

$$Si-O-MgOCH(CH_3)_2 \;+\; H_2O \rightarrow Si-O-MgOH \;+\; (CH_3)_2CHOH \tag{4.9}$$

The ideal solvent would have to both promote negative charge formation, and be inert to the Grignard reagent. As shown above negative surface charges in an organic solvent can be formed either by using a strong donor liquid, or via proton transfer. Since the surface of LTA zeolites comprise of silanol, Si-OH groups, dissociation of the hydroxyl group and proton transfer of the H+ in the presence of a donor liquid appears to be the most suitable mechanism.

$$\underset{zeolite\ surface}{Si-OH} \;+\; \underset{solvent}{D:} \;\rightarrow\; \underset{counterion}{DH^+} \;+\; \underset{charged\ surface}{Si-O^-}$$

Several solvents were investigated to prove this hypothesis and will be discussed in the subsequent sub-sections.

4.5.1. Sol-gel based Grignard treatment using toluene as solvent

Toluene was used as the solvent in the original Grignard treatment process; however, based on the hypothesis discussed earlier with regards to solvent effect on surface charge formation, it was important to reexamine the properties of toluene and compare them to the solvent properties proposed to be suitable for the treatment. Although toluene is inert to Grignard reagent, it lacks lone pair electrons so may not promote negative charge formation on the zeolite surface. This solvent can act as a control system in the investigation of this hypothesis.

This treatment performed by Dr. Liu resulted in bare sieves with 2S DI water, short and scanty $Mg(OH)_2$ crystals with 4S & 6S and $Mg(OH)_2$ flakes with 8S as shown in figure 4.3. With 2S DI water, the hydrolysis of magnesium isopropoxide to $Mg(OH)_2$ is not sufficient so most of the water soluble alkoxide is washed away during the water washing step, leaving the sieves bare. The presence of short scanty $Mg(OH)_2$ crystals with the addition of more water suggests that further hydrolysis and condensation occurred. With the addition of even more water the hydrolysis reaction went even further producing more $Mg(OH)_2$; however, in a toluene environment, it is possible that the sieves do not form the necessary surface charges required for production of nucleating sites. Thus the $Mg(OH)_2$ morphology is as flakes rather than whiskers.

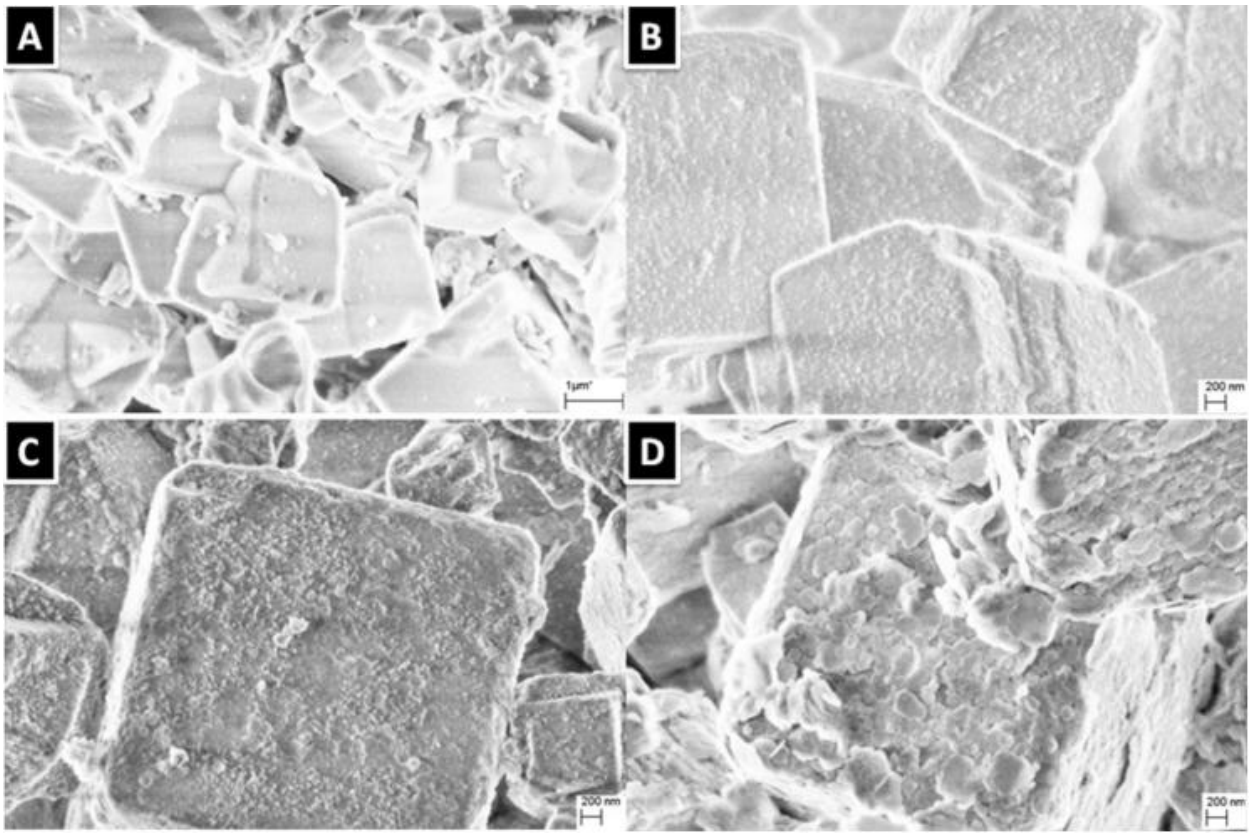

Figure 4.3: Grignard treated commercial LTA sieves with Toluene as solvent (A) 2S, (B) 4S, (C) 6S and (D) 8S of DI water [6]

Lab-made 5A sieves were also treated in a similar way. SEM in figure 4.4 shows that with the addition of 3S DI water, the sieves are practically bare. Addition of up to 5S resulted in flakes. This indicates that toluene may not be the most ideal solvent giving some credence to the hypothesis of surface charge formation.

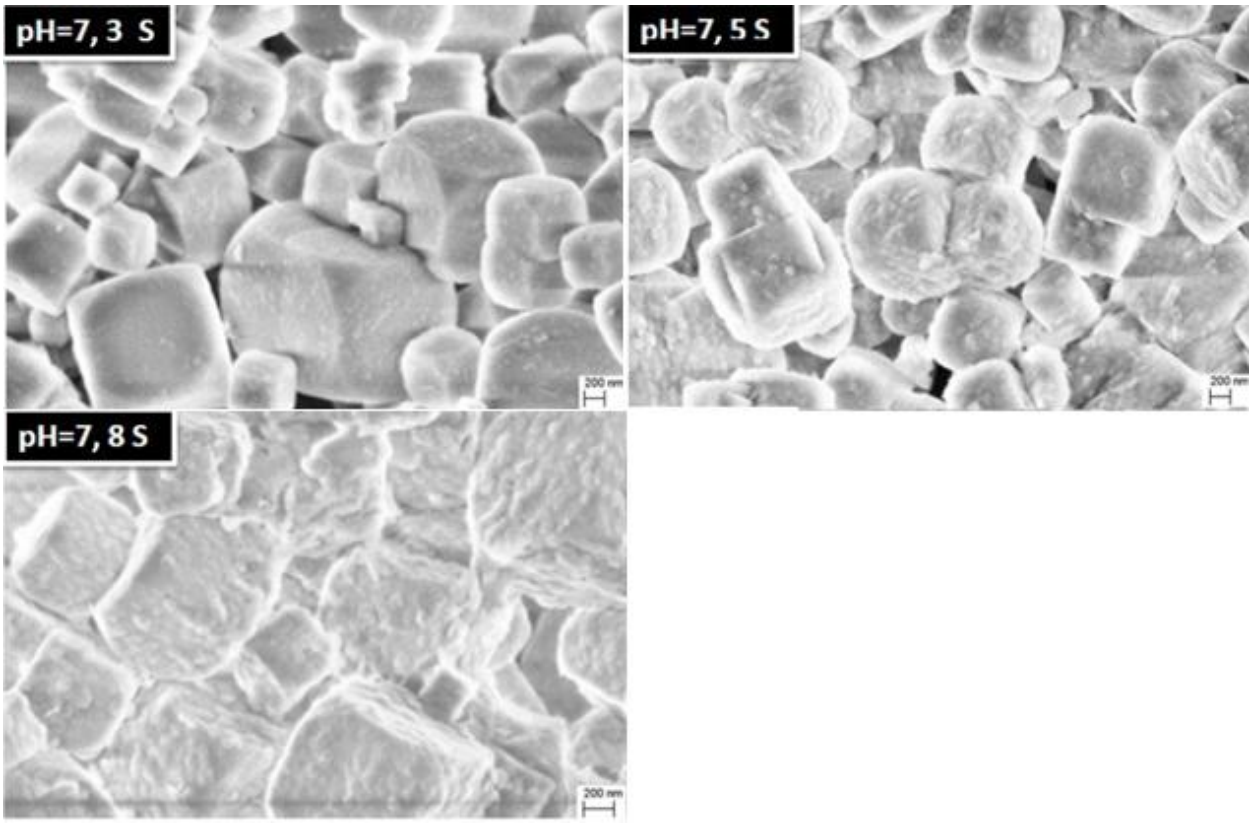

Figure 4.4: Grignard treated lab-made LTA sieves via Sol-gel with Toluene as solvent

4.5.2. Sol-gel based Grignard treatment using tetrahydrofuran as solvent

Another common and readily available solvent is tetrahydrofuran, THF. THF is an ether similar to diethyl ether present in the 3M methyl magnesium bromide reagent used. It is an aprotic solvent thus, inert to the reagent and possesses lone pair electrons that could promote negative surface charge formation. Grignard treatment was performed using THF as the solvent via sol-gel chemistry. SEM in figure 4.5 shows that even with the addition of only 4S DI water, there is evidence of surface roughening of the sieves. The morphology of the surface roughening structures do not appear to be properly formed whiskers. Also amorphous substances around the sieves can be observed, which

are indicative of homogenous nucleation of $Mg(OH)_2$. The SEM pictures suggests that compared to a toluene environment, THF provides a better environment for $Mg(OH)_2$ whisker growth on the sieve surface. Methyl magnesium bromide is very reactive with water and the miscibility of THF in water may make it difficult to control the amount of water in the reaction. This could explain both the homogenous nucleation at low stoichiometric amount of water and the morphology of the whiskers.

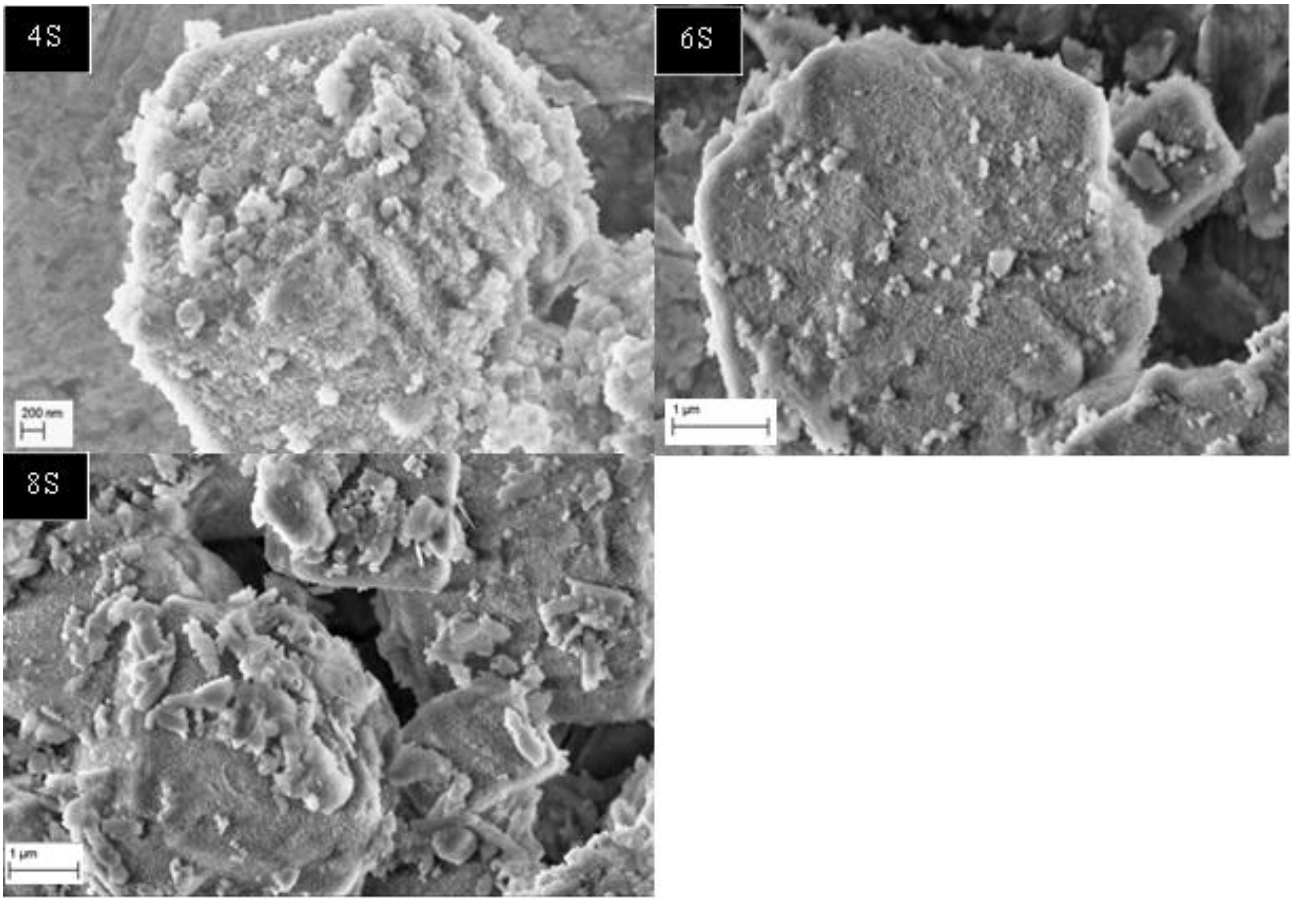

Figure 4.5: Grignard treated commercial LTA sieves via sol-gel with THF as solvent

Treatment of lab-made sieves resulted in $Mg(OH)_2$ flakes on the sieves surface (figure 4.6). Unlike in commercial sieves, it appears that THF was unable to generate

surface charges on lab-made sieves, thus resulting in the flake morphology of $Mg(OH)_2$. This suggests a difference in the surface properties of commercial and lab-made sieves. Stemming from this possible difference, a different environment may be required for the treatment of lab-made sieves.

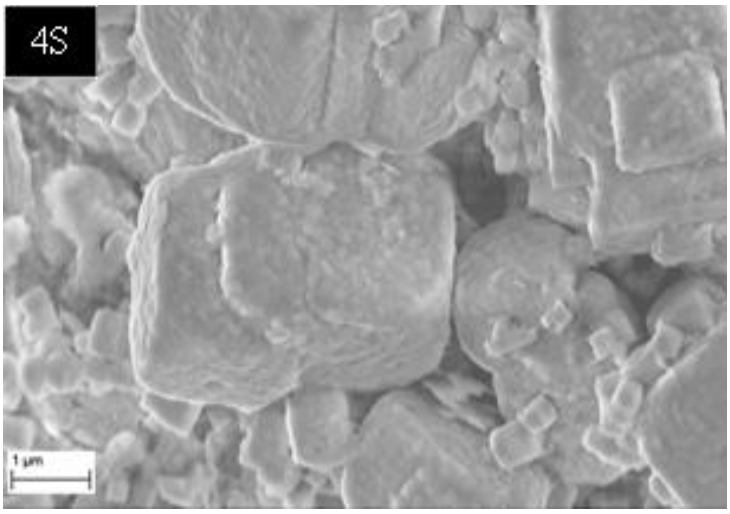

Figure 4.6: Grignard treated lab-made LTA sieves via Sol-gel with THF as solvent

4.5.3. Sol-gel based Grignard treatment using 2-methyltetrahydrofuran as solvent

2-methyltetrahydrofuran, MeTHF is a solvent similar in property to THF but has limited miscibility in water. Grignard treatment was performed using MeTHF as the solvent via sol-gel method. SEM in figure 4.7 shows good whisker formation with 6S DI water. With increase in the amount of water to 8S, the sieves are fully covered with long whiskers, and amorphous homogeneous $Mg(OH)_2$. The homogenous $Mg(OH)_2$ are indicative of excess water. From the SEM, the whiskers appear to be lying horizontally rather than sticking vertically, which may not be a good orientation for proper entanglement with the polymer chains.

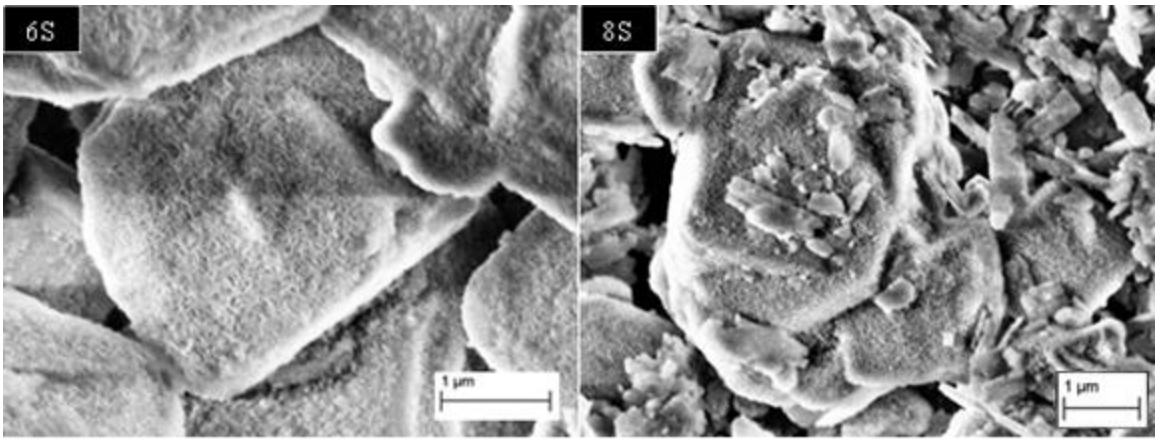

Figure 4.7: Grignard treated commercial sieves with MeTHF as solvent

Of the solvents investigated, MeTHF appears to be the best for the surface modification reaction of commercial LTA 5A. So it was used to treat lab-made sieves. Thus far, treatment of lab-made sieves using other solvents has resulted in either bare sieves or flakes. SEM in figure 4.8 shows that using MeTHF also results in flakes with the addition of 6S DI water. It can be concluded that the surfaces of lab-made and commercial sieves are remarkably different and will require characterization to determine the difference.

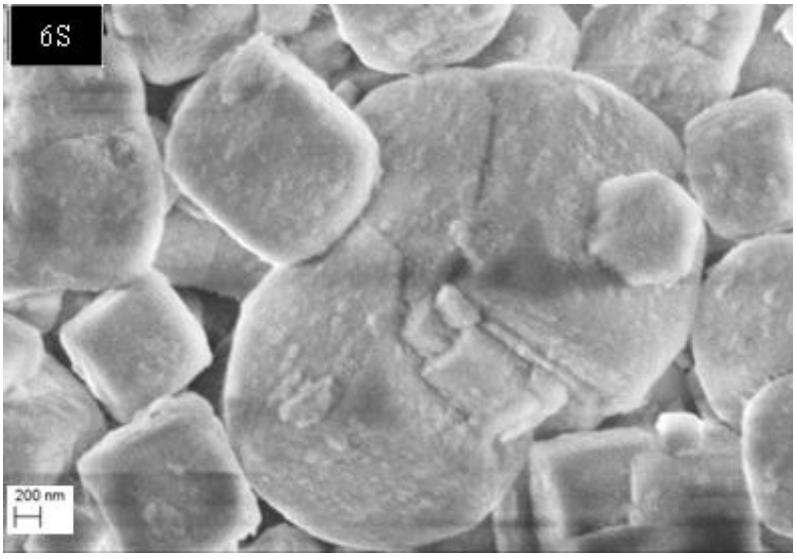

Figure 4.8: Grignard treated lab-made LTA sieves with MeTHF as solvent

4.6. "*SIMPLIFIED*" GRIGNARD TREATMENT PROCESS

Though sol-gel method of Grignard treatment results in good surface modification of commercial 5A, it requires extreme control of the amount of water added, as well as the rate of water addition. These control requirements would make it challenging in industrial application. A "*simplified*" method developed was expected to yield similar results with less need for control, and also prevent homogeneous reactions. This "*simplified*" method is also used to gain insight into the reactivity of the sieve surface. Based on the proposed reaction mechanism, the success of equations 4.8 & 4.9 depends on equation 4.7 being successful; however, equation 4.7 is dependent on the reactivity of the sieves surface. The sieve surface reactivity may be related to the concentration of silanol groups present. To keep the reaction only on the surface of the sieves and avoid homogeneous reactions, the unreacted methyl magnesium bromide is washed away leaving the functional group Si-O-MgBr, which becomes the reactant for reaction with 2-

propanol and water. The "*simplified*" method of Grignard treatment can also provide some support to the hypothesis of solvent effect on Grignard treatment resulting from surface charge formation.

4.6.1. "*Simplified*" Grignard treatment using toluene as solvent

Using toluene as the solvent, commercial LTA 5A sieves were treated via the "*simplified*" Grignard treatment method. The sieves were dispersed in toluene, then reacted with CH_3MgBr and sonicated overnight. The mixture was centrifuged to collect the sieves. Violent reaction of the supernatant with water indicated the presence of unreacted CH_3MgBr, thus indicating that the 'Si-O-' on the surface of the zeolite was the limiting reactant. The sieves were rinsed thoroughly by shaking in toluene and centrifuging 3 times. The sieves were then reacted with 2-propanol, followed by water. Samples for EDS analysis were taken following each reaction step to check for the presence of Mg on the sieves. SEM pictures of the sieves after the final water wash were taken to show proof of whisker formation.

Table 4.1 shows the EDS analysis of samples taken during this treatment. Following the toluene wash, there appears to be a significant amount of Mg present. The magnesium content is shown to drop following IPA and water wash. This suggests that the Mg present after toluene wash was either weakly bound, or simply deposited on the sieve surface.

Table 4.1: EDS analysis of commercial 5A surface treated using Toluene as solvent

	O	Na	Mg	Al	Si	Ca	Total
After Toluene wash	56.36	2.95	5.32	19.56	11.72	4.09	100
After IPA wash	59.83	3.83	0.63	15.35	14.68	5.67	100
After DI water wash	62.54	4.03	0.48	13.47	13.83	5.66	100

The SEM picture (figure 4.9) shows nearly bare sieves after the treatment also supporting the hypothesis that toluene is an undesirable solvent to promote Si-O---Mg-Br bond formation due to its inability to promote surface charge formation on the sieve surface.

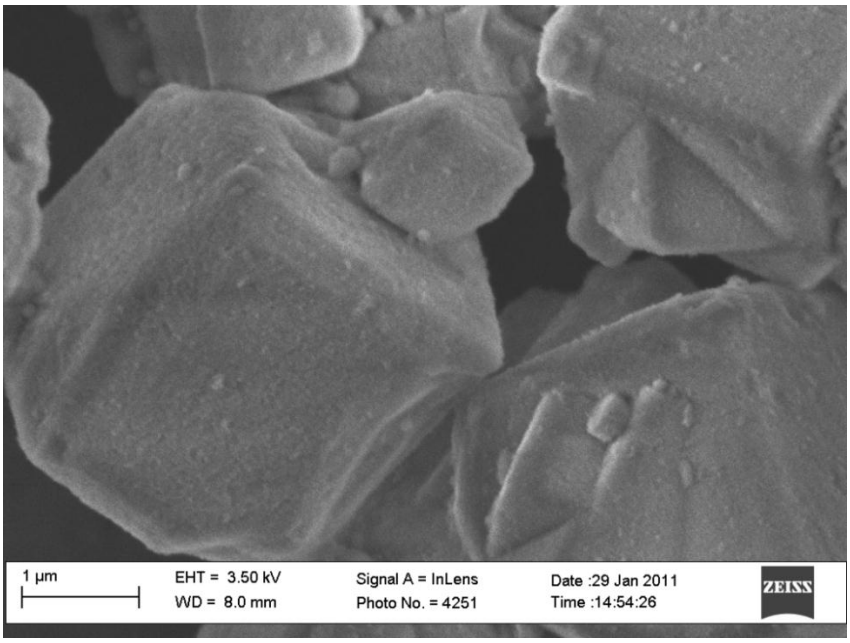

Figure 4.9: Grignard treated commercial LTA sieves via '*simplified* method' with toluene as solvent

4.6.2 *"Simplified"* Grignard treatment using tetrahydrofuran as solvent

The "*simplified*" Grignard treatment process was repeated on commercial sieves using anhydrous tetrahydrofuran as solvent. Based on the SEM pictures in Figure 4.5 for the sol-gel treatment, at 4S DI water, the sieve surface is covered with whiskers and there are signs of homogenous nucleation. The "*simplified*" Grignard treatment process is expected to prevent the occurrence of homogenous nucleation, since the process restricts the reactive sites to the sieve surface. An SEM picture of this treatment in figure 4.10 shows the absence of homogenous nucleation; however, the sieves are sparsely covered with whiskers and flakes.

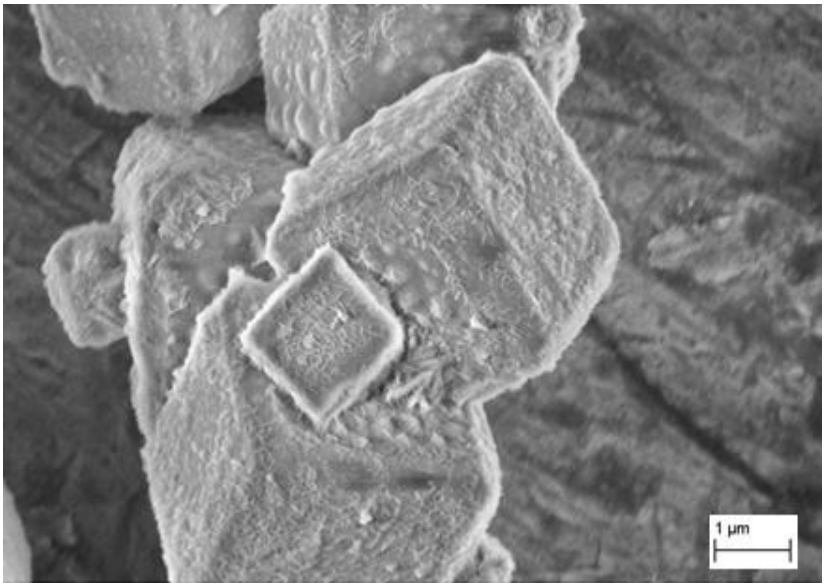

Figure 4.10: Grignard treated commercial LTA sieves via '*simplified* method' with THF as solvent

This poor surface treatment could be due to the introduction of water to the process at stages earlier than the water washing step, due to the infinite solubility of THF in water [10]. The presence of moisture at the early stages of the treatment has the

potential to denature the Grignard reagent thus reducing the amount available for reaction. It could also change the environment from an anhydrous environment that supports deprotonating of the silanol group, to a non-anhydrous environment that reduces the deprotonating power of THF. Labib and Williams [11] studied the effect of moisture on the zeta potential of particles suspended in organic liquids, and concluded that moisture weakens the solid- liquid interactions and makes the solid less acidic. The presence of moisture in some solid/liquid suspensions could result in charge reversal as depicted in the figure 4.11.

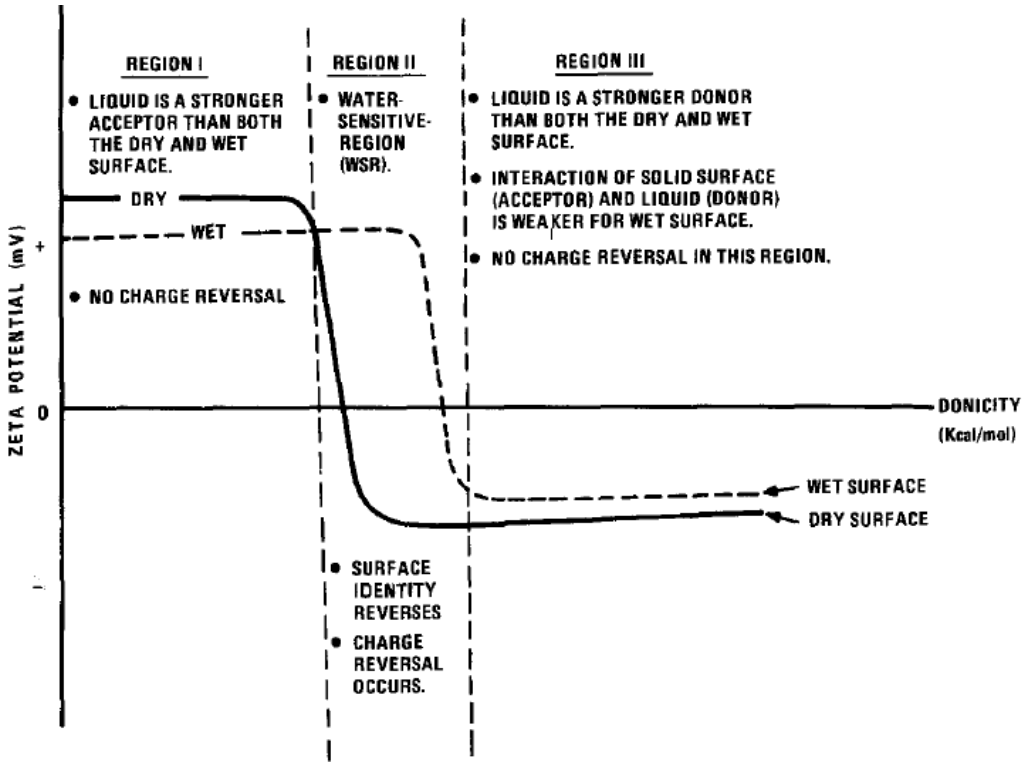

Figure 4.11: Schematic depicting the three regions describing the donor-acceptor interaction of a solid surface and organic liquids in the presence and absence of moisture. The three regions are: Region I – the surface acts as a donor, Region II – the water-sensitive region, and Region III – the surface acts as an acceptor [11]

EDS analysis in table 4.2 shows the magnesium content decreased over the course of the treatment. So compared to toluene, THF provides a better environment; however it does not appear to sufficiently deprotonate the silanol group.

Table 4.2: EDS analysis of commercial 5A surface treated using THF as solvent

	O	Na	Mg	Al	Si	Ca	Total
After THF wash	56.28	3.74	2.14	14.14	14.23	9.47	100
After IPA wash	57.87	4.68	1.95	13.75	12.90	8.86	100
After DI water wash	56.09	3.79	0.65	16.34	15.23	7.91	100

4.6.3. *"Simplified"* Grignard treatment using 2-methyltetrahydrofuran as solvent

MeTHF was used as the solvent in the "*simplified*" Grignard treatment process of commercial LTA 5A. Since MeTHF proved to be a good solvent in the sol-gel process, similar surface modification was expected through the "*simplified*" method. EDS analysis after each step as seen in table 4.3 shows insignificant change in the amount of Mg present after each wash. This suggests that following the reaction with CH_3MgBr, the bond Si-O – Mg-Br was formed by all the available silanol groups on the zeolite surface providing nucleating sites for $Mg(OH)_2$ growth.

Table 4.3: EDS analysis of commercial 5A surface treated using MeTHF as solvent

	O	Na	Mg	Al	Si	Ca	Total
After MeTHF wash	59.89	3.49	1.45	14.62	13.99	6.56	100
After IPA wash	61.28	4.07	1.54	13.8	14.16	5.11	100
After DI water wash	60.47	3.52	1.06	14.82	14.39	5.49	100

The SEM picture in figure 4.12 shows good surface modification of the sieves with whiskers. It was observed that despite not controlling the amount of water added, and the rate of water addition, there are no signs of homogeneous reaction. This is because the only reactive sites following the solvent wash are the Si-O-Mg-Br sites on the sieves surface. The excess CH_3MgBr, that would have reacted with IPA and water independent of the sieves have been washed away. The "*simplified*" method has the potential for easy scale up as it requires little to no control. It should also be noted that there was no need to control the pH of the water used in this treatment. The sieves from this treatment were used to make mixed matrix membranes and their separation enhancement properties will be discussed in chapter 5 and 6.

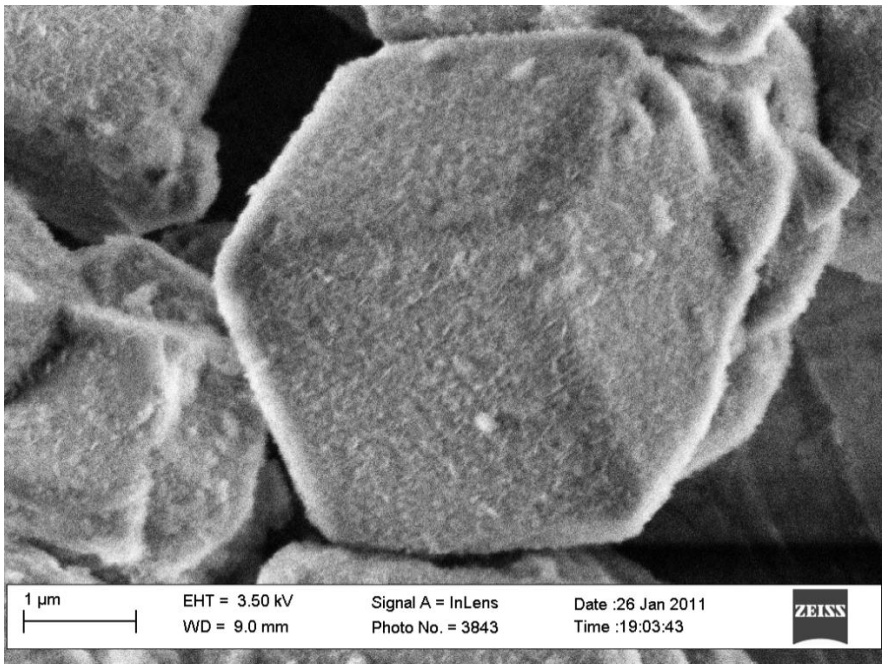

Figure 4.12: Grignard treated commercial LTA sieves via '*simplified* method' with MeTHF as solvent

4.7. EXPLORING THE DIFFERENCE BETWEEN COMMERCIAL AND LAB-MADE LTA SIEVES

FTIR analysis was performed on both commercial and lab made sieves using KBr pellets to investigate the difference in structural property. Using KBr pellets does not allow for surface study; however it allows analysis of skeletal modes. The spectra obtained (shown in figure 4.13) agrees with that obtained by Montanari [12], thus confirming the LTA backbone of the sieves.

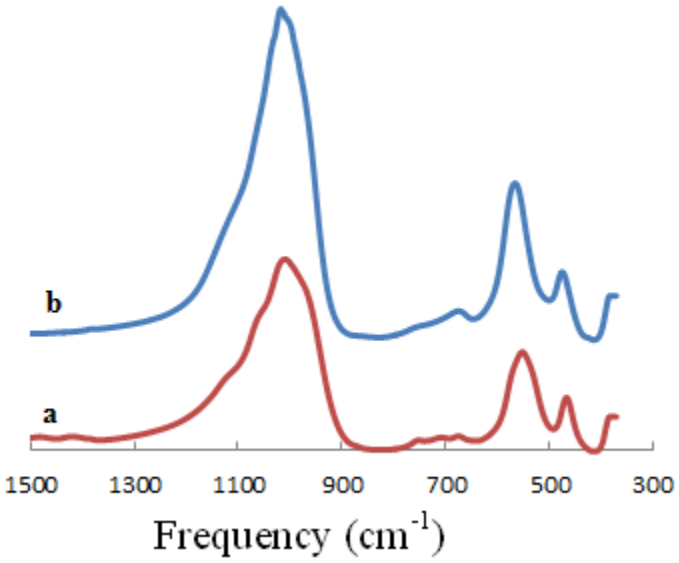

Figure 4.13: FTIR spectra of a) Commercial LTA 5A, and b) Lab-made LTA 4A using KBr pellets

XPS analysis of commercial sieves shown in figure 4.14a indicates the presence of Si, Al, O, Na and Ca which are characteristic of LTA 5A, while figure 4.14b and c indicate the presence of Si, Al, O, Na which are characteristic of LTA 4A. The N peak present in figure 4.14b originates from the template used in synthesis. All carbon peaks

should be ignored as they originate from the carbon tape holding the sample during analysis.

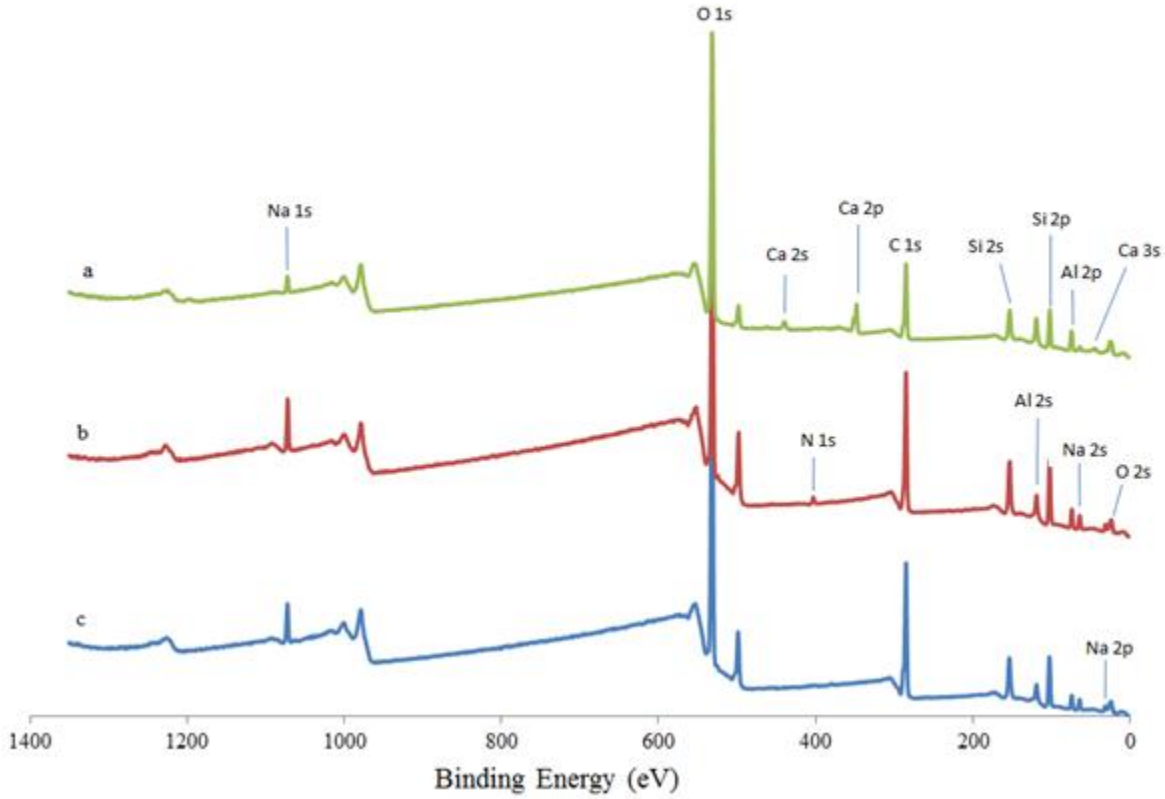

Figure 4.14: XPS spectra of a) commercial LTA 5A, b) uncalcined lab-made LTA 4A, c) lab-made LTA 4A

XPS analysis indicates no unexpected difference in the surface elemental composition between commercial and lab-made LTA.

Based on the hypothesis that surface charges on the sieves are required for reaction with the Grignard reagent to make Si-O-MgBr, zeta-potential measurements were made to compare the extent of charging of LTA. Zeta potential measurements of LTA particles in organic solvents were inconsistent, which may be due to uneven surface charges. Moreover, the mechanism of surface charge formation in organic solvents is

uncertain. Thus zeta potential measurements were made using 0.05g of sieves in 20ml of 1mM NaCl solution. Electrophoresis is calculated using smoluchowski equation.

Table 4.4: Zeta potential values of LTA sieves in aqueous media

LTA Sieves	Zeta Potential (mV)
Commercial LTA	-89
Lab-made LTA Calcined	-55
Lab-made LTA Uncalcined	-85
Lab-made LTA Soaked in Water	-52

The negative zeta potential values indicate negative charges present on the surface of the sieves in the aqueous media. The higher absolute zeta potential value for commercial sieves suggests a higher concentration of silanol groups on their surface compared to lab-made sieves. The lower absolute value for lab-made sieves suggests that the silanol groups may have been dehydroxylated, changing Si-OH to Si-O-Al, which are unreactive with the Grignard reagent. This could occur during calcination. Lab-made sieves were calcined at 550°C, and the commercial sieves used in this work are labeled "undried"; meaning they were synthesized without templates thus, not requiring calcination. It is believed that at calcination temperatures up to 500°C silanol can be dehydroxylated and will be difficult or impossible to rehydroxylate. To verify the effect of calcination on the surface charge of lab-made sieves, zeta potential measurements were made on uncalcined lab-made sieves and seen to be similar to that of commercial sieves. This supports the hypothesis that calcination results in dehydroxylation of the lab-

made sieves. The possibility of rehydroxylation of the sieve surface was tested by soaking calcined lab-made sieves in DI water overnight prior to zeta potential measurements. This rehydroxylation attempt resulted in no significant change in zeta potential. This indicates that the Si-O-Al groups cannot easily be reverted to Si-OH groups. If the concentration of silanol on the sieve surface were the only factor hindering surface modification of lab-made sieves, it could be implied that Grignard treatment of uncalcined lab-made sieves should be successful. Surface modification of uncalcined lab-made sieves via sol-gel method with MeTHF as the solvent resulted in a combination of scanty whiskers and flakes on the sieves along with amorphous $Mg(OH)_2$ (figure 4.15a). Though this is not the ideal morphology, it is remarkably different from figure 4.8, which shows the same treatment on calcined sieves. Treatment of these sieves via "*simplified*" Grignard treatment with MeTHF as the solvent resulted in mostly bare sieves (figure 4.15b) with random particles having whiskers. This leads to the belief that the success in treating commercial sieves is dependent on more than the concentration of silanol groups.

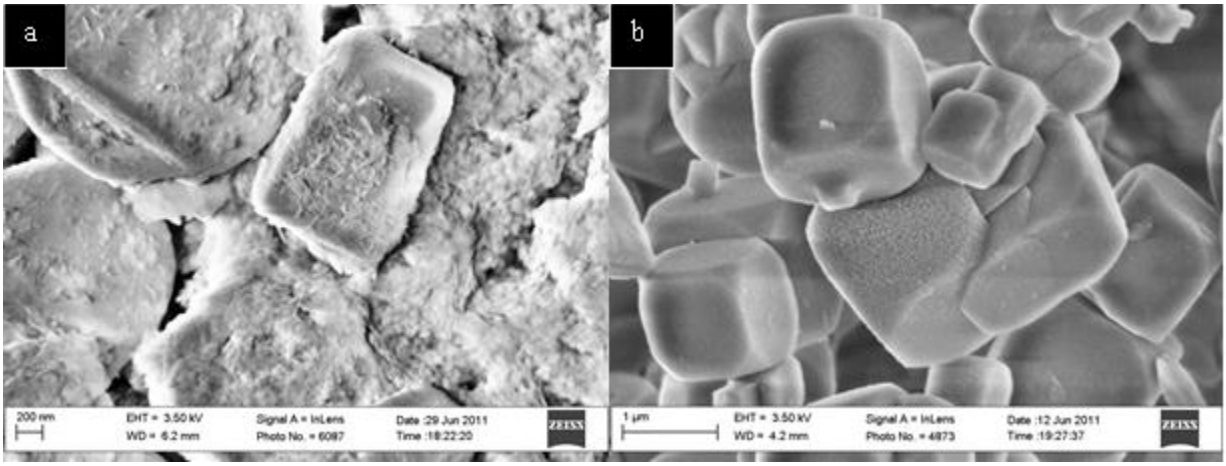

Figure 4.15: a) Treated via sol-gel with 6S DI H20, b) Treated via "simplified" method

Revisiting the investigation carried out by Shu, on the basis of $Mg(OH)_2$ morphology. The presence of NaCl and $AlCl_3$ following dealumination allowed for whisker morphology of $Mg(OH)_2$. Both the sol-gel method and "*simplified*" method of Grignard treatment discussed earlier, did not involve dealumination step, yet whisker morphology was achieved on commercial but not on lab-made sieves. This suggests that, despite the higher concentration of silanol groups present on commercial sieves as evident from zeta potential measurements, there could be some salt or other impurities present that may act as nucleating sites. SEM of the bare sieves shown in figure 4.16a & b, show clean and smooth lab-made sieves, while some amorphous substances are clearly observed on commercial sieves. The identity of these amorphous substances where not identifiable via EDS; which is seen in table 4.5 to show only elements characteristic of LTA. It is possible that these amorphous substances are $Al(OH)_3$ which could be a by-product of the synthesis, and would enhance the reactivity of the surface of commercial LTA. Table 4.5 also shows a slightly higher Si/Al ratio in lab-made sieves compared to commercial sieves and the theoretical Si/Al = 1. Since the number of potential acidic sites equal theoretically the number of Al atoms [13], this suggests that the lab-made sieves are slightly more basic than commercial sieves, and thus would require a different environment for surface modification.

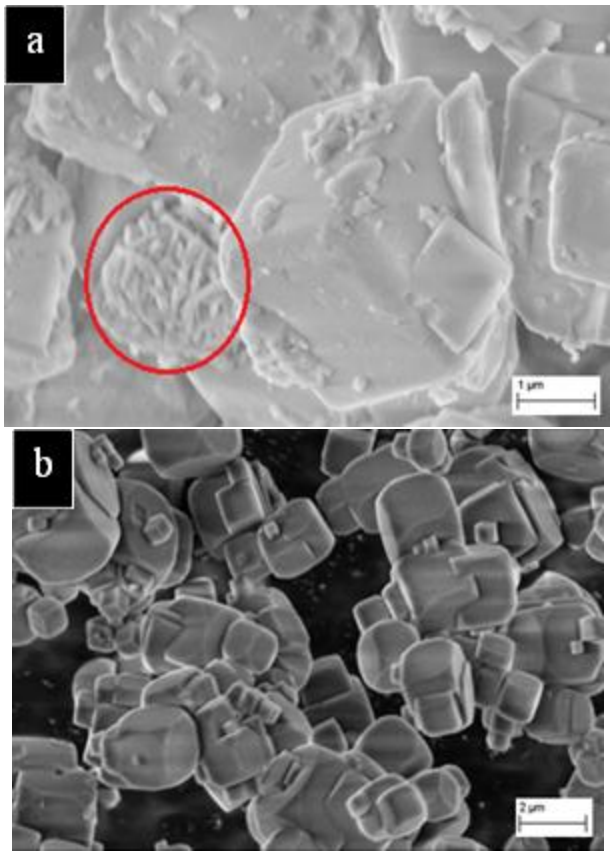

Figure 4.16: SEM of bare LTA, a) Commercial, red outline indicating amorphous substance, b) Lab-made

Table 4.5: EDS analysis of bare LTA

	O	Na	Al	Si	Ca
Comm. 5A	71.17	4.45	10.43	10.40	3.56
Lab-made 4A	66.41	10.08	10.74	12.90	-

Rather than the difference in concentration of silanol groups and the presence of impurities in commercial LTA, it is inconclusive what main difference between commercial and lab-made sieves is responsible for their varying response to Grignard treatment.

4.8. CONCLUSION

Successful surface modification of commercial LTA sieves via Grignard treatment is believed to depend on the ability of the solvent to promote the formation of negative surface charges on the sieve surface. Based on the solvents investigated, MeTHF is an ideal solvent and resulted in dense whiskers on commercial LTA. Following from the discussion above, it can be concluded that the surface properties of lab-made sieves differ from commercial sieves making the current surface modification method unsuccessful on lab-made sieves. Investigation via several characterization techniques indicated a lower concentration of silanol groups on lab-made sieves that could explain its inability to form Si-O-MgBr bond. Also observed was the presence of impurities on commercial that may serve as nucleating sites or enhance its reactivity. Further studies are required to determine the appropriate surface modification treatment for lab-made sieves. NaCl was investigated as an alternative to $AlCl_3$ anchoring and dealumination. Details of this is work is discussed in appendix A.

4.9. REFERENCES

1. Mahajan, R. and W.J. Koros, *Mixed matrix membrane materials with glassy polymers. Part 1.* Polymer Engineering & Science, 2002. **42**(7): p. 1420-1431.

2. Mahajan, R. and W.J. Koros, *Mixed matrix membrane materials with glassy polymers. Part 2.* Polymer Engineering & Science, 2002. **42**(7): p. 1432-1441.

3. Husain, S. and W.J. Koros, *Mixed matrix hollow fiber membranes made with modified HSSZ-13 zeolite in polyetherimide polymer matrix for gas separation.* Journal of Membrane Science, 2007. **288**(1-2): p. 195-207.

4. Shu, S. Husain, and W.J. Koros, *Formation of Nanostructured Zeolite Particle Surfaces via a Halide/Grignard Route.* Chemistry of Materials, 2007. **19**(16): p. 4000-4006.

5. Shu, S., *Engineering the performance of mixed matrix membranes for gas separation*, in *Chemical and Biomolecular Engineering* 2007, Georgia Institute of Technology: Atlanta

6. Liu, J., *Development of next generation mixed matrix hollow fiber membranes for butane isomer separation*, in *Chemical and Biomolecular Engineering*. 2010, Georgia Institute of Technology: Atlanta.

7. Labib, M.E. and R. Williams, *An experimental comparison between the aqueous pH scale and the electron donicity scale.* Colloid & Polymer Science, 1986. **264**(6): p. 533-541.

8. Labib, M.E., *The origin of the surface charge on particles suspended in organic liquids.* Colloids and Surfaces, 1988. **29**(3): p. 293-304.

9. Esumi, K., et al., *Dispersion of uniformly sized palladium particles in organic solvents.* Colloids and Surfaces, 1991. **55**: p. 9-14.

10. http://www.pschem.com/pdfs/methfgrignard6.pdf.

11. Labib, M.E. and R. Williams, *The effect of moisture on the charge at the interface between solids and organic liquids.* Journal of Colloid and Interface Science, 1987. **115**(2): p. 330-338.

12. Montanari, T. and G. Busca, *On the mechanism of adsorption and separation of CO2 on LTA zeolites: An IR investigation.* Vibrational Spectroscopy, 2008. **46**(1): p. 45-51.

13. Barthomeuf, D., *Zeolite acidity dependence on structure and chemical environment. Correlations with catalysis.* Materials Chemistry and Physics. **17**(1-2): p. 49-71.

CHAPTER 5

SINGLE GAS TRANSPORT OF BUTANE ISOMERS IN 6FDA-DAM-BASED DENSE FILMS

5.1. ABSTRACT

This chapter will address the transport of butane isomers through dense 6FDA-DAM films. Annealing effects on the permeation and sorption isotherms were investigated at sub-T_g temperatures of 180°C and 230°C for 24hrs. Increases in selectivity and decreases in permeability were observed at the higher annealing temperature. Annealing at the higher temperature gave a permselectivity increase of ~29% at feed pressures of 25psi, which was attributed mainly to increase in sorption selectivity. The effect of operating temperature was investigated via sorption measurements at temperatures of 50°C and 100°C. As expected, solubility decreased with temperature, while diffusivity increased, consistent with the van't Hoff and Arrhenius equations respectively. The separation performance of mixed matrix membranes was studied in single gas permeation systems at sieve loadings of 25 and 30wt%. Selectivity enhancement was achieved at these sieves loadings. This chapter will also address some factors believed to affect adequate mixed matrix membrane fabrication.

5.2. ANNEALING STUDY ON 6FDA-DAM

Annealing has been shown by various researchers [1-3] to suppress plasticization. Sub-T_g annealing accelerates physical aging of glassy polymers through the thermodynamically driven process of free volume diffusion [4], and lattice contraction [5]. Free volume diffusion and lattice collapse lower the fractional free volume of the glassy polymer, thus resulting in lower sorption capacity and permeability. Through the annealing process, the polymer segments become better packed and may undergo changes in the short range order within the polymer, resulting in changes in electron density. The changes in electron density are attributed to the formation of weak bonds via π–electron transfer between various ring structures, and are often referred to as charge-transfer-complexes (CTCs) [4, 6, 7]. The presence of CTCs can be observed as a color change in the film. Charge-transfer-complexes act as virtual crosslinks between polymer chains, thus increasing the rigidity of the chains, which increases the plasticization resistance, but result in decreased permeability [6].

5.2.1. Annealing effect on sorption

An annealing study on equilibrium and kinetic sorption of n-C4 and i-C4 in neat 6FDA-DAM dense films was performed under isothermal condition of 100°C via the pressure-decay method described in chapter 3. The films tested were annealed at sub-T_g temperatures of 180°C and 230°C for 24hrs. As mentioned earlier, annealing results in a decrease in the unrelaxed fractional free volume trapped in the glassy matrix during passage from the rubbery to the glassy state. The loss in free volume decreases the sorption capacity of the polymer, which can be observed in figures 5.1a &b. The sorption

isotherms can be conveniently described using the dual mode sorption model described in chapter 2. The coefficients for the model provided in table 5.1 reflect a few differences between the two isomers. The most dramatic effect is the large reduction in the saturated sorption capacity, C_H' for i-C4 in the 230°C annealed sample.

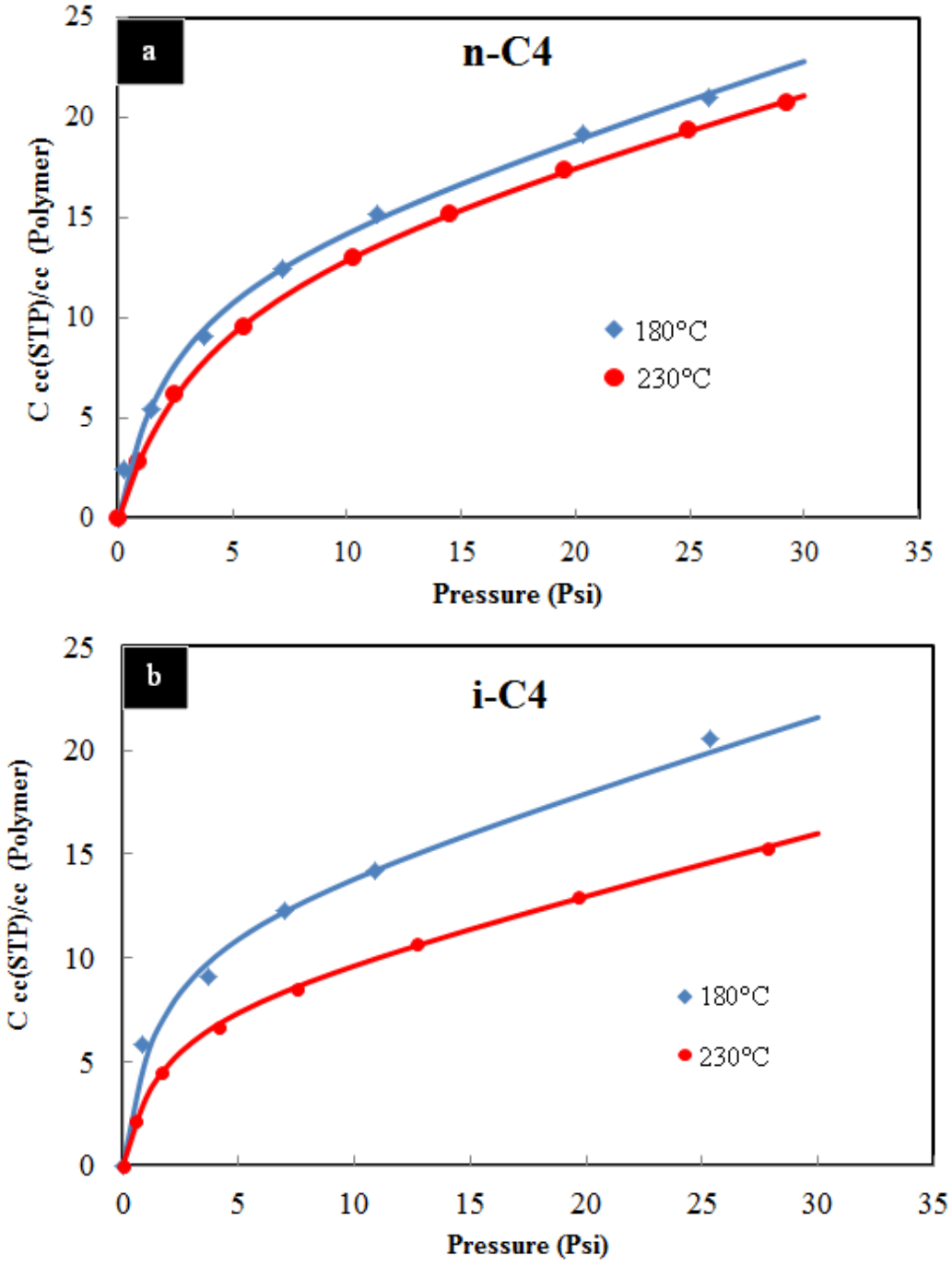

Figure 5.1: Annealing effect on sorption of 6FDA-DAM at operating temperature of 100°C. a) n-C4, and b) i-C4

Table 5.1: Sorption parameters at different annealing conditions, and operating temperature of 100°C

	n-C4			i-C4		
	k_D $\left(\frac{cc(STP)}{cc(poly).psi}\right)$	b (psi^{-1})	C'_H $\left(\frac{cc(STP)}{cc(poly)}\right)$	k_D $\left(\frac{cc(STP)}{cc(poly).psi}\right)$	b (psi^{-1})	C'_H $\left(\frac{cc(STP)}{cc(poly)}\right)$
180°C	0.354 ± 0.1	0.432 ± 0.1	13.1± 1	0.341 ± 0.1	0.676 ± 0.1	11.9 ± 1
230°C	0.295± 0.1	0.252± 0.1	13.9± 2	0.283 ± 0.1	0.602 ± 0.1	7.92 ± 1

This surprising trend suggests a greater effect on the sorption capacity of the more bulky i-C4 versus n-C4. For both n-C4 and i-C4, a decrease in k_D and b was observed. The decrease in k_D can be attributed to rigidification of the Henry's region, while the decrease in the affinity constant can be attributed to change in the nature of the Langmuir sorption site, both of which outcomes could be due to short range ordering from CTCs mentioned above. Normal butane sorption decrease of 7.1%, and a 28.8% increase in sorption selectivity, $S_{n\text{-}C4}/S_{i\text{-}C4}$ at 25psi was observed. This trend may reflect the significant difference in the "bulkiness" of i-C4 and n-C4; however, effects due to annealing on sorption selectivity have not been studied in detail for other gas pairs. This sorption selectivity increase will contribute to the change in permselectivity observed when comparing films annealed at these temperatures.

The diffusion kinetics of n-C4 was calculated and as shown in figure 5.2, an expected decrease in diffusivity with increase in annealing temperature was observed. Diffusion coefficient is directly related to the square of the jump length and the frequency of jump occurrence via;

$$D = \frac{\lambda^2 f}{6} \tag{5.1}$$

The diffusional jump length in glasses are believed to be on the order of magnitude of the penetrant diameter, so the lower diffusion coefficients upon annealing are believed to more reflect the jump frequency than large difference in jump length, λ. Increase in chain rigidification resulting from annealing makes the polymer chains less mobile, which tends to reduce the frequency of diffusional jump occurrence, thereby decreasing the diffusion coefficient as seen in figure 5.2. Kinetic sorption data were analyzed graphically using plots provided in Crank [8] for update by a plane sheet from a stirred solution of limited volume. Diffusivities were determined at half-times, and are plotted against the final external cell pressure to determine changes in the external boundary condition in order to use the graphical solutions in figure 4.6 in Crank [8].

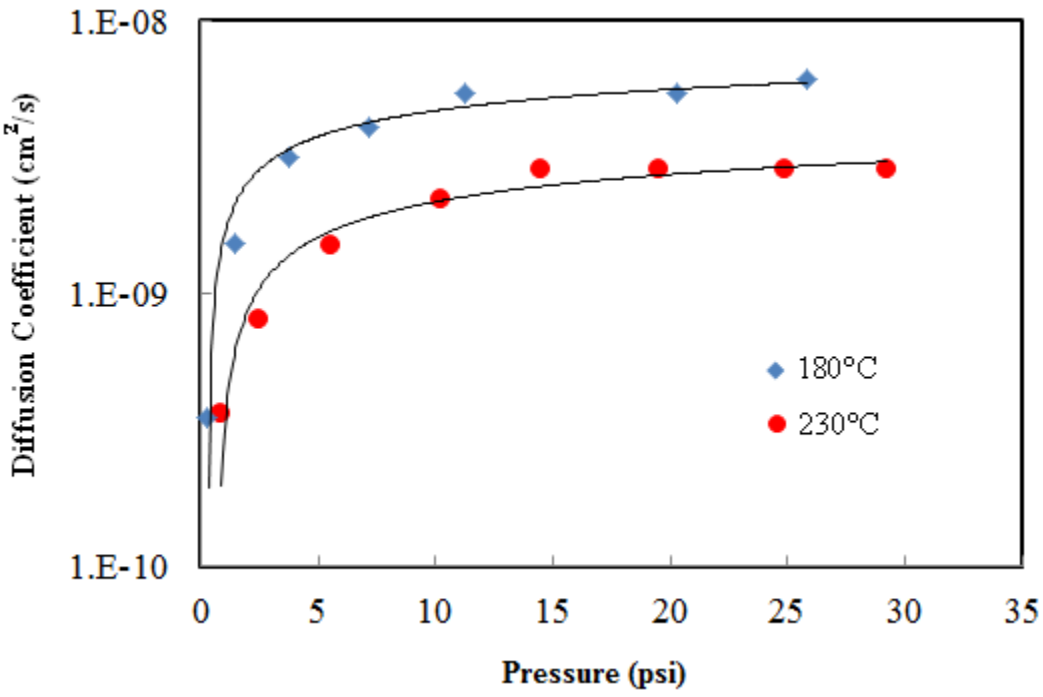

Figure 5.2: Diffusivity of n-C4 in neat 6FDA-DAM at operating temperature of 100°C (data attained via kinetic sorption measurement at different annealing temperatures)

At 25psi approximately a 51% decrease in diffusivity of n-C4 was observed as a result of increasing the annealing temperature from 180°C to 230°C.

Kinetic sorption measurements of i-C4 in neat 6FDA-DAM annealed at 180°C showed deviation from a simple Fickian-controlled diffusion mechanism, to a combination of Fickian and relaxation-controlled diffusion mechanism at low penetrant pressure (observed at 4psi). As a result, the plots provided by Crank [8] were not suitable in making diffusivity estimates. Diffusion of penetrants into glassy polymers causes swelling of the polymer. Both Fickian controlled diffusion and relaxation-controlled swelling contribute to the rate and extent of penetrant sorption in glassy polymers [9]. For a given penetrant-polymer system, over a sufficient range of penetrant activity, the change in the relative contributions of concentration-gradient controlled diffusion and relaxation controlled swelling will give rise to a wide range of behavioral patterns [9]. These patterns range from ideal Fickian to relaxation or swelling controlled sorption. Berens and Hopfenberg developed a model to account for the combination of Fickian and relaxation-controlled diffusion mechanism in polymers [9]. The Berens-Hofpenberg model (equation 5.2) was used to make diffusion coefficient estimates for i-C4 in neat 6FDA-DAM annealed at 180°C. Details of this work are provided in appendix B. Since this diffusion is not simply Fickian controlled, the diffusion coefficient values determined were not used for further analysis.

$$\left(\frac{M_t}{M_\infty}\right)_A = \left[(1-\alpha_R)\left\{1-\sum_{n=0}^{\infty}\frac{8}{\pi^2(2n+1)^2}exp\left(\frac{-D_A(2n+1)^2\pi^2 t}{l^2}\right)\right\}\right] + \left[\alpha_R\left\{1-exp\left({}^{-t}/_{\tau_R}\right)\right\}\right] \quad (5.2)$$

Where, α_R is the fraction of mass uptake occurring via relaxation-controlled process, $(1 - \alpha_R)$ is the fraction of mass uptake occurring via Fickian diffusion, and τ_R is the time constant of the relaxation process.

Diffusion coefficient estimates of i-C4 in neat 6FDA-DAM annealed at 230°C were determined via the plots provided by Crank [8]. It is noteworthy, that by annealing the polymer at a higher temperature, the diffusion mechanism of i-C4 remained purely Fickian over the pressure range tested (i.e. 0 – 28psi). This can be attributed to the ability of thermal annealing to rigidify the polymer matrix, thus suppressing the swelling and relaxation effect of i-C4 sorbed.

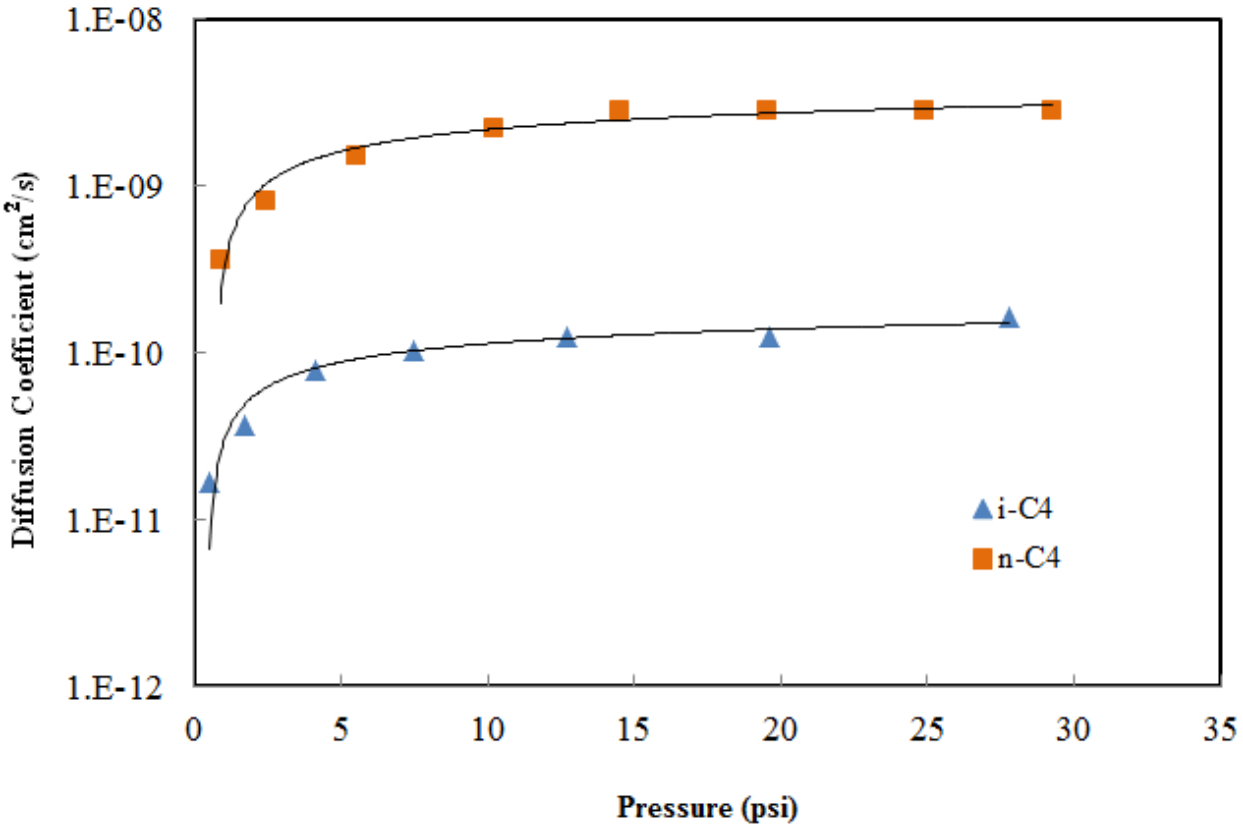

Figure 5.3: Diffusivity of n-C4 and i-C4 in neat 6FDA-DAM annealed at 230°C. Operating temperature of 100°C

Figure 5.3 compares the diffusion coefficient of n-C4 and i-C4 in neat 6FDA-DAM annealed at 230°C. By combining the partial immobilization model in equation 2.14, where $p_B = 0$, with equation 2.2 [10].

$$P = k_D D_D + \frac{C'_H D_H b}{1 + bp} = k_D D_D \left(1 + \frac{KF}{1 + bp}\right) \tag{2.14}$$

$$P = D_{avg} S = k_D D_{avg} \left(1 + \frac{K}{1 + bp}\right) \tag{2.2}$$

D_{avg} can be written in terms of D_D, via equation 5.3.

$$D_{avg} = D_D \left[\frac{1 + (FK/(1 + bp_2))}{1 + (K/(1 + bp_2))}\right] \tag{5.3}$$

In a system where, F = 1, $D_{avg} = D_D$. In this system of butane isomers in neat 6FDA-DAM annealed at 230°C, F < 1, so $D_{avg} < D_D$. Based on equation 5.3, D_{avg} equals:

$$D_{avg} = D_D \left[\frac{1 + FK}{1 + K}\right] \; at\ infinite\ dilution\ (low\ p)$$

$$D_{avg} = D_D \;\; at\ high\ p$$

To avoid confusion, diffusion coefficient values deduced from kinetic sorption measurements will be written with a **superscript k**. By drawing from the plot in figure 5.3, $D_{D_i}^k$ and F_i^k were determined for both n-C4 and i-C4 and used to calculate $D_{avg_i}^k$

values at 25psi. Table 5.2 shows these data. Details of the calculation involved is provided in appendix C.

Table 5.2: Estimated $\boldsymbol{D_{D_i}^k}$ and $\boldsymbol{F_i^k}$ values and calculated $\boldsymbol{D_{avg_i}^k}$ values of butane isomers in neat 6FDA-DAM annealed at 230°C, at external pressure of 25psi and operating temperature of 100°C

	$D_{D_i}^k$ (cm^2/s)	F_i^k	$D_{avg_i}^k$ (cm^2/s)
n-C4	30.0E-10	0.006	11.5E-10
i-C4	1.65E-10	0.008	0.81E-10

From table 5.2, at 25psi, the estimated diffusion selectivity, $\left(D_{avg_{n-C4}}^k / D_{avg_{i-C4}}^k\right)_{230°C} \cong 14.2$ and from table 5.1, the sorption selectivity at 25psi at the same annealing condition can be calculated to be, $(S_{n-C4}/S_{i-C4})_{230°C} \cong 1.34$. These selectivity values suggest a permselectivity of ≅ 18.5 at 25psi.

5.2.2. Annealing effect on permeation

Annealing effect on the permeability of butane isomers in neat 6FDA-DAM dense films was studied at operating temperature of 100°C for annealing conditions of 180°C and 230°C over 24hrs. As discussed earlier, annealing is known to result in permeability decrease in glassy polymers. Such decrease was observed in this system of butane isomers in 6FDA-DAM dense film, as shown in figure 5.4. The parameters for the dual mode transport model for butane isomers in 6FDA-DAM annealed at 230°C are provided in table 5.3. As indicated in table 5.4, a 50% decrease in n-C4 permeability and ~29%

increase in permselectivity was observed by increasing the annealing temperature from 180°C to 230°C.

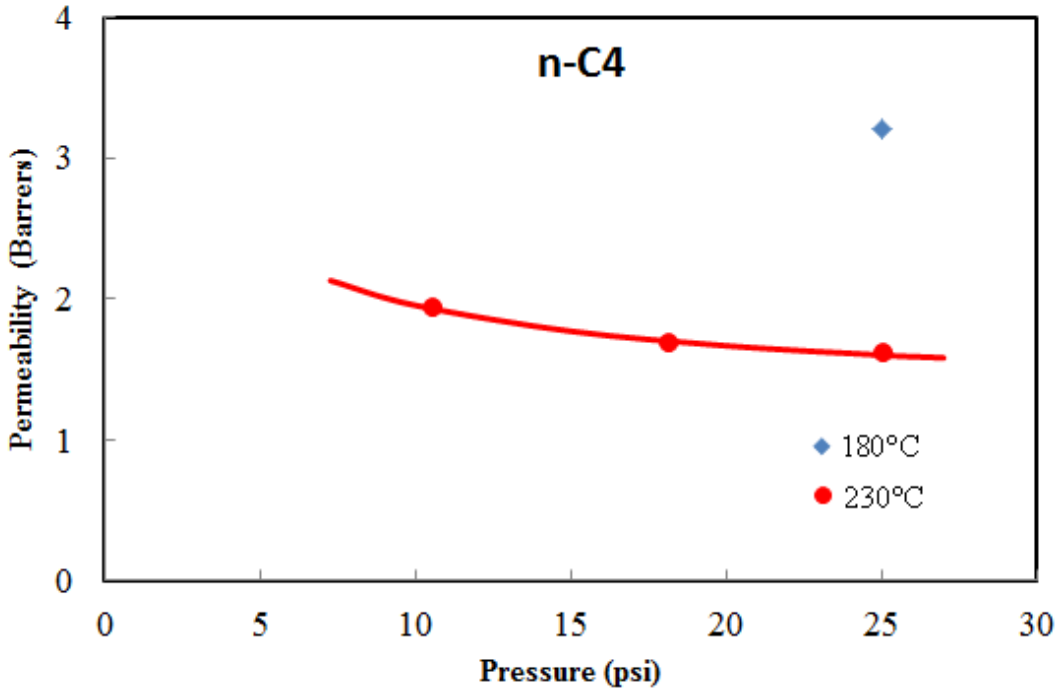

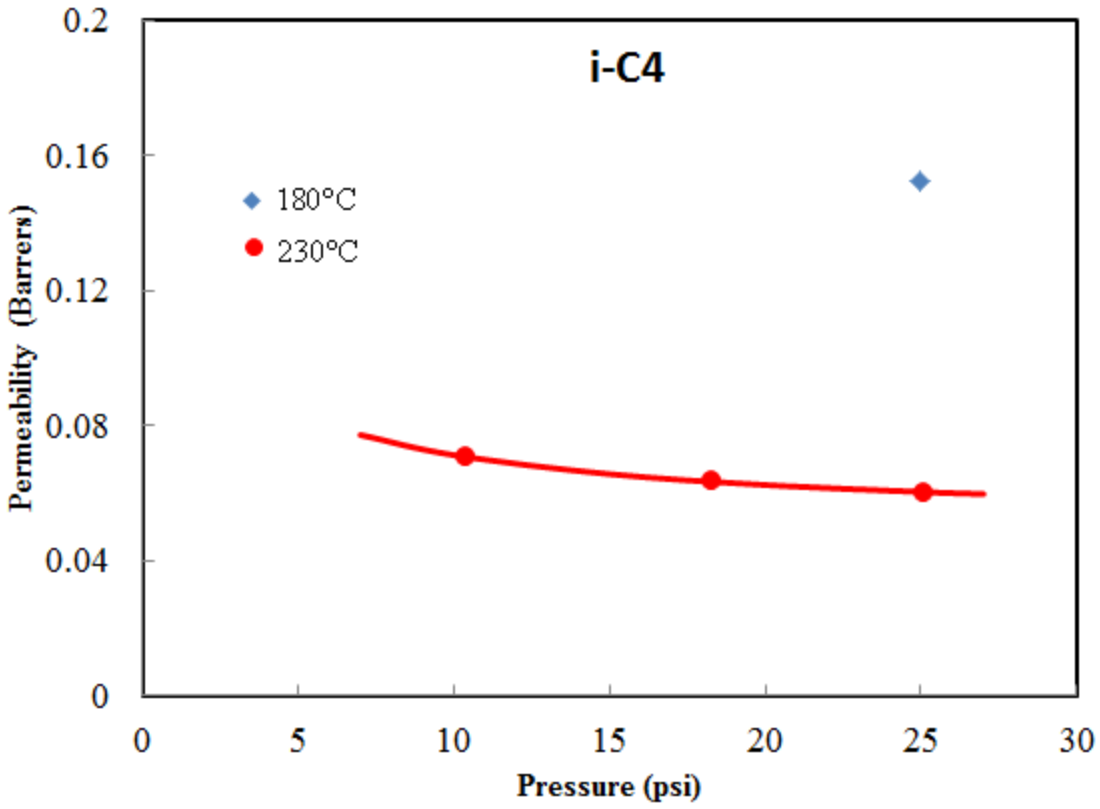

Figure 5.4: Annealing effect on permeability of butane isomers in neat 6FDA-DAM. Operating temperature of 100°C

Table 5.3: Diffusivity of butane isomers in 6FDA-DAM annealed at 230°C. Operating temperature of 100°C

	D_D (*10^{-10} cm^2/s)	D_H (* 10^{-10} cm^2/s)
n-C4	21.4	3.81
i-C4	1.28	0.146

Table 5.4: Annealing effect on separation performance of 6FDA-DAM at 25psi. Operating temperature of 100°C

Annealing Condition	n-C4 Permeability (Barrer)	$\alpha_{n/i}$
180°C	3.2 ± 0.2	21± 1
230°C	1.6 ± 0.2	27± 1

The observed permselectivity at the annealing condition of 230°C is ~ 1.4X greater than the estimated permselectivity from equilibrium and kinetic sorption measurements. Based on the definition of permeability as the product of solubility and diffusivity coefficients, permeability and selectivity data from table 5.4 and equilibrium sorption data from table 5.1 were used to estimate the diffusion coefficient at 25psi for n-C4 and i-C4 in neat 6FDA-DAM annealed at both 180°C and 230°C. These values provided in table 5.5, are compared to the diffusion coefficients estimated from kinetic sorption. The difference between D_{avg} and D_{avg}^{k}, indicates error in kinetic sorption measurements. Better accuracy of kinetic sorption, can be attained by using a more sensitive pressure transducer, and taking smaller pressure jumps; however, the available kinetic sorption data was useful in making close estimates.

Table 5.5: Comparing diffusion coefficient values of butane isomers in neat 6FDA-DAM annealed at different temperatures. Operating temperature of 100°C

	180°C		230°C	
	$D_{avg} = P/S$ (cm^2/s)	D_{avg}^k (cm^2/s)	$D_{avg} = P/S$ (cm^2/s)	D_{avg}^k (cm^2/s)
n-C4	19.8E-10	25.1E-10	10.7E-10	11.5E-10
i-C4	0.997E-10	NA	0.526E-10	0.812E-10

Diffusion selectivity, $D_{avg}{}_{n-C4}/D_{avg}{}_{i-C4}$ of 19.8 and 20.3 at 180°C and 230°C were calculated from table 5.1 & 5.4. This indicates a surprisingly negligible annealing effect on the diffusion selectivity, thus suggesting that both n-C4 and i-C4 experienced the same degree of change in their jump frequency as a result of annealing. Surprisingly, it can be concluded that in this system, the observed increase in permselectivity is mainly a result of the sorption selectivity increase.

As shown in figure 5.4a & b, there is no sign of plasticization over the pressure range tested. Plasticization is generally indicated by an upswing in the permeation isotherm. The pressure at which this upswing begins is noted as the plasticization pressure. Annealing has been observed to shift the plasticization pressure to higher pressures. Plasticization may be observed at higher feed pressures, but that was not the focus of my study. To avoid the added complication of plasticization, experiments were performed within the plasticization-free pressure range.

The selectivity increase that resulted from annealing at 230°C compared to 180°C provided in table 5.4 was attractive for subsequent work. Literature has shown added complexities that may decrease separation performance under mixed gas operation,

which will be discussed in Chapter 6. Due to the possibility of these complexities it was desirable to utilize films conditioned for high separation performance.

5.3. OPERATING TEMPERATURE STUDY ON 6FDA-DAM

The effect of operating temperature on transport of n-C4 through neat 6FDA-DAM was studied at 50°C and 100°C via equilibrium and kinetic sorption measurements. The annealing condition was kept constant at 230°C for 24 hours.

As shown in figure 5.5, n-C4 has relatively high activities for the conditions considered here. The activity increases with decrease in temperature at a given pressure. The presence of hydrocarbons at high activities can promote swelling of the polymer chains, thereby leading to plasticization. The data in figure 5.5, for instance shows that if the studies done here at 25 psia and 100°C were performed at 20°C, the feed activity would be over 0.8 and tend to sorb more strongly and possibly introduce plasticization complications. These complications were avoided in our work at 100°C and feed pressure $\leq$ 25 psia. This is also a suitable temperature to avoid the energy cost associated with cooling or heating the butane isomerization product stream from the butamer^{TM} unit when implemented industrially. As shown in figure 1.4 the butamer^{TM} unit yields a maximum conversion of 60 mol% i-C4 at ~100°C.

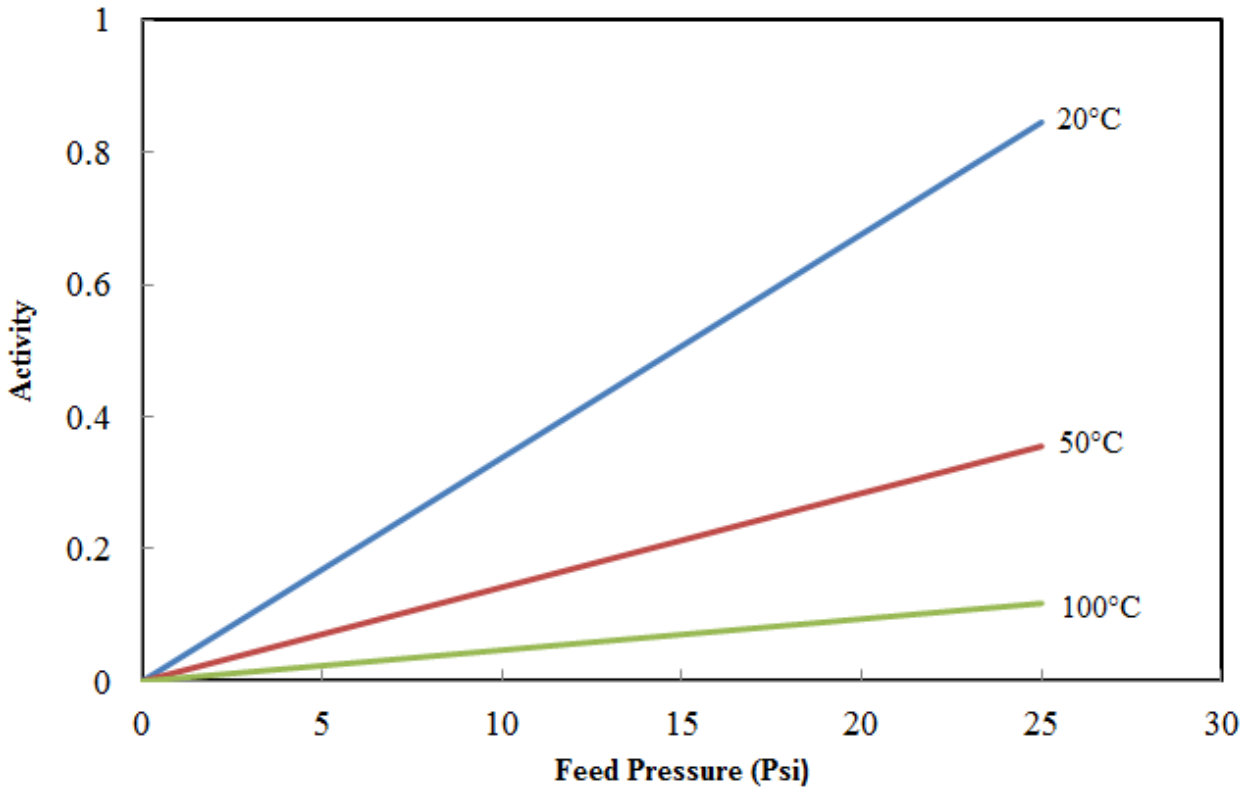

Figure 5.5: Activity of pure n-C4 at varying pressures and temperatures.
Calculated using activity $= \frac{p}{P^{sat}}$, where, P^{sat} is the saturated vapor pressure at a given temperature

Equilibrium sorption measurement (shown in figure 5.6) indicates a higher sorption capacity of n-C4 at the lower temperature. This is because at lower temperatures the condensability of this gas is higher due to its higher activity. Table 5.6 provides the fitting parameters to the dual mode sorption model.

Diffusivities were determined at half-time, and are plotted against the final external cell pressure as seen in figure 5.7. The diffusivity of n-C4 is observed to decrease with operating temperature. This is because gas diffusion rate in polymers is dependent on the frequency and length of diffusion jump, which is governed by thermal

fluctuations in the polymer. These fluctuations decrease with temperature, thus the decrease in diffusivity.

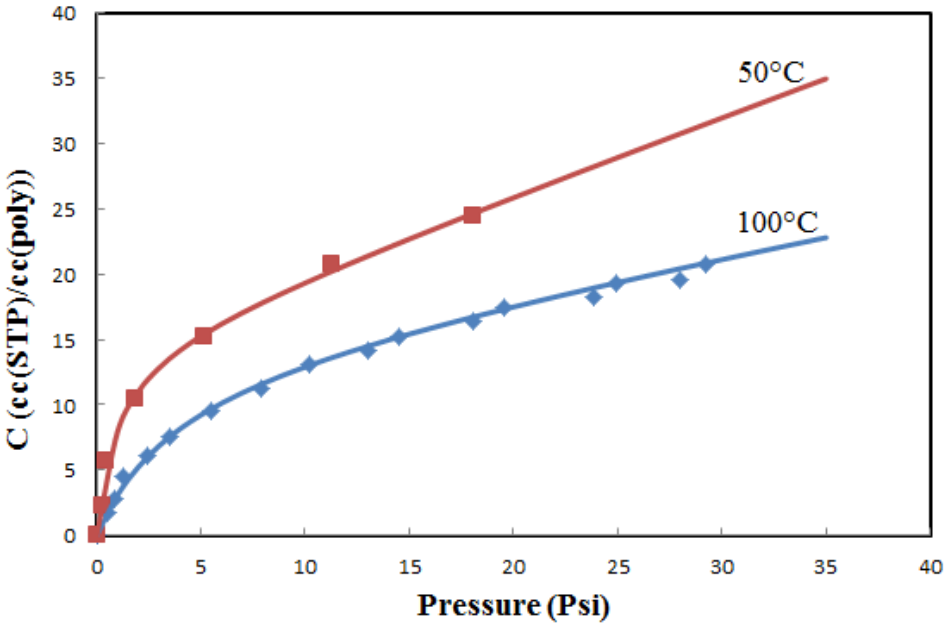

Figure 5.6: Equilibrium sorption of n-C4 in 6FDA-DAM annealed at 230°C

Table 5.6: Dual mode sorption parameters for n-C4 in neat 6FDA-DAM annealed at 230°C under different operating temperatures

	n-C4		
	k_D $\left(\frac{cc(STP)}{cc(poly).psi}\right)$	b (psi^{-1})	C'_H $\left(\frac{cc(STP)}{cc(poly)}\right)$
50°C	0.588± 0.1	0.986± 0.1	14.8± 1
100°C	0.295± 0.1	0.252± 0.1	13.9± 2

The apparent heat of sorption and activation energies of diffusion and permeability can be estimated using equations 2.25 to 2.29; however, experimental data

at other temperatures would be required in order to improve the accuracy of the estimates.

Based on sorption experimental data in table 5.6, the solubility of n-C4 in the film at 25psi, was calculated at operating temperatures of 50°C and 100°C. These values were used in the van't Hoff equation (equation 2.26) at 25psi to estimate the apparent heat of sorption, ΔH_s, and the pre-exponential solubility factor, S_0. The calculated values are provided in table 5.7.

$$S = S_0 \exp\left(\frac{-\Delta H_S}{RT}\right) \tag{2.26}$$

The diffusivities of n-C4 in neat 6FDA-DAM were determined via analysis of kinetic sorption, and are shown in figure 5.7 at operating temperatures of 50°C and 100°C. Diffusivity values determined at the same pressure of 25psi, were used in the Arrhenius equation (equation 2.25) to estimate the apparent activation energy of diffusion, ΔE_D, and the pre-exponential diffusivity factor. These calculated values are provided in table 5.7. Details of the calculation involved are provided in appendix C.

$$D = D_0 \exp\left(\frac{-E_D}{RT}\right) \tag{2.25}$$

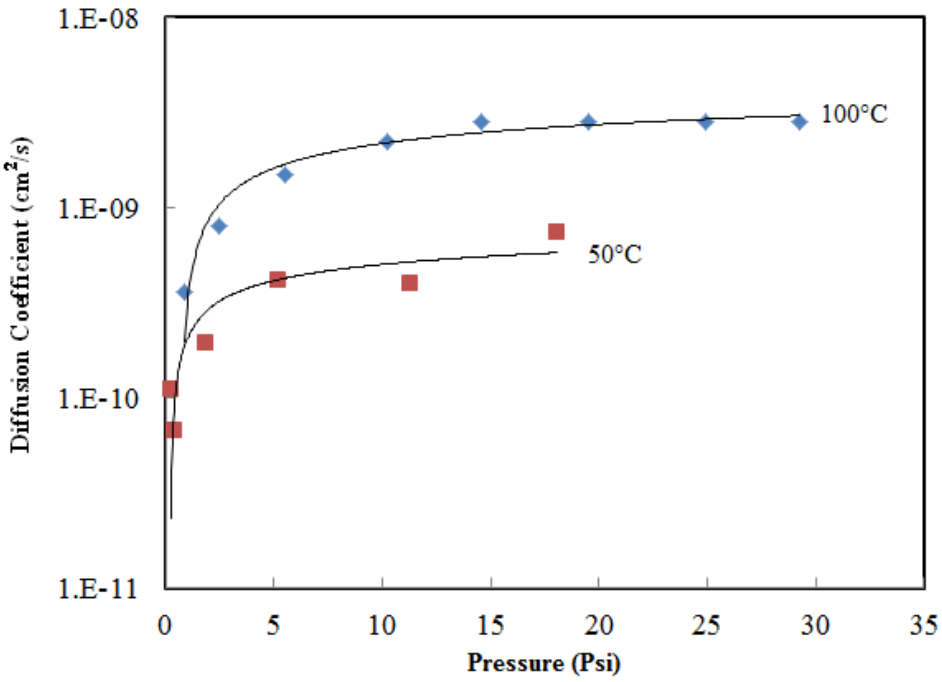

Figure 5.7: Kinetic sorption of n-C4 in 6FDA-DAM annealed at 230°C. Points are experimental data, while solid lines are excel least square regression to a logarithimic equation

Table 5.7: Arrhenius and van't Hoff parameters of n-C4 in 6FDA-DAM annealed at 230°C at external pressure of 25psi

	50°C	100°C
$D_D^k\ (cm^2/s)$	6.21E-10	30.0E-10
F^k	0.038	0.006
$D_{avg}^k\ (cm^2/s)$	3.16E-10	11.5E-10
$\Delta E_D\ (kcal/mol)$	6.26	
$D_{avg_0}^k\ (cm^2/s)$	5.34E-06	
$S\ \left(\frac{cc(STP)}{cm^3.cmHg}\right)$	0.224	0.149
$\Delta H_S\ (kcal/mol)$	-1.92	
$S_0\ \left(\frac{cc(STP)}{cm^3.cmHg}\right)$	1.12E-02	

Comparing the apparent activation energy of sorption and diffusion for n-C4 shown in table 5.7, to that deduced from data provided by Das [1], which indicates $\Delta H_s = -2.1\ kcal/mol$, and $\Delta E_D = 4.9\ kcal/mol$ for C_3H_8 in neat 6FDA-6FpDA annealed at 210°C, our estimated values seem reasonable.

Using equations 2.27 and 2.28, at 25psi, the pre-exponential permeability factor, P_0^k was calculated to be 598 Barrers, while the apparent activation energy of permeation was calculated to be 4.34 kcal/mol. Using equation 2.29, the permeability of n-C4 at 25psi in neat 6FDA-DAM annealed at 230°C was estimated to be $P_{n-C4}^k = 1.72$ Barrers at 100°C which is comparable to $P_{n-C4} = 1.6$ Barrers obtained from permeability measurements at the same conditions.

5.4. GAS TRANSPORT THROUGH LTA 5A

Gas transport through mixed matrix membranes involves simultaneous transport through the sieves and the polymer matrix. As mentioned briefly in Chapter 2, there are matching criteria to be considered while making material selection for a particular gas mixture. As depicted in figure 2.6, if the permeability through the sieve is lower than that through the polymer, the mixed matrix yields decreased permeability with slight increase in selectivity. On the other hand, if the permeability through the sieves is much greater than that through the polymer, the mixed matrix yields increased permeability with negligible selectivity enhancement. In order to achieve both permeability and selectivity enhancement, the permeability of the faster gas through the sieve should be greater than

that through the polymer but less than or equal to 10 times the permeability through the polymer, ($P_M < P_D \leq 10P_M$).

One criterion for sieve selection in membrane-based gas separation is the ability of the sieve to selectively sorb the gases. The sorption selectivity of the sieves was determined by performing single gas sorption test via the pressure-decay method described in chapter 3. Figure 5.8 shows the sorption capacity isotherm of n-C4 in LTA 5A at a temperature of 100°C. Isobutane was observed to have no measurable sorption capacity in 5A [11]. The kinetic diameter of i-C4 is ~6.0Å, which is larger than the 4.3Å pore size of 5A, thus explaining the complete exclusion of i-C4, and infinite selectivity. Table 5.8 provides the sorption fitting parameters to equation 2.30, where $p_B = 0$.

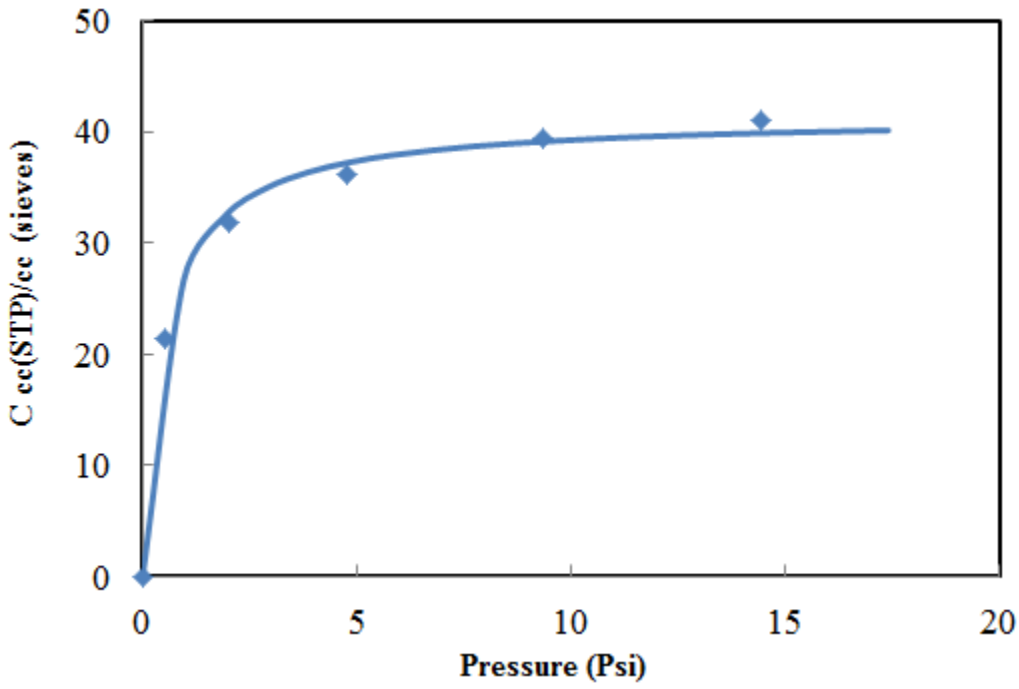

Figure 5.8: Sorption capacity isotherm of n-C4 in bare LTA 5A at operating temperature of 100°C

Table 5.8: Fitting Parameters for n-C4 sorption in bare LTA 5A

	C'_H (cc(STP)/cc(sieves))	b (psi^{-1})
n-C4	41.4 ± 3	1.89 ± 0.5
i-C4 [11]	0	0

$$C_A = \frac{C'_{H_A} b_A p_A}{1 + b_A p_A + b_B p_B} \tag{2.30}$$

Gas permeability through zeolites can be obtained from literature, estimated experimentally via equilibrium and kinetic sorption measurements, or back calculated from mixed matrix permeation data. According to Yucel et al [12] the corrected diffusivity (also known as the mobility diffusion coefficient of the penetrant in the sieves, and estimated to be the diffusion coefficient at low concentration), D_0, of n-C4 in 5A (cation composition of 65% Ca^{2+}, bal. Na^+) at 100°C is $2.1 \times 10^{-9} cm^2/s$, and $6.3 \times 10^{-9} cm^2/s$ in 5A with >95% Ca^{2+}. The average cation % in the commercial 5A used in this work is ~76% Ca^{2+}/bal. Na^+. At cation composition >67% Ca^{2+} the sieves are believed to have fully open CaA pores [11]. Thus, the corrected diffusivity of 6.3E-09 cm^2/s would be expected in the commercial sieves used in this work. Using this corrected diffusivity value and the sorption data in table 5.8, the permeability of n-C4 was estimated via equation 2.34 at 25psi and 100°C to be 70 Barrers. Kinetic sorption measurements of n-C4 in 5A were difficult to make using the equipment available because the diffusion kinetics is very fast. Liu [11] estimated the permeability of n-C4 through surface modified 5A to be 2.5 Barrers. This value was determined by back calculation using mixed matrix membrane experimental data and the Maxwell model.

Table 5.9: Estimated permeability of n-C4 in LTA 5A

	Permeability (Barrers)	Determination method
Yucel (>95% Ca^{2+}) [12]	70	$Eqn. 2.34$
Yucel (Comm.) [12]	0.4	$Eqn. 2.34$
Liu [11]	2.5	Back Calculated

Using sorption data in table 5.8 and the permeability, P = 2.5 Barrer estimated by Liu, the diffusivity value at 25psi was estimated to be 7.96E-10 cm^2/s, which corresponds to a corrected diffusivity value of 2.2E-10 cm^2/s. The estimated lower corrected diffusivity value of n-C4 in the commercial 5A used in Liu's work can be attributed to complete blockage of some of the zeolite windows during synthesis [12, 13]. Yucel [12] measured a low corrected diffusivity value of 3.3E-11cm^2/s in commercial 5A compared to the values in lab-made 5A. Using the commercial 5A from Yucel's work, and the sorption data in table 5.8, n-C4 permeability at 25psi was estimated to be 0.4 Barrers.

5.5. SINGLE GAS PERMEATION THROUGH MIXED MATRIX MEMBRANES

Membranes were fabricated using 6FDA-DAM and surface modified commercial 5A sieves as described in chapter 3. SEM in figure 5.9 shows improved adhesion of the sieves to the polymer compared to mixed matrix membranes made with untreated sieves. The enhanced adhesion is expected to improve the separation performance of the membrane.

Single gas permeation data on films annealed at 180°C and 230°C are presented in table 5.10. The data shows ~20% and 28% increase in selectivity at 20wt% and 30wt% sieve loading respectively.

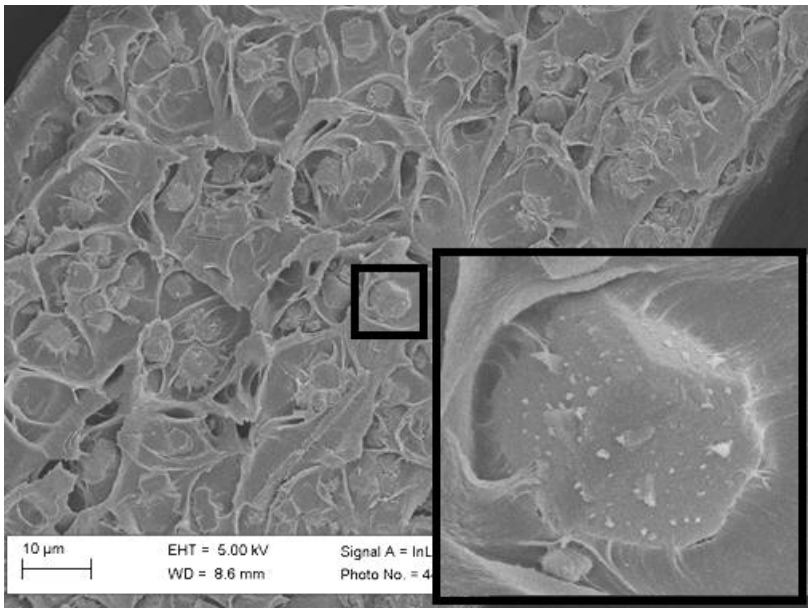

Figure 5.9: SEM picture of 25wt% 5A loading in 6FDA-DAM

Using P_D = 2.5 Barrer and P_D = 0.4 Barrer, Maxwell model selectivity predictions provided in table 5.10 appear to bracket the experimental selectivity data; however, the experimental data leans closer to the higher P_D estimate. The discrepancy in experimental data and Maxwell prediction using P_D = 2.5 Barrers could be due to imperfect adhesion in sections of the film, but overall the selectivity enhancement observed is encouraging.

Table 5.10: Experimental and predicted separation performance of 6FDA-DAM-5A mixed matrix membranes. Operating temperature of 100°C

		Average Exp. Value		Maxwell Pred.			
				P_D = 2.5 Barrer		P_D = 0.4 Barrer	
		$P_{n\text{-}C4}$	$\alpha_{n/i}$	$P_{n\text{-}C4}$	$\alpha_{n/i}$	$P_{n\text{-}C4}$	$\alpha_{n/i}$
180°C	Neat Polymer	3.2	21	-	-	-	-
	25wt% LTA 5A	3.28 ±0.1	25.03 ± 0.3	3.03	28.46	2.39	22.39
	30wt% LTA 5A	3.03	27.36	2.99	30.55	2.23	22.75
230°C	Neat Polymer	1.6	27	-	-	-	-
	25wt% LTA 5A	1.99 ± 0.2	32.05 ± 0.1	1.78	42.62	1.27	30.35

5.6. FACTORS AFFECTING FABRICATION OF MIXED MATRIX MEMBRANES

Gas separation using mixed matrix membranes has been shown to have potential for better separation performance than neat polymers. The efficiency of these membranes is not only based on the matching criteria discussed earlier, but also on proper fabrication. Sieve surface modification discussed in detail in chapter 4 is aimed at improving adhesion of the sieves to polymer thus potentially improving the performance of the mixed matrix membrane. Despite the presence of whiskers on sieve surface, other factors involved in the membrane fabrication, which are not easily quantified, may have an effect on their performance. Some of these factors will be explored in single gas transport system.

5.6.1. Concentration of $Mg(OH)_2$ whiskers

At this point it is difficult to accurately quantify the concentration of $Mg(OH)_2$ whiskers on the sieves surface required for fabrication of good mixed matrix membranes. EDS analysis of surface modified sieves that resulted in selectivity enhancement indicated ~1.55wt% Mg on the sieves. These sieves were modified via the "*simplified*" Grignard treatment method using MeTHF as solvent discussed in chapter 4. It is also difficult to ensure that every sieve is adequately treated. In a single batch treatment, sieves can be unevenly treated as shown in figure 5.10. When these sieves are used in mixed matrix membrane fabrication, there are sections of the membrane that are well adhered and sections that are not. As a result, testing different parts of a large piece of dense film, will give varying results as presented in table 5.11. Films 1 & 2 indicate sieve-in-cage morphology despite the presence of whiskers, while film 3 shows some selectivity enhancement. Sieve batch no. GT144-1 is commercial 5A treated via sol-gel Grignard treatment, using 6S DI water, with MeTHF as the solvent. The schematic in figure 5.11 is provided as a visual aid to clarify the discussion on the effect of even sieve surface treatment on the separation performance of different sections of a mixed matrix membrane. As depicted in figure 5.11, the sieves, represented by circles and squares are from the same batch of Grignard treatment; however, the circles are well treated while the squares are not. After dispersion in polymer and casting into a mixed matrix membrane, section 1 which only has good treated sieves, will be expected to perform better than section 2 which has more poorly treated sieves. The uneven surface modification could be a result of poor dispersion during the whisker growth period. It is believed that $Mg(OH)_2$ whiskers are produced during the water washing step, which is

followed by a period in which the sol stands for 30 minutes. Using the sol-gel method of Grignard treatment, the water addition step is followed by 3 bursts of sonication for 30secs at 50% amplitude. It is possible that the amount of sonication applied is insufficient for adequate dispersion. In the simplified method of Grignard treatment, the water addition step is followed by hand shaking, which may not be sufficient for dispersion. Care should be taken to ensure proper dispersion in order to attain evenly treated sieves. Slow mixing or rolling of the sol between washing steps may help increase uniformity.

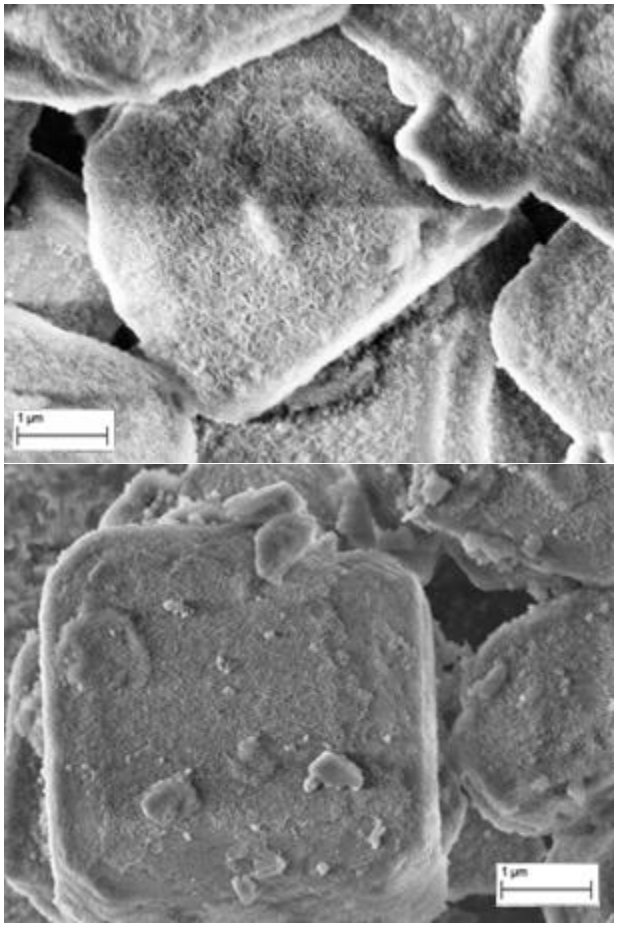

Figure 5.10: SEM of treated 5A showing inconsistency in concentration of whiskers on the sieves

Table 5.11: Varying separation performance from different sections of a mixed matrix membrane Films annealed at 180°C, tested at operating temperature of 100°C

25wt% GT 144-1	P (Barrers)	$\alpha_{n/i}$
Film 1	3.5	21.66
Film 2	3.35	20.98
Film 3	3.43	23.33

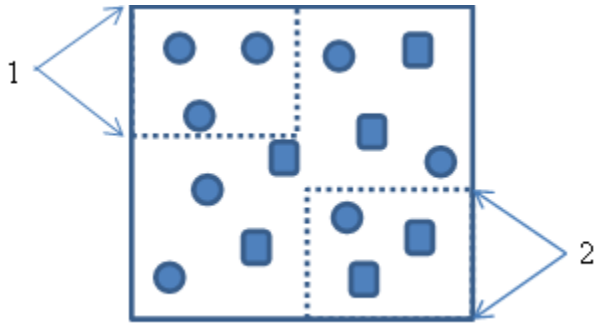

Figure 5.11: Schematic of mixed matrix membrane containing unevenly treated sieves. Circle depict well treated sieves, while squares depict poorly treated sieves

5.6.2. The length of the whiskers

The desired whisker length is not so quantifiable. It is understood that the polymer-sieve adhesion is improved by the entanglement of the polymer chains with the $Mg(OH)_2$ whiskers formed on the sieves; however the depth of entanglement, may play a role in the mixed matrix membrane performance. This can be pictured as in figure 5.12.

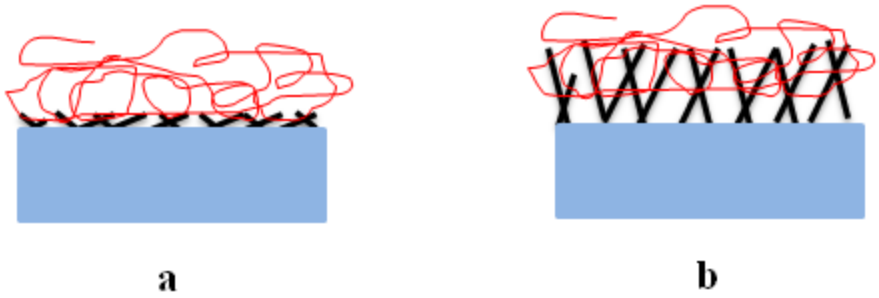

Figure 5.12: Schematic of the effect of chain length on mixed matrix membrane fabrication

Figure 5.12a depicts sieves with short whiskers, such that the polymer chains are unable to entangle adequately. During solvent evaporation, the stress can presumably easily pull the polymer from the sieves, which will result in the so-called sieve-in-cage morphology shown in figure 5.13a. On the other hand, if the whiskers are long as depicted in figure 5.12b, the polymer chains may only penetrate and entangle to a certain depth, thus leaving a leaky interface. The desired whisker length should allow the polymer chains to be adequately entangled through its depth. This will result in a firmer bond as depicted in figure 5.13b. This suggests the desired whisker length should be close to the radius of gyration of the polymer [14]. The length of the whiskers can be roughly estimated via SEM. Using the sieves that occasionally yielded positive selectivity enhancement as model for well treated sieves, the desired whisker length can be estimated to be ~100nm as shown in figure 5.14. The radius of gyration of 6FDA-DAM is estimated to be ~50nm, which is low compared to the whisker length. This size variation could explain some of the discrepancy between experimental mixed matrix membrane performance and Maxwell predictions.

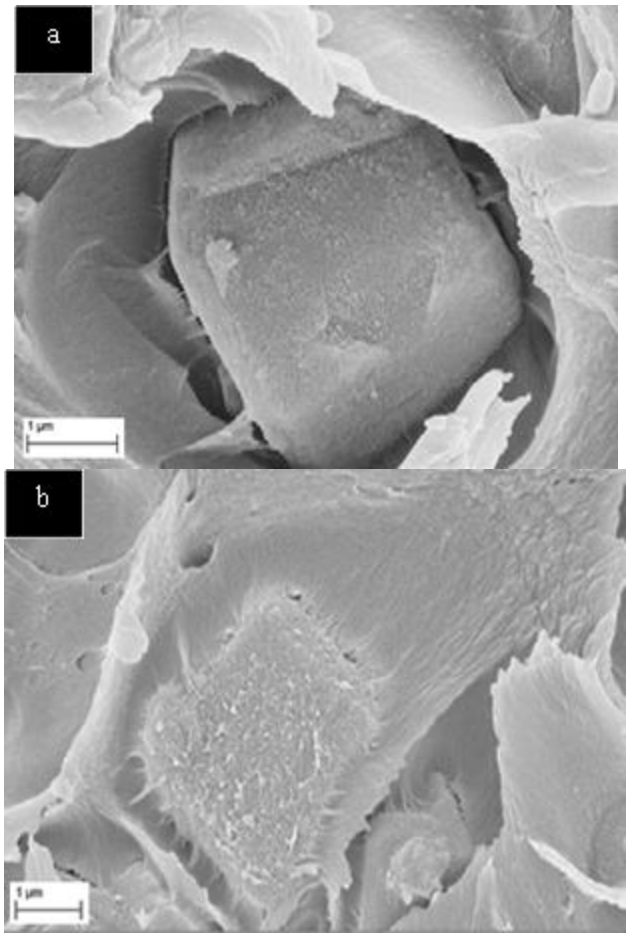

Figure 5.13: SEM of sieve bound to 6FDA-DAM: a) Weak bond resulting in Sieve-in-cage morphology, b) Firmer bond resulting in good adhesion

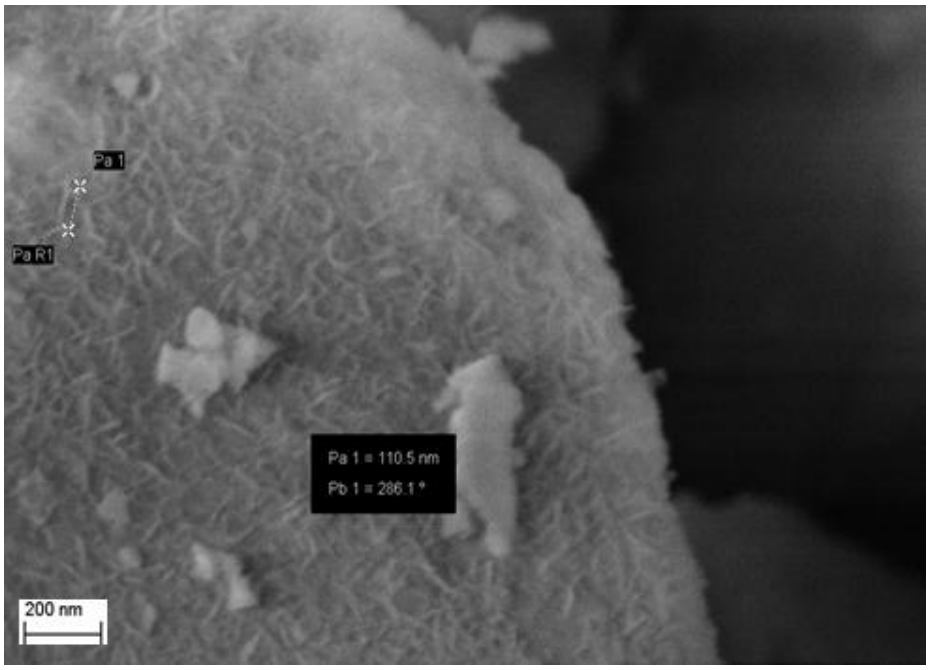

Figure 5.14: Estimate of the whisker length using SEM

There is currently no way to precisely control the length of the whiskers grown; however, the condensing period during sol-gel treatment can be used as a control. The condensing period is the length of time the sol is allowed to stand following dropwise water addition. During this time the hydrolyzed magnesium alkoxide condenses into $Mg(OH)_2$ which grows into the whisker morphology in the presence of nucleating sites. SEM in figure 5.15a-b, show sieves treated via Sol-gel method with condensing periods of 1, and 3 nights. The sieves left to stand for 1 night shows short whiskers or deposits of $Mg(OH)_2$ on their surface, while those left for 3 nights show longer whiskers.

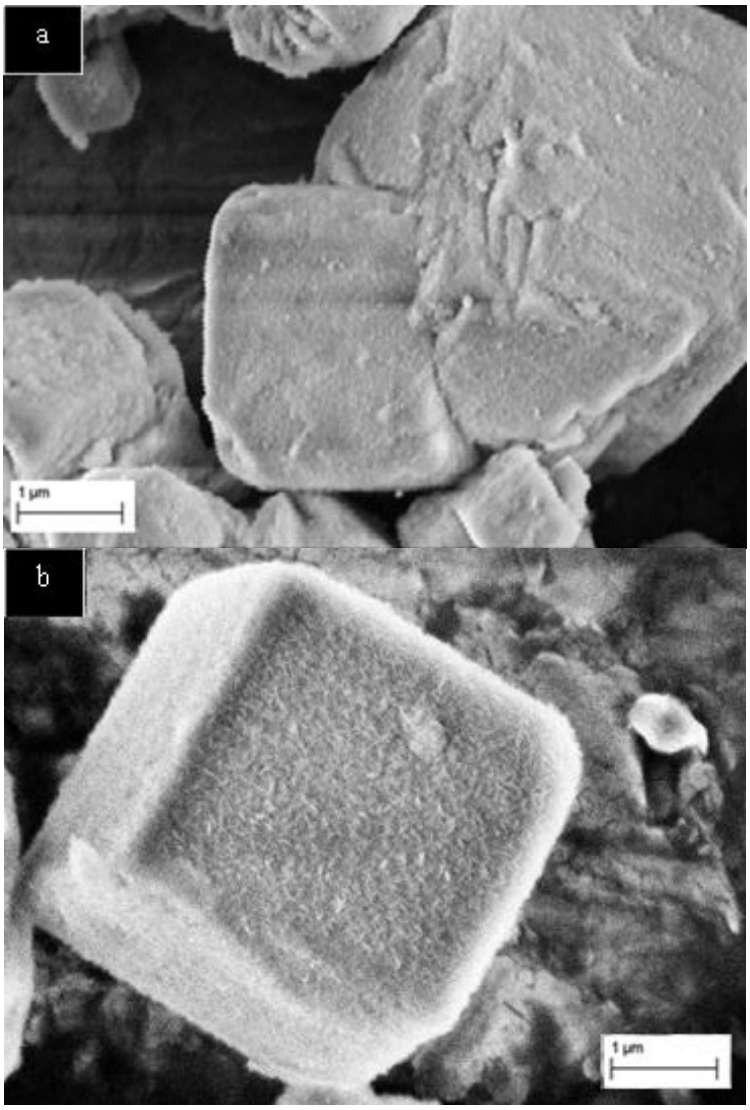

Figure 5.15: SEM showing varying whisker length resulting from varying condensation duration: a) 1 night, and b) 3 nights

5.6.3. Other: evaporation rate, and dope viscosity

Other than the entropy penalty experienced during polymer adhesion to pristine sieves, which is overcome by modification of the sieve surface, poor mixed matrix morphology has been attributed to stress encountered during solvent evaporation. Solvent

evaporation rate was reduced by casting in nitrogen filled glove bag saturated with solvent, and the film was left to sit overnight allowing the solvent to slowly evaporate.

Adams [13] studied the effect of dope viscosity on the successful fabrication of mixed matrix membranes. In his work, he observed that at higher dope viscosity (i.e. less solvent), there was significant improvement in the MMM morphology at high sieves loading, and thus higher selectivity compared to membrane fabricated using less viscous dope. This was hypothesized to relate to onset of percolation resulting from smaller interparticle spacing between the contiguous layers of MMM fabricated from low viscosity dopes [13]. Based on this information, during dope preparation, the viscosity was increased by evaporating some of the solvent using nitrogen, and then the dope was placed on a roller overnight to homogenize. The dope viscosity of the membranes used in this work were not directly measured, but were judged based on experience. An approximate dope viscosity of ~4000cps is believed to be adequate. This approximation was obtained via viscometric measurement of a sample dope.

5.7. REFERENCES

1. Das, M., *Membranes for Olefin/Paraffin Separation*, in *Chemical and Biomolecular Engineering*. 2009, Georgia Institute of Technology: Atlanta, GA.

2. Krol, J.J., M. Boerrigter, and G.H. Koops, *Polyimide hollow fiber gas separation membranes: preparation and the suppression of plasticization in propane/propylene environments.* Journal of Membrane Science, 2001. **184**(2): p. 275-286.

3. Wind, J.D., et al., *Relaxation Dynamics of CO2 Diffusion, Sorption, and Polymer Swelling for Plasticized Polyimide Membranes.* Macromolecules, 2003. **36**(17): p. 6442-6448.

4. Duthie, X., et al., *Thermal treatment of dense polyimide membranes.* Journal of Polymer Science Part B: Polymer Physics, 2008. **46**(18): p. 1879-1890.

5. Kratochvil, A., *Thickness Dependent Physical Aging and Supercritical Carbon Dioxide Conditioning Effects on Crosslinkable Polyimide Membranes for Natural Gas Purification*, in *Chemical and Biomolecular Engineering*. 2008, Georgia Institute of Technology: Atlanta.

6. Bos, A., et al., *Plasticization-resistant glassy polyimide membranes for CO2/CO4 separations.* Separation and Purification Technology, 1998. **14**(1-3): p. 27-39.

7. Wachsman, E.D. and C.W. Frank, *Effect of cure history on the morphology of polyimide: Fluorescence spectroscopy as a method for determining the degree of cure.* Polymer, 1988. **29**(7): p. 1191-1197.

8. Crank, J., *The Mathematics of Diffusion*. 2nd ed. 1975: Oxford Science Publicatios.

9. Berens, A.R. and H.B. Hopfenberg, *Diffusion and relaxation in glassy polymer powders: 2. Separation of diffusion and relaxation parameters.* Polymer, 1978. **19**(5): p. 489-496.

10. Wang, R., C. Cao, and T.-S. Chung, *A critical review on diffusivity and the characterization of diffusivity of 6FDA-6FpDA polyimide membranes for gas separation.* Journal of Membrane Science, 2002. **198**(2): p. 259-271.

11. Liu, J., *Development of next generation mixed matrix hollow fiber membranes for butane isomer separation*, in *Chemical and Biomolecular Engineering*. 2010, Georgia Institute of Technology: Atlanta.

12. Yucel, H. and D.M. Ruthven, *Diffusion in 5A zeolite. Study of the effect of crystal size*. Journal of the Chemical Society, Faraday Transactions 1: Physical Chemistry in Condensed Phases, 1980. **76**: p. 71-83.
13. Adams, R., *High Molecular Sieve Loading Mixed Matrix Membranes For Gas Separations*, in *Chemical and Biomolecular Engineering*. 2010, Georgia Institute of Technology: Atlanta.

14. Shu, S., *Engineering the performance of mixed matrix membranes for gas separation*, in *Chemical and Biomolecular Engineering* 2007, Georgia Institute of Technology: Atlanta

CHAPTER 6

MIXED GAS TRANSPORT OF BUTANE ISOMERS IN 6FDA-DAM-BASED DENSE FILMS

6.1. ABSTRACT

This chapter will address the transport of butane isomer mixtures through dense 6FDA-DAM films. Permeation measurements were made using 3 feed compositions. Experimental mixed gas data indicated some interesting transport behavior, which was hypothesized to result from a combined effect of difference in penetrant size and shape. Two hypotheses were presented; the first attributed the mixed gas transport behavior to hindered transport of n-C4 into the Langmuir environment due to the presence of i-C4. This hypothesis led to the development of a new transport model termed the Hindered Hole Filling (HHF) model. The second hypothesis attributed the observed transport behavior to a change in the accessible fractional free volume of a penetrant due to the presence of a co-penetrant. This hypothesis led to the introduction of a fitting parameter, termed the CAUFFV fit. Both the HHF and CAUFFV fit showed better agreement with experimental data, than the commonly accepted dual mode transport model. Mixed gas sorption measurements were made to further investigate the mixed gas transport behavior in this system. Sorption measurements were not in agreement with the commonly accepted dual mode sorption model and either the HHF model or the CAUFFV fit. This suggests the mixed gas sorption and transport behaviors are not completely understood at

present. With the aim of improving separation performance in mixed gas systems, permeation tests were made using mixed matrix membranes at sieve loadings of 25 wt% and 30 wt% annealed at different temperatures. A selectivity increase of ~9% was observed at 30 wt% sieve loading annealed at 180°C.

6.2. MIXED GAS PERMEATION IN NEAT 6FDA-DAM

Pure gas transport often gives more optimistic separation performance than would be observed under realistic operating conditions of mixtures. As discussed in chapter 2 competitive sorption for the limited Langmuir sites in a glassy polymer, and bulk flow contributions are possible factors that are known to complicate mixture gas transport even in the absence of plasticization of the matrix. Plasticization complications were avoided by restricting the partial pressures of both feed components to values lower than the plasticization range (i.e. pressure range in figure 5.4). The absence of plasticization can be verified by the always concave nature of the pure (see figure 5.4) and mixed gas permeation isotherms vs. the pressure axes (see figures 6.1 – 6.3). The partial immobilization model has been extended to account for competitive sorption and explains decrease in the permeability of a penetrant with increasing partial pressure of the co-penetrant.

As noted in the context of Equations 2.17 - 2.24, Koros and Kamaruddin [1] showed that it can be important to account for the frame of reference effect (bulk flow effect) on the overall flux of a penetrant. Equations 2.17 – 2.24, were used to predict the transport behavior of butane isomer mixtures composing of 5 mol% n-C4/95 mol% i-C4,

42 mol% n-C4/58 mol% i-C4, and 95 mol% n-C4/5 mol% i-C4. These predictions were compared to experimental data as seen in figures 6.1 – 6.3. The dual mode transport model predicts a reduction in n-C4 permeability due to competitive sorption, and a negligible effect of bulk flow for this particular case. Isobutane is predicted to experience a reduction in permeability due to competition, but a small increase in permeability due to bulk flow effect, resulting in an overall decrease in selectivity. Figures 6.1 – 6.3 clearly do not show a good fit of this model to experimental data for n-C4 permeability (Figures 6.1a, 6.2a, 6.3a) or n-C4/i-C4 selectivity (Figures 6.1b, 6.2b, 6.3b). Isobutane permeability plots are provided in appendix D. As seen in Figures 6.1 – 6.3, experimental data suggests that the permeability of n-C4 is more suppressed by the presence of i-C4 than anticipated due to competition effects. This is similar in some respects to complex transport behaviors observed by Raharjo [2, 3] in a system of CH_4 and n-C4 mixture in PTMSP, and by Freeman [4] in a system of H_2 and n-C4. In both of these cases, however, a suppression of the permeability of CH_4 and H_2 were observed, which was described as a blocking effect of the more condensable n-C4. In this work we present a system of n-C4 and i-C4 which have similar condensability as indicated by sorption selectivity near unity (refer to table 5.1), so the observed transport cannot solely be attributed to one gas being more condensable than the other. A similar trend in mixed gas permeability was observed for butane isomer system separation via MFI membranes [5]. It was reported that in a binary mixture, n-C4 diffuses extremely slower and i-C4 diffuses only slightly faster in comparison with the pure components. This was explained via molecular simulation to result from i-C4 molecules preferentially located at the intersections between the straight

and zig-zag channels of the MFI structure. The presence of the slow-diffusing molecules at the intersection obstructs the diffusion of both molecules along the straight channels.

Our work with this C4 isomer pair also shows somewhat similar mixed gas results. While there are not pores per se, in the glassy polyimide we have studied, the rigid polyimide does show complex dual mode sorption behavior suggesting morphological features that the two isomers probe. Two hypotheses have been proposed to explain this mixed gas behavior of butane isomers in 6FDA-DAM.

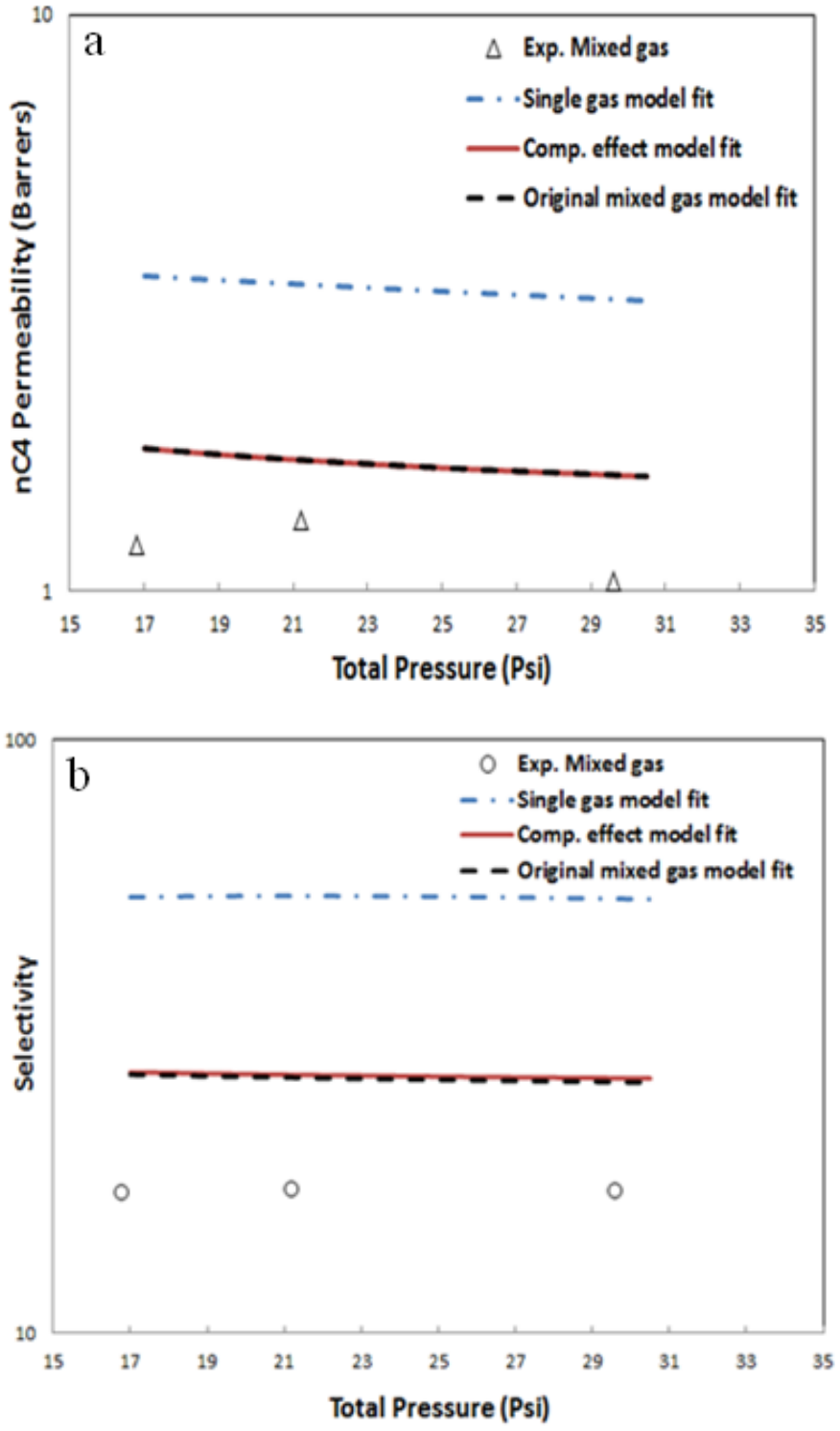

Figure 6.1: Transport performance of 5 mol% n-C4/ 95 mol% i-C4 in neat 6FDA-DAM annealed at 230°C at operating temperature of 100°C. Comparing experimental data with original mixed gas transport model a) n-C4 permeability, b) n-C4/i-C4 selectivity

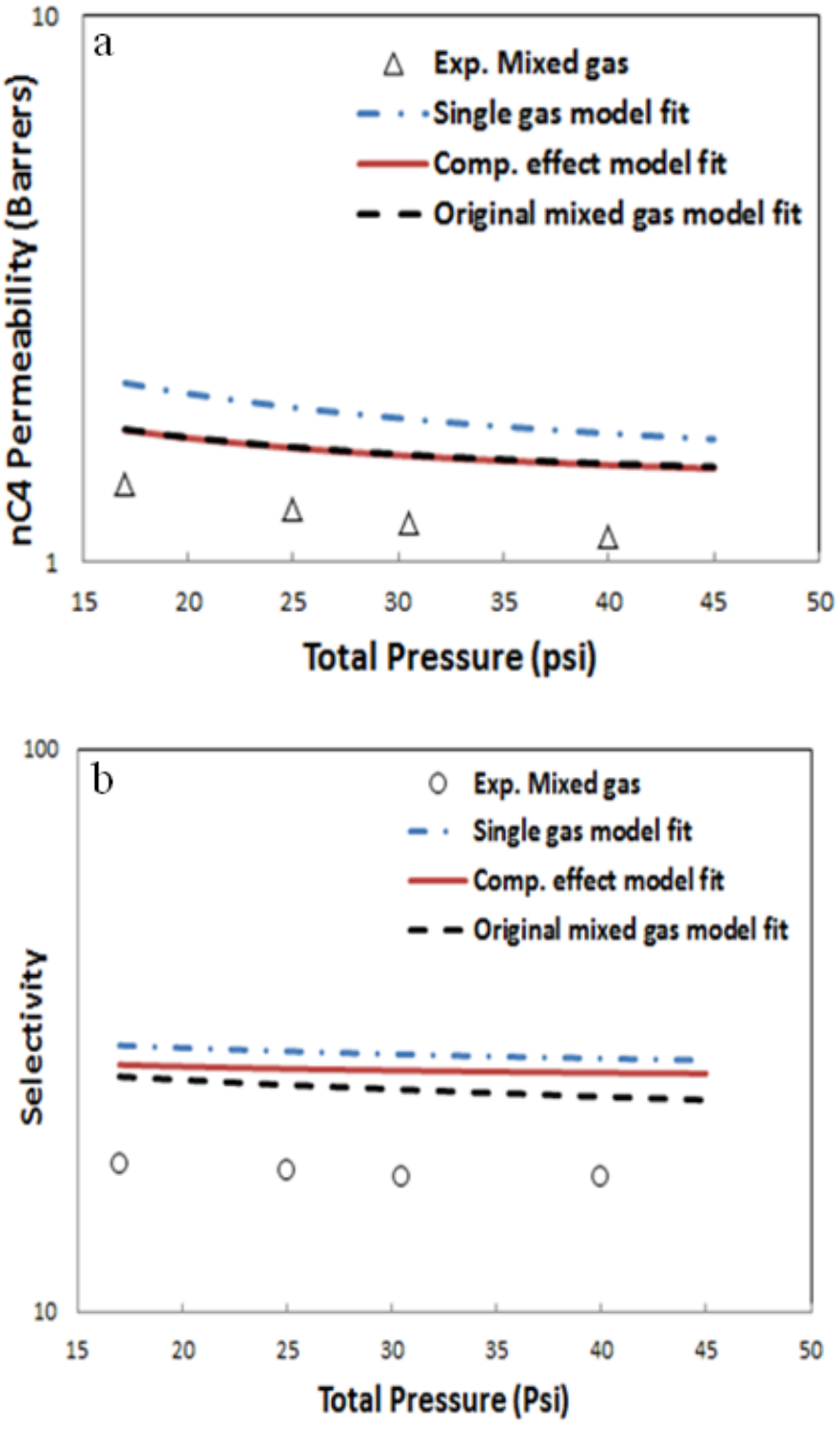

Figure 6.2: Transport performance of 42 mol% n-C4/ 58 mol% i-C4 in neat 6FDA-DAM annealed at 230°C at operating temperature of 100°C. Comparing experimental data with original mixed gas transport model a) n-C4 permeability, b) n-C4/i-C4 selectivity

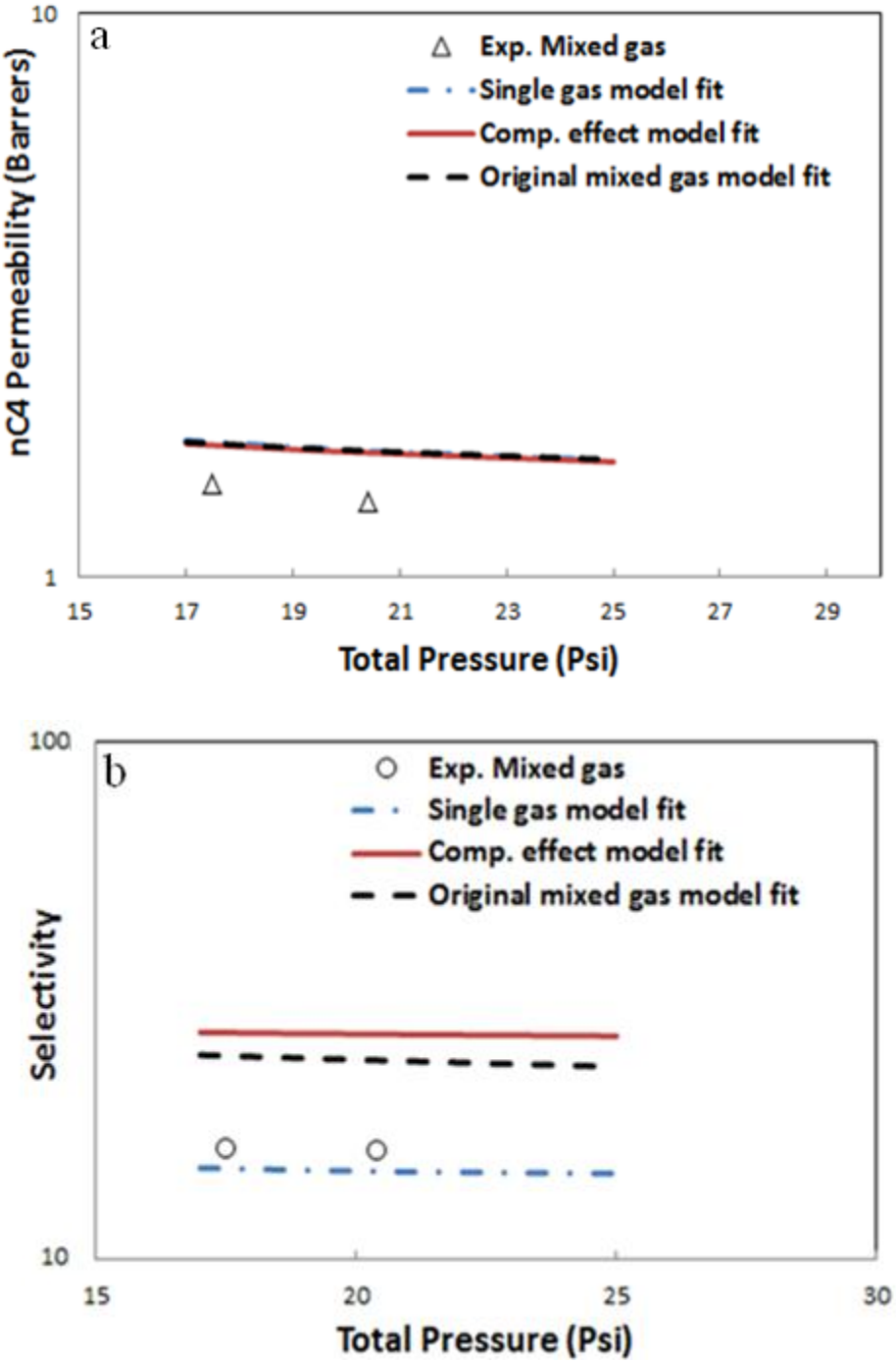

Figure 6.3: Transport performance of 95 mol% n-C4/ 5 mol% i-C4 in neat 6FDA-DAM annealed at 230°C at operating temperature of 100°C. Comparing experimental data with original mixed gas transport model a) n-C4 permeability, b) n-C4/i-C4 selectivity

6.2.1. Hypothesis 1: Change in equilibrium isotherm of n-C4

In a mixture system of butane isomers, although local equilibrium is still believed to exist, the nature of that local equilibrium can be altered in a mixed gas vs. the pure gas case. For instance, the slower moving molecule; i-C4, is expected to take longer to vacate microvoids due to its lower Langmuir mode diffusivity, shown in Table 6.1, versus the corresponding value for n-C4. This fact notwithstanding, the good fit of the permeation data for pure i-C4 as well as n-C4 (see figure 5.4) suggests that the assumption of local equilibrium is valid for the pure components. On the other hand, in the mixture feeds, it appears possible that the exchange rate of i-C4 relative to the local diffusion rate of n-C4 could restrict local equilibrium access of n-C4 to those sites. This does *not* imply a breakdown of local equilibrium, but it does reflect an added complication that has not been observed in prior work with other systems involving smaller penetrants such as CO_2, CH_4, C_3H_6, and C_3H_8. As a control study, permeation tests were performed on a mixture of C_3H_8/C_3H_6 using 6FDA-DAM with the same conditioning, and experimental results in figure 6.4 appear to show fewer problems with the simple assumptions leading to local sorption equilibrium model predictions using equations 2.17 – 2.24. The observed difference in the transport of butane isomer mix vs propane/propylene mix could be due to the combination of two factors: (1) the larger difference in the kinetic diameter and consequently diffusion coefficients, between i-C4 and n-C4 compared to propane and propylene (see table 6.1), (2) the more compact shape of propane and propylene illustrated in Figures 6.5c & d respectively, compared to the spheroid i-C4 vs linear n-C4 illustrated in Figures 6.5a & b respectively. Table 6.1 summarizes collision diameters for the hydrocarbon pair. The 0.1Å difference in kinetic diameter for

propane/propylene compared to the larger 2Å difference for n-C4/i-C4 suggests a larger difference in the diffusion coefficient for the butane isomers. Experiments show that C_3H_8 has a D_H of 4.76e-10 cm^2/s, and that of C_3H_6 is 3.2e-09 cm^2/s which comprises only a 6.8X difference, compared to the 26X difference in the D_H values of n-C4 and i-C4. Difference in the diffusion coefficient can be related to the difference in the kinetic diameters of the penetrants, with diffusion coefficients generally decreasing strongly with increasing effective diameters [6]. The difference in diffusion coefficients alone will not accurately explain the observed mixed gas transport behavior of C4 isomers. For example, Kamaruddin [1] observed 34X difference in D_H values for CO_2 and CH_4 in 6FDA-TADPO polypyrrolone and Das [7] observed a 62X difference in D_H values for propane and propylene in 6FDA-6FpDA. Despite the large differences in diffusion coefficients their mixed gas transport data were in good agreement with the dual mode model.

Table 6.1: Diffusion coefficients of penetrants in 6FDA-DAM annealed at 230°C

	D_D (10^{-10} cm^2/s)	D_H (10^{-10} cm^2/s)	F	Kinetic Diameter
$n\text{-}C_4H_{10}$	21.4	3.80	0.178	~3.95 - 4Å
$i\text{-}C_4H_{10}$	1.28	0.146	0.114	6.0Å
C_3H_6	321	32	0.097	3.82Å
C_3H_8	38	4.76	0.125	3.95Å

The above results, which we are quite sure are correct, suggest to us that there may be an additional feature present for the n-C4/i-C4 pair that is not present in the other pairs. While this feature is not currently identified, we suspect it may reflect the much

larger difference in kinetic diameter (roughly 1.0Å – 2.0Å) vs. 0.3 – 0.5Å for CO_2/CH_4 and C_3H_8/C_3H_6. We suggest that this difference in kinetic diameter can significantly affect mixed gas transport through a "rigid" glass, and that although the diffusion coefficients D_H & D_D from pure gas analyses are valid, in the presence of a mixture, we suspect but cannot yet prove, that the scale of the required perturbation in local segmental morphology of the glass to enable transport of i-C4 vs. nC4 is partly responsible for the observed difficulties in mixed gas predictions. This mixed gas behavior can be exacerbated in mixed matrix membranes, where apparent selectivity enhancements vs. pure polymer fall below expected levels as predicted by Maxwell model and dual mode transport model respectively. Of course, many factors related to complex adhesion and rigidification due to the presence of the dispersed phase may also be factors, so the mixed matrix membrane cases are even more difficult to analyze definitively.

To explain the observed mixed gas transport behavior by introducing the simplest additional fundamental feature (Occam's razor [8]), we explore two speculative features to help improve the description of mixed gas data

Due to the rigid nature of the polymer chains, the linearity and compact nature of gas molecules such as CO_2, CH_4, n-C4, propane and propylene favors entrance and exit of microvoids, which will be more difficult for bulky i-C4 molecules. Hence, in a system of n-C4 and i-C4 mixture, due to the difficulty i-C4 encounters in exiting the microvoids, there may be much less vacant microvoids (even beyond that accounted for by simple Langmuir competition based on the respective pure component affinity constants) available for n-C4. Although the shape difference may play a more significant role in the observed transport behavior, it is difficult to quantify and predict.

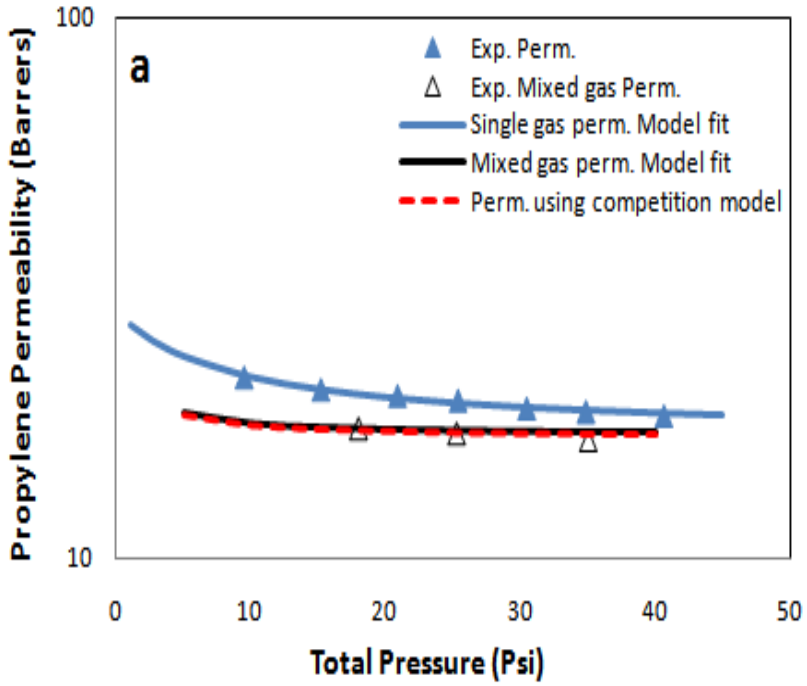
a
Exp. Perm.
Exp. Mixed gas Perm.
Single gas perm. Model fit
Mixed gas perm. Model fit
Perm. using competition model
Propylene Permeability (Barrers)
100
10
0
10
20
30
40
50
Total Pressure (Psi)

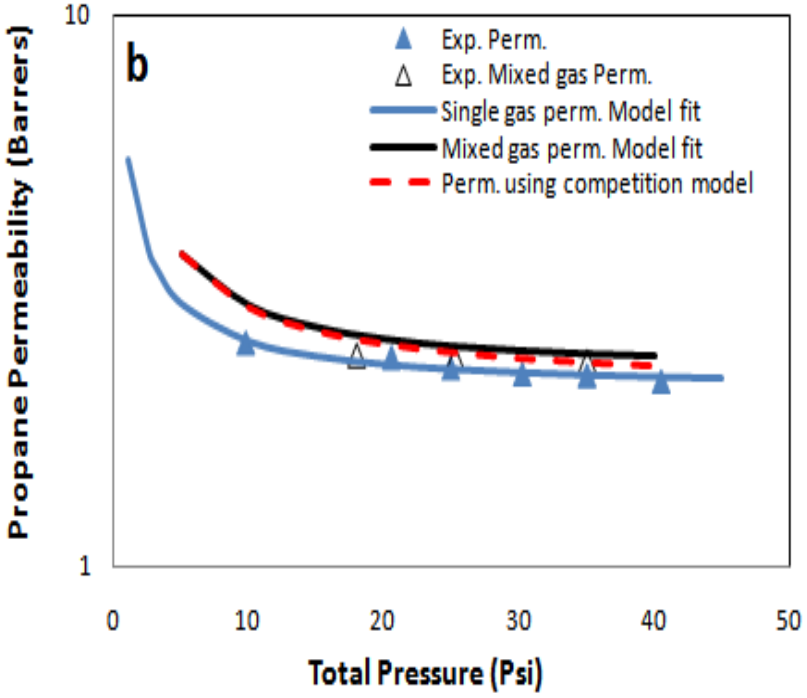
b
Exp. Perm.
Exp. Mixed gas Perm.
Single gas perm. Model fit
Mixed gas perm. Model fit
Perm. using competition model
Propane Permeability (Barrers)
10
1
0
10
20
30
40
50
Total Pressure (Psi)

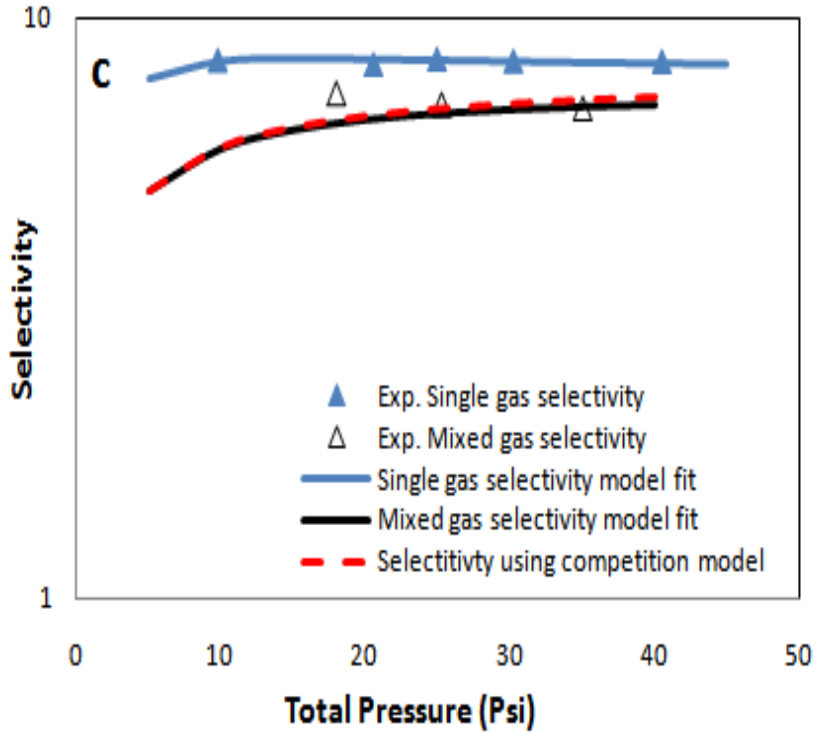

Figure 6.4: Separation performance of neat 6FDA-DAM annealed at 230°C, at operating temperature of 100°C in pure gas and 50 mol% C_3H_6/50 mol% C_3H_8 mixture permeation system a) C_3H_6 permeability, b) C_3H_8 permeability, and c) C_3H_6/C_3H_8 selectivity

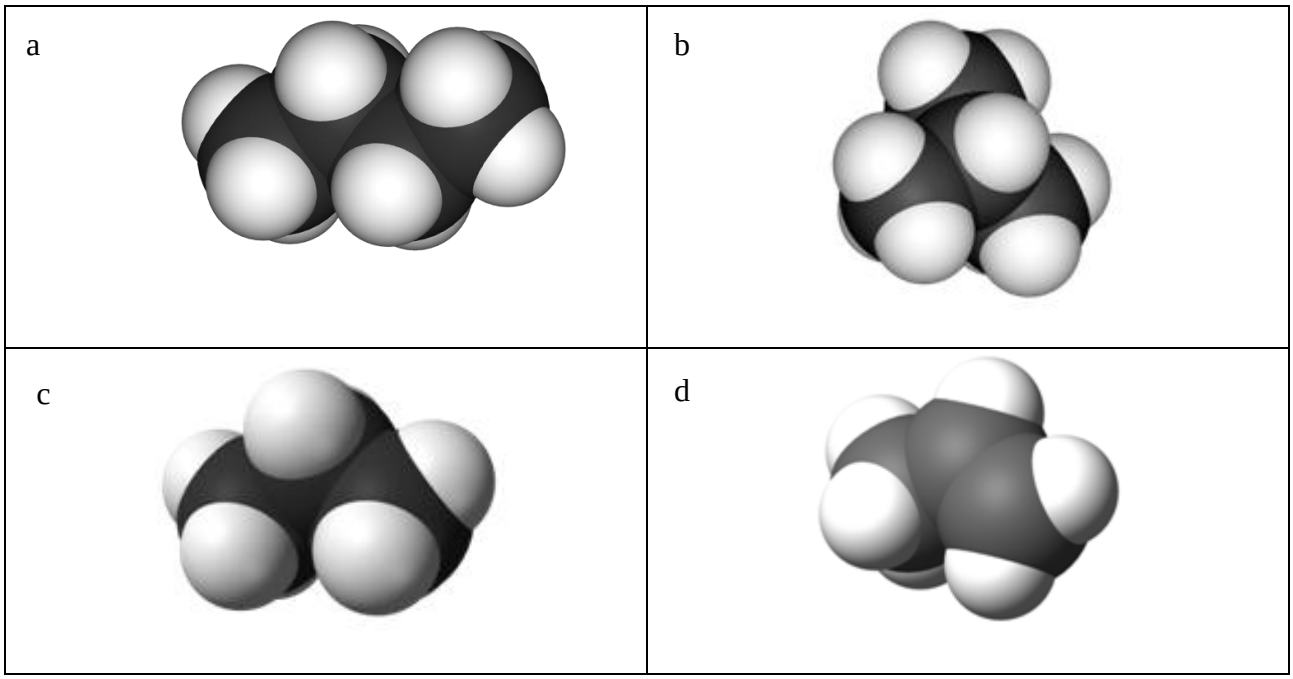

Figure 6.5: Molecular diagrams of: a) n-butane, b) Isobutane, c) propane, and d) propylene

Based on our hypothesis, we suggest that the restriction of n-C4 access to microvoids can result in an unusual change in local equilibrium for n-C4 that is not captured by the simple expression in Equation 2.14.

$$P_A^* = k_{D_A} D_{D_A} + \frac{C'_{H_A} D_{H_A} b_A}{1 + b_A p_A + b_B p_B} = k_{D_A} D_{D_A} \left(1 + \frac{K_A F_A}{1 + b_A p_A + b_B p_B}\right) \qquad (2.14)$$

Hindrances of access to the local microvoids by the slow exchange between i-C4 Henry's law and microvoid populations effectively reduces their availability to n-C4. This does not mean that local equilibrium of either n-C4 or i-C4 has broken down; however, it effectively means only that the affinity constant for n-C4 has been altered in the mixture. In this case, the n-C4 does not kinetically impede i-C4, but i-C4 impedes n-

C4 exchange between Henry's environment and microviods. Thus the standard classical dual mode sorption model cannot adequately describe n-C4 in 6FDA-DAM when in a mixture with i-C4. Since i-C4 does not experience this change in apparent affinity coefficient, its transport through microvoids is unrestricted and it only experiences simple competition and the bulk flow effect with n-C4.

If the above picture is valid, the affinity parameter, $b_{n\text{-}C4}$, can no longer be considered a constant equal to the ratio of a forward and reverse kinetic rate constant as is common as is the case for the classical Langmuir model, viz, [9]:

$$\text{site} + \text{gas molecule} \underset{k_{-1}}{\overset{k_1}{\rightleftharpoons}} \text{site–molecule complex}$$

$$b_{n-C4} = \frac{k_1}{k_{-1}} \tag{6.1}$$

Local equilibrium is attained when at any depth across the area of a film; the chemical potential of a particular gas is the same in both the dissolved and Langmuir environment

$$at\ any\ l = x, \qquad \mu_{n-C4}^{Dissolved} = \mu_{n-C4}^{Langmuir} = \mu_{n-C4}$$

For the case in which the forward "reaction" is restricted, the ratio no longer remains constant. The affinity parameter of n-C4 is proposed here to depend upon the feed composition and an appropriate measure of microvoid occupancy. This relationship expressed in Equation 6.2 will be referred to as the "Hindered Hole Filling (HHF) Model" and is shown to give a better fit (shown in Figures 6.6 – 6.8) to experimental data

as compared to the model using competition and bulk flow (Equations 2.17 – 2.24). Isobutane permeability plots are provided in appendix D. As a result of the "hindered holes", a new local equilibrium is attained.

$$\text{site}^* + \text{gas molecule} \underset{k_{-1}}{\overset{k_1^*}{\rightleftharpoons}} \text{site}^* - \text{molecule complex}$$

$$b'_{n-C4} = \frac{k_1^*}{k_{-1}} \tag{6.2}$$

$$at\ any\ l = x, \qquad \mu^*_{n-C4,Dissolved} = \mu^*_{n-C4,Langmuir} = \mu^*_{n-C4}$$

$$where\ \ \mu^*_{n-C4} \neq \mu_{n-C4}$$

We propose the simplest form of a modified affinity constant to address this added complication, since this avoids the need for an empirical adjustable parameter, viz,

$$b'_{n-C4} = b_{n-C4}(1 - \theta_{i-C4}) \tag{6.3}$$

$$\theta_{i-C4} = \frac{b_{i-C4}p_{i-C4}}{1 + b_{i-C4}p_{i-C4}} \tag{6.4}$$

$$\lim_{p_{i-C4}\to\infty} b'_{n-C4} = 0$$

$$\lim_{p_{i-C4}\to 0} b'_{n-C4} = b_{n-C4}$$

The Hindered Hole Filling (HHF) model, describes a system, in which the probability of a microvoid being available to participate in a diffusion jump of a faster moving molecule, from the dissolved environment to the hole (D-H Jump), is reduced due to the presence of a slow diffusing Langmuir sorbed molecule. According to this model, the probability of a D→H diffusion jump is not negligible as otherwise stated in

chapter 2. Although the Barrer model, provided in equation 2.11, could be extended to mixture gas systems, we do not expect it would account for this phenomenon, since the model would maintain the assumption that the affinity coefficient remains constant. In describing the mixed gas transport of CH_4 and n-C4 mixture through PTMSP, Raharjo [2] defined D_H as an exponential relation to the product of the average concentration of n-C4 in the microvoids and an *empirical* parameter that quantifies the blocking effect in the microvoid. Although this gave a good fit to their experimental data, it does not allow for predictions, and there is no known physical basis for the empirical parameter. The HHF model provides a much simpler first order model *with no additional required parameters*.

The dual mode permeability expression for n-C4, while accounting for the "Hindered Hole", is given in Equation 6.5. The derivation details are presented in Appendix D.

$$P^*_{n-C4} = k_{D_{n-C4}} D_{D_{n-C4}} + \frac{C'_{H_{n-C4}} b'_{n-C4} D_{H_{n-C4}}}{1 + b'_{n-C4} p_{n-C4} + b_{i-C4} p_{i-C4}} \tag{6.5}$$

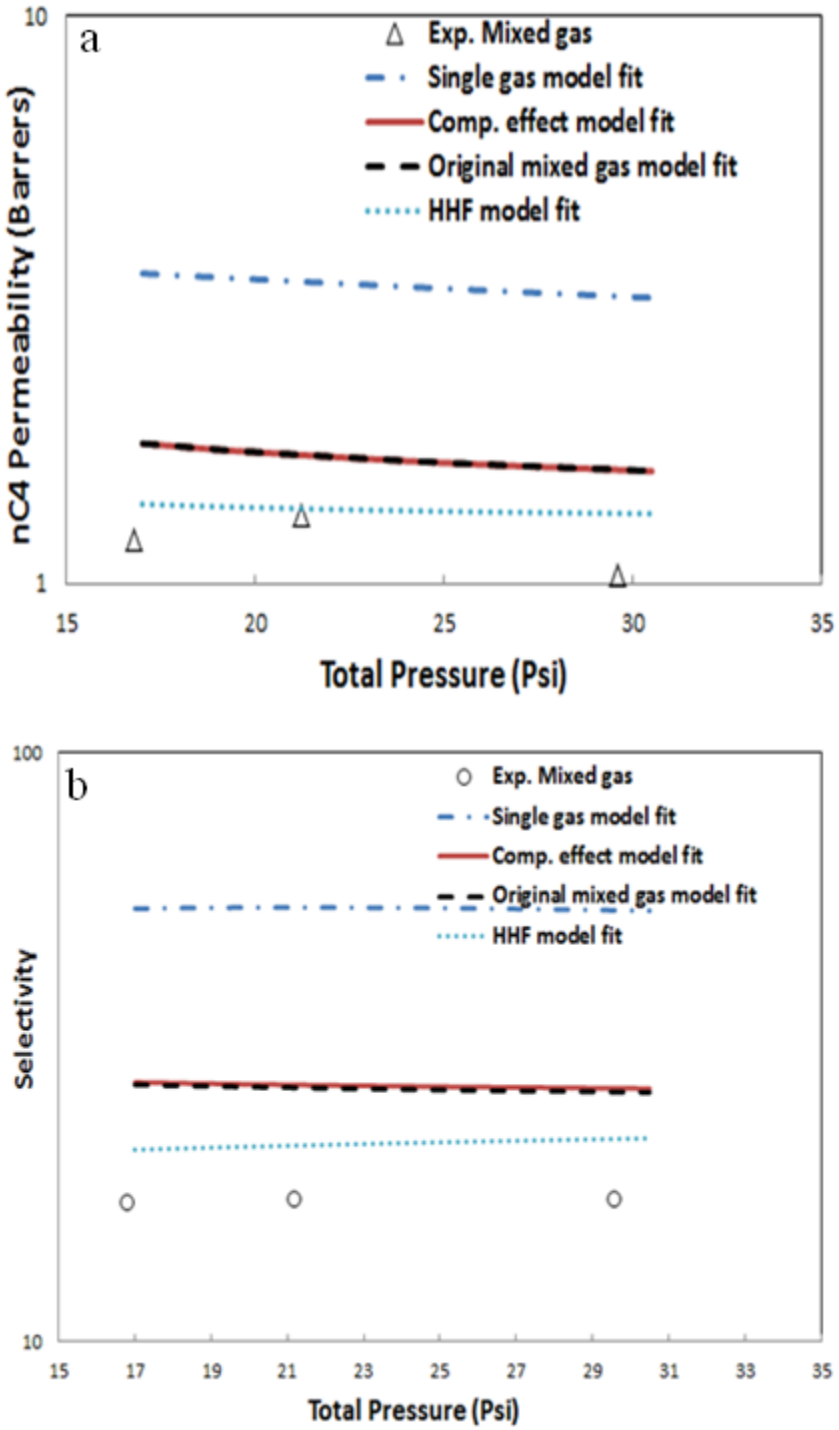

Figure 6.6: Transport performance of 5 mol% n-C4/ 95 mol% i-C4 in neat 6FDA-DAM annealed at 230°C, at operating temperature of 100°C. Comparing experimental data with HHF model, a) n-C4 permeability, b) n-C4/i-C4 selectivity

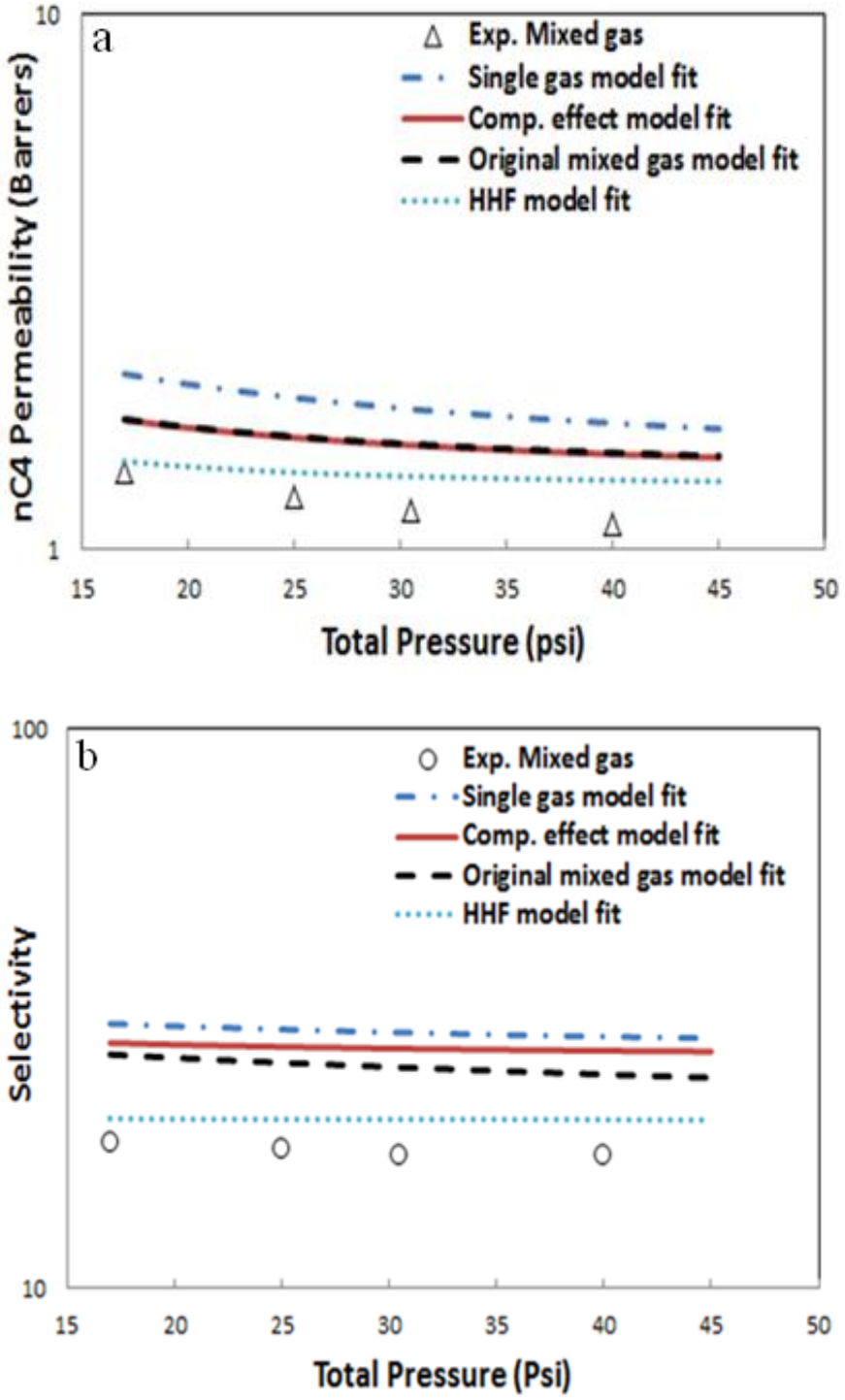

Figure 6.7: Transport performance of 42 mol% n-C4/ 58 mol% i-C4 in neat 6FDA-DAM annealed at 230°C, at operating temperature of 100°C. Comparing experimental data with HHF model, a) n-C4 permeability, b) n-C4/i-C4 selectivity

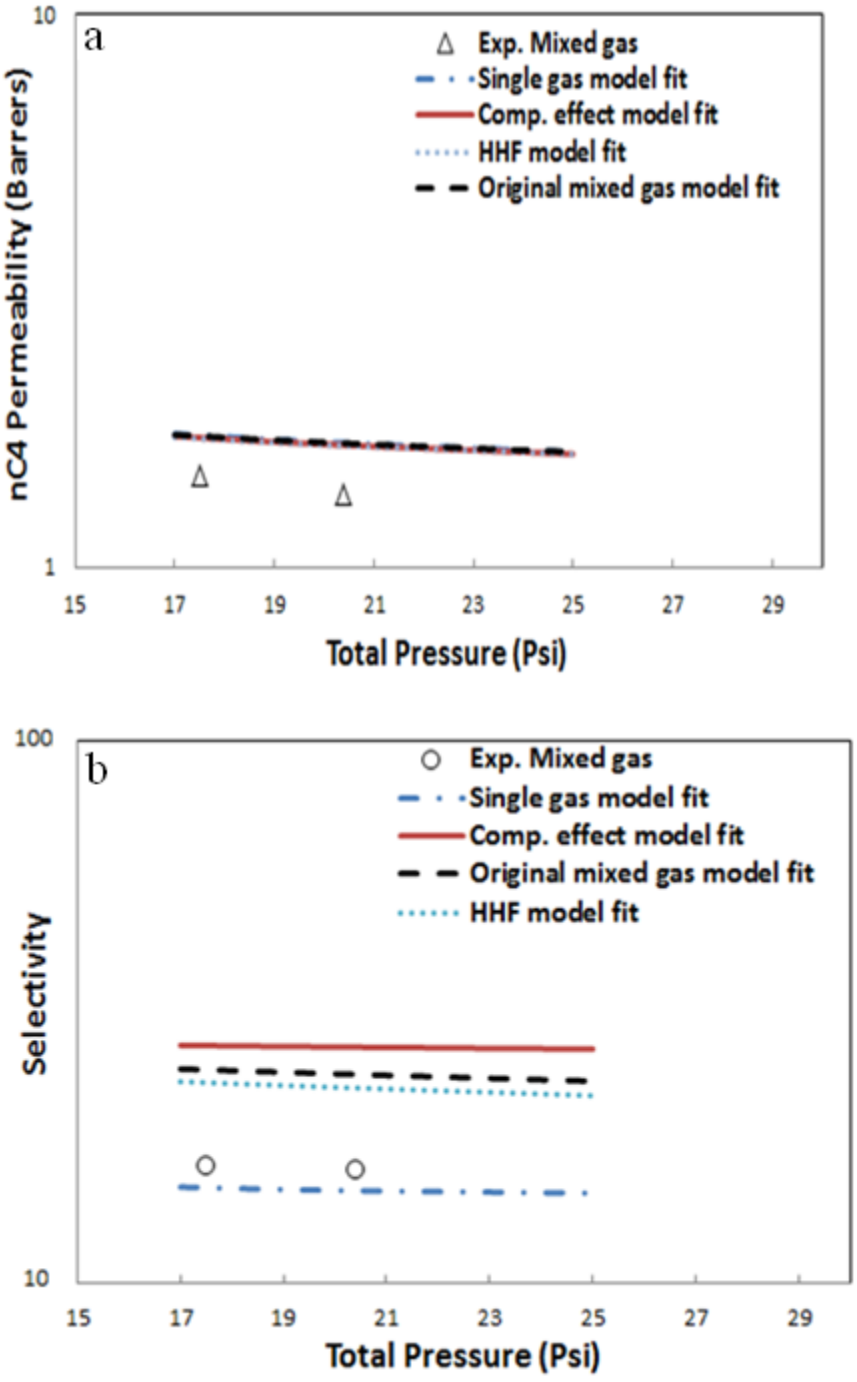

Figure 6.8: Transport performance of 95 mol% n-C4/ 5 mol% i-C4 in neat 6FDA-DAM annealed at 230°C, at operating temperature of 100°C. Comparing experimental data with HHF model, a) n-C4 permeability, b) n-C4/i-C4 selectivity

Errors resulting from HHF predictions were compared to those from the dual mode model predictions (Equations 2.17 – 2.24). This comparison is shown in Appendix D. The comparison shows that the HHF model gives significantly less error, especially for feed compositions of 42 mol% and 5 mol% n-C4. On average for the feed composition of 5 mol% n-C4, the selectivity deviation of the HHF model is ~2X smaller than that of the competition and bulk flow model. The deviation is ~3X smaller for 42 mol% n-C4 feed composition. There is little improvement in the deviation for 95 mol% n-C4 feed composition suggesting the HHF model breaks down at low i-C4 concentrations, thus not fully describing the system.

6.2.2. Hypothesis 2: Change in accessible unrelaxed fractional free volume

Park and Paul [10], explain that for every polymer, each gas has access to a different FFV, as a result of their variation in size and structure. The commonly accepted definition of FFV is:

$$FFV = \frac{(V - V_0)}{V} \tag{6.6}$$

$$V_0 = 1.3 \sum_{k=1}^{K} (V_W)_k \tag{6.7}$$

where, K is the total number of groups into which the repeat unit structure of the polymer is divided, $(V_W)_k$ is the van der Waals volume of the various groups in the polymer structure obtained from tables by van Krevelen [11], V is the specific volume of the glass at a specific temperature, and V_0 is the occupied specific volume of the polymer chain.

In the new correlation, Park and Paul [10] define the FFV with an empirical factor dependent on a gas.

$$(FFV)_n = \frac{(V - (V_0)_n)}{V} \tag{6.8}$$

$$(V_0)_n = \sum_{k=1}^{K} \gamma_{nk}(V_W)_k \tag{6.9}$$

where, γ_{nk} represents a set of empirical factors to be determined that depend on gas n and group k.

Given that C_H' is related to the FFV of the polymer [12-15] via equation 2.7, it follows that its value can differ with gas structure and shape. The dual mode model that accounts for competition in the microvoid assumes negligible effect of mixture on the C_H' value of a gas. One could argue that there exists a mutual effect on C_H' for each gas. The presence of two gases with different sizes and structures might change the FFV *available to each gas*.

$$C_{H_A}' = \left(\frac{V_g - V_l}{V_g}\right)\rho_A^* \tag{2.7}$$

To pursue this concept, it is hypothesized that in the presence of n-C4, i-C4 gains access to more unrelaxed free volume than it could have in a pure gas system. The initial presence of an n-C4 molecule in a hole (originally too small to fit an i-C4 molecule), may cause the polymer chains to be flexible enough to allow entrance of an i-C4 molecule, once n-C4 vacates the hole. This gives i-C4 access to more unrelaxed free volume in a mixture; however, due to the slow diffusion rate of i-C4 out of a microvoid, n-C4

experiences a reduction in the amount of accessible free volume. We have used an empirical parameter, $\varepsilon_{i,j}$, to illustrate the degree of this effect of a gas j on gas i.

Based on this hypothesis, we now define the diffusion-based permeability as Equation (6.10).

$$P_i^* = k_{D_i} D_{D_i} + \frac{\varepsilon_{i,j} C'_{H_i} b_i D_{H_i}}{1 + b_i p_i + b_j p_j} \tag{6.10}$$

and the mobile weight fraction as Equation (6.11).

$$\omega_i = \left(1 + \frac{\varepsilon_{i,j} F_i K_i}{1 + b_i p_i + b_j p_j}\right) \frac{k_{D_i} p_i M_i}{22400\rho} \tag{6.11}$$

Figures 6.9 – 6.11 show the fit of experimental data to the model. Isobutane permeability plots are provided in appendix D. The best fit values of $\varepsilon_{i,j}$, are given in table 6.2.

Table 6.2: Approximate values of $\boldsymbol{\varepsilon_{ij}}$

	n-C4	i-C4
ε_{ij}	0.14	2.10

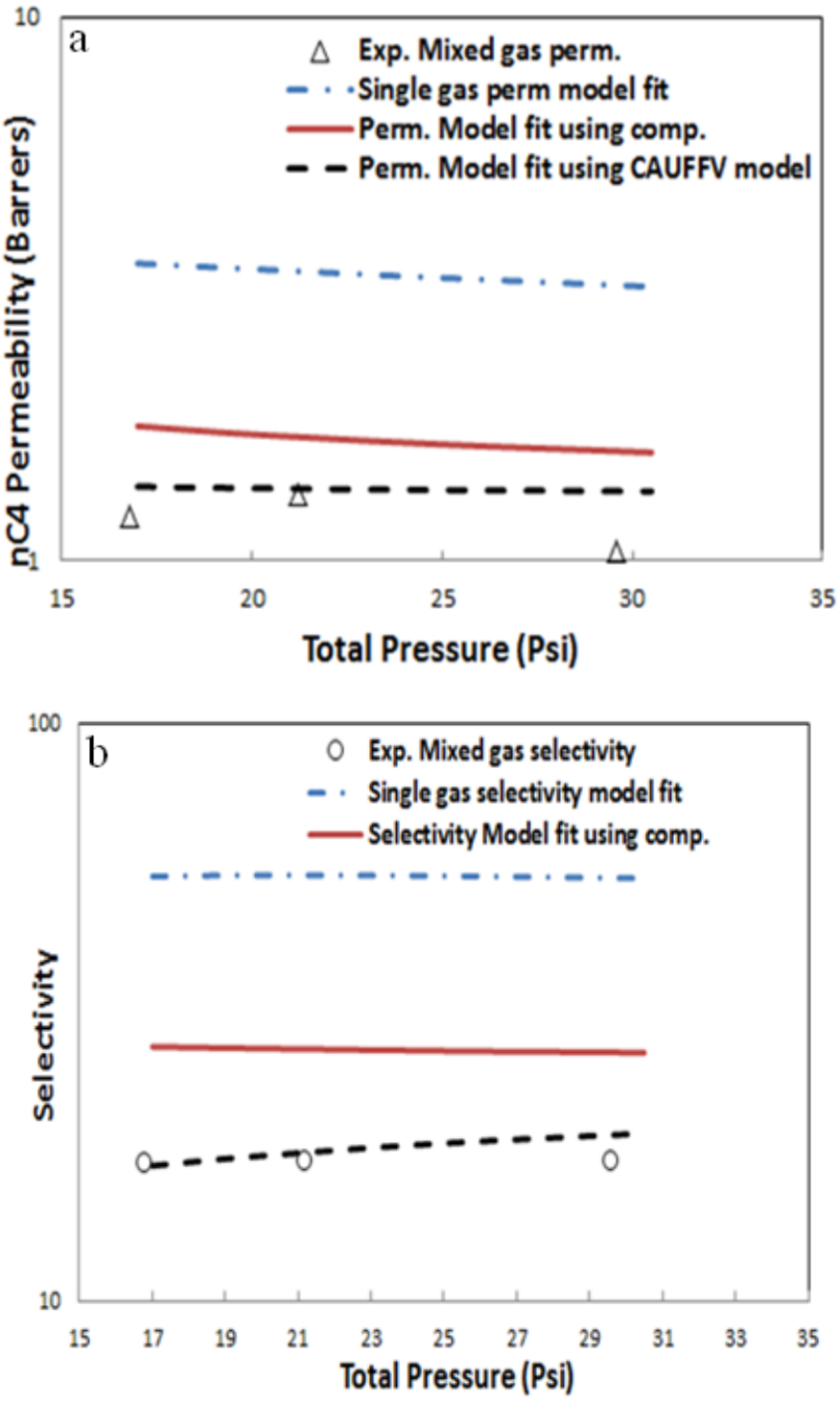

Figure 6.9: Transport performance of 5 mol% n-C4/ 95 mol% i-C4 in neat 6FDA-DAM annealed at 230°C, at operating temperature of 100°C. Comparing experimental data with CAUFFV fit, a) n-C4 permeability, b) n-C4/i-C4 selectivity

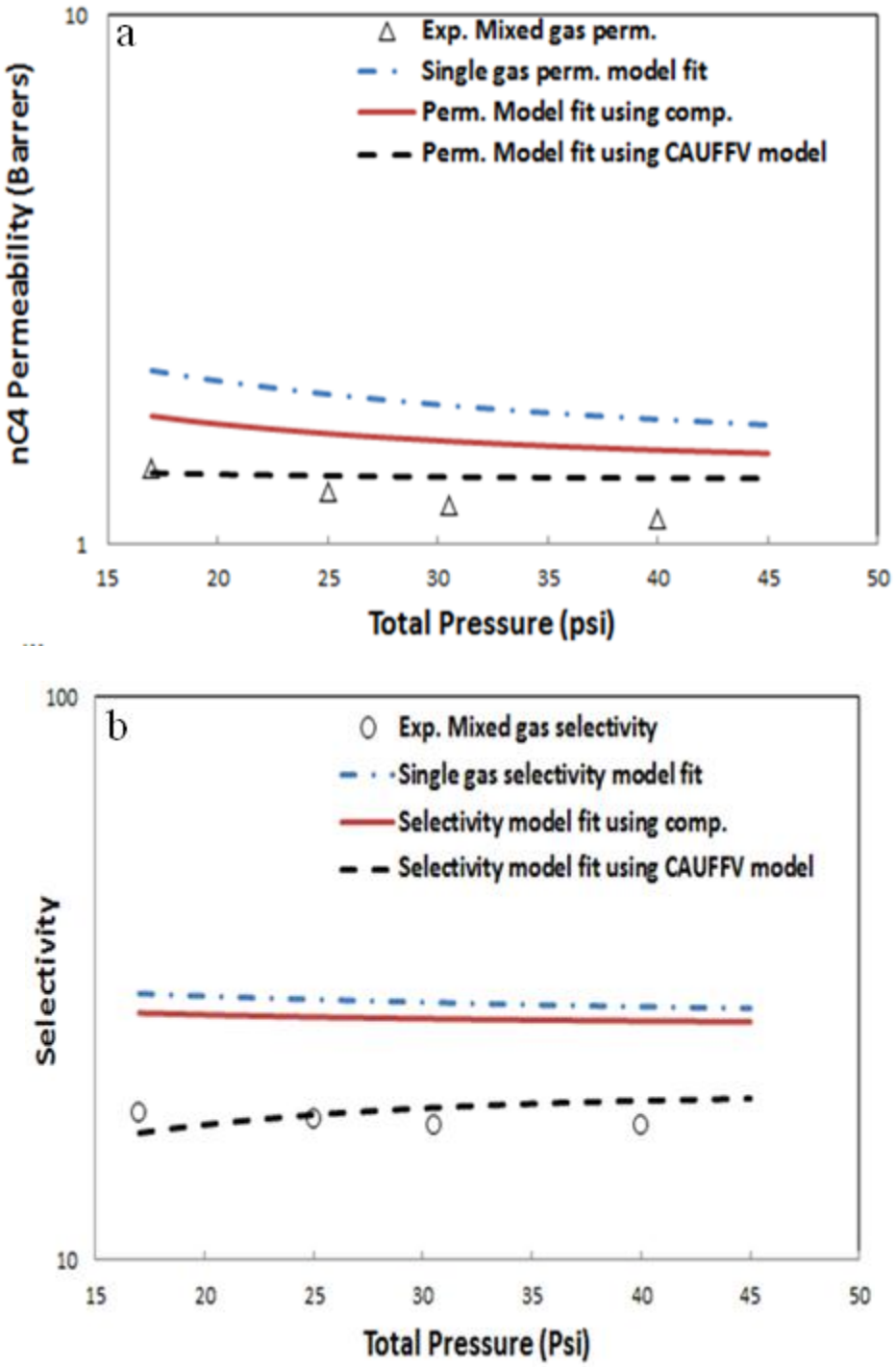

Figure 6.10: Transport performance of 42 mol% n-C4/ 58 mol% i-C4 in neat 6FDA-DAM annealed at 230°C, at operating temperature of 100°C. Comparing experimental data with CAUFFV fit, a) n-C4 permeability, b) n-C4/i-C4 selectivity

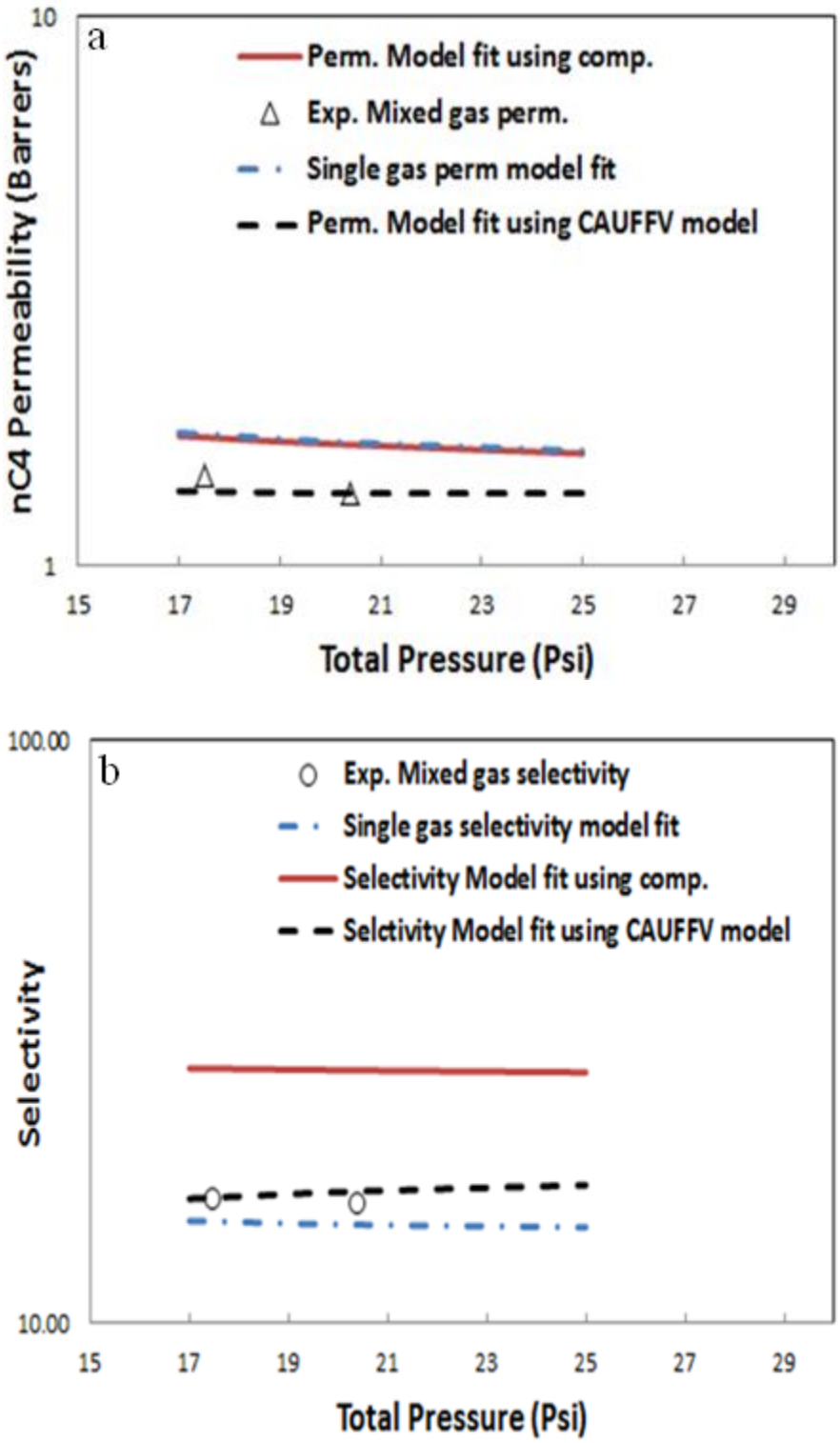

Figure 6.11: Transport performance of 95 mol% n-C4/ 5 mol% i-C4 in neat 6FDA-DAM annealed at 230°C, at operating temperature of 100°C. Comparing experimental data with CAUFFV fit, a) n-C4 permeability, b) n-C4/i-C4 selectivity

Appendix D shows the absolute errors resulting from the CAUFFV fit. The inclusion of the CAUFFV fitting parameters results in minimal deviation from experimental result, with a minimum average selectivity deviation of ~3% in 95 mol% n-C4 feed composition, and a maximum selectivity deviation of ~7% in 42 mol% n-C4 feed composition. On average for the feed composition of 5 mol% n-C4, the selectivity deviation of the CAUFFV fit is ~10X smaller than that of the competition and bulk flow model. The deviation is ~6X smaller for 42 mol% n-C4, and ~19X smaller for 95 mol% n-C4. This suggests that the CAUFFV hypothesis can effectively describe this system within an acceptable error range. Despite this improvement, it does require the introduction of two additional adjustable parameters, whereas, the HHF approach does not. It is also clear that the lack of a truly physical basis for the ε_{ij} values in table 6.2 makes this approach currently only a "curve fitting" approach. We hope eventually to make a fundamental link to ε_{ij} values, but this is not yet possible.

6.3. MIXED GAS SORPTION IN NEAT 6FDA-DAM

Mixed gas sorption measurements were made at 100°C via the pressure-decay method as described in chapter 3. The dual mode sorption model has been extended for binary gas sorption, by accounting for competition effects in the Langmuir environment. The model assumes that the saturated sorption capacity, C_H', affinity constant, b, and Henry's constant, k_D of each penetrant are constant values independent on the presence of a competing penetrant.

$$C_i = k_{D_i} p_i + \frac{C'_{H_i} b_i p_i}{1 + b_i p_i + b_j p_j} \tag{2.8}$$

Mixed gas sorption measurements were performed using three reservoir gas compositions (5, 42, and 95 mol% n-C4 bal. i-C4). The final partial pressures of the gases in the cell were determined via GC analysis, and used in equation 2.8, to make sorption predictions. The mixed gas experimental data were compared with pure gas experimental data in figure 6.12. Predictions were also made using the HHF model (equation 6.12) and the CAUFFV fit (equation 6.13) using the fitting parameters provided in Table 6.2. The predicted values were compared with experimental data shown in figures 6.13.

$$C_{n-C4} = k_{D_{n-C4}} p_{n-C4} + \frac{C'_{H_{n-C4}} b'_{n-C4} p_{n-C4}}{1 + b'_{n-C4} p_{n-C4} + b_{i-C4} p_{i-C4}} \tag{6.12}$$

$$C_i = k_{D_i} p_i + \frac{\varepsilon_{ij} C'_{H_i} b_i p_i}{1 + b_i p_i + b_j p_j} \tag{6.13}$$

As expected, the dual mode sorption model, which accounts for competition, predicts sorption capacity of a co-penetrant to be lower than in the pure gas system. As shown in figure 6.13, the dual mode sorption model over-predicts the sorption capacity of both n-C4 and i-C4. Based on mixed gas transport behavior discussed in section 6.1, the HHF model, and the CAUFFV fit, would imply n-C4 sorption capacity in the mixed gas system to be lower than in the pure gas system, while that of i-C4 to be higher. Experimental data shows penetrant sorption capacity values lower than in pure gas

system for both n-C4 and i-C4 (see figure 6.12), thus not in exact agreement with any existing model or fit.

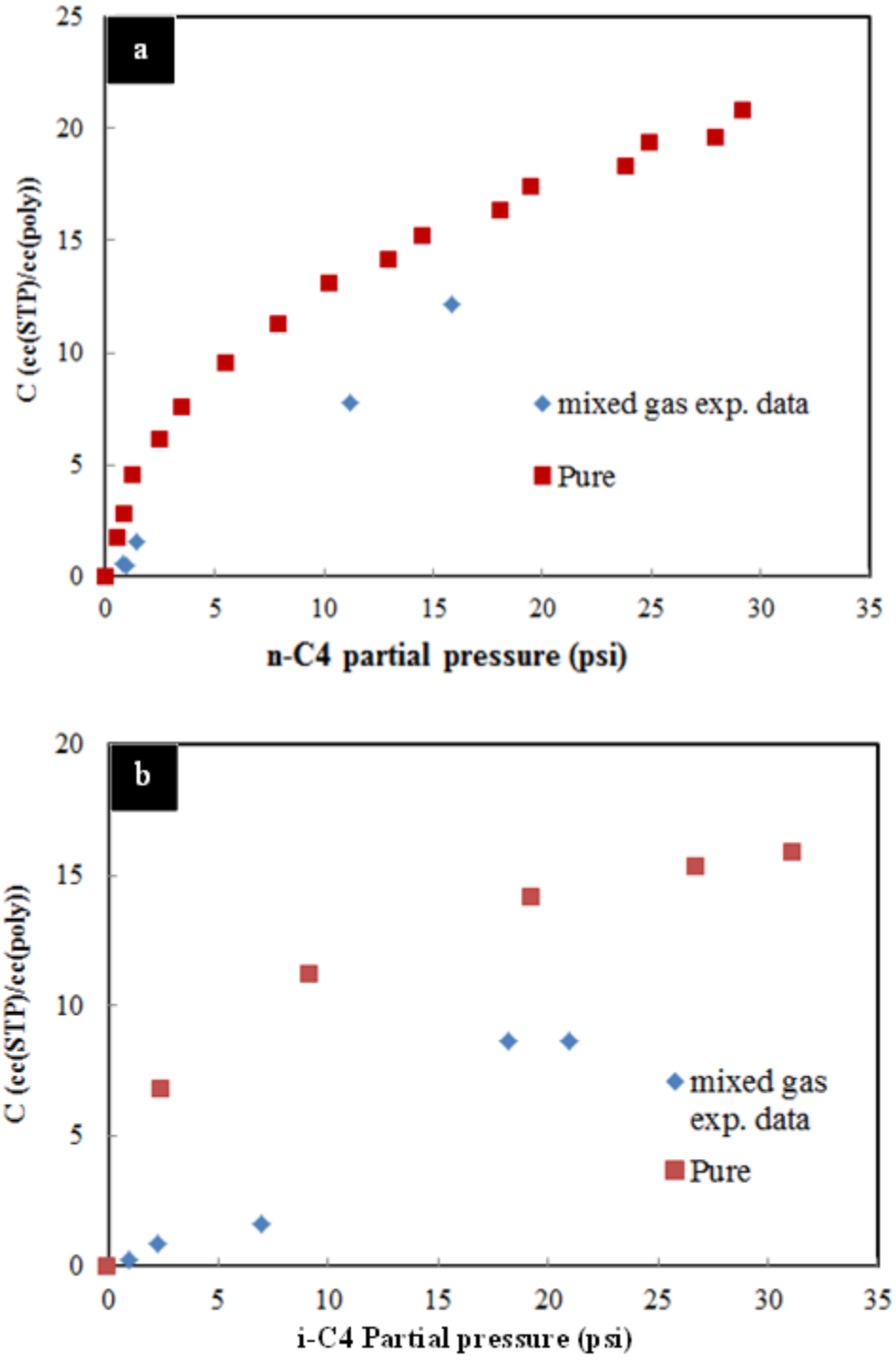

Figure 6.12: Comparing of sorption capacity of butane isomer in neat 6FDA-DAM in pure gas system to sorption capacity in mixed gas system. Films were annealed at 230°C, and measurements were made at operating temperature of 100°C. a) n-C4, and b) i-C4

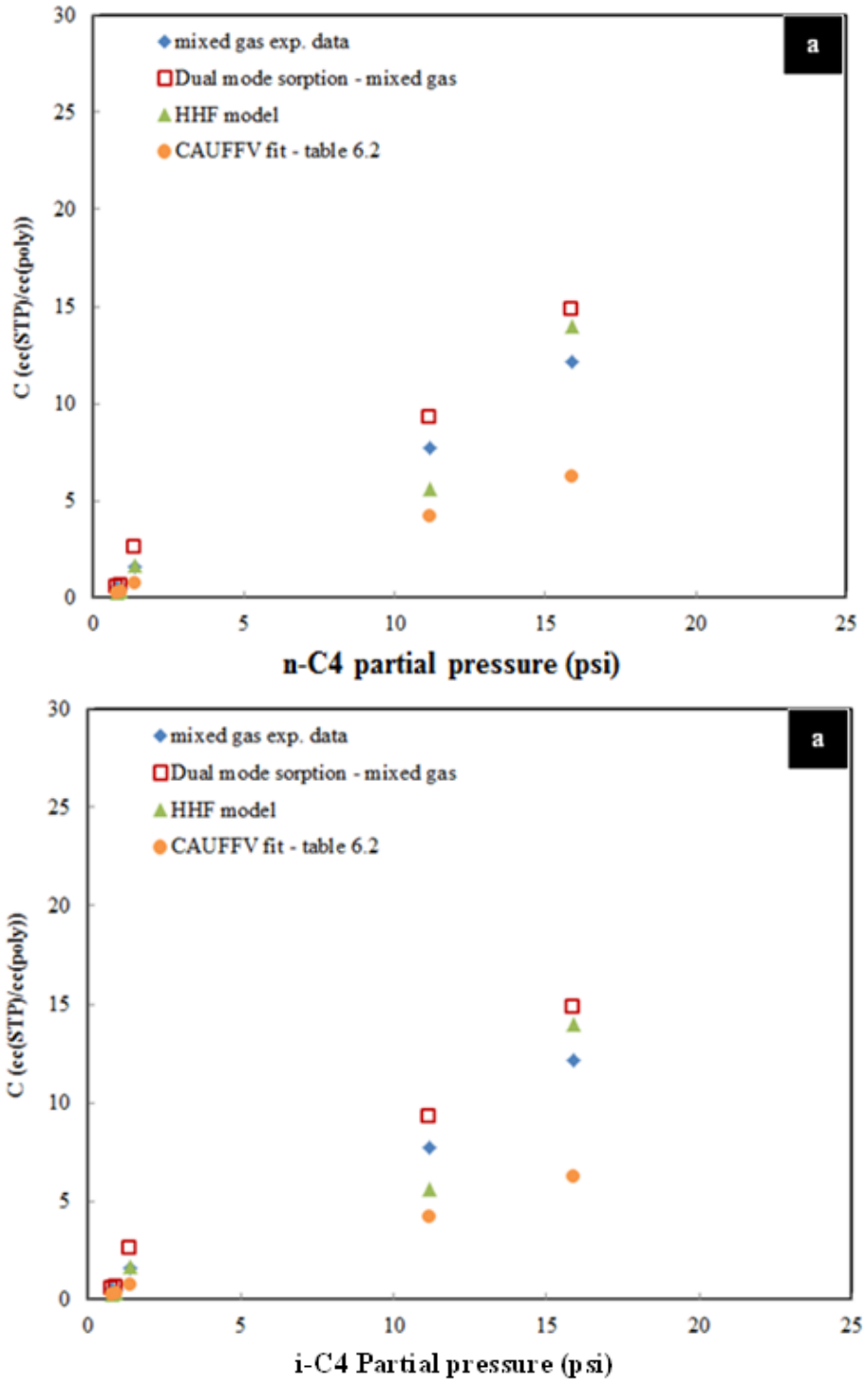

Figure 6.13: Comparing experimental data of sorption capacity of butane isomer in neat 6FDA-DAM in mixed gas system with predictions using various models. Films were annealed at 230°C, and measurements were made at operating temperature of 100°C. a) n-C4, and b) i-C4

It can also be observed in figure 6.13 that the experimental data lie closer to the predictions made using the extended dual mode sorption model and the HHF model than to CAUFFV fit. The observed mixed gas sorption behavior of this system suggests that the transport system is more complicated than currently understood, and cannot easily be described by changes in sorption parameters such as the affinity constant, b, or the saturated sorption capacity, C_H', but rather may also be due to changes in the diffusivity of each penetrant in the presence of the co-penetrant. We currently do not have a means of determining diffusion coefficient of a penetrant in a mixed gas system, but a combination of the permeation and sorption experimental data would suggest an increase in $D_{H_{i-C4}}$, and decrease in $D_{H_{n-C4}}$; however, such changes in D_H cannot be explained at present. Notwithstanding the above shortcomings, the HHF model is still suitable for an approximate description of the separation performance of the membrane for the mixed gas system. As might be anticipated due to the difficulties in predicting the mixed gas performance for pure polymer, the mixed matrix, mixed gas case is even more difficult. To make the problem tractable, we will use the observed mixed gas results in neat polymer in making hybrid (mixed matrix) predictions with the Maxwell model.

6.4. MIXED GAS PERMEATION IN MIXED MATRIX MEMBRANE

Mixed gas permeation measurements were made on mixed matrix membranes as described in chapter 3. Using 42 mol% n-C4/58 mol% i-C4 feed compositions, a fresh film with 25 wt% sieve loading, annealed at 230°C was used for mixed gas permeation measurements. The obtained selectivity of 15.5 is lower than in neat polymer, and the n-

C4 permeability of 1.6 Barrers is larger than predicted using the Maxwell equation where P_D = 2.5 Barrers. It should be noted that since this film did not undergo pure gas test to confirm good adhesion; which would have been indicated by an ideal selectivity of 32 (see table 5.10), it is possible that the low mixed gas selectivity was due to poor adhesion. Pure gas measurements were not made on this film in an attempt to cut down on time that would be required to vacuum the film between measurements of each individual gas and before mixed gas measurement. This turned out not to be a good idea as it made it impossible to pinpoint the reason for the observed low selectivity. Table 6.3 shows 9% increase in selectivity at sieve loading of 30 wt% annealed at 180°C. Mixed gas permeation measurements were performed on this film of 30 wt% sieve loading after good adhesion had been indicated via pure gas permeation test; which yielded an ideal selectivity of 27 (see table 5.10) compared to 21 in neat polymer under similar condition. This observed selectivity increase in the mixed gas system is significantly lower than predicted via Maxwell equation using P_D = 2.5 Barrers. As stated in chapter 5, P_D = 2.5 Barrers gave Maxwell predictions closer to experimental mixed matrix performance in pure gas system. The deviation observed between mixed gas Maxwell predictions and experimental data, may reflect a combined effect of imperfect adhesion as discussed in chapter 5, possible blocking of some of the sieve pore windows by i-C4 molecules; which have a relatively large kinetic diameter of 6.0Å compared to the sieve pore size of 4.2Å as well as complexities related to the observed effects noted in the previous section for pure polymer mixed gas. It is understood that due to the various factors involved in fabrication of successful mixed matrix membranes, repeatability is difficult. Although more permeation measurements will be desired to support the observed selectivity

enhancement in this mixed gas system, the available experimental result showing some selectivity enhancement at 30 wt% sieve, loading is encouraging.

Table 6.3: Separation performance of 6FDA-DAM-5A in mixed gas system of n-C4/i-C4. Operating temperature of 100°C

		Average Exp. Value		Maxwell Pred.			
				P_D = 2.5 Barrer		P_D = 0.4 Barrer	
		$P_{n\text{-}C4}$	$\alpha_{n/i}$	$P_{n\text{-}C4}$	$\alpha_{n/i}$	$P_{n\text{-}C4}$	$\alpha_{n/i}$
180°C	Neat Polymer	3.17	15.7	-	-	-	-
	30 wt% LTA 5A	2.73	17.1	2.98	22.9	2.21	17.0
230°C	Neat Polymer	1.25	17.8	-	-	-	-
	25 wt% LTA 5A	1.62	15.5	1.47	29.9	1.02	20.64

6.5. REFERENCES

1. Kamaruddin, D.H. and W.J. Koros, *Some observations about the application of Fick's first law for membrane separation of multicomponent mixtures.* J. Mem. Sci., 1997. **135**(2): p. 147-159.

2. Raharjo, R.D., et al., *Pure and mixed gas CH4 and n-C4H10 permeability and diffusivity in poly(1-trimethylsilyl-1-propyne).* Polymer, 2007. **48**(25): p. 7329-7344.

3. Raharjo, R.D., B.D. Freeman, and E.S. Sanders, *Pure and mixed gas CH4 and n-C4H10 sorption and dilation in poly(1-trimethylsilyl-1-propyne).* Polymer, 2007. **48**(20): p. 6097-6114.

4. Pinnau, I., et al., *Hydrocarbon/hydrogen mixed gas permeation in poly(1-trimethylsilyl-1-propyne) (PTMSP), poly(1-phenyl-1-propyne) (PPP), and PTMSP/PPP blends.* J. Poly. Sci. Part B: Poly. Phys., 1996. **34**(15): p. 2613-2621.

5. Fernandez, M., et al., *Mixture diffusion in zeolites studied by MAS PFG NMR and molecular simulation.* Microporous and Mesoporous Materials, 2007. **105**(1-2): p. 124-131.

6. Okamoto, K., et al., *Permeation and separation properties of polyimide membranes to 1,3-butadiene and n-butane.* J. Mem. Sci., 1997. **134**(2): p. 171-179.

7. Das, M., *Membranes for Olefin/Paraffin Separation*, in *Chemical and Biomolecular Engineering*. 2009, Georgia Institute of Technology: Atlanta, GA.

8. http://www.math.ucr.edu/home/baez/physics/General/occam.html.

9. Tshudy, J.A. and C. Von Frankenberg, *A model incorporating reversible immobilization for sorption and diffusion in glassy polymers.* J. Poly. Sci.: Poly. Phys. Ed., 1973. **11**(10): p. 2027-2037.

10. Park, J.Y. and D.R. Paul, *Correlation and prediction of gas permeability in glassy polymer membrane materials via a modified free volume based group contribution method.* J. Mem. Sci., 1997. **125**(1): p. 23-39.

11. vanKrevelen, D.W., *Properties of Polymer*. 3rd ed. 1990, New York: Elsevier.

12. Wonders, A.G. and D.R. Paul *Effect of CO2 exposure history on sorption and transport in polycarbonate.* J. Mem. Sci., 1979. **5**: p. 63-75.

13. Koros, W.J. and D.R. Paul, *CO2 sorption in poly(ethylene terephthalate) above and below the glass transition.* J. Poly. Sci.: Poly. Phys. Ed., 1978. **16**(11): p. 1947-1963.

14. Koros, W.J. and D.R. Paul, *Transient and steady-state permeation in poly(ethylene terephthlate) above and below the glass transition.* J. Poly. Sci.: Poly. Phys. Ed., 1978. **16**(12): p. 2171-2187.

15. Kanehashi, S. and K. Nagai, *Analysis of dual-mode model parameters for gas sorption in glassy polymers.* J. Mem. Sci., 2005. **253**(1-2): p. 117-138.

CHAPTER 7
CONCLUSIONS AND RECOMMENDATIONS

7.1. SUMMARY AND CONCLUSIONS

The aim of this research study as stated in Chapter 1 was to both understand and model the performance of hybrid inorganic-organic membranes under realistic operating conditions for hydrocarbon gas/vapor separation. Butane isomers were utilized as the model vapors, and a hybrid membrane of 6FDA-DAM-5A zeolites was used as an advanced separation hybrid membrane. In order to achieve this goal, specific objectives were established.

7.1.1. Objective 1: Characterize and analyze the factors that impact the separation performance of dense 6FDA-DAM membranes for the model isobutane/n-butane system.

Plasticization was identified as one major factor affecting gas separation via polymeric membranes. It is well documented that high temperature annealing can be used to suppress plasticization [1-4]. In addressing this objective, the effects of annealing on the transport properties of neat 6FDA-DAM were studied using films annealed at 180°C and 230°C for 24hrs. These studies of effects focused on sorption and permeation characterizations. As expected a decrease in permeability was observed at the higher annealing temperature. Analysis of equilibrium sorption measurements showed a decrease in sorption capacity of both isomers at the higher annealing temperature, as well as increase in sorption selectivity in favor of n-C4. Experimental data at 25 psi showed a 28% increase in sorption selectivity. An increase in permselectivity was observed by

changing the annealing temperature from 180°C to 230°C. At 25 psi, this increase was about 29%, thus suggesting an insignificant change in diffusion selectivity. Plasticization was not observed over the pressure range tested in this work. Due to possible complexities that may lower the separation performance of the membranes even in the absence of plasticization, annealing condition of 230°C was chosen for mixed gas analysis, to take advantage of the higher ideal permselectivity.

The effect of operating temperature was investigated via sorption measurements of n-C4 at 50°C and 100°C. Analysis of equilibrium sorption showed an expected decrease in sorption capacity with increase in temperature. This observed behavior is in accordance to van't Hoff equation. Estimates of the apparent heat of sorption, ΔH_S, and the pre-exponential solubility factor, S_0, where made at 25 psi. Analysis of kinetic sorption showed an increase in diffusivity with increase in operating temperature, which is in accordance to the Arrhenius equation. Estimates of the apparent activation energy of diffusion, ΔE_D, and the pre-exponential diffusivity factor, D_0, were made. These values are useful in making estimates of n-C4 permeability at 25 psi, under various operating temperatures. Additional measurements at other temperatures are necessary for more accurate estimates. Operating temperature of 100°C was chosen for the rest of this project as it avoids the energy cost associated with heating/cooling the product stream from the butamer™ unit when this membrane is implemented industrially.

7.1.2. Objective 2: Identify and model factors affecting separation performance of dense 6FDA-DAM membranes for gas/vapor mixtures of the model n-butane/isobutane system.

There are three common factors known to influence mixed gas transport though glassy polymers. As stated in chapter 1, these are: 1) Competitive sorption in the limited Langmuir environment present in glassy polymers, 2) Bulk flow effect or convective flow effect, which may be important when the bulk contribution to the overall flux (i.e. the bulk fraction), which is related to the sorption level of the penetrant and the flux of both mobile components is significant [5] and 3) Plasticization of the polymer in the presence of highly condensable gases. To avoid the influence of plasticization, transport measurements were performed within the pressure range identified in Chapter 5 to be plasticization free. In addressing this objective, mixed gas permeation measurements were made using feed compositions of 5 mol% n-C4/ 95 mol% i-C4, 42 mol% n-C4/58 mol% i-C4 and 95 mol% n-C4/ 5 mol% i-C4. Transport predictions using the dual mode transport model were compared to the experimental mixed gas permeation data. Despite accounting for competition effect in the Langmuir environment, and bulk flow effect, the predictions showed significant error when compared to experimental data. Two hypotheses were presented to explain the interesting transport behavior observed. The first hypothesis attributed the observed lower n-C4 permeability to hindered transport into the Langmuir environment resulting from a combined effect of the difference in size and shape of the butane isomers in the mixture. The Hindered Hole Filling (HHF) model, was developed to account for the hypothesized hindered transport, and was shown to better fit the experimental data. The second hypothesis attributed the observed transport behavior to change in the accessible fractional free volume of each penetrant due to the

presence of the co-penetrant. The Change in Unrelaxed Fractional Free Volume (CAUFFV) fitting parameter was introduced to the dual mode transport model. Although there is no known physical basis for the empirical parameter, its introduction gave better fit to experimental data than both the dual mode transport model and the HHF model. As noted, however, this latter approach at the present time is really only curve fitting.

Mixed gas sorption measurements were made to further investigate the transport behavior. The experimental data showed deviation from predictions made using the original dual mode sorption model, the HHF model and CAUFFV fit introduced in Chapter 6. These data, however, suggest that the HHF model is still suitable for an approximate description of the separation performance in the mixed gas system.

7.1.3. Objective 3: Extend analysis to include hybrid inorganic-organic membranes in realistic operating conditions.

In addressing this objective, modifications were made to the existing sieves surface modification process via Grignard treatment. In collaboration with Dr. Liu [6], a Grignard treatment method involving sol-gel chemistry was explored, and shown to successfully grow $Mg(OH)_2$ whiskers on the surface of commercial 5A zeolite, but without success for the nominally identical lab-made sieves. This work explored the effect of solvent on sieves surface modification. It was hypothesized that the presence of –ve charges on the surface of the sieves will promote bond formation with the +MgBr from the Grignard reagent, which will further promote $Mg(OH)_2$ whisker growth. To explore this hypothesis, it was suggested that the ideal solvent would need to be inert to Grignard reagents in order to prevent side reactions. The ideal solvent would also possess lone pair electrons in order to promote –ve surface charge formation on the sieves. Toluene, Tetrahydrofuran (THF) and 2-Methyltetrahydrofuan (MeTHF) were used in this

study. Toluene, which was used in the original Grignard treatment method [7] served as a control since it is inert to the reagent but does not possess lone pair electrons. It was concluded that MeTHF was an ideal solvent for the treatment reaction. Unfortunately, despite the success with commercial sieves, still no success was made in treating lab-made sieves.

Due to the inconvenient amount of control required in the sol-gel method, a "*simplified*" method was developed to make the process suitable on an industrial scale. This method avoids the need to control the amount of water added as in the sol-gel method. It also prevented homogenous nucleation of $Mg(OH)_2$, by limiting the reactive sites to the surface of the sieves.

Commercial and lab-made sieves were characterized via SEM, FTIR, XPS and zeta potential in an attempt to determine the difference responsible for their varying responses to Grignard treatment. Zeta potential measurements suggested a lower silanol concentration on the surface of lab-made sieves; which was attributed to calcination. SEM showed the presence of impurities on commercial sieves, which were thought to be $Al(OH)_3$ left during synthesis. FTIR and XPS showed no identifiable difference. No conclusion was made regarding what main difference in these sieves is responsible for their varying response to Grignard treatment.

Permeation measurements were made under single gas systems using 6FDA-DAM-5A at sieves loadings of 25 and 30 wt%. Selectivity enhancement of about 20% and 28% were observed at 25 and 30 wt% sieve loadings respectively. The transport values showed a close fit to Maxwell predictions made using P_D = 2.5 Barrers, as suggested by Liu. Errors in predictions were attributed to possible imperfect adhesion in

sections of the film. Permeation measurements were also made under mixed gas system with 42 mol% n-C4/58 mol% i-C4 using 6FD-DAM-5A at sieve loadings of 25 and 30 wt%. No selectivity enhancement was achieved on the film with 25 wt% loading. This was attributed to possible poor adhesion of the sieves to the polymer. Good adhesion was confirmed in the film with 30 wt% sieve loading via pure gas permeation measurements. A 9% increase in mixed gas selectivity was achieved; however, the permeability and selectivity was significantly lower than predicted via Maxwell model. This observation was hypothesized to reflect a combined effect of imperfect adhesion in some sections of the film, possible blocking of some of the sieve pore windows by i-C4, as well as complexities related to the observed effects in the pure polymer mixed gas system.

7.2. RECOMMENDATIONS

7.2.1. Objective 1: Characterize and analyze the factors that impact the separation performance of dense 6FDA-DAM membranes for the model isobutane/n-butane system.

Implementation of membranes industrially will involve non-vacuum downstream. The introduction of a positive downstream may affect the separation performance of the membrane. It is recommended that these membranes be tested at such positive downstream conditions. In the absence of plasticization, introduction of positive downstream is expected to reduce the driving force, thus decrease flux, and possibly selectivity. Equation 7.1 was used to make ideal permselectivity predictions of n-C4/i-C4 in 6FDA-DAM annealed at 230°C. The feed pressure for each penetrant was set at 25 psi and the selectivity was calculated over various pressure ratios (i.e. pressure ratio = feed

pressure/permeate pressure) via equation 7.1. Selectivity loss of 1.3% was predicted using equation 7.1 resulting from a decrease in pressure ratio for both n-C4 and i-C4 from infinite to 18.

$$P = \frac{D_D}{(p_2 - p_1)}\left[k_D(p_2 - p_1) + FC'_H b\left(\frac{p_2}{1 + bp_2} - \frac{p_1}{1 + bp_1}\right)\right] \tag{7.1}$$

Using the ideal case analysis, 1.3% loss in selectivity is quite insignificant; however, predictions in mixed gas system vary using different models. By assuming a feed composition of 50 mol% n-C4/50 mol% i-C4, and total feed pressure of 25 psi, selectivity predictions of n-C4/i-C4 in neat 6FDA-DAM annealed at 230°C were made by varying the pressure ratio of both n-C4, and i-C4. As shown in figure 7.1, using the original mixed gas model [5, 8], a selectivity loss of 1.9% is predicted, while the HHF and CAUFFV models predict a selectivity increase of 2.8% and 6.6% respectively.

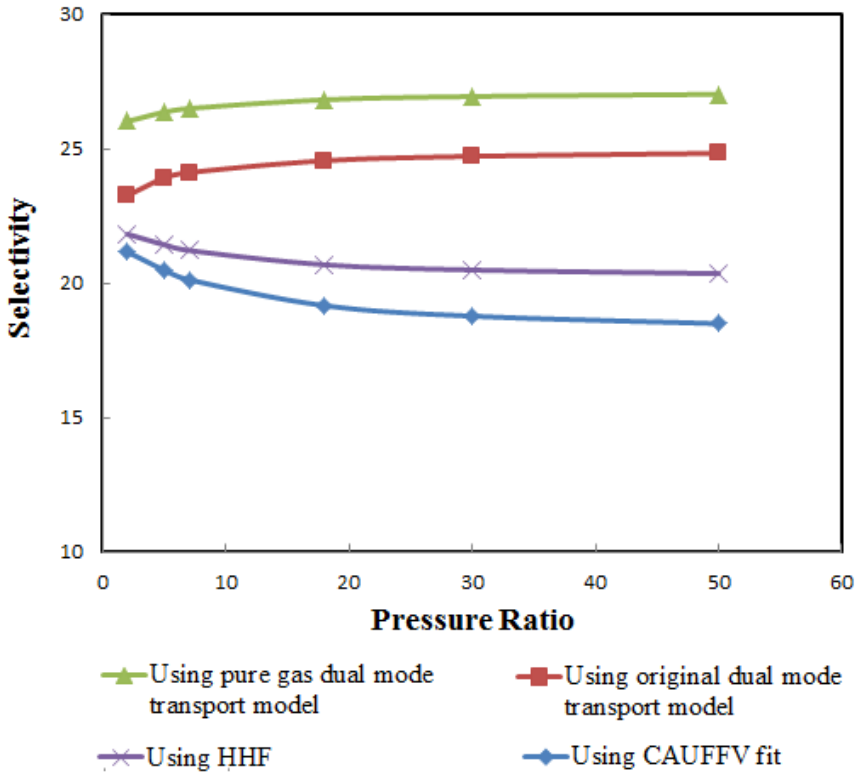

Figure 7.1: Prediction of pressure ratio effect on separation performance by varying both the pressure ratio of n-C4 and i-C4. Hypothetical case maintains a total feed pressure of 25 psi, feed composition of 50 mol% n-C4/ bal. i-C4, operating temperature of 100°C, and neat 6FDA-DAM dense films annealed at 230°C

In the case were only the pressure ratio of n-C4 is varied while maintaining infinite pressure ratio of i-C4, the ideal selectivity is predicted to decrease by 5.6% due to a decrease in n-C4 pressure ratio from infinite to 18. As shown in figure 7.2, a 6.3% loss in selectivity is predicted using the original dual mode transport model [5, 8], while a smaller loss of ~0.96% and ~0.8% is predicted by using the HHF model and CAUFFV fitting values provided in chapter 6 respectively. The variation of the mixed gas permeability model described by Kamaruddin [5], to account for positive downstream pressure is provided in appendix F.

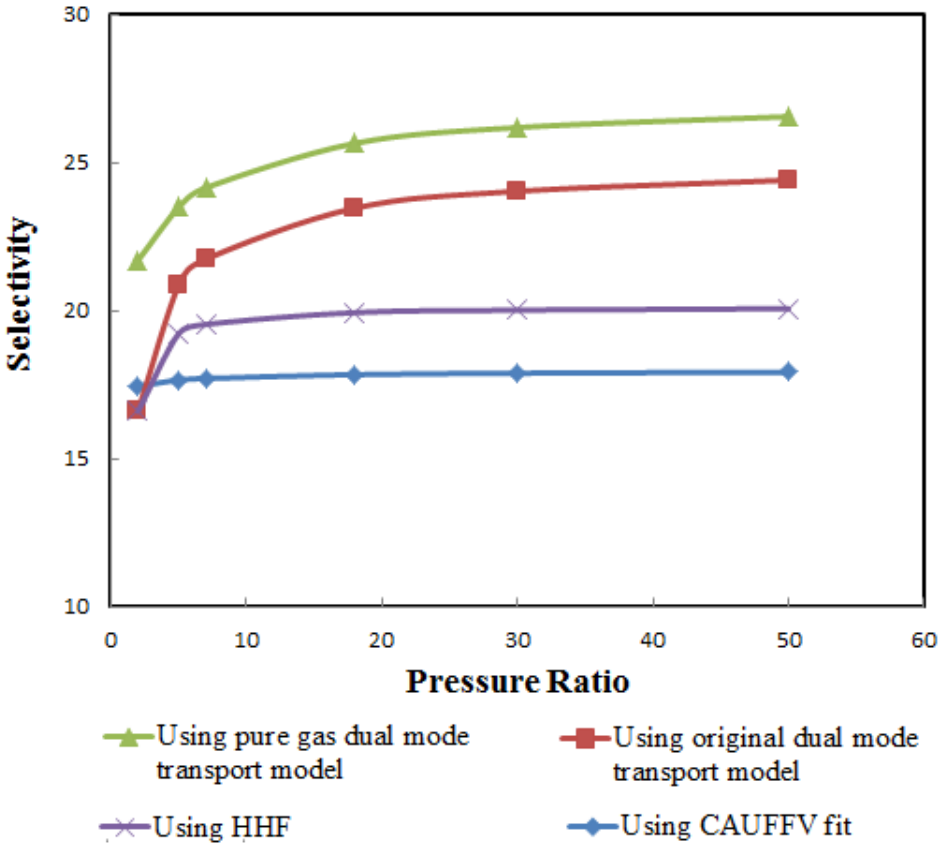

Figure 7.2: Prediction of pressure ratio effect on separation performance by varying the pressure ratio of only n-C4 and maintaining infinite pressure ratio of i-C4. Hypothetical case maintains a total feed pressure of 25 psi, feed composition of 50 mol% n-C4/ bal. i-C4, operating temperature of 100°C, and neat 6FDA-DAM dense films annealed at 230°C

It will be important to know how much selectivity loss is expected by implementing positive downstream pressure. There is also the possibility of taking advantage of pressure ratio to engineer the most suitable operating condition. For example, model predictions suggest that by decreasing the pressure ratio of i-C4 in the hypothetical mixed gas case discussed earlier, a selectivity increase is expected, and predictions made using the CAUFFV fit move towards those using the original dual mode model.

It is also recommended to make mixed gas permeation test on hollow fibers, as they are the industrially favored configuration.

7.2.2. Objective 2: Identify and model factors affecting separation performance of dense 6FDA-DAM membranes for gas/vapor mixtures of the model n-butane/isobutane system.

Further investigation is required to determine the factors contributing to the observed mixed gas transport. It is hypothesized to be dependent on the difference in penetrant sizes and shape as well as the rigidity of the polymer.

To study the effect of polymer rigidity, it is recommended to test the gas mixture using less rigid polymers. Though the polymer may have lower ideal permselectivity, if it does not experience the mixed gas behavior transport as in 6FDA-DAM, it could possibly show a higher selectivity in mixed gas systems. Another option is to test a different gas pair such as propane/propylene using a more rigid polymer such as 6FDA-TADPO polypyrrolone. 6FDA-TADPO has been studied to be more permeable and selective than polyimides due to its repeat unit of two benzene rings joined by two fused five-membered rings polymer, which impacts rigidity, and inhibits packing, thus increasing its fractional free volume [9]. This rigid polymer may cause the relatively small kinetic diameter difference of propane and propylene to impact its mixed gas transport behavior in a similar way to what was observed with n-C4/i-C4 in 6FDA-DAM.

To investigate the size and shape effect, other gas pairs such as Isobutane and Isopentane should be tested using 6FDA-DAM. It will be useful to determine which gas pairs would require introduction of the HHF model in predicting their transport behavior. To achieve this, a series of experimentation would be recommended. Mixed gas systems

of n-C4/propane, n-C4/propylene, i-C4/propane, i-C4/propylene and i-C4/SF6 could provide such useful information.

7.2.3. Objective 3: Extend analysis to include hybrid inorganic-organic membranes under realistic operating conditions.

As shown in figure 5.11, one factor affecting the fabrication of good mixed matrix membranes is uneven surface treatment of sieves. There is also the challenge of treating lab-made sieves and fabricating good mixed matrix membranes. I recommend:

- Studying the effect of sonication. By using controlled sonication intensity it may help attain even sieve treatment
- Introducing impurities to serve as nucleating sites on lab-made sieves. One could explore the introduction of some metals that may acts at acidic sites
- Properly controlling factors such as mixed matrix dope viscosity

As discussed in section 4.7, calcination of lab-made sieves may be responsible for lower silanol concentration. To confirm this, I recommend heating commercial sieves up to 550°C (the calcination temperature) prior to zeta-potential measurement. The calcinated commercial sieves would be expected to have lower zeta-potential value.

Since polymer adhesion to sieves is understood to occur in the dope phase (i.e. in the presence of the solvent), the radius of gyration of the polymer in the dilated state becomes an important factor for proper adhesion. An alternative to controlling the length of whiskers could be to use a solvent that produces the ideal radius or gyration of the polymer.

Further experimentation is recommended on mixed gas transport through mixed matrix membranes. The hypothesized blocking of some sieve windows by i-C4 requires further probing using different feed composition.

7.3. REFERENCES

1. Duthie, X., et al., *Thermal treatment of dense polyimide membranes.* Journal of Polymer Science Part B: Polymer Physics, 2008. **46**(18): p. 1879-1890.

2. Das, M., *Membranes for Olefin/Paraffin Separation*, in *Chemical and Biomolecular Engineering*. 2009, Georgia Institute of Technology: Atlanta, GA.

3. Krol, J.J., M. Boerrigter, and G.H. Koops, *Polyimide hollow fiber gas separation membranes: preparation and the suppression of plasticization in propane/propylene environments.* Journal of Membrane Science, 2001. **184**(2): p. 275-286.

4. Wind, J.D., et al., *Relaxation Dynamics of CO2 Diffusion, Sorption, and Polymer Swelling for Plasticized Polyimide Membranes.* Macromolecules, 2003. **36**(17): p. 6442-6448.

5. Kamaruddin, D.H. and W.J. Koros, *Some observations about the application of Fick's first law for membrane separation of multicomponent mixtures.* J. Mem. Sci., 1997. **135**(2): p. 147-159.

6. Liu, J., *Development of next generation mixed matrix hollow fiber membranes for butane isomer separation*, in *Chemical and Biomolecular Engineering*. 2010, Georgia Institute of Technology: Atlanta.

7. Shu, S. Husain, and W.J. Koros, *Formation of Nanostructured Zeolite Particle Surfaces via a Halide/Grignard Route.* Chemistry of Materials, 2007. **19**(16): p. 4000-4006.

8. Thundyil, M.J., Y.H. Jois, and W.J. Koros, *Effect of permeate pressure on the mixed gas permeation of carbon dioxide and methane in a glassy polyimide.* Journal of Membrane Science, 1999. **152**(1): p. 29-40.

9. Walker, D.R.B. and W.J. Koros, *Transport characterization of a polypyrrolone for gas separations.* Journal of Membrane Science, 1991. **55**(1-2): p. 99-117.

APPENDIX A

NACL AS NUCLEATING SITE FOR GRIGNARD TREATMENT OF LAB-MADE LTA

As mentioned in chapter 4, Liu [1] studied the effect of $AlCl_3$ anchoring on surface treatment of lab-made LTA sieves. The sieves were successfully treated although they were inadequate for use in mixed matrix membranes. $AlCl_3$ anchoring was used to simulate the deposits from thionyl chloride dealumination. Shu hypothesized that depositing NaCl on the surface of any sieve prior to Grignard treatment would aid formation of $Mg(OH)_2$ in whisker morphology. Based on this hypothesis, I attempted to deposit NaCl on the surface prior to Grignard treatment. This was performed in two ways. The first was similar to the anchoring procedure used with $AlCl_3$, while the second was similar to the seeding procedure used by Shu [2] with silica particles.

A.1. CASE 1: NACL ANCHORING METHOD

In this case, 1g of sieves dried under vacuum overnight at 120°C was sonicated in MeTHF for 3hrs, and then heated in an oil bath to ~60°C, while maintaining a low nitrogen sweep. When the temperature reached 60°C, 0.08g of NaCl was added and the mixture was allowed to stir at that temperature for 4hrs. The mixture was cooled to room temperature and 2.5ml of 3M CH_3MgBr was added and sonicated overnight in a sonication bath. The rest of the reaction was as described in the sol-gel procedure in chapter 3, using 6S DI water. Following the addition of CH_3MgBr, some salt crystals

were observed to settle at the bottom of the flask due to its low solubility in the organic solvent. Its poor solubility would have made it difficult to disperse in the mixture, so it is possible that an insignificant amount of the salt got to the sieve surface (see table A.1). SEM in figure A.1 shows $Mg(OH)_2$ flakes on the surface of the sieves indicating that this method was unsuccessful.

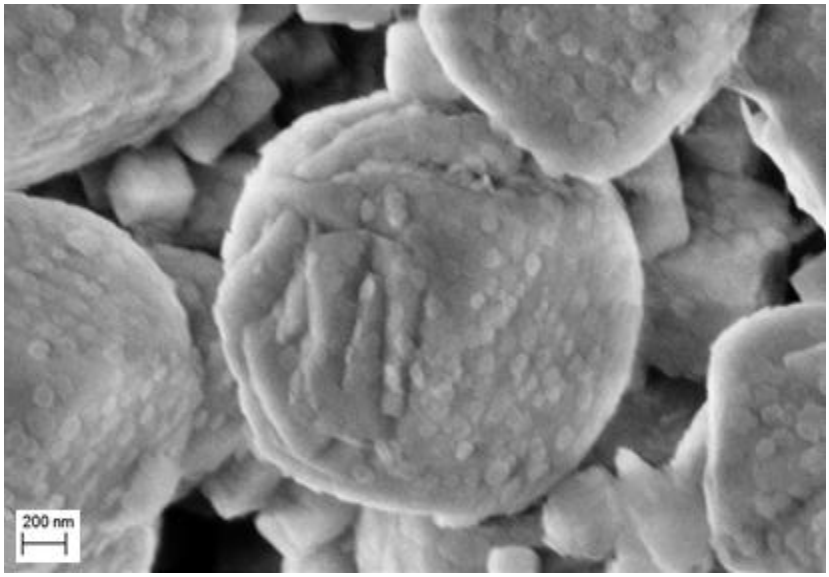

Figure A.1: Treated lab-made LTA via NaCl anchoring method using MeTHF as solvent

Table A.1: EDS analysis of lab-made LTA 4A treated via NaCl anchoring method using MeTHF as solvent

O	Na	Mg	Al	Si	Cl
61.92	9.38	2.43	11.69	14.36	0.22

A.2. CASE 2: NACL SEEDING METHOD

In this case, 1g of lab-made LTA was sonicated overnight in 10ml of supersaturated NaCl solution. The mixture was evaporated while continuously being stirred, and then dried under vacuum at 120°C overnight (~12hrs). Grignard treatment followed via sol-gel method as described in chapter 3 using MeTHF as solvent, and 6S DI water. Prior to addition of DI water, the mixture was observed to be more viscous than usual. SEM samples were taken following 3 times IPA wash and 4 times DI water wash. As shown in figure A.2a after washing in IPA, the sieves appear to be covered with a gel-like substance, which is most likely magnesium isopropoxide. EDS analysis of this sample in table A.1, indicates the high atomic % of Cl present which is definitely from the NaCl added. It is difficult to say exactly if the NaCl is on the sieve surface of just stuck in the gel. Following DI water wash, there are large homogenous $Mg(OH)_2$ around the sieves, and some flakes on the sieve surface (see figure A.2b).

Table A.2: EDS analysis of treated lab-made LTA via NaCl seeding method using MeTHF as solvent

	O	Na	Mg	Al	Si	Cl
IPA wash	49.28	22.51	2.95	6.81	6.77	11.69
DI H2O wash	68.43	7.40	10.21	5.59	7.36	0.99

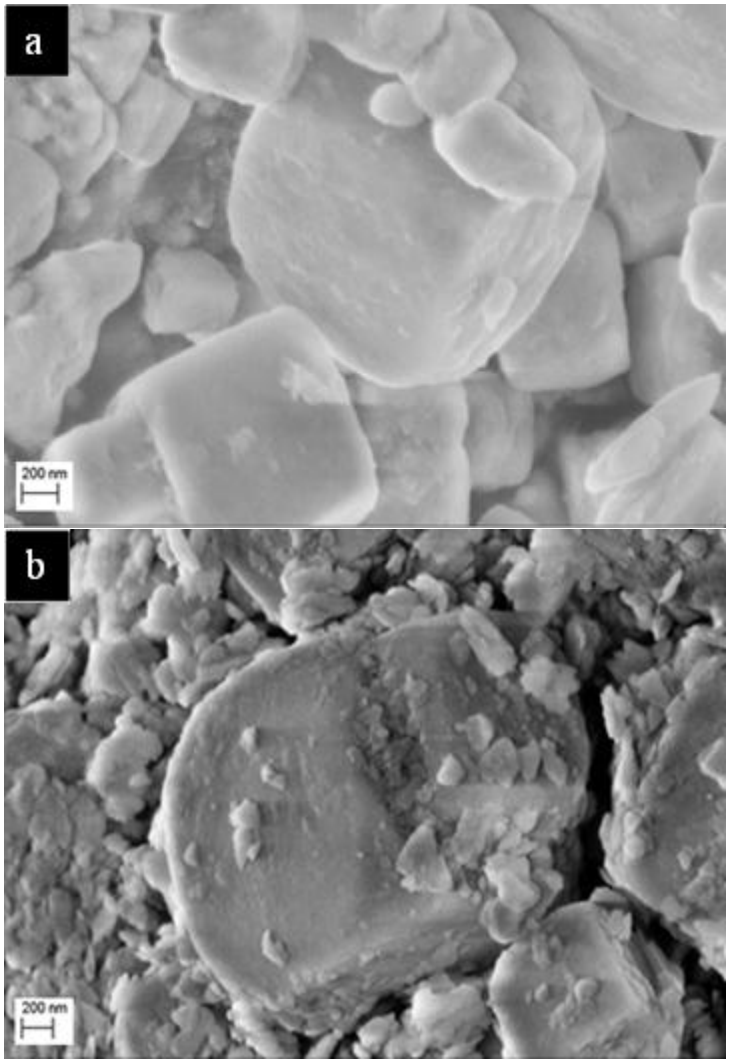

Figure A.2: Treated lab-made LTA via NaCl seeding method. a) after 3 times IPA wash, and b) after 4 times DI water wash

EDS analysis shows that a significant amount of NaCl was washed off, thus explaining the drop in atomic % of Na and Cl. The homogeneous nucleation suggests that the salt was not deposited on the surface but rather was stuck in the isopropoxide, which reacted with water to give $Mg(OH)_2$. It is probable that, the sieve acting as a substrate is essential for attaining whisker morphology.

A.3. CONCLUSION

This work has investigated NaCl anchoring and seeding as an alternative to thionyl chloride dealumination and $AlCl_3$ anchoring. Based on the presented results, it is likely that NaCl cannot be attached to the sieve surface in the same manner as $AlCl_3$, and thus will not act as a suitable nucleating site.

A.4. REFERENCES

1. Liu, J., *Development of next generation mixed matrix hollow fiber membranes for butane isomer separation*, in *Chemical and Biomolecular Engineering*. 2010, Georgia Institute of Technology: Atlanta.

2. Shu, S., *Engineering the performance of mixed matrix membranes for gas separation*, in *Chemical and Biomolecular Engineering.* 2007, Georgia Institute of Technology: Atlanta

APPENDIX B

DIFFUSION OF ISOBUTANE IN 6FDA-DAM

As mentioned in chapter 5, Kinetic sorption measurements of i-C4 in neat 6FDA-DAM annealed at 180°C showed deviation from a simple Fickian-controlled diffusion mechanism, to a combination of Fickian and relaxation-controlled diffusion mechanism at low penetrant pressures. The Berens-Hofpenberg model was used to make diffusion coefficient estimates for i-C4 in neat 6FDA-DAM annealed at 180°C.

$$\left(\frac{M_t}{M_\infty}\right)_A = \left[(1-\alpha_R)\left\{1-\sum_{n=0}^{\infty}\frac{8}{\pi^2(2n+1)^2}exp\left(\frac{-D_A(2n+1)^2\pi^2 t}{l^2}\right)\right\}\right] + \left[\alpha_R\{1-exp(^{-t}/_{\tau_R})\}\right]$$

This model was fit to experimental data by varying the unknown parameters, α_R, D_A, and τ_R to obtain the best fit. Table B.1 provided the fitting parameter for each pressure interval measured. Figures B.1 and B.2 show examples of simultaneous diffusion and relaxation-controlled uptake and simple diffusion controlled uptake for i-C4 sorption in neat 6FDA-DAM annealed at 180°C and 230°C for similar pressure change respectively.

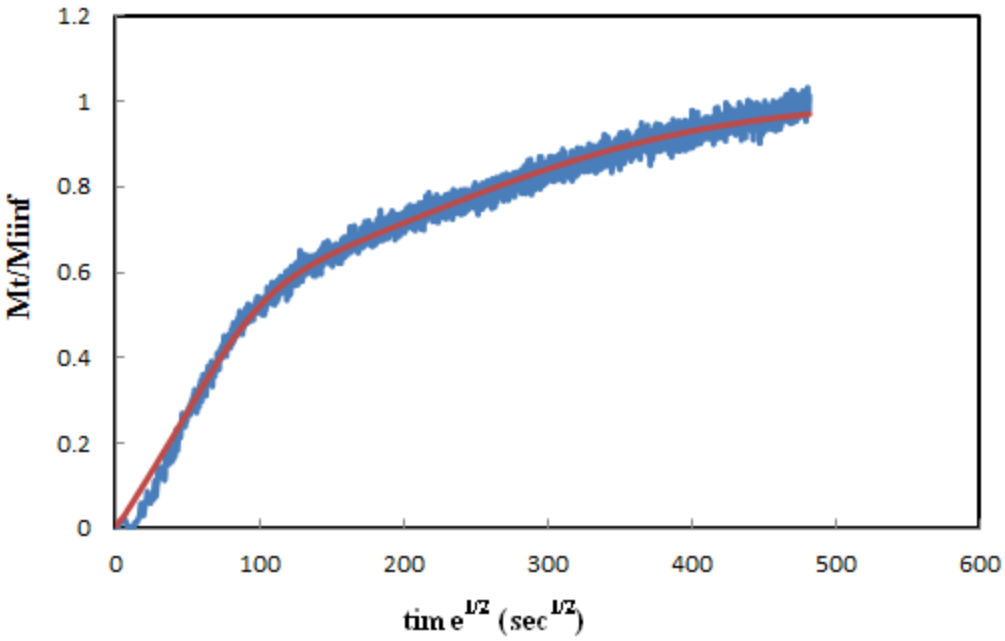

Figure B.1: Simultaneous diffusion and relaxation-controlled uptake for i-C4 sorption in neat 6FDA-DAM annealed at 180°C from the pressure change of 3.7 psi to 7 psi

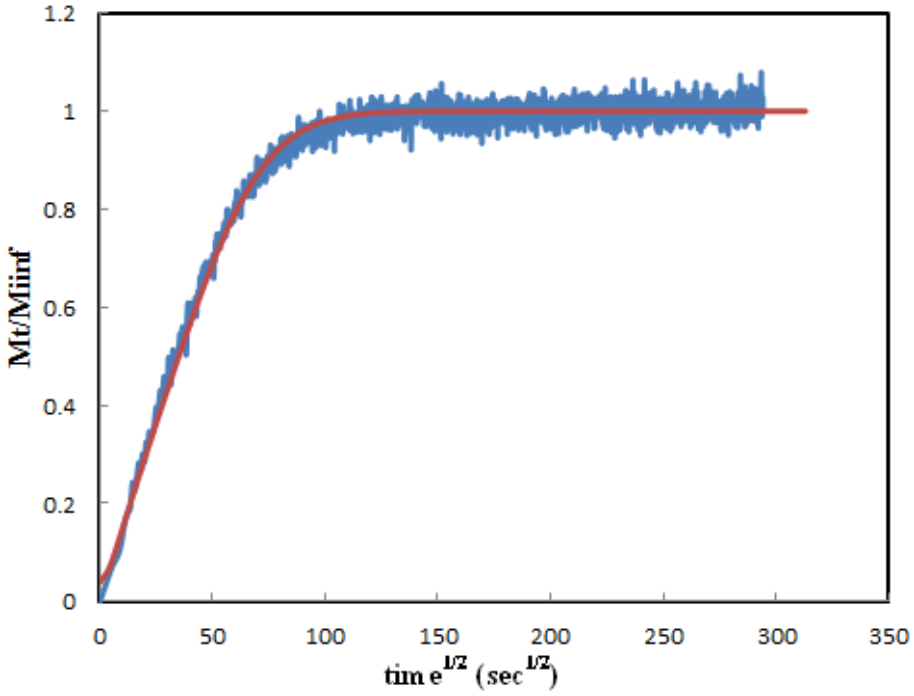

Figure B.2: Simultaneous diffusion and relaxation-controlled uptake for i-C4 sorption in neat 6FDA-DAM annealed at 230°C from the pressure change of 4.1 psi to 7 psi

Table B.1: Fitting parameters for Berens-Hofpenberg model for i-C4 sorption in neat 6FDA-DAM annealed at 180°C, with operating temperature of 100°C

Pressure Interval (psi)	D (cm^2/s)	α_R	τ_R (s)
0 – 0.882	9.58E-11	0.36	40500
0.882 – 3.719	7.45E-11	0.27	35800
3.719 – 7.001	8.08E-11	0.45	85565
7.001 – 10.86	1.62E-10	0.45	26241
10.86 – 25.36	1.38E-10	0.48	47940
25.36 – 35.63	2.18E-10	0.67	38199

Permeation isotherm measurements were not made for films annealed at 180°C, so it was not possible to compare the diffusion coefficient determined at the low pressure interval of 0 – 0.882 psi to D_{avg} at infinite dilution.

APPENDIX C

SAMPLE CALCULATIONS USING KINETIC SORPTION DATA

1. Using plots of diffusion coefficient versus final external cell pressure to determine, values for D_D^k, F^k and D_{avg}^k.

Sample calculation.

Kinetic sorption data for n-C4 in neat 6FDA-DAM annealed at 230°C, at operating temperature of 100°C.

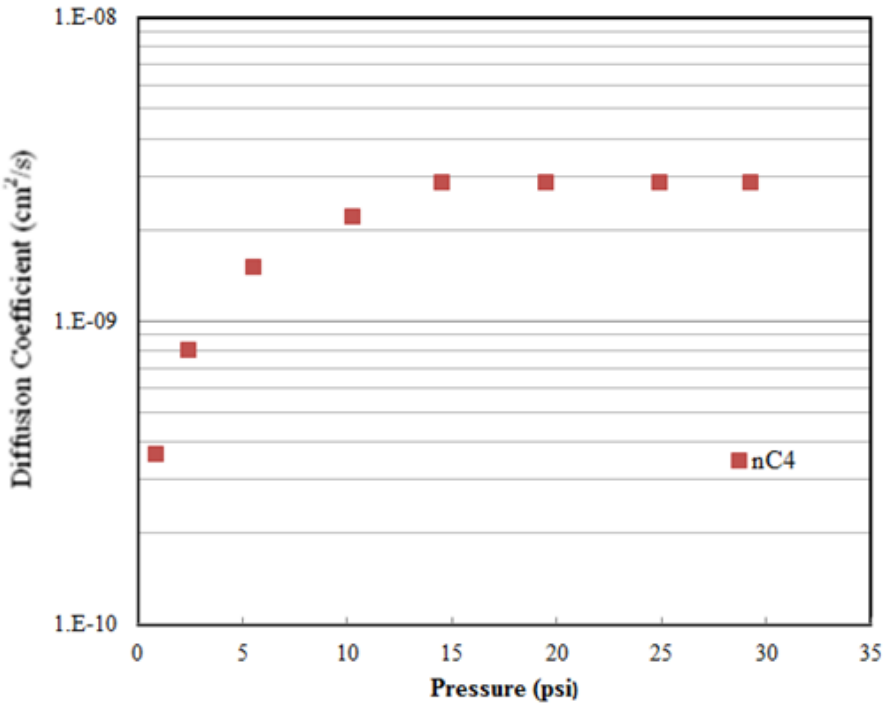

Figure C.1: Diffusion coefficient plot of n-C4 in neat 6FDA-DAM annealed at 230°C with operating temperature of 100°C. Values were determined via kinetic sorption analysis

Using the equation,

$$D_{avg}^{k} = D_{D}^{k}\left[\frac{1+\left(\frac{FK}{1+bp_2}\right)}{1+\left(\frac{K}{1+bp_2}\right)}\right] \qquad (C.1)$$

At high values of p,

$$D_{avg}^{k} = D_{D}^{k} \qquad (C.2)$$

At infinite dilution (low values of p),

$$D_{avg}^{k} = D_{D}^{k}\left[\frac{1+FK}{1+K}\right] \qquad (C.3)$$

By reading the plot, at high p values, $\boldsymbol{D_{avg}^{k} \cong 3E-09\, cm^2/s = D_{D}^{k}}$ and at low p values, $D_{avg}^{k} \cong 2.5E-10\, cm^2/s$. Substitute these values into equation C.1

$$2.5E-10\, cm^2/s = 3.0E-09\, cm^2/s\left[\frac{1+F^{k}(11.874)}{1+11.874}\right]$$

$$\boldsymbol{F^{k} = 0.006}$$

At cell pressure of 25psi,

$$\boldsymbol{D_{avg}^{k}} = 3E-09\left[\frac{1+\left(\frac{0.006*11.874}{1+(0.252*25)}\right)}{1+\left(\frac{11.874}{1+(0.252*25)}\right)}\right] = \boldsymbol{11.5E-10\, cm^2/s}$$

2. Determine the fitting parameter for the operating temperature dependence of transport factors.

Sample calculation

Using the solubility equation

$$S = k_D + \frac{C_H' bp}{1 + bp} \qquad (C.4)$$

At 25psi of n-C4, in neat 6FDA-DAM annealed at 230°C:

$$S_{100℃} = 0.295 + \frac{13.9 * 0.252}{1 + (0.252 * 25)} = 0.775 \frac{cc(STP)}{cm^3.psi}$$

$$S_{100℃} = 0.149 \frac{cc(STP)}{cm^3.cmHg}$$

$$S_{50℃} = 0.588 + \frac{14.8 * 0.986}{1 + (0.986 * 25)} = 1.157 \frac{cc(STP)}{cm^3.psi}$$

$$S_{50℃} = 0.224 \frac{cc(STP)}{cm^3.cmHg}$$

Using the van't Hoff equation

$$S = S_0 \exp\left(\frac{-\Delta H_S}{RT}\right) \qquad (C.5)$$

$$\ln\left(\frac{0.149}{0.224}\right) = \frac{-\Delta H_S}{1.987}\left[\frac{1}{373.15} - \frac{1}{323.15}\right]$$

$$\boldsymbol{\Delta H_S = -1.92\ kcal/mol}$$

$$0.149 \frac{cc(STP)}{cm^3.cmHg} = S_0 exp\left(\frac{-(-1923)}{1.987 * 373.15}\right)$$

$$\boldsymbol{S_0 = 0.112\ \frac{cc(STP)}{cm^3.cmHg}}$$

APPENDIX D

TRANSPORT OF BUTANE ISOMER MIXTURES IN NEAT 6FDA-DAM FILM: ADDITIONAL INFORMATION

D.1. DERIVATION OF THE DUAL MODE TRANSPORT MODEL TO ACCOUNT FOR THE HYPOTHESIZED APPARENT AFFINITY CONSTANT OF NC4, b'_{nC4}.

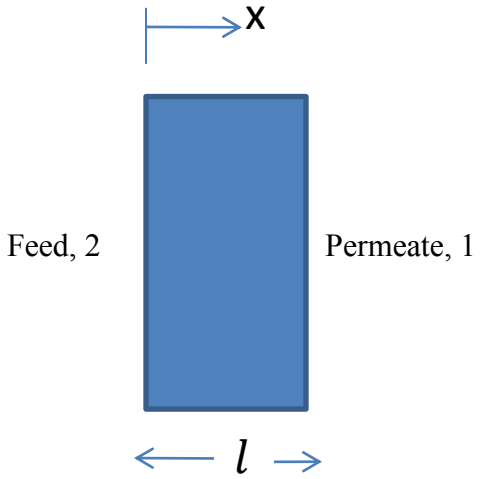

Figure D.1: Schematic of dense film

The diffusion-based permeability of a penetrant through a membrane is defined as the flux of the penetrant normalized by the difference in partial pressure of the penetrant across the membrane, and the thickness of the membrane. This is mathematically expressed in Eq. D.1.

$$P_i^* = \frac{N_i^{diff}}{\Delta p_i / l} \qquad (D.1)$$

where,

$$N_i^{diff} = -D_{D_i} \frac{dC_{M_i}}{dx} \qquad (D.2)$$

from the partial immobilization model, C_M is the total mobile concentration of a penetrant, defined as:

$$C_{M_i} = C_{D_i} + F_i C_{H_i} \qquad (D.3)$$

Where, F_i is the mobile concentration fraction of penetrants sorbed in the microviod, C_{H_i} and C_{M_i} are the concentrations of the penetrant in the Langmuir and Henry's environments respectively

Taking the integral of the flux of n-C4 across the film thickness

$$\int_l^0 N_{nC4} = -\int_{C_{M_{nC4_1}}}^{C_{M_{nC4_2}}} D_{D_{nC4}}\, dC_{M_{nC4}} \qquad (D.4)$$

$$N_{nC4} * l = \int_{C_{M_{nC4_1}}}^{C_{M_{nC4_2}}} D_{D_{nC4}}\, dC_{M_{nC4}} \qquad (D.5)$$

$$C_{M_{nC4}} = C_{D_{nC4}} + F_{nC4} C_{H_{nC4}} \qquad (D.6)$$

$$C_{D_{nC4}} = k_{D\,nC4} p_{nC4} \qquad (D.7)$$

$$C_{H_{nC4}} = \frac{C'_{H_{nC4}} b_{nC4} \left[1 - \frac{b_{iC4} p_{iC4}}{1 + b_{iC4} p_{iC4}}\right] p_{nC4}}{1 + b_{nC4} \left[1 - \frac{b_{iC4} p_{iC4}}{1 + b_{iC4} p_{iC4}}\right] p_{nC4} + b_{iC4} p_{iC4}} \qquad (D.8)$$

$$C_{M_{nC4}} = C_{D_{nC4}} \left[1 + \frac{F_{nC4} K_{nC4} \left[1 - \frac{b_{iC4} p_{iC4}}{1 + b_{iC4} p_{iC4}}\right]}{1 + \alpha_{nC4} C_{D_{nC4}} \left[1 - \frac{b_{iC4} p_{iC4}}{1 + b_{iC4} p_{iC4}}\right] + b_{iC4} p_{iC4}}\right] \qquad (D.9)$$

where,

$$K_{nC4} = \frac{C'_{H_{nC4}} b_{nC4}}{k_{D_{nC4}}}, \qquad F_{nC4} = \frac{D_{H_{nC4}}}{D_{D_{nC4}}} \quad and \quad \alpha_{nC4} = \frac{b_{nC4}}{k_{D_{nC4}}}$$

$$\frac{\partial C_{M_{nC4}}}{\partial C_{D_{nC4}}} = 1 + \frac{\left[1 + \alpha_{nC4} C_{D_{nC4}} \left[1 - \frac{b_{iC4} p_{iC4}}{1 + b_{iC4} p_{iC4}}\right] + b_{iC4} p_{iC4}\right] \left[F_{nC4} K_{nC4} \left[1 - \frac{b_{iC4} p_{iC4}}{1 + b_{iC4} p_{iC4}}\right]\right] - \left[\alpha_{nC4} \left[1 - \frac{b_{iC4} p_{iC4}}{1 + b_{iC4} p_{iC4}}\right]\right] \left[F_{nC4} K_{nC4} \left[1 - \frac{b_{iC4} p_{iC4}}{1 + b_{iC4} p_{iC4}}\right]\right]}{\left[1 + \alpha_{nC4} C_{D_{nC4}} \left[1 - \frac{b_{iC4} p_{iC4}}{1 + b_{iC4} p_{iC4}}\right] + b_{iC4} p_{iC4}\right]^2}$$

$$\frac{\partial C_{M_{nC4}}}{\partial C_{D_{nC4}}} = 1 + \frac{\left[F_{nC4}K_{nC4}\left[1 - \frac{b_{iC4}p_{iC4}}{1 + b_{iC4}p_{iC4}}\right]\right][1 + b_{iC4}p_{iC4}]}{\left[1 + \alpha_{nC4}C_{D_{nC4}}\left[1 - \frac{b_{iC4}p_{iC4}}{1 + b_{iC4}p_{iC4}}\right] + b_{iC4}p_{iC4}\right]^2} \qquad (D.10)$$

$$N_{nC4} * l = D_{D_{nC4}}k_{D_{nC4}}\int_{C_{D_{nC4_1}}}^{C_{D_{nC4_2}}}\left[1 + \frac{\left[F_{nC4}K_{nC4}\left[1 - \frac{b_{iC4}p_{iC4}}{1 + b_{iC4}p_{iC4}}\right]\right][1 + b_{iC4}p_{iC4}]}{\left[1 + \alpha_{nC4}C_{D_{nC4}}\left[1 - \frac{b_{iC4}p_{iC4}}{1 + b_{iC4}p_{iC4}}\right] + b_{iC4}p_{iC4}\right]^2}\right]dC_{D_{nC4}} \qquad (D.11)$$

$$C_{D_{nC4}} = k_{D_{nC4}}p_{nC4}$$

$$\frac{\partial C_{D_{nC4}}}{\partial p_{nC4}} = k_{D_{nC4}} \qquad (D.12)$$

$$N_{nC4} * l = D_{D_{nC4}}k_{D_{nC4}}\int_{P_{nC4_1}}^{P_{nC4_2}}\left[1 + \frac{\left[F_{nC4}K_{nC4}\left[1 - \frac{b_{iC4}p_{iC4}}{1 + b_{iC4}p_{iC4}}\right]\right][1 + b_{iC4}p_{iC4}]}{\left[1 + b_{nC4}p_{nC4}\left[1 - \frac{b_{iC4}p_{iC4}}{1 + b_{iC4}p_{iC4}}\right] + b_{iC4}p_{iC4}\right]^2}\right]dp_{nC4} \qquad (D.13)$$

$$N_{nC4} * l = D_{D_{nC4}}k_{D_{nC4}}\left[p_{nC4_2} + \frac{F_{nC4}K_{nC4}\left[1 - \frac{b_{iC4}p_{iC4_2}}{1 + b_{iC4}p_{iC4_2}}\right]}{1 + b_{nC4}p_{nC4_2}\left[1 - \frac{b_{iC4}p_{iC4_2}}{1 + b_{iC4}p_{iC4_2}}\right] + b_{iC4}p_{iC4_2}}\right] \qquad (D.14)$$

$$P^*_{nC4} = \frac{N_{nC4} * l}{p_{nC4_2}} = D_{D_{nC4}} k_{D_{nC4}} \left[1 + \frac{F_{nC4} K_{nC4} \left[1 - \frac{b_{iC4} p_{iC4_2}}{1 + b_{iC4} p_{iC4_2}} \right]}{1 + b_{nC4} p_{nC4_2} \left[1 - \frac{b_{iC4} p_{iC4_2}}{1 + b_{iC4} p_{iC4_2}} \right] + b_{iC4} p_{iC4_2}} \right] \quad (D.15)$$

$$P^*_{nC4} = k_{D_{nC4}} D_{D_{nC4}} + \frac{C'_{H_{nC4}} b'_{nC4} D_{H_{nC4}}}{1 + b'_{nC4} p_{nC4} + b_{iC4} p_{iC4}} \quad (D.16)$$

$$\omega_{nC4} = \left(k_{D_{nC4}} p_{nC4} + \frac{C'_{H_{nC4}} b'_{nC4} p_{nC4}}{1 + b'_{nC4} p_{nC4} + b_{iC4} p_{iC4}} \right) \frac{M_{nC4}}{22400 \rho} \quad (D.17)$$

D.2. ISOBUTANE PERMEABILITY PLOTS

D.2.1. Original mixed gas model fit

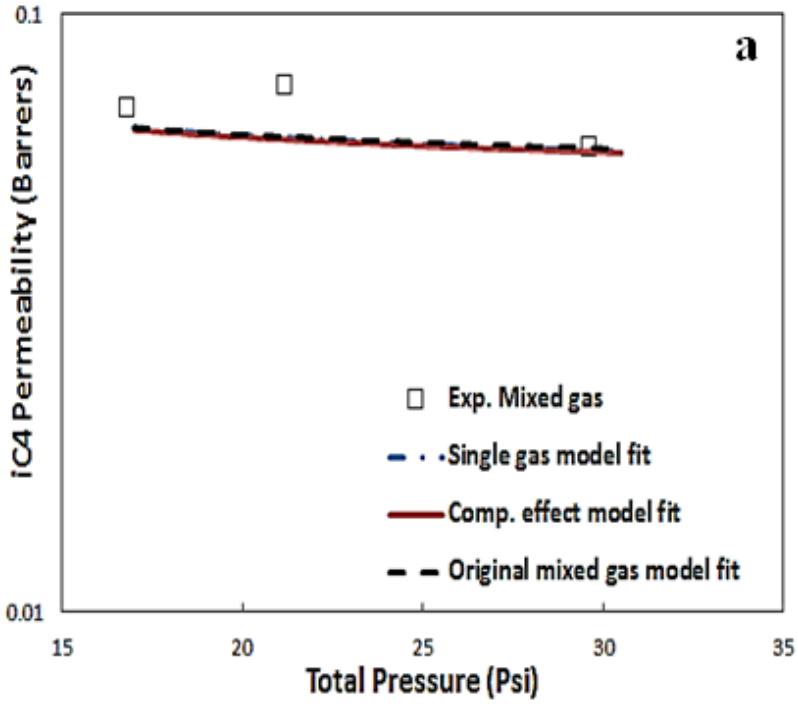

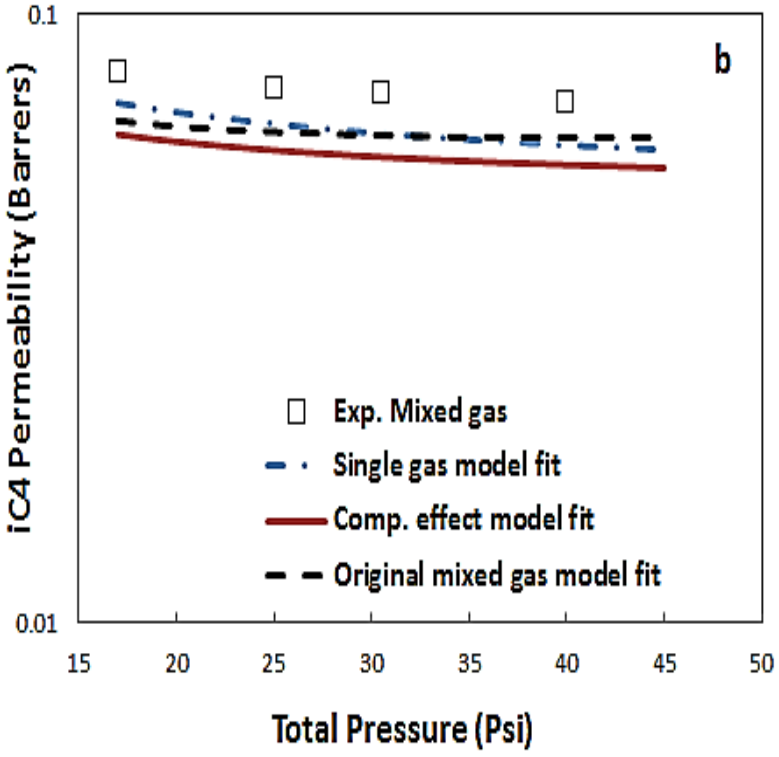

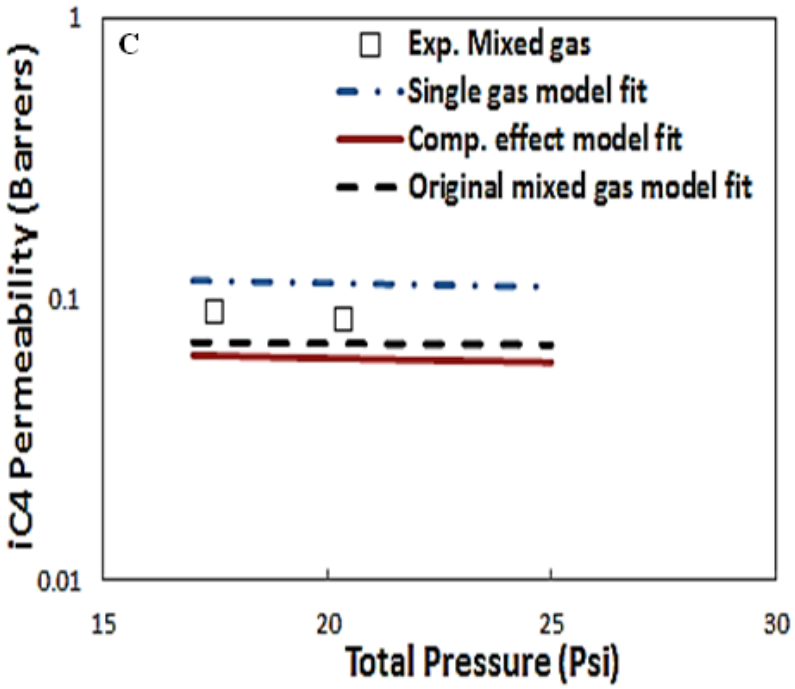

Figure D.2: Permeability of i-C4 in neat 6FDA-DAM annealed at 230°C at operating temperature of 100°C. Comparing experimental data with original mixed gas transport model. Feed compositions of: a) 5 mol% n-C4/ 95 mol% i-C4, b) 42 mol% n-C4/ 58 mol% i-C4, and c) 95 mol% n-C4/5 mol% i-C4

D.2.2. Hypothesis 1: HHF model

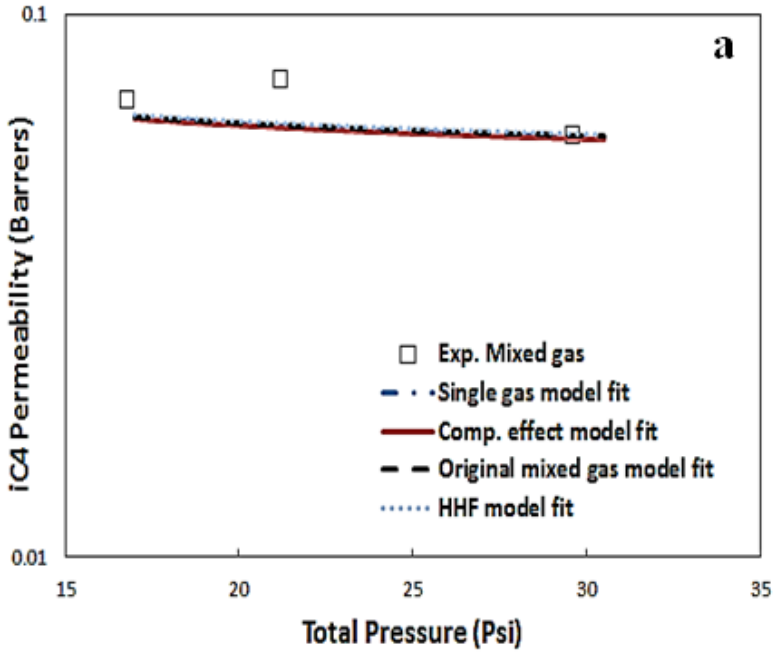

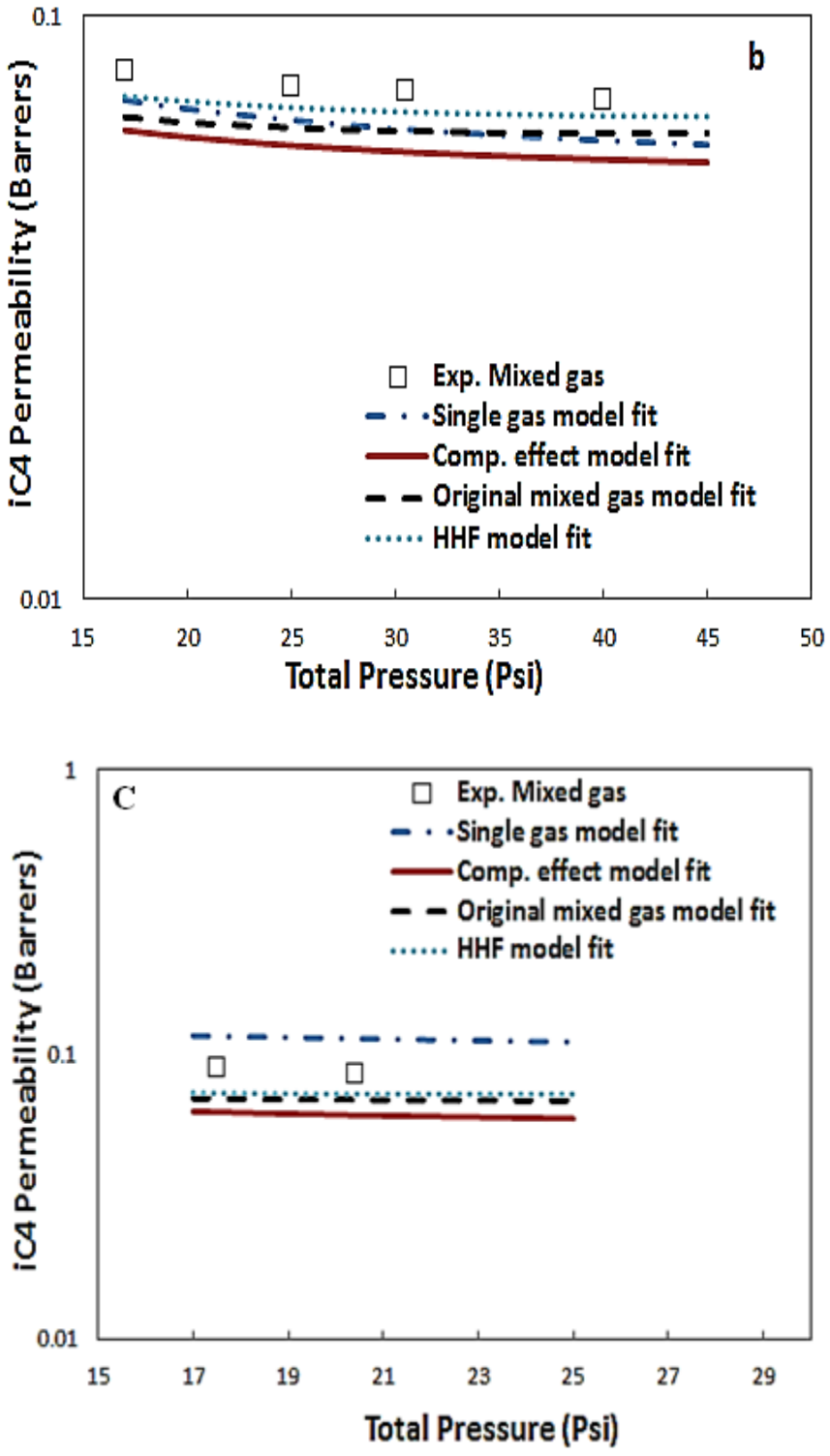

Figure D.3: Permeability of i-C4 in neat 6FDA-DAM annealed at 230°C at operating temperature of 100°C. Comparing experimental data with HHF model. Feed compositions of: a) 5 mol% n-C4/ 95 mol% i-C4, b) 42 mol% n-C4/ 58 mol% i-C4, and c) 95 mol% n-C4/5 mol% i-C4

D.2.3. Hypothesis 2: CAUFFV fit

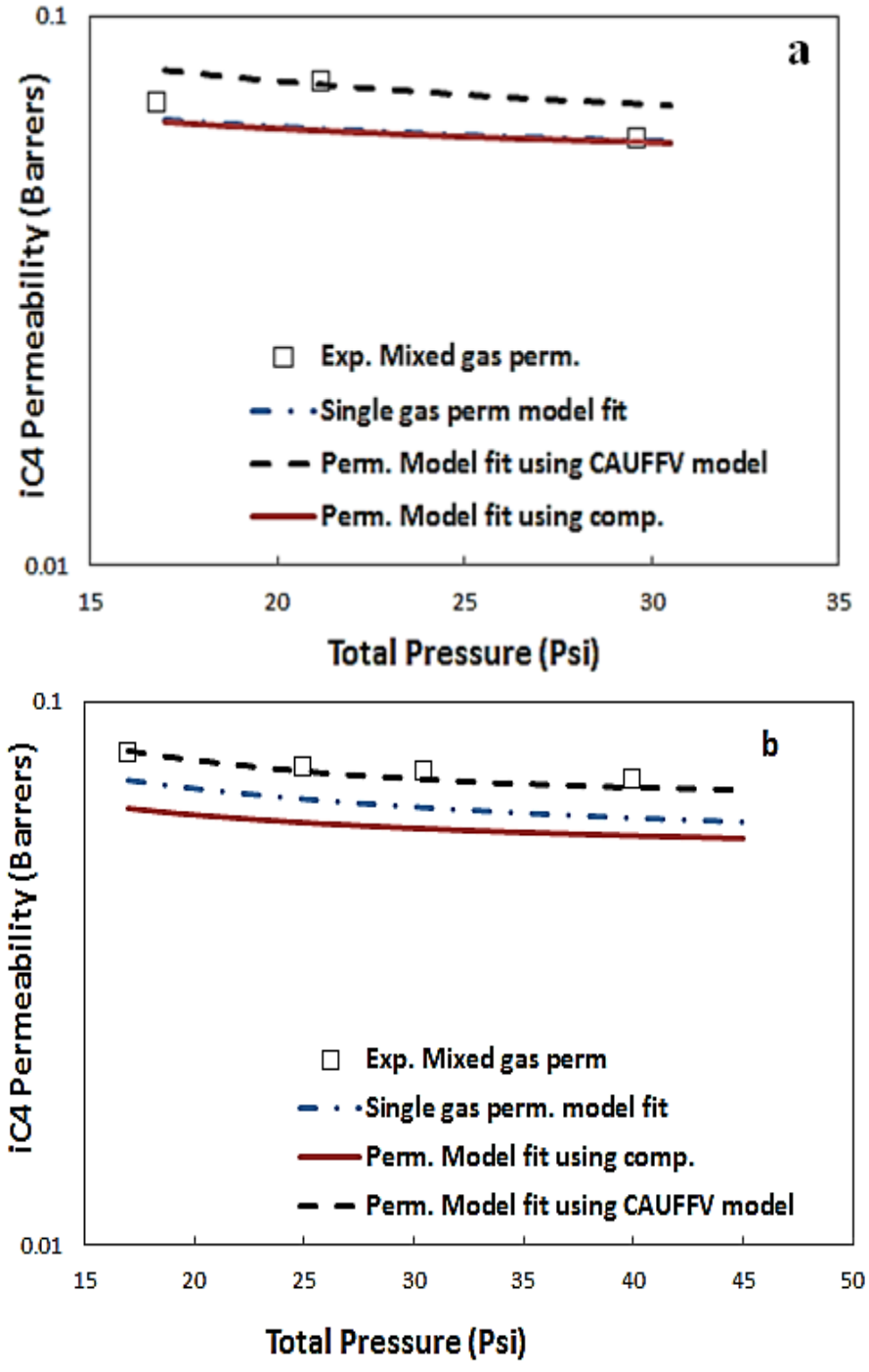

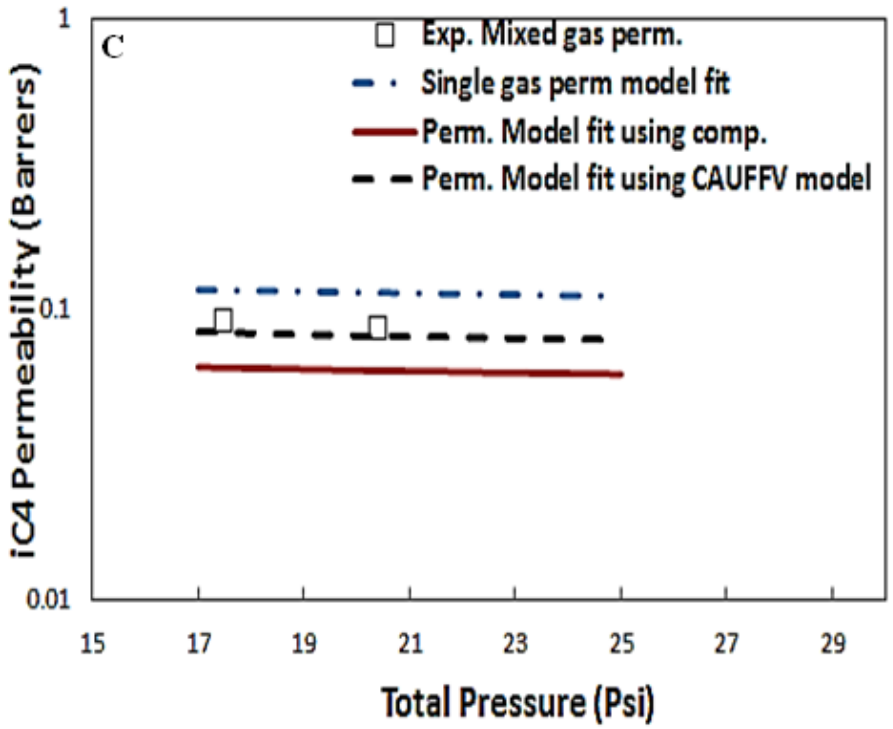

Figure D.4: Permeability of i-C4 in neat 6FDA-DAM annealed at 230°C at operating temperature of 100°C. Comparing experimental data with CAUFFV model. Feed compositions of: a) 5 mol% n-C4/ 95 mol% i-C4, b) 42 mol% n-C4/ 58 mol% i-C4, and c) 95 mol% n-C4/5 mol% i-C4

D.3. ERROR ANALYSIS OF THE HHF MODEL

Table D.1: Absolute %Δ at feed composition 5 mol% n-C4/ 95 mol% i-C4

Absolute %ΔHHF = (HHF pred. – Exp. Data)/(Exp Data)*100			
Total Pressure (psi)	**n-C4**	**i-C4**	**Selectivity**
16.8	2.38	17.07	23.46
21.2	15.38	6.06	27.08
29.2	28.14	0.83	22.82
Absolute %ΔComp. & Bulk = (Comp & Bulk pred. – Exp. Data)/(Exp Data)*100			
Total Pressure (psi)	**n-C4**	**i-C4**	**Selectivity**
16.8	27.33	17.72	54.75
21.2	47.69	6.86	58.56
29.2	52.89	0.16	52.64
Absolute %ΔComp. = (Comp pred. – Exp. Data)/(Exp Data)*100			
Total Pressure (psi)	**n-C4**	**i-C4**	**Selectivity**
16.8	27.24	18.68	56.47
21.2	47.60	7.76	60.02
29.2	52.74	1.39	54.89
Absolute %ΔPure = (Pure gas pred. – Exp. Data)/(Exp Data)*100			
Total Pressure (psi)	**n-C4**	**i-C4**	**Selectivity**
16.8	193.87	6.81	215.34
21.2	156.96	17.94	213.14
29.2	208.74	0.65	210.77

Table D.2: Absolute %Δ at feed composition 42 mol% n-C4/ 58 mol% i-C4

Absolute %ΔHHF = (HHF pred. – Exp. Data)/(Exp Data)*100			
Total Pressure (psi)	**n-C4**	**i-C4**	**Selectivity**
17.0	4.67	9.60	10.13
25.0	11.24	7.79	12.70
30.5	15.96	7.70	15.94
40.0	20.65	5.78	15.76
Absolute %ΔComp. & Bulk = (Comp & Bulk pred. – Exp. Data)/(Exp Data)*100			
Total Pressure (psi)	**n-C4**	**i-C4**	**Selectivity**
17.0	25.41	16.83	43.41
25.0	29.79	14.82	42.34
30.5	33.25	14.40	43.64
40.0	35.74	12.03	39.50
Absolute %ΔComp. = (Comp pred. – Exp. Data)/(Exp Data)*100			
Total Pressure (psi)	**n-C4**	**i-C4**	**Selectivity**
17.0	25.02	20.98	50.49
25.0	29.24	20.57	51.99
30.5	32.58	21.17	55.21
40.0	34.89	20.71	53.80
Absolute %ΔPure = (Pure gas pred. – Exp. Data)/(Exp Data)*100			
Total Pressure (psi)	**n-C4**	**i-C4**	**Selectivity**
17.0	52.42	10.98	62.85
25.0	53.40	12.24	63.28
30.5	54.90	13.82	65.86
40.0	54.16	14.53	63.07

Table D.3: Absolute %Δ at feed composition 95 mol% n-C4/ 5 mol% i-C4

Absolute %ΔHHF = (HHF pred. – Exp. Data)/(Exp Data)*100			
Total Pressure (psi)	**n-C4**	**i-C4**	**Selectivity**
17.5	16.83	18.26	42.92
20.4	22.21	14.02	42.14
Absolute %ΔComp. & Bulk = (Comp & Bulk pred. – Exp. Data)/(Exp Data)*100			
Total Pressure (psi)	**n-C4**	**i-C4**	**Selectivity**
17.5	18.12	21.74	50.94
20.4	23.48	17.98	50.56
Absolute %ΔComp. = (Comp pred. – Exp. Data)/(Exp Data)*100			
Total Pressure (psi)	**n-C4**	**i-C4**	**Selectivity**
17.5	17.34	29.84	67.25
20.4	22.56	27.50	69.04
Absolute %ΔPure = (Pure gas pred. – Exp. Data)/(Exp Data)*100			
Total Pressure (psi)	**n-C4**	**i-C4**	**Selectivity**
17.5	18.48	29.53	8.53
20.4	23.66	34.58	8.11

D.4. ERROR ANALYSIS OF THE CAUFFV MODEL

Table D.4: Absolute %ΔCAUFFV at feed composition 5 mol% n-C4/ 95 mol% i-C4

Absolute %ΔCAUFFV = (CAUFFV – Exp. Data)/(Exp Data)*100			
Total Pressure (psi)	**n-C4**	**i-C4**	**Selectivity**
16.8	13.92	14.82	0.78
21.2	2.23	1.39	3.67
29.2	13.92	15.67	11.55

Table D.5: Absolute %ΔCAUFFV at feed composition 42 mol% n-C4/ 58 mol% i-C4

Absolute %ΔCAUFFV = (CAUFFV – Exp. Data)/(Exp Data)*100			
Total Pressure (psi)	**n-C4**	**i-C4**	**Selectivity**
17.0	2.37	0.84	7.91
25.0	7.55	1.32	1.81
30.5	13.49	2.90	7.84
40.0	19.40	2.74	10.98

Table D.6: Absolute %ΔCAUFFV at feed composition 95 mol% n-C4/ 5 mol% i-C4

Absolute %ΔCAUFFV = (CAUFFV – Exp. Data)/(Exp Data)*100			
Total Pressure (psi)	**n-C4**	**i-C4**	**Selectivity**
17.5	6.73	7.29	0.61
20.4	0.00	4.62	4.84

D.5. COMBINATION OF HHF AND CAUFFV

Mixed gas predictions were made using a combination of both hypotheses. Best fit values for CAUFFV fit were determined after implementing the HHF model correction. The best fit values are shown in table D.7. Comparing these values to those in table 6.2, by first making the HHF model correction, it can be implied that the effect of i-butane on the accessible free volume of n-butane is ~80% less than the CAUFFV fit only suggested, while the effect on i-butane is ~20% less.

Table D.7: Approximate values of ε_{ij}

	n-C4	i-C4
ε_{ij}	0.3	1.7

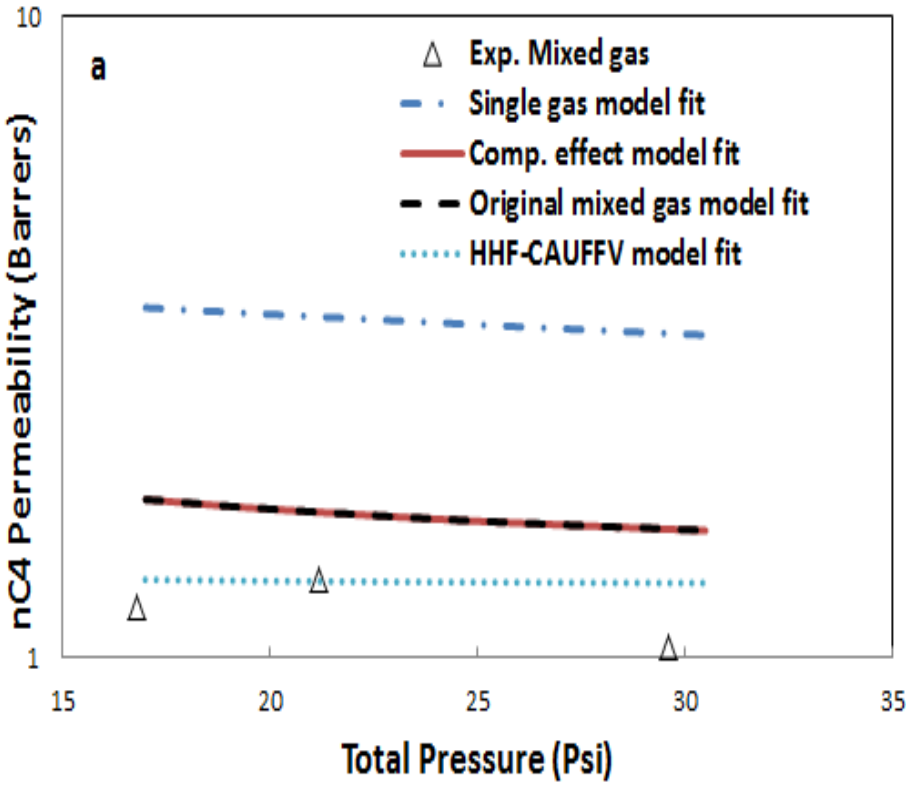

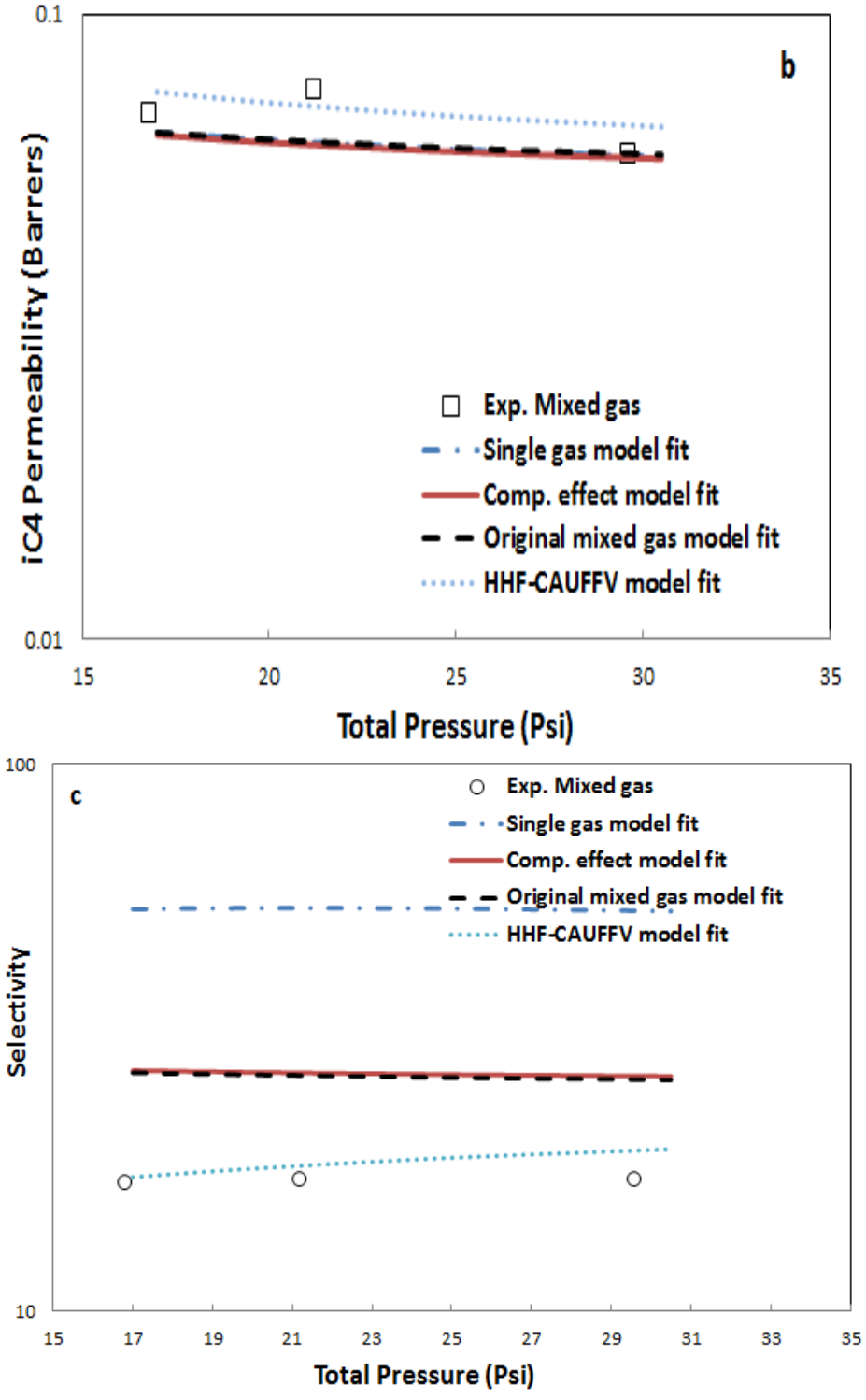

Figure D.5: Transport performance of 5 mol% nC4/ 95 mol% iC4 in neat 6FDA-DAM annealed at 230°C, at operating temperature of 100°C. Comparing experimental data with HHF-CAUFFV fit, a) n-C4 permeability, b) i-C4 permeability, and c) n-C4/i-C4 selectivity

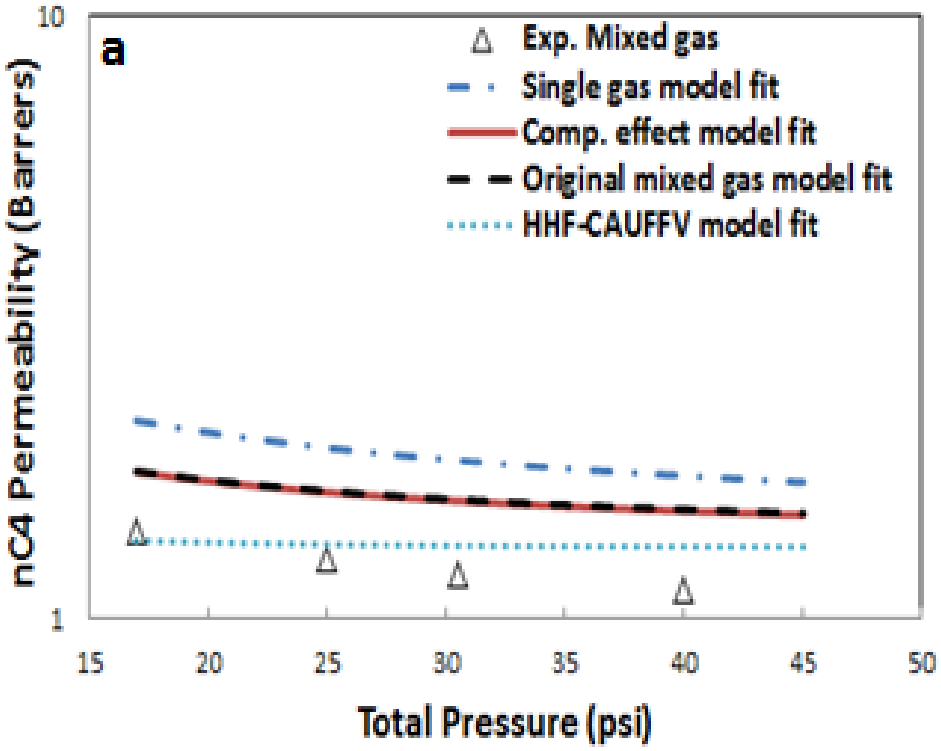
a
Exp. Mixed gas
Single gas model fit
Comp. effect model fit
Original mixed gas model fit
HHF-CAUFFV model fit
nC4 Permeability (Barrers)
10
1
15
20
25
30
35
40
45
50
Total Pressure (psi)

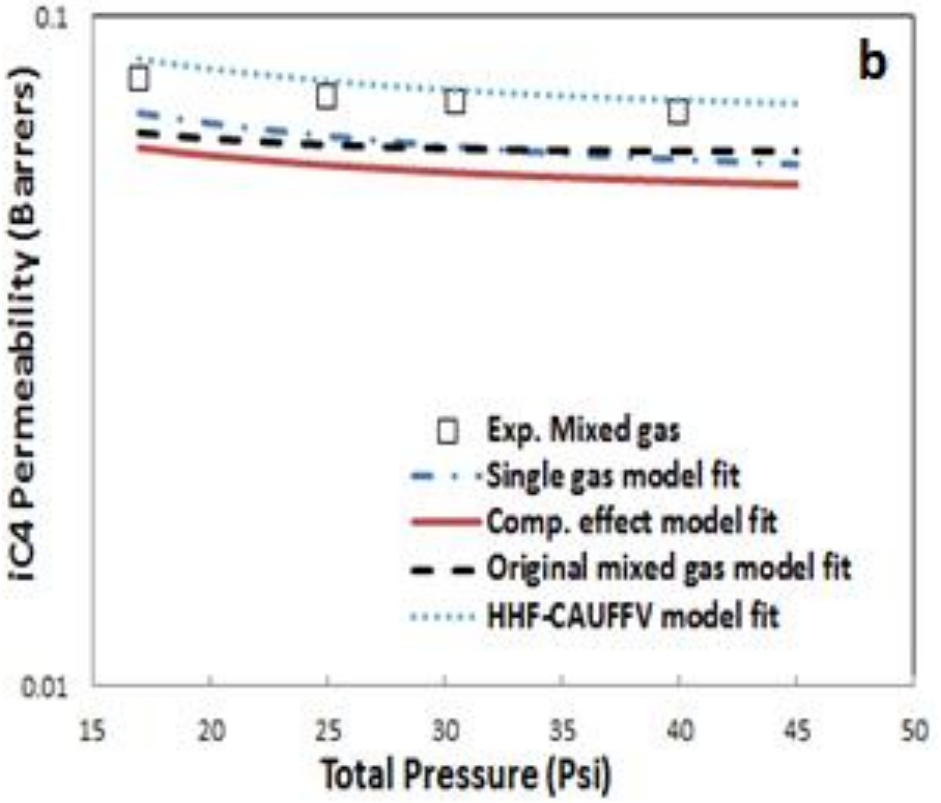
b
Exp. Mixed gas
Single gas model fit
Comp. effect model fit
Original mixed gas model fit
HHF-CAUFFV model fit
iC4 Permeability (Barrers)
0.1
0.01
15
20
25
30
35
40
45
50
Total Pressure (Psi)

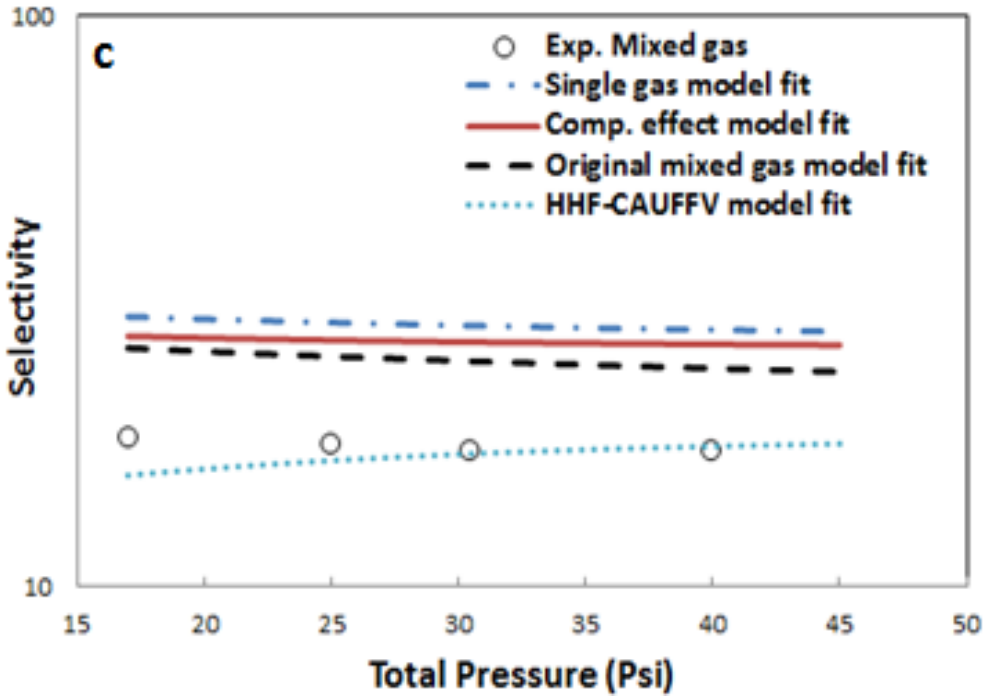

Figure D.6: Transport performance of 42 mol% nC4/ 58 mol% iC4 in neat 6FDA-DAM annealed at 230°C, at operating temperature of 100°C. Comparing experimental data with HHF-CAUFFV fit, a) n-C4 permeability, b) i-C4 permeability, and c) n-C4/i-C4 selectivity

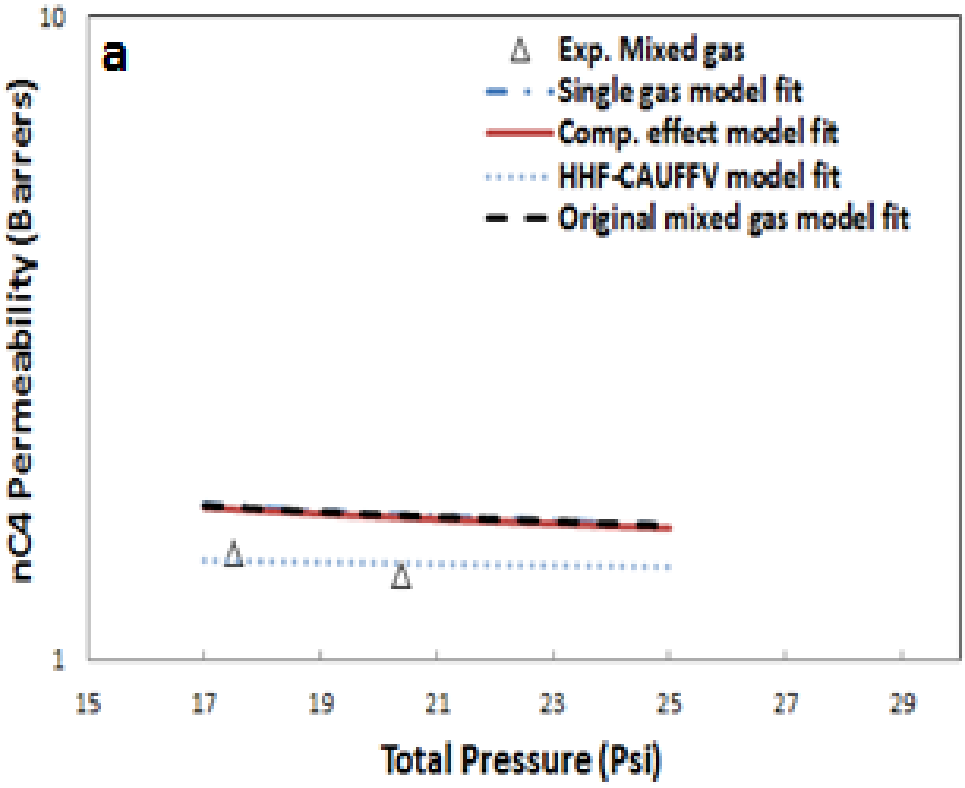
a
Exp. Mixed gas
Single gas model fit
Comp. effect model fit
HHF-CAUFFV model fit
Original mixed gas model fit
nC4 Permeability (Barrers)
10
1
15
17
19
21
23
25
27
29
Total Pressure (Psi)

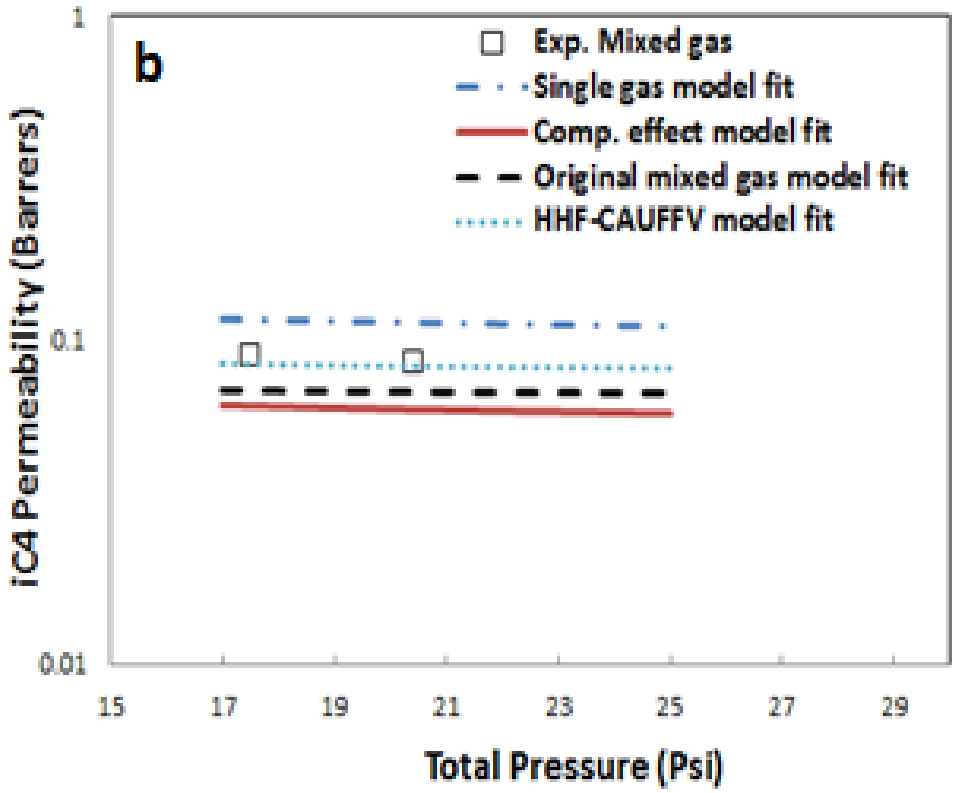
b
Exp. Mixed gas
Single gas model fit
Comp. effect model fit
Original mixed gas model fit
HHF-CAUFFV model fit
iC4 Permeability (Barrers)
1
0.1
0.01
15
17
19
21
23
25
27
29
Total Pressure (Psi)

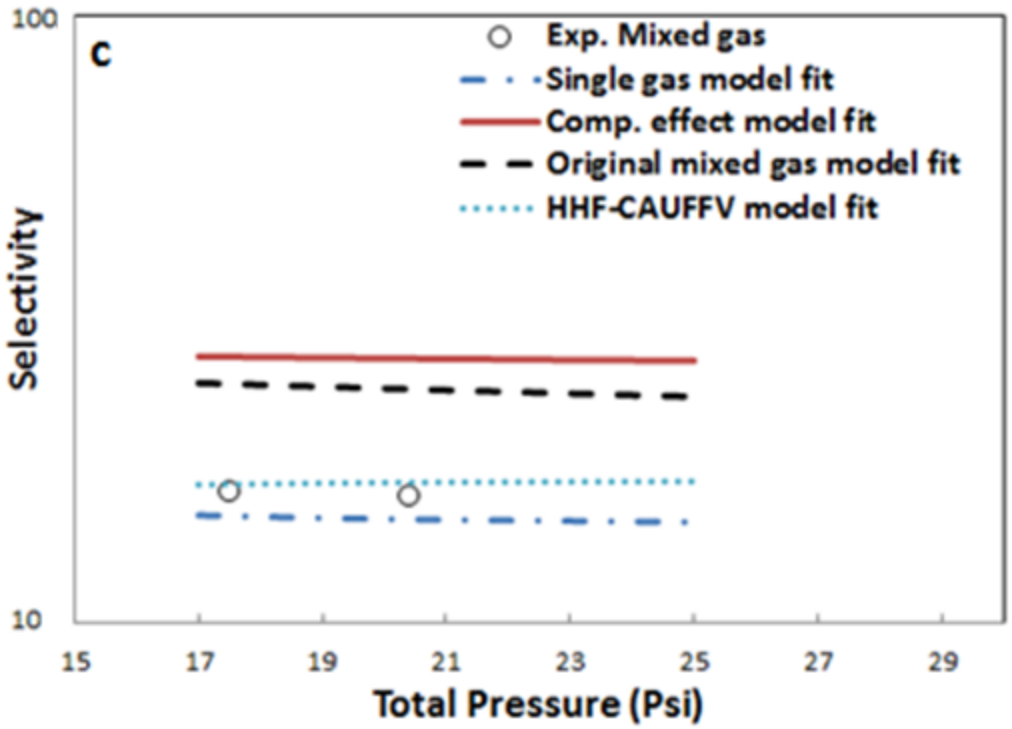

Figure D.7: Transport performance of 95 mol% nC4/ 5 mol% iC4 in neat 6FDA-DAM annealed at 230°C, at operating temperature of 100°C. Comparing experimental data with HHF-CAUFFV fit, a) n-C4 permeability, b) i-C4 permeability, and c) n-C4/i-C4 selectivity

APPENDIX E

MIXED GAS DATA ANALYSIS ACCOUNTING FOR FUGACITY

The effect of the non-ideality of butane was checked by analyzing data using fugacity rather than partial pressure. Figure E.1a & b compares mixed gas experimental data to predictions made using the original mixed gas transport model given in equations 2.17 – 2.24. No significant difference was observed between figure E.1a, which uses fugacity, and figure E.1b, which uses partial pressure. It can be concluded that within the pressure range tested it is safe to assume the gases behave as ideal gases. We can thus justify analyzing the data in the work using partial pressure rather than fugacity.

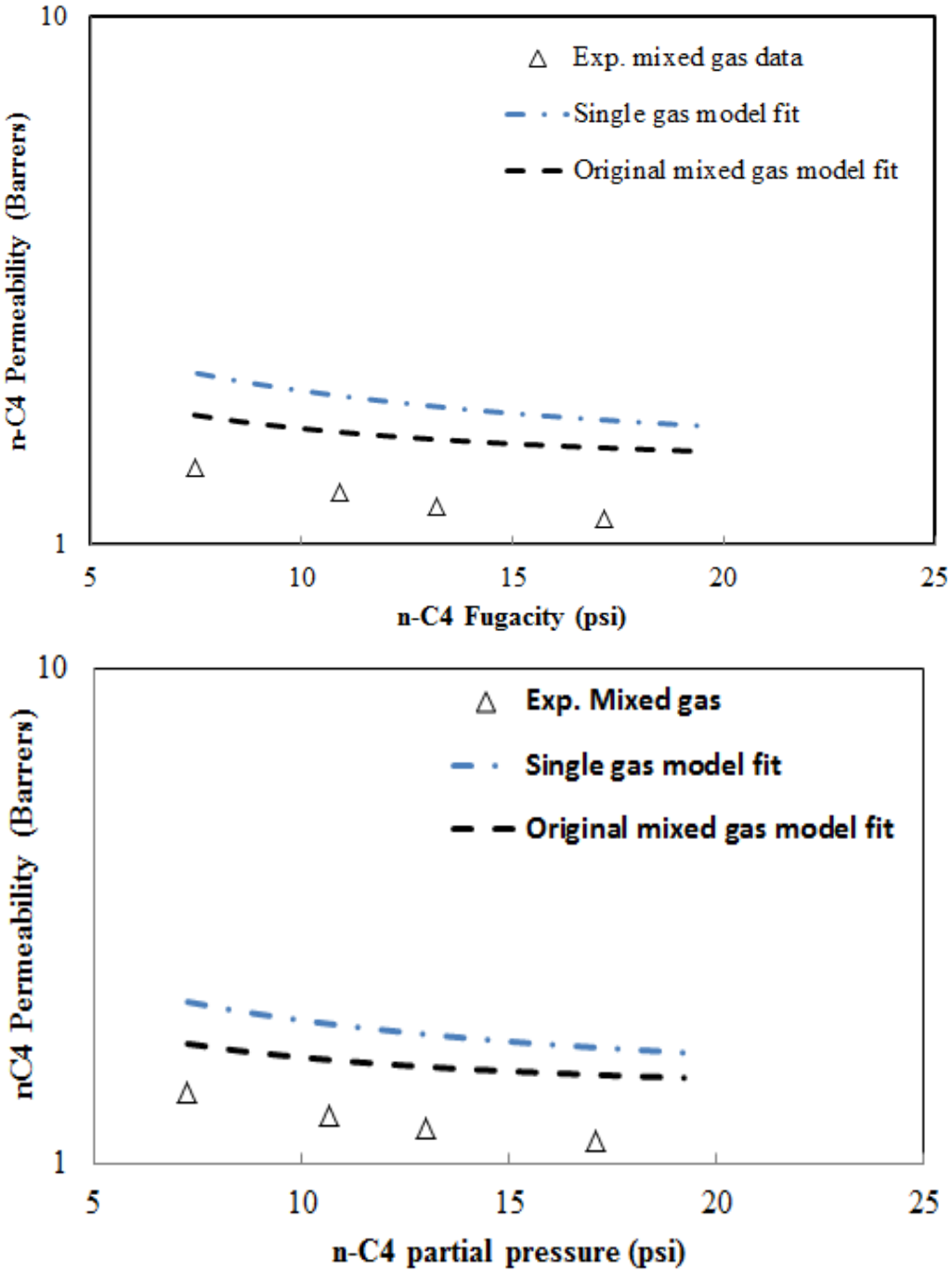

Figure E. 1: Transport performance of 42 mol% n-C4/ 58 mol% i-C4 in neat 6FDA-DAM annealed at 230°C at operating temperature of 100°C. Comparing experimental data with original mixed gas transport model Plot of n-C4 permeability versus a) fugacity of n-C4, b) partial pressure on n-C4

APPENDIX F

DERIVATION OF MIXED GAS TRANSPORT MODEL TO ACCOUNT FOR POSITIVE PERMEATE PRESSURE

Obtained from Kamaruddin [1], the mobile weight fraction at any point in the dense film can be obtained by equations F.1 and F.2.

$$\omega_A(x) = \frac{1 - \left(1 - \omega_{A1}(1 + 1/r)\right) exp\left(\frac{n_A x(1 + 1/r)}{\rho D_{D_A}}\right)}{(1 + 1/r)} \qquad (F.1)$$

$$\omega_B(x) \frac{1 - \left(1 - \omega_{B1}(1 + r)\right) exp\left(\frac{n_B x(1 + r)}{\rho D_{D_B}}\right)}{(1 + r)} \qquad (F.2)$$

The average mobile weight fraction inside the membranes can be obtained via equations F.3 and F.4.

$$\omega_A^{avg} = \frac{\int_0^l \omega_A(x)dx}{\int_0^l dx} = \left(\frac{1}{\left(1 + \frac{1}{r}\right)}\right)\left\{1 - \left(\frac{\left(1 - \omega_{A1}(1 + 1/r)\right)\rho D_{D_A}}{n_A l(1 + 1/r)}\right)\left(exp\left(\frac{n_A l(1 + 1/r)}{\rho D_{D_A}}\right) - 1\right)\right\} \qquad (F.3)$$

$$\omega_B^{avg} = \frac{\int_0^l \omega_B(x)dx}{\int_0^l dx} = \left(\frac{1}{(1 + r)}\right)\left\{1 - \left(\frac{\left(1 - \omega_{B1}(1 + r)\right)\rho D_{D_B}}{n_B l(1 + r)}\right)\left(exp\left(\frac{n_B l(1 + r)}{\rho D_{D_B}}\right) - 1\right)\right\} \qquad (F.4$$

Using the boundary conditions:

$$x = 0; \quad \omega_A(x) = \omega_{A1}$$

$$\omega_{A1} = \frac{1 - \left(1 - \omega_{A1}(1 + 1/r)\right)}{(1 + 1/r)} \tag{F.5}$$

$$x = l; \quad \omega_A(x) = \omega_{A2}$$

$$\omega_{A2} = \frac{1 - \left(1 - \omega_{A1}(1 + 1/r)\right) exp\left(\frac{n_A l(1 + 1/r)}{\rho D_{D_A}}\right)}{(1 + 1/r)} \tag{F.6}$$

Substituting equations F.5 and F.6 into F.1, equation F.1 can be simplified to equation F.7

$$\omega_A^{avg} = \frac{1}{(1 + 1/r)} - \frac{(\omega_{A1} - \omega_{A2})}{ln\left[\frac{1 - \omega_{A2}\left(1 + \frac{1}{r}\right)}{1 - \omega_{A1}\left(1 + \frac{1}{r}\right)}\right]} \tag{F.7}$$

Similarly, using the boundary conditions;

$$x = 0; \quad \omega_B(x) = \omega_{B1}$$

$$\omega_{B1} = \frac{1 - \left(1 - \omega_{B1}(1 + r)\right)}{(1 + r)} \tag{F.8}$$

$$x = l; \quad \omega_B(x) = \omega_{B2}$$

$$\omega_{B2} = \frac{1 - \left(1 - \omega_{B1}(1 + r)\right) exp\left(\frac{n_B l(1 + r)}{\rho D_{D_B}}\right)}{(1 + r)} \tag{F.9}$$

Substituting equations F.8 and F.9 into F.2, equation F.2 can be simplified to equation F.10

$$\omega_B^{avg} = \frac{1}{(1+r)} - \frac{(\omega_{B1} - \omega_{B2})}{ln\left[\frac{1-\omega_{B2}(1+r)}{1-\omega_{B1}(1+r)}\right]} \quad (F.10)$$

So the fraction of bulk contribution to the overall flux can be defined as equation F.11 and F.12

$$\pi_A^{bulk} = (1+1/r)\omega_A^{avg} = 1 - \frac{(\omega_{A1} - \omega_{A2})(1+1/r)}{ln\left[\frac{1-\omega_{A2}(1+1/r)}{1-\omega_{A1}(1+1/r)}\right]} \quad (F.11)$$

$$\pi_B^{bulk} = (1+r)\omega_B^{avg} = 1 - \frac{(\omega_{B1} - \omega_{B2})(1+r)}{ln\left[\frac{1-\omega_{B2}(1+r)}{1-\omega_{B1}(1+r)}\right]} \quad (F.12)$$

The diffusion based permeability is thus related to the observed permeability via equations F.13 and F.14.

$$P_A^* = \left(1 - \pi_A^{bulk}\right)P_A = \frac{(\omega_{A1} - \omega_{A2})(1+1/r)P_A}{ln\left[\frac{1-\omega_{A2}(1+1/r)}{1-\omega_{A1}(1+1/r)}\right]} \quad (F.13)$$

$$P_B^* = \left(1 - \pi_B^{bulk}\right)P_B = \frac{(\omega_{B1} - \omega_{B2})(1+r)P_B}{ln\left[\frac{1-\omega_{B2}(1+r)}{1-\omega_{B1}(1+r)}\right]} \quad (F.14)$$

Where the diffusion-based permeability is defined as in equation F.15,

$$P_A^* = \frac{D_D}{\left(p_{A_2} - p_{A_1}\right)}\left[k_D\left(p_{A_2} - p_{A_1}\right) + FC_H' b\left(\frac{p_{A_2}}{1 + bp_{A_2} + bp_{B_2}} - \frac{p_{A_1}}{1 + bp_{A_1} + bp_{B_1}}\right)\right] \quad (F.15)$$

F.1. REFERENCE

1. Kamaruddin, D.H. and W.J. Koros, *Some observations about the application of Fick's first law for membrane separation of multicomponent mixtures*. J. Mem. Sci., 1997. **135**(2): p. 147-159.

VITA

Omoyemen E. Esekhile

Esekhile was born in Benin city, Edo state, Nigeria. She obtained a BSc. in Chemical Engineering from the University of Minnesota Duluth in 2006, worked for nine months at SouthWest Research Institute in San Antonio Texas, before coming to Georgia Tech in 2007 to pursue a doctorate in Chemical Engineering.